



Delft University of Technology

Visualizing response to DNA damage in bacteria

Deb Roy, Sumit

DOI

[10.4233/uuid:dfdfb7e1-795b-4939-be5c-96da4efc21dd](https://doi.org/10.4233/uuid:dfdfb7e1-795b-4939-be5c-96da4efc21dd)

Publication date

2020

Document Version

Final published version

Citation (APA)

Deb Roy, S. (2020). *Visualizing response to DNA damage in bacteria*. [Dissertation (TU Delft), Delft University of Technology]. <https://doi.org/10.4233/uuid:dfdfb7e1-795b-4939-be5c-96da4efc21dd>

Important note

To cite this publication, please use the final published version (if applicable).
Please check the document version above.

Copyright

Other than for strictly personal use, it is not permitted to download, forward or distribute the text or part of it, without the consent of the author(s) and/or copyright holder(s), unless the work is under an open content license such as Creative Commons.

Takedown policy

Please contact us and provide details if you believe this document breaches copyrights.
We will remove access to the work immediately and investigate your claim.

Visualizing response to DNA damage in bacteria

Sumitabho DEB ROY

Visualizing response to DNA damage in bacteria

Dissertation

for the purpose of obtaining the degree of doctor

at Delft University of Technology

by the authority of the Rector Magnificus Prof.dr.ir. T.H.J.J. van der Hagen

chair of the Board for Doctorates

to be defended publicly on

Wednesday 3 June 2020 at 10:00 o'clock

by

Sumitabho DEB ROY

Master of Science in Biotechnology, Berhampur University, India

born in Shillong, India

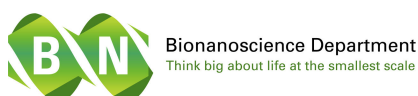
This dissertation has been approved by the promotor.

Composition of the doctoral committee:

Rector Magnificus	chairperson
Prof. dr. N. H. Dekker	Delft University of Technology, promotor

Independent members:

Prof. dr. A.M. Dogterom	Delft University of Technology
Prof. dr. ir. S. J. Tans	Delft University of Technology
Prof. dr. T Shimizu	AMOLF
Dr. G. E. Bokinsky	Delft University of Technology



Keywords: DNA damage, DNA repair, DNA replication, bacterial replisome, translesion polymerases, live cell imaging, single-molecule fluorescence microscopy

Printed by: Gildeprint

Front: S. Deb Roy (Image analyses: Supersegger)

Copyright © 2020 by Sumitabho Deb Roy

Casimir PhD Series, Delft-Leiden 2020-12

ISBN 978-90-8593-439-4

An electronic copy of this dissertation is available at
<http://repository.tudelft.nl>

Contents

1. Introduction: DNA replication and replication fork stalling	1
1.1 Introduction	2
1.2 DNA replication and the <i>Escherichia coli</i> replisome	3
1.3 Accessory components of the replisome	4
1.3.1 Accessory Helicases	5
1.3.2 Translesion DNA polymerases	5
1.4 Impediments to replication fork stalling	6
1.5 Types of DNA damage	7
1.6 The motivation for this thesis: questions of biological significance	11
1.7 Outline of the thesis	12
References	13
2. A review: Live cell imaging- Single molecule fluorescence microscopy (SMFM)	19
2.1 Introduction	20
2.2 Fluorescence and 'Molecular Flashlights': The concept	20
2.3 Live cell imaging: A brief history of development	22
2.4 Single molecule fluorescence microscopy (SMFM): A brief history of development	24
2.5 <i>Live cell imaging</i> modalities with <i>Single molecule fluorescence microscopy</i> : The common combinations	25
2.6 Why single molecule imaging in live cells?	30
2.7 Single molecule fluorescence imaging pioneering research in live bacteria	31
2.8 A technical perspective: Why Live Cell Imaging - (Wide-field Epi-fluorescence) Single molecule fluorescence microscopy combination?	33
2.9 A biological perspective: Why Live Cell Imaging- (Wide-field Epi-fluorescence) Single molecule fluorescence microscopy combination?	35
2.10 Finding the right scheme for imaging: DNA replication and repair mechanisms	36
2.11 Coda	38
References	40
3. What happens to DnaB upon DNA damage?	47
3.1 Introduction	48
3.2 Number of replisomes and number of foci: related but different concepts	52
3.3 How to assess DnaB behavior? The parameters	54

3.4 Results.....	56
3.4.1 Strain engineering and validation.....	56
3.4.2 DnaB behavior in undamaged cells.....	60
3.4.2.1 DnaB foci characteristics in undamaged cells.....	60
3.4.2.2 DnaB stoichiometry in undamaged cells.....	61
3.4.2.3 DnaB foci and stoichiometry (combined) in undamaged cells.....	62
3.4.2.4 DnaB overall characteristics (foci & spatial distribution) with respect to the replisome.....	64
3.4.2.5 Spatial distribution of DnaB foci (categorized: 1, 2 and 3) with respect to the replisome.....	66
3.4.3. DnaB behavior after UV exposure.....	67
3.4.3.1 DnaB foci behavior after UV exposure with respect to the replisome.....	68
3.4.3.2 DnaB stoichiometry after UV exposure.....	70
3.4.3.3 Spatial distribution of DnaB foci after UV exposure, with respect to the replisome.....	73
3.5 Discussion.....	77
3.6 Materials and methods.....	80
3.7 Supplementary information.....	86
References.....	96

4. Drug dosage and timing influence the spatial distribution of DNA Polymerase IV.....99

4.1 Introduction.....	100
4.2 Results.....	103
4.2.1 Strain creation with fluorescently labelled DNA Polymerase IV and β -clamp.....	103
4.2.2 Observing <i>in vivo</i> Pol IV response to DNA damage drugs.....	103
4.2.3 The spatial distribution of Pol IV depends on dosage of DNA damage drugs and elapsed time.....	106
4.2.4 Examination at the single-cell level of colocalization between Pol IV and the replisome in the presence of DNA damage drugs.....	109
4.3 Discussion.....	111
4.4 Materials and methods.....	115
4.5 Supplementary information.....	120
References.....	139

Summary.....143

Samenvatting.....145

Acknowledgments.....149

Curriculum Vitae153

List of publications155

1

Introduction: DNA replication and replication fork stalling

Genome replication is faithfully carried out by the bacterial replisome. However, the replisome has to overcome obstacles, emanating from internal and external sources, in its onward DNA journey. The replisome has its core components, but may also be aided by accessory factors under such circumstances. Unable to overcome obstacles in the path, replication forks may be stalled posing threat to cell survival.

1.1 Introduction

Cell growth and division are essential to life, whether it is for prokaryotes or eukaryotes. A key process contributing to cell growth and division, is replication of the genome of the organism. The four nucleotide bases of Adenine, Thymine, Guanine and Cytosine, organise in various combinations to form the strands of Deoxyribonucleic acid (DNA), which further on, gives rise to the genome. The genome codes for all cellular processes essentially and thereby, functionally regulates the organism as well.

An understanding of the genome and its replication, thus forms a fundamental basis of understanding biology in general and organism function in particular. An understanding of which is also incomplete, without considering how genomes deal with various kinds of impediments and DNA breaks in its path, during the process of genome replication.

Inevitably, this brings us to appreciating the concept of DNA damage and how genomes repair and cope with it (1,2). DNA may be damaged, due to causative external factors, including Ultraviolet (UV) radiation and chemicals, and internal factors, like spontaneous mutation and cellular metabolites. At the molecular level, apart from strand breaks, adducts and lesions, which also emanate from the aforementioned causative factors, contribute as obstacles to replication progress.

The subsequent step of how these breaks and impediments are resolved, show the plethora of pathways available to the cell, some of which target the damage incurred for repair, while others help the cell tolerate damage or further in certain cases, even lead to programmed cell death (3-5). With error prone pathways of damage tolerance, which will be discussed in chapter 4 later, mutations arise in DNA and these have significant consequences.

A framework of understanding on how DNA damage is managed and how underlying mutations (causal or consequential) which exist and get repaired or are tolerated, is critical for comprehending all kinds of biological phenomena that arise later phenotypically. We are only beginning to appraise, how mutation rates have a direct bearing on antibiotic resistance evolution (6-9). Notably, the threat emanating from antibiotic resistance in this age and time cannot be overemphasized (10-13), as public health crises looms large.

Most importantly, furthering fundamental knowledge on replication during DNA damage, has implications for mechanisms of cancer and aging, in no uncertain terms (14-17).

Therefore, the scope and goal of this thesis has been to advance our understanding on genome replication, in the context of DNA damage. I, along with my team of researchers, have inflicted DNA damage on cells, and in different ways (UV and chemically different DNA damage agents) and compared these results with the undamaged replication condition. Using live cell imaging as our main tool, we have probed replicative factors, some of which may have distinct functions in the DNA damaged cells, as compared to undamaged ones.

In this introductory chapter, followed by chapters of scientific investigation, we describe in detail, how the replicative helicase (DnaB) and a translesion DNA polymerase (Pol IV), as

specific cases, behave during DNA replication when perturbed by DNA damage and work to avert cellular crises.

This thesis, does proverbially stand on the shoulders of research performed by various groups, which have advanced techniques for imaging in live cells with single molecule sensitivity (18-25), for me and my research team to come in now and probe questions of biological significance. The technical advancement has come through years of painstaking research of others and sets up our ability to image proteins of interest, using bright fluorophores with superior properties, simultaneously encompassing electronic devices that capture faintest of signals to amplify and 'machine learning' analyses algorithms to harvest patterns amidst a deluge of signals and data, just to name a few.

1.2 DNA replication and the *Escherichia coli* replisome

Biochemical, biophysical and genetic research over the decades, has rendered the replicative process in *Escherichia coli*, as one of the best understood amongst all organisms studied (26-28).

The *E.coli* replisome is multi-protein complex tasked with DNA synthesis for its genome. Composed of more than 12 different subunits, the replisome travels at an average speed of 600-1000 bp/s (37°C) bidirectionally, to cover the 4.6 Mbp genome (27,29). DNA synthesis is catalysed by the main replicase DNA polymerase III (referred as Pol III hereafter) (30,31), which consists of three core subunits (α , ϵ , θ , encoded by *dnaE*, *dnaQ* and *holE* genes, respectively) and is present in three molecular copies (core) at the replisome (32,33). Pol III interacts with the pentameric clamp loader complex ($\tau_3\delta\delta'$), via the τ subunit, which is referred as Pol III* complex. The clamp loader further functions to load the sliding β clamp dimer on DNA, which makes Pol III synthesis processive. Pol III* complex in association with sliding β clamp dimer is called the Pol III HE (holoenzyme).

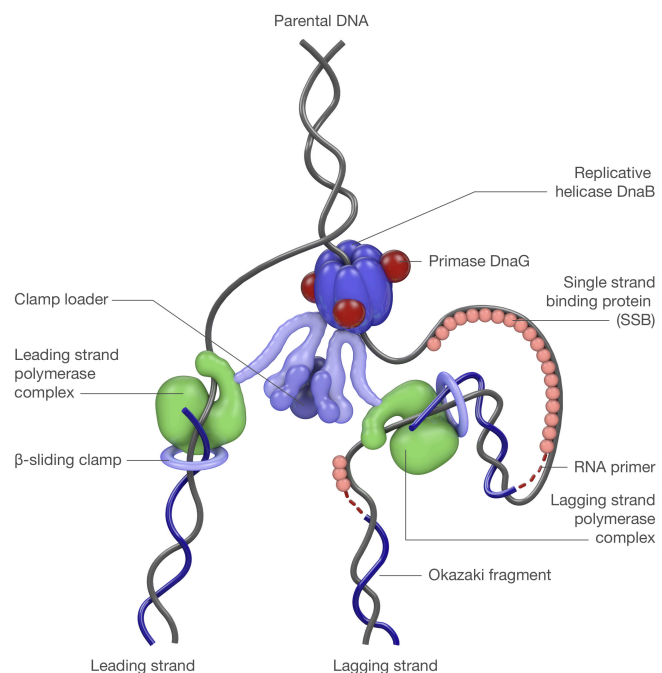


Figure 1.1 The *Escherichia coli* replisome with its multiple components, unwinding the double stranded parental DNA to synthesize new complementary strands.

The Pol III HE is estimated to have a molecular copy number of 10-20 per cell (5,34) and carries out a primer-initiated DNA synthesis in 5'-3' orientation, while also possessing a 3'-5' proofreading exonuclease capability. (Of the Pol III core components, the α -subunit is known

for polymerase activity, the ϵ subunit contributes to the proofreading activity, while the θ subunit adds to the stability of the core complex).

At the forefront of this molecular machinery, is the DnaB helicase responsible for unwinding of DNA, which by its interaction with τ subunit of the clamp loader, is also coupled with the Pol III HE. DnaG primase, which generates RNA primers for initiation of replication synthesis, is also recruited by DnaB helicase. Conventionally, due to the antiparallel nature of DNA strands and the directional processivity of the replisome (5'-3'), the synthesis of one of the strands has been thought to be discontinuous (lagging strand), and to occur in short fragments of ~1200 bp (Okazaki fragments), while the other strand has been modeled to be replicated in the continuous fashion (leading strand) (26,35).

DNA Polymerase I (Pol I) has been known to seal gaps between Okazaki fragments by removing RNA primers and synthesizing complementary DNA between gaps, thereby accomplishing complete synthesis for both strands. Pol I was the first polymerase discovered, encoded by the *polA* gene, and estimated to be at a molecular copy of ~400 per cell (34,36). This single polypeptide of 103 kDa, possesses a three-fold ability, of DNA synthesis (5'-3'), exonuclease (5'-3') as well as exonuclease (3'-5').

Interestingly, in recent years, the replisome has been cast somewhat in new light, with evidences emerging of both strands being replicated in a discontinuous fashion (27).

The *E.coli* replisome being a multi-subunit complex, has components with varying stability on DNA (bound time on DNA) (27). The DnaB helicase has a reported bound time of 913 ± 508 s, ~15 min (27), (DnaB mean lifetime reported by another group is ~9 min (37)), which is much higher than that of other replisome components, for example the sliding β -clamp (47.2 ± 2.9 s) and the Pol III component ϵ (10.4 ± 0.8).

This has particular significance for our research and implies that individual components inside the replisome, may not be a reliable marker or proxy for replisome behaviour as a whole. When imagining the replisome as multi-component machine, during its onward journey colliding with a lesion, adduct or a strand break, individual replisome components may be hypothesized to behave differently, in response to DNA damage. For example, the components with longer bound times or lifetimes, may persist at the damage sites, while the ones with shorter lifetimes may be easily dissociated, whereby the single strand DNA (ssDNA) gaps may be exposed for other downstream factors to come in and repair DNA.

1.3 Accessory components of the replisome

The replisome besides having its integral components, also has factors which have been found to associate with, or have been debated to be in the vicinity of, the replisome, especially during critical cellular scenarios.

Some of these critical cellular scenarios include nucleoprotein barriers in the path of the replisome during transcription and impediments arising from DNA damage. In the following section, I introduce two of the most common class of factors, which avert or resolve such critical cellular scenarios. Understanding some of these factors has been a focus of this thesis.

1.3.1 Accessory helicases

One of these factors, called accessory helicases are known to exist in viruses, bacteria and eukaryotes and there are three such known helicases in *E.coli* (38-42). These helicases may also mitigate or resolve replication-transcription conflicts, when the moving replication complex meets the transcription complex (moving or stalled), either co-directionally or head-on, by promoting fork movement through nucleoprotein barriers, apart from DNA repair activities (43,44).

Rep, UvrD and DinG constitute the three known accessory helicases in *E.coli*. Interestingly, Rep and UvrD also share a 40% homology at the amino acid level (45,46), and perhaps not surprisingly, both seem to have overlapping functions at the replication fork or elsewhere.

While Rep has been discovered to play an important role in removing nucleoprotein barriers and clearing the path ahead for the progressing replisome (41,47), its role in DNA repair has also been documented (48,49). Similarly, while UvrD has been a central player in DNA repair processes, participating in pathways of the nucleotide excision repair (NER) pathway and methyl directed mismatch repair (MMR) (50-52), it has also been evidenced how stalled RNA polymerases (potential nucleoprotein barriers), work with UvrD in Transcription coupled repair (TCR) (43,53), wherein these stalled RNA polymerases act as sensors of DNA damage. Thus, UvrD clears the nucleoprotein roadblocks and helps prevent replication transcription conflicts, a role also ascribed to Rep helicase (40,54). Furthermore, strains lacking both Rep and UvrD are 'inviable' in rich media, which does indicate cooperativity between these helicases, at least under certain conditions (55). In this regard, these two helicases have been investigated *in vitro* recently, for their competitiveness at the replication fork (45). The authors reported that Rep and UvrD 'antagonize' or thwart the presence of one another.

In relation to the replisome, Rep has been shown to interact with the DnaB helicase (55,56), while absence of Rep reduces the replisome speed (57). A recent study has shed light on how the Rep- replisome interaction may occur in the undamaged cell cycle *in vivo* (47). 70% of Rep foci were found to colocalize with the replisome, and analysis of these foci revealed a hexameric stoichiometry.

1.3.2 Translesion DNA polymerases

E.coli has at least five different DNA polymerases, of which three of them, are categorised as translesion DNA polymerases (34,58-60). Broadly, translesion polymerases represent the last line of defence through error prone DNA synthesis, when error free pathways have failed to repair DNA damage. Therefore, at the cost of mutation and molecular evolution which has wider ramifications, translesion polymerases provide damage tolerance and boost survival. All three translesion polymerases are under the regulatory control of SOS response, mediated by the LexA operator, which serves to upregulate gene expression of proteins involved in DNA damage repair and rescue (3).

Apart from Pol I and Pol III, discussed above (section 1.2), which take part in regular processes of replication, the remaining polymerases are Pol II, Pol IV and Pol V, are encoded by different

genes. Pol II, encoded by the gene *dinA/ polB* (61,62), is an 88 kDa polypeptide with 3'-5' exonuclease activity, whose function has been largely unknown (34,58), apart from its participation in replication restart and certain stress response pathways (63,64).

Pol IV, a 39.5 kDa polypeptide encoded by the gene *dinB* (65), is without 3'-5' exonuclease activity and thus, a low fidelity polymerase. Pol IV has high molecule copy number in undamaged cells (250 molecules/cell), which is further upregulated 10 fold by SOS response (34,66). However, these numbers have been revised in a recent study, which reported a lower molecule copy number in undamaged cells (20 molecules/cell) (67). Pol IV action has been particularly implicated in bypassing certain types of DNA adducts (N₂-dG) (68) or CH₃ (69), among other types. Pol IV has also been known to cause -1 frameshift mutations, when highly overexpressed (60,70).

Pol V, was the last translesion polymerase identified (71), encoded by genes *umuDC* and is a 72 kDa heterotrimer complex of UmuD'₂C polypeptides. Unlike Pol II and Pol IV, Pol V has low presence in undamaged cells (15 molecules/ cell, or fewer), and is upregulated further during SOS response (~200 molecules/cell). Similar to Pol IV, Pol V is also a low fidelity polymerase and works without 3'-5' proofreading ability. Pol V has been well characterized as a principal player in UV mediated damage and by-passing photoproducts, such as pyrimidine dimers (60,72).

1.4 Impediments to replication fork stalling

The understanding of DNA and DNA replication is incomplete, without the associated understanding of what happens when DNA replication is halted or even disrupted, due to many factors, internal and external (73-75). This is referred in this thesis as 'replication fork stalling', when the replisome at the Y-shaped fork structure, the junction of DNA unwinding by the replicative helicase, is stopped from proceeding any further.

The internal factors which contribute to replication fork stalling, exist as natural roadblocks and contribute to genome instability (40,75). They may be summarized briefly, below:

- **DNA binding proteins**, such as replication termination proteins of the Ter-Tus complex.
- **Transcription**, because the replisome and RNA polymerase share DNA as their template and can collide either head-on or co-directionally. Apart from this, RNA-DNA hybrids (R-loops), may also pose problems.
- **DNA secondary structures and unusual structures**, which may form cruciform, hairpin or triplex DNA, including structures like G-quadruplexes, H-DNA, Z-DNA or S-DNA.

While these are natural impediments potentially leading to replication fork stalling, this thesis has focused on impediments of another kind, that which is arisen due to DNA damage (73,74). An adduct, lesion or strand break may arise due to DNA damage and lead to replication fork stalling. Unlike the above-mentioned internal factors leading to replication fork stalling, DNA damage can be both externally inflicted or internally generated (see following **section 1.5.**). The types of DNA damage are discussed in the next section.

1.5 Types of DNA damage

DNA, being the genetic blueprint for the development of an organism, any damage to it (DNA) carries grave risk. On a hypothetical argument, damage to the other factors of the central dogma (RNA and proteins) does not pose as much risk as it does for DNA. This is simply because damage to DNA can be passed on for generations and is not limited to a cellular lifetime (one cycle of cell birth to cell division) only, due to its ability to code for RNA and proteins.

DNA damage, broadly can be classified into two major categories (based on origin): exogenous and endogenous (1). Given the scope of this introductory chapter in particular and the thesis in general, which inclines towards the functional consequences of DNA damage, we briefly mention the major categories of DNA damage (based on origin, as mentioned above) without going deeper into the details. For the interested reader, there have been many excellent reviews over the years to refer to, for further interest (1,2,76).

For a quick glance on general information about DNA damage as an overview, please refer to **Table 1.1.** for DNA damage agents, DNA damage substrates and DNA repair pathways. The table is partly adapted from the ref. (1) .

DNA damage agents	Alkylating agents Base deamination Replication errors	Oxidative damage Electrophiles	Ionizing radiation UV radiation Cross linking agents Aromatic compounds Heat cold hypoxia
Damaged DNA	Mismatches Uracil Abasic sites Adducts	Lesions Single strand breaks Double strand breaks	Bulky lesions Strand crosslinks Single strand breaks Double strand breaks
DNA repair pathways	Mismatch repair Base excision repair	Base excision repair Single strand break repair Double strand break repair	Nucleotide excision repair Interstrand crosslink repair Single strand break repair Double strand break repair Translesion synthesis

Table 1.1 A general overview on DNA damage agents, damaged DNA and DNA repair pathways. Adapted from ref. (1)

A. Exogenous DNA damage:

- **Ionizing radiation (IR)**

IR, consisting of alpha, beta, gamma, neutrons and X-rays, is abundantly produced on earth, coming with cosmic radiation and from rocks, soil and medical devices as well. A 'spectrum' of base lesions, is produced, including 8-oxo-guanine, thymine glycol and formamidopyrimidines. IR may also produce single strand breaks (SSBs) and double strand breaks (DSBs) (1).

- **Ultraviolet radiation (UV)**

UV rays typically, coming from the sun, can be classified into 3 sub-parts based on its wavelength:

- a. UV-A (320-400 nm)
- b. UV-B (290-320 nm)
- c. UV-C (190-290 nm)

Maximal absorption occurs at 260 nm for DNA, beyond which its photo-absorption 'drops dramatically' (1). UV inflicts damage on cells in two ways-direct and indirect. In a direct type of damage, if biological matter can absorb UV for excitation, then it leads to their photochemical modification. In an indirect type of damage, when UV is not directly absorbable by biological matter, energy transfer from neighbouring molecules (photosensitizers) may perturb structural or chemical properties.

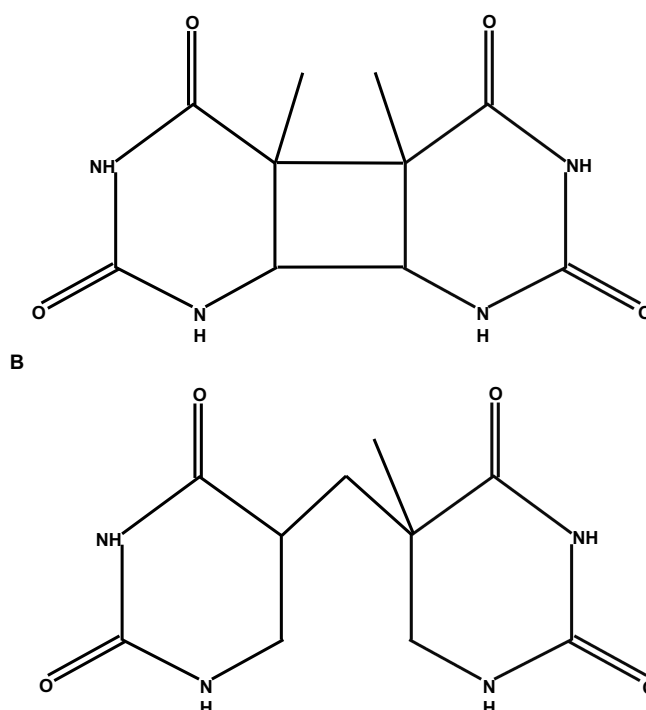


Figure 1.2 showing the representative structures of **A. Cyclobutane pyrimidine dimer (CPD). B. Pyrimidine (6-4) pyrimidone photoproduct.**

Two major photoproducts of UV radiation are, cyclobutane pyrimidine dimers (CPDs) and pyrimidine (6-4) pyrimidone photoproducts [(6-4) PPs], a consequence of covalent linkages between two adjacent pyrimidine bases of DNA (**Figure 1.2., adapted from ref. (1)**). Wavelength and dose of light dictate the relative formation of these two photoproducts, although the former (CPDs) have a higher yield known (1).

UV-C has been widely reported in laboratory studies, due to its maximal absorption by DNA (1,76). UV-B may also cause pyrimidine dimer formation, but apparently does so with lower efficiency. UV-A may damage DNA by adduct formation, through photo-oxidation reactions, and by the excitation of endogenous (porphyrins and flavins) and exogenous (psoralens, tetracycline, promazine, and methylene blue) photosensitizers, amongst others (1,76).

UV-C has been used to study the behavior of replicative helicase DnaB in this thesis (chapter 3).

- **Chemical sources**

DNA damage under this category, is caused by many different agents of dissimilar chemical properties. They are highlighted below, but briefly:

a. Alkylating agents

Emanating from dietary components, tobacco smoke and biomass burning, amongst others, these agents react with 'increased affinity' to the highly nucleophilic nitrogen base rings (1).

Some of the most common alkylating agents used in laboratory studies include methyl methanesulfonate (MMS), ethyl methanesulfonate (EMS), N-methyl-N'-nitro-N-nitrosoguanidine (MNNG), and methylnitrosourea (MNU), which react with DNA to form mutagenic and carcinogenic lesions.

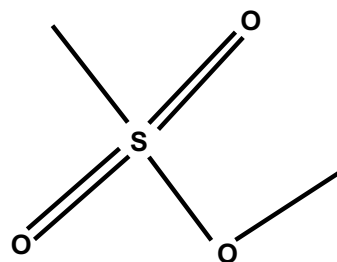


Figure 1.3. showing the representative structure of methyl methanesulfonate (MMS).

MMS (**figure 1.3.**, adapted from reference (1)) has been used in this thesis to study the action of DNA Polymerase IV (chapter 4).

b. Aromatic amines

Aromatic amines are produced from cigarette smoke, fuel, coal and industrial dyes, amongst others. C8-guanines lesions from aminofluorenes are known to be 'persistent' and mutagenic.

c. Polycyclic aromatic hydrocarbons

Coming from common sources such as tobacco smoke, automobile exhaust, fossil fuels amongst others, these carbon compounds with two or more aromatic rings are widely distributed carcinogens in the environment.

d. Other reactive electrophiles

Of the miscellaneous types of agents here, N-nitrosamines are potent carcinogens, which are produced from tobacco smoke and found in preserved meats. Of note, the hormone estrogen, used frequently in Hormonal Replacement

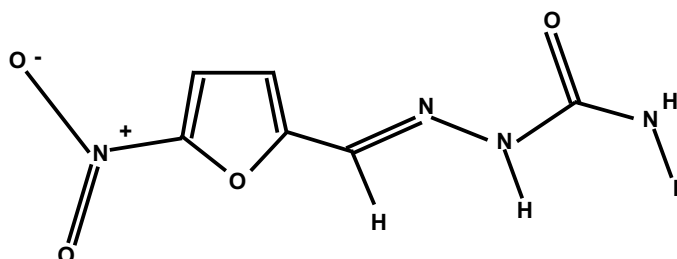


Figure 1.4. showing the representative structure of Nitrofurazone (NFZ).

Therapy (HRT), poses cancer risk after prolonged use (1).

It is important to note that 4- nitroquinoline 1-oxide (4-NQO), having both mutagenic and carcinogenic, can form covalent adducts with C8 or N² of guanines (N²-dG) and N⁶ of adenines. Similarly, Nitrofurazone (**NFZ**) can also form N²-dG adducts and has been used in this thesis to study DNA polymerase IV (chapter 4) as the encoding gene *dinB* was shown to be sensitive both these molecules (77). **Figure 1.4.** (as adapted from the website of Pubchem, US National Library of Medicine) shows a representative chemical structure of NFZ.

e. *Toxins*

These are biological products produced as part of defence mechanisms, secreted by bacteria and fungi, which possess genotoxicity and carcinogenicity. (e.g., Aflatoxins produced by *Aspergillus flavus* and *Aspergillus parasiticus*).

- **Environmental stresses**

Environmental sources of stress like extreme heat, extreme cold, hypoxia, and oxidative stress, to name a few common ones, fall under this category (1). These stresses have been reported to be mutagenic at trinucleotide repeats, associated with neurodegenerative disorders, among other observations.

B. Endogenous DNA damage:

- **Replication errors**

While genome replication remains a high-fidelity process, base substitutions, single base insertions and deletion still accumulate.

- **Spontaneous Base Deamination**

This phenomenon wherein bases lose their exocyclic amines, contributes to spontaneous mutagenesis in cells.

- **Abasic Sites**

Abasic or AP (apurinic/apyrimidic) sites, which are created in the DNA when the N-glycosyl bond linking the nitrogenous base and the sugar phosphate bond is hydrolysed or cleaved, are inherently unstable and readily form single strand breaks (SSBs).

- **Oxidative DNA Damage**

Reactive Oxygen Species (ROS) are byproducts of the cellular metabolism, which can attack DNA backbone and generate single strand breaks (SSBs), amongst other consequences.

- **DNA Methylation**

Methylated bases, are contributed by methyl transferases, of which O⁶- methylguanine and the related residues O⁴-methylthymine and O⁴-ethylthymine are highly mutagenic.

1.6 The motivation for this thesis: questions of biological significance

Without any overstatement, it is true to say that the motivation for my undertaking of this thesis work has been fueled by my curiosity for understanding the replication fork stalling mechanisms. Because without understanding how DNA deals with stalled replication forks, as a consequence of DNA damage, our understanding of DNA and its function in replication is incomplete.

Some of the general questions, that came to my mind at the outset of my PhD, prior to asking specific questions in the following chapters, were the following:

- What happens to the replisome components in general, when the replisome faces DNA damage obstacles head on?
- What happens to the replisome components specifically at the forefront (DnaB/ DnaG) of the replisome machinery?
- How do the accessory factors of the replisome, like translesion polymerases come to the replisome?
- Do these accessory factors come to the replisome only during situations of DNA damage or are they always part of the replisome, undetected to be so yet?
- Is there 'switching' of the regular polymerase and the translesion polymerases at the replisome, to trigger their specialized translesion functions during DNA damage? (For example, does the regular polymerase fall away from the replisome and the translesion polymerases become the sole occupants at the replisome for DNA synthesis?)
- Considering that some translesion polymerases (e.g., DNA polymerase IV in *E.coli*), have presence in both undamaged and DNA damaged states of the same cell, how does the transition work or appear to be, for such polymerases?

Overarching questions such as the above, have formed the basis of specific questions in the following chapters on research. A careful perusal of the literature and references mentioned in the thesis will inform the interested reader, that we as a research community, have still not found 'to-the-point' answers to the above questions, although we (our research group and others) have generated insightful observations that have contributed knowledge and narrowed down hypotheses to more probable ones.

1.7 Outline of the thesis

In this thesis, chapter 1 provides introductory information on DNA replication and the *Escherichia coli* replisome. We also bring up the context of accessory components of the replisome which may help during replication fork stalling, followed by the discussion of impediments leading to replication fork stalling in general and DNA damage specifically. A brief description of the overarching research goals is provided, the curiosity of which forms the motivation for this thesis work and which are also unresolved scientific questions for the research field, to our knowledge.

In chapter 2, we introduce the concept of fluorescence as 'Molecular flashlight' and provide brief histories of technical development in the fields of 'Live cell imaging' and 'Single Molecule Fluorescence Microscopy'. This is followed by a comparison of imaging modalities which can be used both for live cell imaging and single molecule fluorescence microscopy (i.e., the two techniques in combination). Additionally, we discuss next why single molecule imaging in live cells in general and in bacteria particularly, is a rewarding labor for understanding biological concepts, which elude deeper investigation by 'ensemble average' techniques. In **section 2.8.**, we bring the reader an overview of the advantages of these techniques and potential problems to be circumvented. Subsequently in **sections 2.9.** and **2.10.**, we discuss why these techniques are suited for biological studies and how these techniques have contributed to an advancement for the discipline of DNA replication and repair particularly. In this regard, we cite seminal studies of DNA replication and repair in bacteria over the years using single molecule imaging, which have paved the way for our research.

In chapter 3, we provide results on what happens to the replisome component and helicase motor DnaB, at the forefront of replicative machinery when DNA damage is inflicted. We attempt to find the 'fate' of DnaB upon UV mediated DNA damage, as to whether it stays on, falls off the DNA or shows uncoupling with the other components of the replisome, upon such DNA damage conditions.

In chapter 4, we bring up our investigation on how we track the translesion polymerase DNA polymerase IV (Pol IV), from the undamaged state of the cell to the DNA damage one, with the objective of visualizing the transition in real-time and analyzing whether Pol IV behavior changes (as defined by its spatial distribution in the cellular long axis, with respect to the spatial distribution of the replisome, across time).

Finally, I summarize our research findings and discuss what our data may mean for the wider biological function and context. I also delve into the outlook for the future of such investigations and predict where we should be headed for.

References

1. Chatterjee, N. and Walker, G.C. (2017) Mechanisms of DNA damage, repair, and mutagenesis. *Environ Mol Mutagen*, **58**, 235-263.
2. Friedberg, E.C. (2003) DNA damage and repair. *Nature*, **421**, 436-440.
3. Kreuzer, K.N. (2013) DNA damage responses in prokaryotes: regulating gene expression, modulating growth patterns, and manipulating replication forks. *Cold Spring Harb Perspect Biol*, **5**, a012674.
4. Fuchs, R.P. and Fujii, S. (2013) Translesion DNA synthesis and mutagenesis in prokaryotes. *Cold Spring Harb Perspect Biol*, **5**, a012682.
5. Fijalkowska, I.J., Schaaper, R.M. and Jonczyk, P. (2012) DNA replication fidelity in *Escherichia coli*: a multi-DNA polymerase affair. *FEMS Microbiol Rev*, **36**, 1105-1121.
6. Denamur, E. and Matic, I. (2006) Evolution of mutation rates in bacteria. *Molecular microbiology*, **60**, 820-827.
7. Pope, C.F., O'Sullivan, D.M., McHugh, T.D. and Gillespie, S.H. (2008) A practical guide to measuring mutation rates in antibiotic resistance. *Antimicrob Agents Chemother*, **52**, 1209-1214.
8. Ragheb, M.N., Thomason, M.K., Hsu, C., Nugent, P., Gage, J., Samadpour, A.N., Kariisa, A., Merrikh, C.N., Miller, S.I., Sherman, D.R. *et al.* (2019) Inhibiting the Evolution of Antibiotic Resistance. *Mol Cell*, **73**, 157-165 e155.
9. Long, H., Miller, S.F., Strauss, C., Zhao, C., Cheng, L., Ye, Z., Griffin, K., Te, R., Lee, H., Chen, C.C. *et al.* (2016) Antibiotic treatment enhances the genome-wide mutation rate of target cells. *Proc Natl Acad Sci U S A*, **113**, E2498-2505.
10. Hofer, U. (2019) The cost of antimicrobial resistance. *Nat Rev Microbiol*, **17**, 3.
11. Cassini, A., Hogberg, L.D., Plachouras, D., Quattrocchi, A., Hoxha, A., Simonsen, G.S., Colomb-Cotinat, M., Kretzschmar, M.E., Devleesschauwer, B., Cecchini, M. *et al.* (2019) Attributable deaths and disability-adjusted life-years caused by infections with antibiotic-resistant bacteria in the EU and the European Economic Area in 2015: a population-level modelling analysis. *Lancet Infect Dis*, **19**, 56-66.
12. Chatterjee, A., Modarai, M., Naylor, N.R., Boyd, S.E., Atun, R., Barlow, J., Holmes, A.H., Johnson, A. and Robotham, J.V. (2018) Quantifying drivers of antibiotic resistance in humans: a systematic review. *Lancet Infect Dis*, **18**, e368-e378.
13. Peterson, E. and Kaur, P. (2018) Antibiotic Resistance Mechanisms in Bacteria: Relationships Between Resistance Determinants of Antibiotic Producers, Environmental Bacteria, and Clinical Pathogens. *Front Microbiol*, **9**, 2928.
14. Fuss, J.O. and Cooper, P.K. (2006) DNA repair: dynamic defenders against cancer and aging. *PLoS Biol*, **4**, e203.
15. Hoeijmakers, J.H. (2009) DNA damage, aging, and cancer. *N Engl J Med*, **361**, 1475-1485.
16. Sperka, T., Wang, J. and Rudolph, K.L. (2012) DNA damage checkpoints in stem cells, ageing and cancer. *Nat Rev Mol Cell Biol*, **13**, 579-590.
17. Fitzgerald, D.M., Hastings, P.J. and Rosenberg, S.M. (2017) Stress-Induced Mutagenesis: Implications in Cancer and Drug Resistance. *Annu Rev Cancer Biol*, **1**, 119-140.
18. Stylianidou, S., Brennan, C., Nissen, S.B., Kuwada, N.J. and Wiggins, P.A. (2016) SuperSegger: robust image segmentation, analysis and lineage tracking of bacterial cells. *Molecular microbiology*, **102**, 690-700.

19. Deich, J., Judd, E.M., McAdams, H.H. and Moerner, W.E. (2004) Visualization of the movement of single histidine kinase molecules in live *Caulobacter* cells. *Proc Natl Acad Sci U S A*, **101**, 15921-15926.
20. Watanabe, N. and Mitchison, T.J. (2002) Single-molecule speckle analysis of actin filament turnover in lamellipodia. *Science (New York, N.Y.)*, **295**, 1083-1086.
21. Ritchie, K., Lill, Y., Sood, C., Lee, H. and Zhang, S. (2013) Single-molecule imaging in live bacteria cells. *Philos Trans R Soc Lond B Biol Sci*, **368**, 20120355.
22. Ha, T. (2014) Single-molecule methods leap ahead. *Nat Methods*, **11**, 1015-1018.
23. Xie, X.S., Choi, P.J., Li, G.W., Lee, N.K. and Lia, G. (2008) Single-molecule approach to molecular biology in living bacterial cells. *Annu Rev Biophys*, **37**, 417-444.
24. Yu, J. (2016) Single-Molecule Studies in Live Cells. *Annu Rev Phys Chem*, **67**, 565-585.
25. Shashkova, S. and Leake, M.C. (2017) Single-molecule fluorescence microscopy review: shedding new light on old problems. *Biosci Rep*, **37**.
26. Beattie, T.R. and Reyes-Lamothe, R. (2015) A Replisome's journey through the bacterial chromosome. *Front Microbiol*, **6**, 562.
27. Beattie, T.R., Kapadia, N., Nicolas, E., Uphoff, S., Wollman, A.J., Leake, M.C. and Reyes-Lamothe, R. (2017) Frequent exchange of the DNA polymerase during bacterial chromosome replication. *Elife*, **6**.
28. van Oijen, A.M. and Loparo, J.J. (2010) Single-molecule studies of the replisome. *Annu Rev Biophys*, **39**, 429-448.
29. Kurth, I. and O'Donnell, M. (2013) New insights into replisome fluidity during chromosome replication. *Trends Biochem Sci*, **38**, 195-203.
30. Gefter, M.L., Hirota, Y., Kornberg, T., Wechsler, J.A. and Barnoux, C. (1971) Analysis of DNA polymerases II and 3 in mutants of *Escherichia coli* thermosensitive for DNA synthesis. *Proc Natl Acad Sci U S A*, **68**, 3150-3153.
31. McHenry, C. and Kornberg, A. (1977) DNA polymerase III holoenzyme of *Escherichia coli*. Purification and resolution into subunits. *J Biol Chem*, **252**, 6478-6484.
32. Reyes-Lamothe, R., Sherratt, D.J. and Leake, M.C. (2010) Stoichiometry and architecture of active DNA replication machinery in *Escherichia coli*. *Science (New York, N.Y.)*, **328**, 498-501.
33. McInerney, P., Johnson, A., Katz, F. and O'Donnell, M. (2007) Characterization of a triple DNA polymerase replisome. *Mol Cell*, **27**, 527-538.
34. Curti, E., McDonald, J.P., Mead, S. and Woodgate, R. (2009) DNA polymerase switching: effects on spontaneous mutagenesis in *Escherichia coli*. *Molecular microbiology*, **71**, 315-331.
35. Balakrishnan, L. and Bambara, R.A. (2013) Okazaki fragment metabolism. *Cold Spring Harb Perspect Biol*, **5**.
36. Bessman, M.J., Kornberg, A., Lehman, I.R. and Simms, E.S. (1956) Enzymic synthesis of deoxyribonucleic acid. *Biochim Biophys Acta*, **21**, 197-198.
37. Mangiameli, S.M., Merrikh, C.N., Wiggins, P.A. and Merrikh, H. (2017) Transcription leads to pervasive replisome instability in bacteria. *Elife*, **6**.
38. Bruning, J.G., Howard, J.L. and McGlynn, P. (2014) Accessory replicative helicases and the replication of protein-bound DNA. *J Mol Biol*, **426**, 3917-3928.
39. Boubakri, H., de Septenville, A.L., Viguera, E. and Michel, B. (2010) The helicases DinG, Rep and UvrD cooperate to promote replication across transcription units in vivo. *EMBO J*, **29**, 145-157.

40. Merrikh, H., Zhang, Y., Grossman, A.D. and Wang, J.D. (2012) Replication-transcription conflicts in bacteria. *Nat Rev Microbiol*, **10**, 449-458.
41. Hawkins, M., Dimude, J.U., Howard, J.A.L., Smith, A.J., Dillingham, M.S., Savery, N.J., Rudolph, C.J. and McGlynn, P. (2019) Direct removal of RNA polymerase barriers to replication by accessory replicative helicases. *Nucleic Acids Res*, **47**, 5100-5113.
42. Lohman, T.M., Tomko, E.J. and Wu, C.G. (2008) Non-hexameric DNA helicases and translocases: mechanisms and regulation. *Nat Rev Mol Cell Biol*, **9**, 391-401.
43. Epshtein, V., Kamarthapu, V., McGary, K., Svetlov, V., Ueberheide, B., Proshkin, S., Mironov, A. and Nudler, E. (2014) UvrD facilitates DNA repair by pulling RNA polymerase backwards. *Nature*, **505**, 372-377.
44. Kamarthapu, V. and Nudler, E. (2015) Rethinking transcription coupled DNA repair. *Curr Opin Microbiol*, **24**, 15-20.
45. Liu, X., Seet, J.X., Shi, Y. and Bianco, P.R. (2019) Rep and UvrD Antagonize One Another at Stalled Replication Forks and This Is Exacerbated by SSB. *ACS Omega*, **4**, 5180-5196.
46. Makurath, M.A., Whitley, K.D., Nguyen, B., Lohman, T.M. and Chemla, Y.R. (2019) Regulation of Rep helicase unwinding by an auto-inhibitory subdomain. *Nucleic Acids Res*, **47**, 2523-2532.
47. Syeda, A.H., Wollman, A.J.M., Hargreaves, A.L., Howard, J.A.L., Bruning, J.G., McGlynn, P. and Leake, M.C. (2019) Single-molecule live cell imaging of Rep reveals the dynamic interplay between an accessory replicative helicase and the replisome. *Nucleic Acids Res*.
48. Mahdi, A.A., Buckman, C., Harris, L. and Lloyd, R.G. (2006) Rep and PriA helicase activities prevent RecA from provoking unnecessary recombination during replication fork repair. *Genes Dev*, **20**, 2135-2147.
49. Courcelle, C.T., Landstrom, A.J., Anderson, B. and Courcelle, J. (2012) Cellular characterization of the primosome and rep helicase in processing and restoration of replication following arrest by UV-induced DNA damage in Escherichia coli. *J Bacteriol*, **194**, 3977-3986.
50. Epshtein, V. (2015) UvrD helicase: an old dog with a new trick: how one step backward leads to many steps forward. *Bioessays*, **37**, 12-19.
51. Goosen, N. and Moolenaar, G.F. (2008) Repair of UV damage in bacteria. *DNA Repair (Amst)*, **7**, 353-379.
52. Newton, K.N., Courcelle, C.T. and Courcelle, J. (2012) UvrD Participation in Nucleotide Excision Repair Is Required for the Recovery of DNA Synthesis following UV-Induced Damage in Escherichia coli. *J Nucleic Acids*, **2012**, 271453.
53. Kisker, C., Kuper, J. and Van Houten, B. (2013) Prokaryotic nucleotide excision repair. *Cold Spring Harb Perspect Biol*, **5**, a012591.
54. Garcia-Muse, T. and Aguilera, A. (2016) Transcription-replication conflicts: how they occur and how they are resolved. *Nat Rev Mol Cell Biol*, **17**, 553-563.
55. Guy, C.P., Atkinson, J., Gupta, M.K., Mahdi, A.A., Gwynn, E.J., Rudolph, C.J., Moon, P.B., van Knippenberg, I.C., Cadman, C.J., Dillingham, M.S. *et al.* (2009) Rep provides a second motor at the replisome to promote duplication of protein-bound DNA. *Mol Cell*, **36**, 654-666.
56. Atkinson, J., Gupta, M.K. and McGlynn, P. (2011) Interaction of Rep and DnaB on DNA. *Nucleic Acids Res*, **39**, 1351-1359.

57. Atkinson, J., Gupta, M.K., Rudolph, C.J., Bell, H., Lloyd, R.G. and McGlynn, P. (2011) Localization of an accessory helicase at the replisome is critical in sustaining efficient genome duplication. *Nucleic Acids Res*, **39**, 949-957.
58. Goodman, M.F. and Woodgate, R. (2013) Translesion DNA polymerases. *Cold Spring Harb Perspect Biol*, **5**, a010363.
59. Andersson, D.I., Koskiniemi, S. and Hughes, D. (2010) Biological roles of translesion synthesis DNA polymerases in eubacteria. *Molecular microbiology*, **77**, 540-548.
60. Henrikus, S.S., van Oijen, A.M. and Robinson, A. (2018) Specialised DNA polymerases in Escherichia coli: roles within multiple pathways. *Curr Genet*.
61. Bonner, C.A., Hays, S., McEntee, K. and Goodman, M.F. (1990) DNA polymerase II is encoded by the DNA damage-inducible dinA gene of Escherichia coli. *Proc Natl Acad Sci U S A*, **87**, 7663-7667.
62. Iwasaki, H., Nakata, A., Walker, G.C. and Shinagawa, H. (1990) The Escherichia coli polB gene, which encodes DNA polymerase II, is regulated by the SOS system. *J Bacteriol*, **172**, 6268-6273.
63. Dapa, T., Fleurier, S., Bredeche, M.F. and Matic, I. (2017) The SOS and RpoS Regulons Contribute to Bacterial Cell Robustness to Genotoxic Stress by Synergistically Regulating DNA Polymerase Pol II. *Genetics*, **206**, 1349-1360.
64. Frisch, R.L., Su, Y., Thornton, P.C., Gibson, J.L., Rosenberg, S.M. and Hastings, P.J. (2010) Separate DNA Pol II- and Pol IV-dependent pathways of stress-induced mutation during double-strand-break repair in Escherichia coli are controlled by RpoS. *J Bacteriol*, **192**, 4694-4700.
65. Wagner, J., Gruz, P., Kim, S.R., Yamada, M., Matsui, K., Fuchs, R.P. and Nohmi, T. (1999) The dinB gene encodes a novel E. coli DNA polymerase, DNA pol IV, involved in mutagenesis. *Mol Cell*, **4**, 281-286.
66. Kim, S.R., Matsui, K., Yamada, M., Gruz, P. and Nohmi, T. (2001) Roles of chromosomal and episomal dinB genes encoding DNA pol IV in targeted and untargeted mutagenesis in Escherichia coli. *Mol Genet Genomics*, **266**, 207-215.
67. Henrikus, S.S., Wood, E.A., McDonald, J.P., Cox, M.M., Woodgate, R., Goodman, M.F., van Oijen, A.M. and Robinson, A. (2018) DNA polymerase IV primarily operates outside of DNA replication forks in Escherichia coli. *Plos Genet*, **14**, e1007161.
68. Jarosz, D.F., Cohen, S.E., Delaney, J.C., Essigmann, J.M. and Walker, G.C. (2009) A DinB variant reveals diverse physiological consequences of incomplete TLS extension by a Y-family DNA polymerase. *Proc Natl Acad Sci U S A*, **106**, 21137-21142.
69. Scotland, M.K., Heltzel, J.M., Kath, J.E., Choi, J.S., Berdis, A.J., Loparo, J.J. and Sutton, M.D. (2015) A Genetic Selection for dinB Mutants Reveals an Interaction between DNA Polymerase IV and the Replicative Polymerase That Is Required for Translesion Synthesis. *Plos Genet*, **11**, e1005507.
70. Kuban, W., Banach-Orlowska, M., Bialoskorska, M., Lipowska, A., Schaaper, R.M., Jonczyk, P. and Fijalkowska, I.J. (2005) Mutator phenotype resulting from DNA polymerase IV overproduction in Escherichia coli: preferential mutagenesis on the lagging strand. *J Bacteriol*, **187**, 6862-6866.
71. Tang, M., Shen, X., Frank, E.G., O'Donnell, M., Woodgate, R. and Goodman, M.F. (1999) UmuD'(2)C is an error-prone DNA polymerase, Escherichia coli pol V. *Proc Natl Acad Sci U S A*, **96**, 8919-8924.
72. Krishna, S., Maslov, S. and Sneppen, K. (2007) UV-induced mutagenesis in Escherichia coli SOS response: a quantitative model. *PLoS Comput Biol*, **3**, e41.

73. Cox, M.M., Goodman, M.F., Kreuzer, K.N., Sherratt, D.J., Sandler, S.J. and Mariani, K.J. (2000) The importance of repairing stalled replication forks. *Nature*, **404**, 37-41.
74. Yeeles, J.T., Poli, J., Mariani, K.J. and Pasero, P. (2013) Rescuing stalled or damaged replication forks. *Cold Spring Harb Perspect Biol*, **5**, a012815.
75. Mirkin, E.V. and Mirkin, S.M. (2007) Replication fork stalling at natural impediments. *Microbiology and molecular biology reviews : MMBR*, **71**, 13-35.
76. Rastogi, R.P., Richa, Kumar, A., Tyagi, M.B. and Sinha, R.P. (2010) Molecular mechanisms of ultraviolet radiation-induced DNA damage and repair. *J Nucleic Acids*, **2010**, 592980.
77. Jarosz, D.F., Godoy, V.G., Delaney, J.C., Essigmann, J.M. and Walker, G.C. (2006) A single amino acid governs enhanced activity of DinB DNA polymerases on damaged templates. *Nature*, **439**, 225-228.

2

A review: Live cell imaging- Single molecule fluorescence microscopy (SMFM)

Live cell imaging enables real-time monitoring of cells. When coupled to Single Molecule Fluorescence Microscopy (SMFM), cellular behaviour can be also quantitated. Beginning with a conceptual introduction and a brief history of technical development, I describe different imaging modalities. I also describe the merits of studying live cells by single molecule imaging and how such studies have produced an upheaval in the field of bacterial cell biology. Subsequently, I consider the technical and biological considerations driving the choice of such imaging (live cell imaging-single molecule fluorescence microscopy) techniques. The chapter concludes by bringing up how the usage of these two techniques is suitable for our research, by reviewing how these single molecule imaging has led to recent progress of DNA replication and repair mechanisms particularly.

2.1 Introduction

The opportunity to see any phenomenon or mechanism unravel itself, is a profound and enriching experience, if one were to go by the adage “seeing is believing” (1). Imaging living cells is therefore, one of the direct ways to see and understand biology at work.

The history of observing life using microscopy, goes centuries back. Usage of light microscopy in biology of the modern era, arguably dates back to English natural philosopher, Robert Hooke (1635-1703) and his famous manuscript “Micrographia”. Unsurprisingly perhaps, he is also credited with coining the term “cell”. Hooke’s studies included specimens of fossils and insects, among other things (2).

Inspired by Hooke, the Dutch polymath in Delft, considered by some as a founder of microscopy, Antonie van Leeuwenhoek (1632-1723) pursued observations of ‘living animalcules’, with single-lens microscope (3). His studies spanned a wide variety of specimens from bacteria to spermatozoa, and were meticulously documented (3).

From these humble beginnings to ultra-modern and sophisticated microscopes in the hands of a modern biologist, as we know it now, we have come a long way across the centuries. Consisting of hundreds of mechanical and optical components, microscopes today mostly are computer controlled. Images are not plainly seen by eyes, but using sensitive detectors and advanced cameras, three dimensional pictures are projected on computer monitors. Candles have been replaced by lasers, even the mounting stage is electronically controlled and chemically engineered glass has replaced molten glass.

2.2 Fluorescence and ‘Molecular Flashlights’: The concept

In 1852, the term ‘fluorescence’ attributed to have been coined, by the physicist George Gabriel Stokes to describe a phenomenon associated with the mineral fluorite, which upon ultraviolet radiation, emits light in the visible spectrum (4). Thus, ‘fluorescence’ is the emission of light typically of longer wavelength, in a span of nanoseconds, following upon the absorption of light which is typically of shorter wavelength (5) (**figure 2.1**).

Quite naturally it follows that, using fluorescent proteins (FPs) as “molecular flashlights”, genes of interest can be tagged and the resulting fusion protein product may be followed in biological processes. Observing living cells, using this concept of fluorescence-based gene tagging, is at the heart of the ‘Live Cell Imaging’ process, which is described in further detail, under the sections 2.5., 2.8. and 2.9. In this thesis, we have used this principle (of fluorescence combined with live cell imaging) to monitor processes of DNA replication and repair, as described in the following chapters.

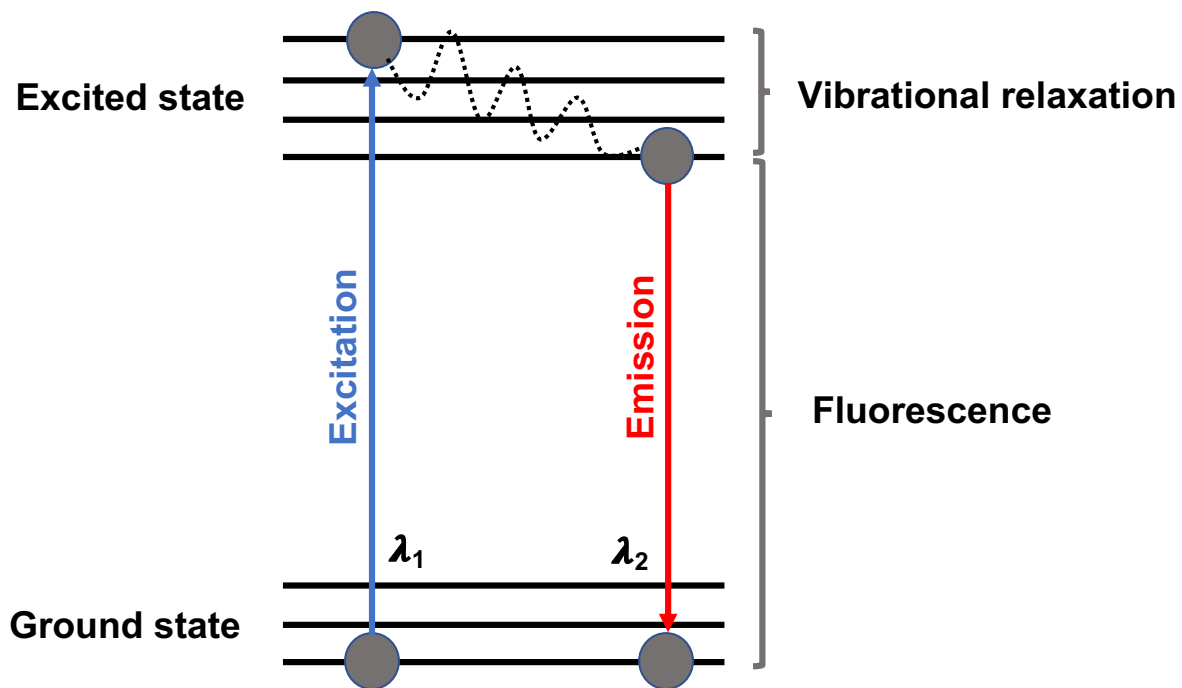


Figure 2.1 Fluorescence emission due to electron excitation. When excitation light is incident on the fluorescent molecules, the energy carried by photons is transferred to the fluorescent molecules. Consequently, this energy raises the electrons in the fluorescent molecules from the “Ground state” to the “Excited state”. Excited states (higher energy of electrons) tend to be relatively short-lived ones, as electrons will return to the ground state (lower energy of electrons), losing the excess energy in the form of non-radiative transitions (e.g. vibration relaxation, whereby the vibrational energy of excited fluorescent molecules is transferred to the neighbouring fluorescent molecules by direct interactions) or via radiative transitions (such as fluorescence), or both.

Additionally, named after George Stokes, the difference between the peaks of excitation and emission light or spectra, is referred as Stokes shift (**figure 2.2**). This key principle underpins the operation of a modern fluorescence microscope by the ability to illuminate specimen with light of a particular wavelength and filtering the return light, such that only the desired light of longer wavelength is seen or detected (5). The magnitude of the Stokes shift depends ‘considerably’ on the type of fluorescent protein used. With a larger shift or difference between the excitation and emission spectra, the filtering of return light is easier.

It is noteworthy, that not all fluorophores emit light of longer wavelength upon excitation. (A minority of ground state fluorophores exist in a ‘higher vibrational states’ (5), and consequently, the excitation-emission spectra may overlap) (5). As a corollary, the choice of fluorophores is particularly pertinent, when it comes to imaging a sample with multiple fluorophores.

The discovery of Green Fluorescent Protein (GFP) in *Aequorea victoria*, which came to be called as the “GFP revolution” later, has led to a paradigm shift in the field of cell biology through biological imaging (6-12). Fittingly, for this discovery, the researchers - Osamu Shimomura, Martin Chalfie, and Roger Tsien - were awarded the Nobel prize in Chemistry (2008). The impact and potential of this discovery can also be gauged by the fact that, blue, cyan, and yellow variants of GFP were engineered shortly afterwards (12-15). Further

discoveries of fluorescent proteins (FPs) were reported in Anthozoa species (coral reefs), which extended the “fluorescent protein rainbow” to red and other colors with the passage of time (16,17).

However, with these fascinating discoveries of reef-derived fluorescent proteins, came the realization of fluorophore

oligomerization in many of them (which could

lead to higher order complex aggregation after successful gene labeling) (6,18). ‘Heroic’ efforts entailed to engineer monomeric proteins, beginning with the red fluorescent protein (mRFP1) (19), and further extended to other colors, resulting in the “mFruits” family of monomeric fluorescent proteins (20,21).

In the past decade or so, there has been a rising tide of progress in generating bright monomeric FPs and now we have the luxury of carefully choosing an appropriate tag for a gene of interest, based on biological conditions and requirements (4,22-26).

The choice of fluorophores today is quite complex and daunting. As a class, FPs (DNA encoded) offer two distinct advantages over other fluorescent molecules or dyes (27). FPs can be tagged at the genome level (thus, being specific for the protein of interest) and they also circumvent the necessity for membrane permeability, may be required in the case of molecules or dyes. As of today, a vast of body of literature exists on FPs, which is only ever growing since the GFP revolution of the 1990s. The curious reader is directed here towards important references summarizing the research on FPs in recent years, which may be of potential interest to him or her (27-30).

In this thesis, we have harnessed the suitability of FPs for biological research questions, using live cell imaging.

2.3 Live cell imaging: A brief history of development

“Most cell biologists these days are also cinematographers. Making movies of the cells, tissues and embryos that we study under a microscope is a regular occurrence in the laboratory.” The above sentences, quoted verbatim for emphasis, form the opening lines of an essay by Stramer and Dunn, 2015 (31).

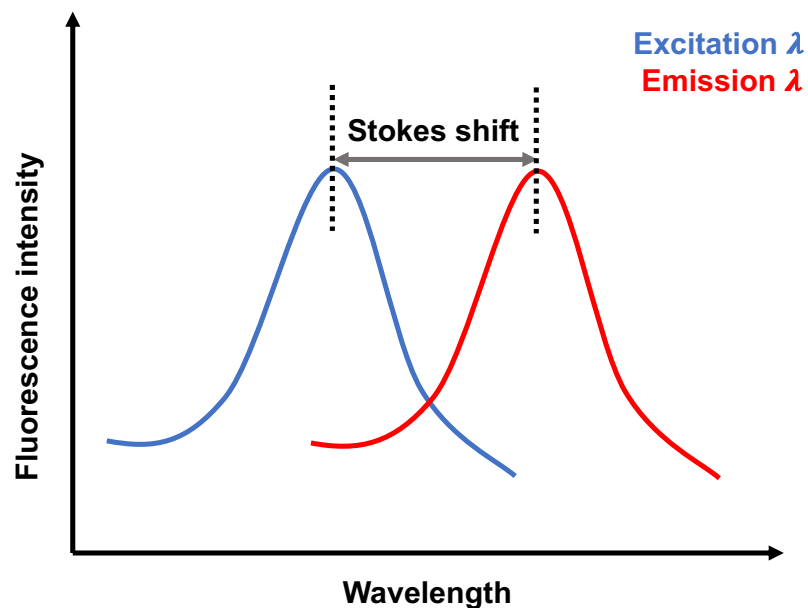


Figure 2.2 Stokes shift. Sketch of the excitation and emission spectra of a typical fluorescent molecule.

Fluorescence imaging is a powerful technique in its own right. Offering unparalleled and piercing insight into the dynamic cellular processes, it is when fluorescence imaging is combined with the ability to image in *real time* as cells grow and divide, through their lifetimes, that we draw our attention to the words 'cinemicroscopy' or 'cinematography' and what they mean and envisage.

Although with the important distinction wherein biological cells and conditions dictate the results, many aspects of laboratory microscopy in the modern era resonate with approaches of filming. We choose the microscope, lens and cameras for viewing and we play around with the 'lighting' of our actors- the cells.

The reader may find it interesting to note that 'the very first purpose' of motion picture photography was directed at experimentation, rather than entertainment and furthermore, some scientists claimed that "*motion picture 'originated' in the biological laboratory*" (31).

In 1872, Eadweard Muybridge used a series of cameras with automatic shutters, to observe the stages of horses trotting. Around the turn of the 20th century and with the advent of motion picture cameras, such cinematographers took up microscopic specimens for study. In 1891, Etienne Jules Marey filmed red blood cells traversing through a capillary. In 1903, the first microorganisms (cheese mites) were filmed. Julius Ries, France, 1907, then as a way of teaching 'cell theory' to medical students, made films on the fertilization and development of sea urchin eggs. Unsurprisingly, he thought he would provide 'moving, living evidence' to the skeptical students of the era, who would have found it hard to have the conviction that 'all cells came from other cells' (32). In 1909, Jean Comandon, considered as a pioneer of cinematography for scientific pursuits, filmed the syphilis microbe at Pasteur Institute, France. In 1913-14, Jean Comandon worked with his colleague Justin Jolly, to give lectures on films they captured about cell division (32). Comandon did a service by arguing that the steps of cell division were not arbitrary, rather followed a sequential continuity.

While filming as a technique was ready, it took some time for its adoption in the laboratory owing to the expense of cameras, film stock and most importantly, the ability to grow or 'culture' live cells (tissue culture was discovered around 1907) (31). The first commercially available 'microcinematic' apparatuses became available in Europe around 1914. The biological research community has not looked back ever since, with early cinematography on 'pinocytosis' (drinking by cells, literally) by the embryologist Warren H. Lewis in United States of America, 1931 and the seminal studies on cellular locomotion by Michael Abercrombie, in United Kingdom (1950s-1970s) (32-34). Ronald Canti, a London pathologist, was also an early adopter of filming and carried out studies on migration of different cell types, amongst other things (31).

Shortly after the advent of cell culture, scientists trained their sights (or film cameras) on mammalian cells as well. Alexis Carrel pioneered cinematography to investigate locomotion of fibroblasts and macrophages (35). Heinz Rosenberger, an assistant to Alexis Carrel, published a methods article in the journal *Science* (36), who presciently commented back in 1929, "*The greatest value of the motion picture as applied to science lies in its domination of time, for by its use it becomes possible to analyze thoroughly motions which are too fast or too slow to be perceived with the naked eye. Very rapid movements photographed with the slow-motion camera and very slow movements taken with the time lapse camera are translated into perceptible speeds.*"

Cinematography received further fillip with the invention of phase contrast in 1932 by the Dutch scientist Frits Zernike (32,37). Phase contrast allowed unprecedented details to cover, when combined with film camera and video technology later. During the 1950s, David Rogers of Vanderbilt University, USA, captured a video on 16 mm film of a neutrophil cell chasing a bacterium (38).

The entry of the confocal laser scanning microscope in biological research, as a prototype in 1986 in MRC laboratory, Cambridge UK, was no trivial achievement (39), after the invention of confocal microscope by Marvin Minsky in 1955 (40,41). A confocal microscope uses the resolving power of objective lenses, but twice, first by focusing light on a diffraction limited spot and then by detecting light through a “pin-hole” which already rejects out of focus light. Concomitant advances in laser technology had to be waited for, until the confocal laser scanning microscope was widely adopted.

While static techniques like X-ray crystallography and electron microscopy also gained popularity during the latter part of 20th century, the cloning of GFP in 1992 (see **section 2.2.**), made cinematography or live cell imaging, made it all but inevitable as a mainstream technique in biological research labs.

For an excellent general commentary on the chronological order of microscopy technology development and its impact on biology research, the interested reader may like to see Dunn and Jones, 2004 (40).

Finally, one cannot conclude this section, without at least a perfunctory mention of how versatile imaging today is, with many different modalities to choose from, ranging from multiphoton, total internal reflection fluorescence (TIRF), light sheet method to super resolution imaging (41-48). As in this thesis, we have not used some of these relatively recent techniques, I refrain from commenting deeply and pass over with a cursory mention. However, with section 2.5. and onwards, I provide rationale for choosing the appropriate imaging scheme, for addressing our biological questions, described in this thesis.

2.4 Single molecule fluorescence microscopy (SMFM): A brief history of development

In the preceding sections, I have introduced the principle of fluorescence as a ‘molecular flashlight’ and summarized a brief history of development of ‘live cell imaging’. In this section, I bring a third, and related concept- ‘single molecule imaging’ (49-51), which when used in conjunction with the other two concepts- fluorescence and live cell imaging, as in this thesis, allows one to perform ‘Single Molecule Fluorescence Microscopy’ in living cells and observing cellular processes in real time, with quantitative information.

Put in a simple language, single molecule imaging offers the ability to image singular molecules, if they exist so, in the biological state.

The first report, to my knowledge, on single molecule fluorescence microscopy, dates back to 1961 (52,53), wherein a method for measuring single beta-D-galactosidase enzyme molecules was described. The first ‘direct detection’ of immobilized single molecules by fluorescence microscopy (globulin molecules), which were labelled by an organic dye

fluorophore, was documented in 1976 (54,55). More than a decade later, in 1990, single molecules were detected in solution using laser beams at room temperature (55,56).

Literature also credits a seminal publication in 1989, towards laying ground for 'direct' single molecule imaging (51,57). At liquid helium temperature, single molecules of pentacene were observed in a solid p-terphenyl crystal. Using near field optics, single immobilized fluorescent dye molecules were also first observed in 1993 (58). While in 1996, the first wide field imaging report of single dye molecules in a lipid bilayer emerged (59).

Fascinating to note, while bacterial systems generally offer a simple model for initial discoveries, many early developments in single molecule imaging happened in mammalian cells (51). Apart from the clinical aspects of working with such cells, immortalized mammalian cells offered the ease of 'plating' and handling perhaps.

2.5 Live cell imaging modalities with *Single molecule fluorescence microscopy*: The common combinations

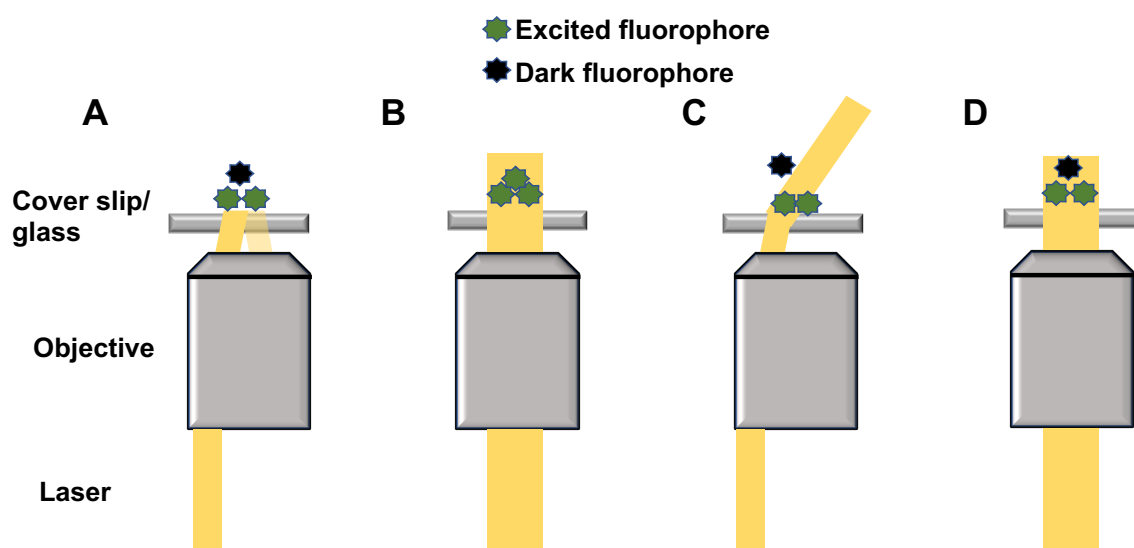


Figure 2.3 Live Cell Imaging modalities, common with Single Molecule Fluorescence Microscopy. Four different imaging modalities, shown here (confocal microscopy shown in Figure 2.5. separately): **A. Total Internal Reflection Microscopy (TIRF).** The light beam (yellow) is modulated such that the light is incident at the sample- cover slip/glass interface, at an angle for shallow penetration into the sample (~150 nm, Z axis) and only fluorophores in this limited Z plane are excited. **B. Wide-field Epifluorescence microscopy.** Without any light modulation, all fluorophores in the whole cell are excited. **C. Oblique Epi-fluorescence microscopy.** Similar to TIRF, the light is also modulated in this imaging scheme, but with a greater depth (> ~150 nm, Z axis) of fluorophore excitation, suited for visualizing non-surface processes of cells. **D. Localization microscopy.** Using spatial or temporal modulation of light (activation/ excitation), only a subset of fluorophores in a biological sample are excited.

Choosing the appropriate microscope system for single molecule fluorescence microscopy, with the express purpose of and in combination with live cell imaging, is not a trivial task and does require much deliberation and consultation. Each system offers some advantages, which are offset nevertheless by some drawbacks too, as this researcher finds (38,42,53,60,61).

By and large, light microscopy and its variants have been the workhorse of single molecule fluorescence microscopy for live cells (51). **Figures 2.3 and 2.5** shows some of the common SMFM imaging schemes (for live cell imaging).

A key facet of most microscopes, broadly speaking, is the role played by the objectives. The performance of the objective is much dependent on its magnification and **numerical aperture (NA)**. The objective magnification implies how large the image of the sample would be at the camera, relative to the actual size; 100X objective would provide a 100-fold enlargement on the sample. Mathematically, the NA is defined as the sine of the largest angle of the light emitted from the sample ($\sin\theta$), multiplied by the refractive index (n) of the sample. In the XY plane (plane which is perpendicular to the focus axis), the theoretical resolution limit is given by:

Resolution limit = $0.61\lambda / n\sin\theta$ (where λ is the wavelength of light)

The resolution limit of a conventional light microscope is ~250 nm in the X, Y axes and >450-700 nm in the Z axis. This limit, also called the **Point Spread Function (PSF)**, corresponds to the size of the spread of a single point source of light visible which is diffracted through the microscope. This spatial distance of ~250 nm sets the **diffraction limit** of the microscope in the XY plane, and no two PSFs are distinguishable as separate below this distance. **Super-resolution microscopy**, (see **section 2.5.d.**, on Localization microscopy for details) breaks this diffraction limit or barrier, by spatial or temporal modulation of light (activation/ excitation) (46).

Additionally, the correction of aberrations also play a role in good imaging, as the technical terms 'Achromat' and 'Plan Apochromat' imply manufacturer's guidelines should be consulted (42).

a) **Total Internal Reflection Microscopy (TIRF)**: Many single molecule studies, including *in vivo* research (42,53,62,63), have employed TIRF technique, wherein the illuminating laser is incident at the cover slip-aqueous media (above the cover slip) interface, at an angle such that an evanescent field is created at this interface (48).

This evanescent field is only a 'few hundred' nanometers into the sample. The advantage of this technique being that only fluorophores near the cover slip- media interface (few hundred nanometers) are illuminated. This method is particularly well suited to track biological processes at the vicinity of cell membranes, as it reduces or eliminates the problem of 'out-of-focus' fluorescence from background cytoplasm. Both mammalian and bacterial systems have been investigated by this technique (63). Figure 2.3.A shows a general TIRF imaging scheme.

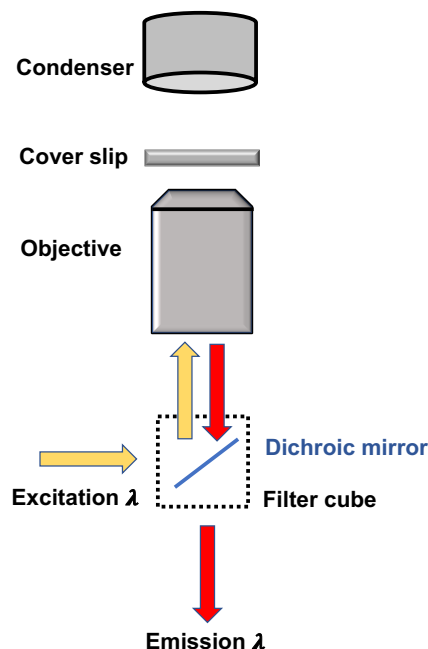


Figure 2.4. An inverted fluorescence microscope schematic. The dichroic mirror plays a central role in this design, filtering the excitation and emission wavelengths in the same light path. This mirror directs the excitation wavelength at, and collects the emission wavelength from, the objective.

b) **Wide-field epi-fluorescence microscopy:** By far, 'most' studies have been done in cell biology with this technique (42). An inverted fluorescence microscope has been the workhorse for live cell imaging. In the simplest design, cells are left open at the top, while imaging happens through a coverslip below those cells (but above the objective). While this design (cells left open at the top) may not be an exclusive feature for just this type of microscopy, in our research, this design has nevertheless played to our advantage when combined with widefield fluorescence (Further technical considerations in **section 2.8**). DNA damage drugs could seep onto the cells from the top (passing through the agarose pad), while images could be captured below, due to the inverted microscope design

In contrast to TIRF imaging, wherein the excitation light penetrates shallow into the sample and creates an evanescent field (~150 nm) (63), widefield imaging captures total fluorescence in a cellular volume (X, Y, Z axes). While this method may not be first choice for visualization of processes at the cell membrane *per se*, nevertheless the method does offer the overall versatility to image whole cells for long times (time lapse, at least 10-12 h in our case) with low phototoxicity and non-selective illumination. (**Figure 2.3.B.** shows the widefield operating scheme, while **figure 2.4.** shows a schematic on inverted fluorescence microscope used in this thesis research).

While the choice of TIRF surely is based on the research question at hand, it stands to reason that bacterial cells, owing to their small size and high curvature, typically 'preclude' the usage of TIRF 'due to their limited depth of illumination' (51). Epi-fluorescence therefore remains a preferred option for many laboratories.

c) **Oblique epi-fluorescence microscopy:** An alternative approach has been to use the TIRF beam such that the angle of incidence is altered to capture non-surface processes. Also referred as HILO (Highly Inclined Laminated Optical sheet) or 'Near TIRF', this usage of a 'high angle' renders it suitable for studies on both bacterial and mammalian cells (51,53). This technique comes with the added advantage of visualizing with 'greater depth' of non-surface processes (53) in a cell, when compared to TIRF (a schematic is represented by the **figure 2.3.C**).

d) **Localization microscopy:** Of late, the popularity of 'single molecule localization' or 'super resolution microscopy' has been burgeoning, in no modest way either, after the 2014 Nobel prize in chemistry, in recognition to its proponents (Eric Betzig, Stefan W. Hell and William E. Moerner). Both eukaryotic and prokaryotic research have benefited from these approaches, which emanate from the superior ability of some fluorophores to be activated or re-activated by laser (one of the other methods, Stimulated Emission Depletion **STED**, relies much on the hardware). These probes are imaged until bleached, followed by another round of probe activation and imaging until bleached. The final image can be reconstructed by sophisticated algorithms, with the advantage of localizing the center or source of the fluorescent probe. Stochastic reconstruction microscopy (STORM), photoactivated

localization microscopy (PALM) and fluorescence PALM have been widely adopted methods (64-66). (**Figure 2.3.D** shows the general operating scheme of these localization techniques).

e) **Confocal laser scanning microscopy:** Conceptually, this method involves moving the sample, by moving the stage (as conceived by Marvin Minsky, see **section 2.3.**) or by laser line scanning nowadays. Confocal microscopy is known to significantly improve signal to noise ratio, by filtering out of focus light due to the usage of two pin-holes, one for excitation light and the other for emission light. (**Figure 2.5** demonstrates the principle underlying confocal imaging).

Most studies use one or more of these modalities which investigate biological processes by the *combination* of single molecule fluorescence microscopy and live cell imaging. This includes ingenious examples like the relatively recent milestones of **single molecule Forster Resonance Energy Transfer (smFRET)** in live cells (67) using one or more of these above systems or usage of confocal microscopy for single molecule and super resolution imaging (68).

There are still other promising microscopy approaches, apart from the widely recognized ones mentioned above, with capability to harness single molecule sensitivity with live cell imaging, as in **Selective Plane Illumination Microscopy (SPIM)** (69-71) and light sheet approaches (43), wherein the sample is illuminated from one side with a thin sheet of light and fluorescence collected in the orthogonal direction.

For a deeper understanding on the timeline of development of these imaging techniques, the interested reader is diverted towards an insightful review on single molecule microscopy, especially from the vantage point of live cell imaging (71).

Adapted and summarized from the same reference (71), is a brief and selective overview (**Table 2.1**) for comparison for some of these techniques and also a brief timeline of technical developments leading to single molecule imaging (**figure 2.6**). The enlightened reader may

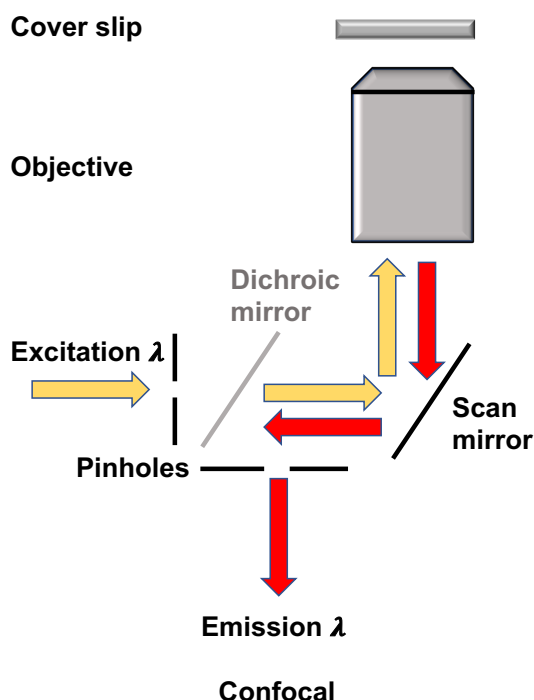


Figure 2.5. Live Cell Imaging modality, common with Single Molecule Fluorescence Microscopy: Confocal microscopy. The two pinholes, one for excitation wavelength and the other for emission wavelength, reduce out-of-focus background fluorescence, and thereby improve the signal to noise ratio. Dichroic mirror filters excitation and emission wavelengths in the same light path, while the scan mirror facilitates specimen excitation in horizontal and vertical directions.

also find a 2017 review quite informative on the latest developments and challenges facing the field (44).

Technique	Spatial resolution	Time resolution	Phototoxicity	Measurable properties	Cellular position	Compatible labels
TIRF	200–250 nm	5 ms	Low	Position and movement	Cover slip interface	FPs, organic dyes
Wide-field (Epi-fluorescence)	200–250 nm	5 ms	Medium	Position and movement	Whole	FPs, organic dyes, Q-dots, colloidal particles
Super resolution	20 nm	~100 ms	High	Position	5–10 μ m from the cell surface	Organic dyes, FPs, PA-FP, PC-FP
Photo-activation/ photo - conversion	200–250 nm	~1 s	High	Position and movement	Whole	PA-FP, PC-FP, tetracycline
SPIM	200–250 nm	5 ms	Low	Position and movement	Whole	FPs, organic dyes
smFRET	200–250 nm (Donor–acceptor 1–10 nm)	~100 ms	Low	Position, movement and conformation	Whole	Donor– acceptor fluorophores

Table 2.1 A comparison of some of the Single Molecule Fluorescence Microscopy techniques, which are also compatible with Live Cell Imaging.

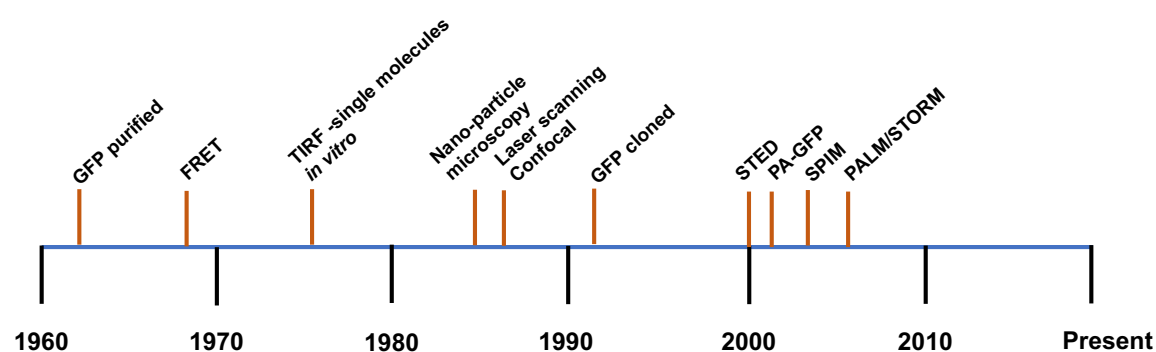


Figure 2.6 A timeline of developments leading to single molecule imaging techniques. Partly adapted from reference (71).

2.6 Why single molecule fluorescence imaging in live cells?

The preceding sections of **2.2.** and **2.3.**, perhaps make it abundantly clear that fluorescence imaging since 1990s (referring to the GFP revolution) and live cell imaging since the past few decades have been around and have gained acceptance with researchers. Indeed, with credit to decades of painstaking research of numerous laboratories using fluorescence microscopy and live cell imaging, we stand at a threshold where we are just beginning to understand how cells (prokaryotes and eukaryotes) function. However, the depth of our understanding of fundamental cellular processes is anything but closer to complete and comprehensive.

One of the major reasons for this, has been that our understanding so far comes from experimental data of the 'ensemble average' nature, drawn from population level observations (53). A critical aspect of laboratory cell cultures, is that this bulk population may contain cells of wide genetic and phenotypic variation, stemming from different physical, chemical and biological properties. This '**cell to cell heterogeneity**' (53,72), which plays a significant role in evolution of strains over a time course, by promoting survival opportunities in severe conditions through different cellular properties in a population, also means that such heterogenous behaviour may get masked or may go unnoticed as 'noise', if one were to consider the population level signature as the only metric to study. This (so called) 'noise' may harbour interesting information on how such heterogeneity at the individual cell level, may give rise eventually to cellular adaptability under severe environmental conditions or DNA damage, and higher order organization towards population growth and maintenance (e.g., bacterial colony formation) under stress conditions, amongst other crucial information towards our holistic understanding of fundamental processes.

Furthermore, as an example, ensemble studies 'will not pinpoint' the antibiotic or DNA damage drug resistant bacterial cells in a general cellular population, albeit perhaps with great difficulty, just confirm the presence of such cells somewhere in the culture (53). This pinpointing has great applications for translational research in the future, when one thinks of modern phenomena like antibiotic resistance in bacteria or drug resistance in cancer cells for multicellular organisms.

Even within a unicellular organism, there is great variance and can be thought of a 'heterogenous system at the molecular level' (53,73,74). This is because a cell, can exhibit heterogenous behaviour dependent on state of cell cycle (G1, S, G2, M) or growth phase (lagging, exponential and stationary), talking of just one parameter (cell cycle/ growth phase) influencing unicellular behaviour, amongst others like nutrition or environmental stress (53,75). This '**molecular heterogeneity**' alone, apart from cell to cell heterogeneity which is also important unquestionably, makes for the most convincing case towards using single-molecule studies for biological investigations.

Single molecule biophysics research holds the key, without overstating, to understanding cell behaviour in all its complexities and aspects, when complemented with population level studies. In the course of studying this thesis, the reader will find illustrative examples of molecular heterogeneity, as the same protein forms punctate structures called 'foci', during certain times of the cell lifetime, while at other times remaining in the diffusive cytoplasmic

pool. Such molecular heterogeneity may functionally mean different roles for the same protein, depending on the biological context.

Indeed, tracking a single biomolecule of interest in living cells, with ‘millisecond time resolution and nanometer spatial precision’, would be an ideal scenario (76). This would unravel all sorts of information on the specific biomolecule, ranging from its kinetics to its dynamics, all the while being in physiological growing conditions.

In summary, the advantages of single molecule imaging in live cells can be noted, as shown below:

- **Copy number:** Not all biomolecules are present in high copy, for some which are present in low copies (for example in the latter case, certain DNA polymerases and transcription factors), ‘single molecule sensitivity in single cells’ is necessitated (76).
- **Stochasticity:** Biological factors which are present in low copy and participate in cellular mechanisms (for example DNA replication or repair), often exhibit stochastic reaction events. In layman terms, this would mean that a particular feature (e.g., time trace of a biomolecule) ‘may not be reproducible’ and consequently, unable to be synchronized with that of a neighbouring cell, even though ‘statistical properties’ are reproducible (76).
- **Steady state biochemical reactions:** Often biochemical reactions (for example, many enzymatic reactions during replication, transcription or translation) occur inside a cell with the help of constant supply of free energy and substrates, as nonequilibrium steady state reactions. However, in stark contrast, conventional ensemble kinetic studies (e.g., stop flow experiments), occur under nonequilibrium non-steady state, wherein the concentrations of reaction constituents vary with time. Single molecule experiments (*in vivo*, as in this thesis) ‘usually occur’ in nonequilibrium steady state conditions (76).
- **Holistic complexity:** As opposed to the orthodox reductionist approach wherein individual biochemical reactions are studied in isolation, live cell experiments with single molecule sensitivity provide the opportunity to probe details in real-time and in physiological conditions.

Although population level studies would never be redundant in the future, as we inch ever and ever closer to systems biology, single molecule studies would complement population studies by probing biomolecules at greater detail.

2.7 Single molecule fluorescence imaging pioneering research in live bacteria

If the guiding rationale is that, a cell is more than just a bag of chemicals or a test tube with reaction mixtures, it does argue for experimentation with living cells to capture all kinetics and

dynamics, including their exquisite spatio-temporal regulation. This then, further goads us to consider the easiest or simplest way to do so.

Inevitably, our thought veers towards the simple unicellular organisms like *Escherichia coli* as an experimental model for fundamental research purposes. This idea of using *E.coli* is further attractive due to the wide availability of background literature and information databases.

As per the understanding of this researcher, in 2000, one of the first 'definitive' single molecule investigation was performed in a living sample Sako *et al.*, (74) wherein the authors investigated fluorescently labelled epidermal growth factor ligands (A431 carcinoma cells) using Total Internal Reflection Microscopy (**TIRF**) (77). Also in 2000, Byassee *et al.*, studied fluorescently labelled transferrin molecules (HeLa cells) undergoing endocytosis using confocal microscopy (78).

This was followed by a flurry of exciting research in live cell single molecule imaging (73,74), which led to remarkable strides of progress, enhancing our understanding of how functional molecular complexes operate inside cells (79,80). Research on molecular complexes which operate in gene expression, or as components of molecular motors and in DNA replication, to name just a few prominent cell biology sub-disciplines, were trailblazing. Below, I highlight here some of the pioneering studies in this regard, interestingly but not surprisingly, which all have employed bacteria, mostly *E.coli*, as the experimental workhorse.

- **Measuring gene expression:** A seminal study in 2006 conducted by the research group of X. Sunney Xie, Harvard University, shed new light on the central dogma of molecular biology (DNA to RNA to proteins, the conventional order of biological information flow). In the study using an epifluorescence microscope, the authors fluorescently tagged the membrane protein Tsr with yellow fluorescent protein (YFP) variant called Venus, and put it under the regulation of endogenous (genome) *lac* promoter to observe gene expression burst in *E.coli* (81). They observed the real-time production of single protein molecules, to discover that protein molecules are produced in bursts, wherein each burst originated from a 'stochastically transcribed' single mRNA molecule.
- **Transcription factor dynamics:** Also performed in the Xie laboratory but in 2007, the authors brought up quantitative information on a *lac* repressor in *E.coli* (fluorescently labelled gene by Venus in the chromosome), specifically on the kinetics and dissociation of the repressor upon metabolic signals (82). They further characterized the non-specific binding, 1-D diffusion and 3-D translocation of the repressor, during its search for the operator sequences in live cells with single molecule sensitivity.
- **Counting components of molecular motors:** Another ground-breaking single molecule imaging research in live cells, was conducted using *E.coli* in 2006 as well, shedding light on the functionality of bacterial flagellar motor complexes (83). They investigated the stoichiometry, turnover and dynamics of MotB, a motor constituent labelled with GFP, in live cells with single molecule precision. By tethering a live *E.coli* cell on a cover slip and using TIRF, the researchers laid bare fine details of MotB operation.

- **Architecture of DNA replication machinery:** In 2010, the research group of David Sherratt in Oxford University in collaboration with Mark Leake, York University, UK, published results on the 'stoichiometry and architecture' of replisomes in *E.coli* (84). A major finding reported therein was the presence of three molecules of the replicative polymerase in an active replisome, challenging the hitherto accepted view of two such polymerases.

Apart from the above-mentioned pioneering studies, this field has been shaped by other noteworthy studies as well - the stoichiometry and turnover of bacterial (*E.coli*) switch protein FliM (85), stoichiometry of ion channels (86), counting and tracking of molecular machines involved in protein translocation (Tat system in *E.coli*) (87), ATP generation in *E.coli*, by way of oxidative phosphorylation (88,89),

The above studies although have been performed in a simple prokaryotic system like *E.coli*, carry much significance even for higher systems (82). Over the years, there have been many wide encompassing reviews by the leading experts of the live cell single molecule imaging field. The interested reader is directed here towards some of them (51,53,61,71,74,76,79,90,91).

2.8 A technical perspective: Why the combination of Live Cell Imaging- (Wide-field Epi-fluorescence) with single molecule fluorescence microscopy?

As described above in **section 2.5.**, the modern biologist has a wide repertoire of tools and techniques available for cell biology imaging. While this is an advantage surely, the decision to choose any particular technique rests on a multitude of factors in general.

Of these factors, some **general ones** are enumerated:

- Ease of instrumentation and software operation
- Affordability and maintenance of the instrumentation and software
- Sample preparation feasibility
- Availability of fluorophores commercially
- Of course, the suitability towards biological investigation

Apart from these general factors mentioned, for weighing on a decision to choose an imaging scheme, in theory, epi-fluorescence illumination, 'suffices' to see single molecules (71), if the copy number (protein expression level) of biological factor is low, the molecules are not moving very fast and the tagging is specific with an analyzable signal to noise ratio. However, in practice, one does encounter issues like auto-fluorescence of the cell, transient high molecule density (especially relevant for proteins which get upregulated during a biological pathway or mechanism) and quenching of fluorescent tag signal over time.

In section **2.8.1.**, I first discuss the potential advantages of Live cell imaging. Next, in section **2.8.2.**, I discussion the technical challenges and advantages of Wide-field epi-fluorescence microscopy, with objective towards achieving single molecule sensitivity.

2.8.1 Live cell Imaging

Considering that Live Cell Imaging has always been an attractive option for tracking real time processes since many decades, as its exciting history shows (**see section 2.3.**), I also list out some of its direct advantages for the ease of the reader:

- Foremost, the ability to track cells and processes in real-time, as they happen.
- Scientific observations stem from physiological conditions (*in vivo*), unlike the reductionist approach of *in vitro* conditions.
- The ability to observe the full cell cycle and beyond, due to long time lapse imaging, especially for studies wherein the cell division is delayed (e.g., filamentation due to DNA damage).
- As a derivative of the above point, when combined with fluorescence microscopy, the ability to observe specific proteins which are active only during certain times of the cell cycle, but remain localized elsewhere or diffused in the cytoplasm at other times, to understand the dynamics.

For live cell imaging to be of potential use, one has to pair this imaging technique with a fluorescence imaging option (see **section 2.5.**), in which at the very least, reaping the benefits of Live Cell Imaging, is not troublesome due to the pairing.

2.8.2 Single Molecule Fluorescence Microscopy (SMFM)

Wide-field epifluorescence comes as a first option, to the best understanding of this researcher, which could be paired with Live Cell Imaging, for Single Molecule Fluorescence Microscopy (SMFM). This is because some of the following **specific advantages** of wide-field epifluorescence in gathering single molecule fluorescence, when combined with live cell imaging:

- Whole cell imaging and not just a shallow region of focus, like TIRF. This may be an advantage, perhaps pertinent mostly to bacterial studies.
- Ease of handling: One of the most straightforward methods to visualize for a biologist, without prior knowledge of sophisticated software, as may be required for some of the advanced techniques for post capture reconstruction of super-resolution images.
- Lower phototoxicity of general FPs, as compared to photoactivable or photoconvertible FP variants, many of which require far-UV 405 nm for activation. While phototoxicity depends largely on the power of laser used (also exposure times), and can be minimized by tuning down the laser, the ideal situation would still be to avoid any UV light keeping in mind direct and indirect methods of DNA damage (see **section 1.5.**).
- Ability for long time lapse imaging in hours.

Alongside the specific advantages, the potential drawbacks (see below) of epi-fluorescence microscopy can be thoughtfully circumvented as well, for example with decisions, such as the following:

- **Auto-fluorescence: How to circumvent it?**
 - a. By choice of alternative fluorophores (DNA encoded), which emit light of different wavelength.

- b. By designing control experiments and analyses tools, which delineate signal from noise.
- **High molecule density: How to circumvent it (when it is a problem)?**
 - a. By choice of minimal media, a consequent advantage has been the ability of restricted growth and thus following processes with ease and efficiency.
 - b. By defining analyses algorithms to consider or restrict certain biological properties, such as punctate structures or foci, rather the whole cell fluorescence.
 - c. One may consider using localization microscopy (e.g., PALM) to complement epifluorescence microscopy, in such situations, to probe protein details with greater ease.
- **Signal quenching: How to circumvent it?**
 - a. By tuning down laser power and reducing fluorescence signal frame capture interval.
 - b. By choosing superior quality fluorophores with higher brightness and quantum yield.

2.9 A biological perspective: Why the combination of Live Cell Imaging- (Wide-field Epi-fluorescence) with single molecule fluorescence microscopy?

From the time of discovery of the DNA structure in 1953, passing through the Human Genome Project and to the present era of personalized medicine (92-96), the humble *Escherichia coli* has contributed to seminal discoveries in the DNA replication and repair, beginning with discoveries of the first DNA polymerase (97-99) and Okazaki fragment intermediates (100,101).

We, as a scientific community, stand at crossroads wherein we understand ever more about genome replication and repair (102-105), yet the specific details of dynamics and kinetics about these processes, elude us, and to put it euphemistically, have only begun to unravel and yield (84,106,107).

In this thesis thus, I have harnessed the combined power of Live Cell Imaging and SMFM to ask and address such questions in DNA replication and repair. In Chapter 3, I and my team have delved on what happens to the bacterial replicative helicase in the immediate aftermath of DNA damage. In chapter 4, we have investigated the behavior of a bacterial translesion DNA polymerase (Polymerase IV) during the onset and prevalence of DNA damage.

With the combined usage of both techniques, we have benefitted in probing the replicative helicase DnaB (*E.coli*), which has been subject to extensive debate and discussion on its 'fate', in the aftermath of DNA damage. With real time tracking for minutes and single molecule sensitivity alongside (with respect to the replisome), we have attempted to gain insights into biological processes which are not just dynamic (for example, protein stoichiometry which may change), but may also be dependent on time and recovery post DNA damage.

Similarly, we have been able to track how Pol IV appears in the undamaged state (in the beginning of the experiment) and later transitions into complex formation (foci) in response to DNA damage. Without the dual usage of these two imaging techniques, one would not have been able to gauge on how long Pol IV takes to respond from the undamaged state to DNA damage. Conventionally, Pol IV has been thought to be a late participant in DNA damage (error prone pathways of DNA repair and tolerance) and has presence and stoichiometry, in the diffusive cytoplasm (mobile population) as well as in agglomerated foci (immobile population). Even accounting for the fact that the usage of growth media (rich or minimal) may have a bearing on the timelines of Pol IV response (which can be rationally assumed to be quicker or slower depending on the media), this study has been the first to track Pol IV for close to 10 hours.

Not all biological molecules or factors however, exist as 'single molecules' in the literal sense, as they may function by being part of a macromolecular assembly or complex (foci). Sometimes, these molecules may even be fleetingly diffuse or be apparently moving at random, in the cytosol of the cell, existing as single molecules at a timepoint and as a complex, in the next. Thus, a technique (in this case SMFM) is only as useful, as the biological mechanisms allow it to be.

In the case of chapter 3, we (apart from others) show that the replicative helicase DnaB, a hexameric helicase, may show a stoichiometry of 6 and 12 molecules when DNA bound. In the case of chapter 4, Polymerase IV builds up as foci in response to DNA damage (observations from other groups included). So, with Live Cell Imaging allied with SMFM, we can observe DNA-bound biological proteins that appear in the microscope as stable foci. However, with the fundamental concept of fluorophore calibration, as reported in the first single molecule imaging study for an *in vivo* bacterial model (108), I and my team have used this principle as a basis for single molecule 'sensitivity' towards multimolecular and complex biological interactions. What this translates into in layman's terms is that we have had the ability to see biological processes as close to the *in vivo* scenario, as a real time experiment would allow us. Fluorophore calibration informs us about the fluorescence intensity from one fluorophore molecule, in theory and thus the single molecule sensitivity of our studies.

2.10 Finding the right scheme for imaging: DNA replication and repair mechanisms

As the following chapters in the thesis demonstrate, my research has delved on DNA replication and repair mechanisms. As a corollary, the first criterion has been to choose a technique, thus cinematography or live cell imaging, which can monitor processes in real time and for more than a few minutes. This is because, firstly, genome replication is not a process of short time order (average doubling time *Escherichia coli* in Luria Bertani broth is ~20 min) (109), which may get further elongated (>100 min), if a minimal media like M9-glycerol is chosen for low background fluorescence.

Secondly, the replicative processes may even come to a halt, and therefore more time required for monitoring biological markers, if the replication fork is stalled or blocked due to DNA damage. Furthermore, depending on the biological factors under investigation, some are reported to be first-line responders to DNA damage (error free pathways), while others act with a time-delay (error prone pathways). In our case, the reliance on live cell imaging has

been quite indispensable, as we have also constantly and concomitantly tried to compare and contrast the biological factor of interest, with a proxy for replisome position. Such phenomena are described in detail in the chapter 4.

Since different proteins or protein complex may have different turnover times (stability), it is only natural that the safest bet would have been to monitor processes real time for time dependent processes. Therefore, live cell imaging has been a choice, marked by prudence. While probing for biological details in real-time as well as for long duration has its inherent advantages for DNA replication and repair studies, the advent of single molecule fluorescence imaging in bacteria over the past two decades or so, has enhanced our depth of understanding and provides quantitative information with 'molecular resolution' for real-time observations, when in used in combination (110).

The field of DNA replication is undergoing a revolution, without overemphasizing, through single molecule studies in general and imaging in particular. The discovery of how unstable the replisome components are inherently while synthesizing DNA has been a discovery thanks to such techniques (110). Using single molecule-based fluorescence recovery after photobleaching (**FRAP**) in live *E. coli*, the research revealed the respective DNA bound times of individual replisome components (111).

A different laboratory provided further evidence on the instability of replisome components in *E. coli* (including *Bacillus subtilis*), with research focused on understanding bacterial transcription (112). Employing single molecule fluorescence microscopy and fluorophore photobleaching, they reported on how the 'replicative helicase complexes' are 'short-lived'. Furthermore, a recent report on *B. subtilis*, using photobleaching and single particle tracking has described the organization and dynamics of replicative polymerase PolC in live cells (113). Combining *in vitro* and *in vivo* approaches, a recent study further 'visualized' polymerase turnover and dynamicity at the *E. coli* replisome, using rolling circle DNA assays and single molecule FRAP (114).

While single molecule fluorescence microscopy has already unearthed details on the *E. coli* replisome core components (84,115), single molecule visualization has come quite recently to the accessory components of the replisome as well. Rep accessory helicase, believed to be critical for removing nucleoprotein barriers for the progressive replisome, has been found to have a hexameric stoichiometry, when it associates with 70% of the replication forks and an average dwell time of 6.5 ms (116). The study was conducted with slim field microscopy and genomically encoded fluorescent proteins.

Translesion DNA polymerases of *E. coli* have also been put under the spotlight through single molecule visualization in recent years. Two reports published at almost the same time from different laboratories, using photoactivated localization microscopy (PALM) and wide-field microscopy, have brought up various details- the kinetics of Pol IV molecules by single particle tracking, spatial distribution of Pol IV population before and after DNA damage, Pol IV colocalization with the replisome, to name a few observations (117,118). An invigorated discussion rages as to why these studies find Pol IV not always at the replisome, amidst different hypotheses (119). Additionally, the accessory helicase Rep, aforementioned, has also been evidenced to associate with Pol IV, thereby raising more exciting questions, as comes from another study harnessing sensitivity of single molecule imaging (120).

To put in broad perspective, single molecule fluorescence microscopy has yielded insights on not just replication *per se*, but it has also led us to realize how DNA replication and DNA repair are intimately connected and understanding in pursuit of one leads to another (110).

Providing mechanistic insight into this DNA replication- repair connection and by tracking MutS single molecules, a study has shown how live *B. subtilis* cells carry out DNA mismatch repair (**MMR**), a highly conserved pathway wherein replication errors which have evaded DNA polymerase proofreading, are corrected (121). MutS foci were found to colocalize with the replisome, the latter fluorescently marked by β -clamp or the clamp loader protein DnaX, and were further found to be unperturbed after treatment for DNA mismatch formation by 2-aminopurine (2-AP). With the power of single molecule imaging, the ability to see 'transient dwelling events' after DNA damage has come to the fore (110).

Other mutagens have been explored as well, notably the adaptive response towards alkylation (methyl methanesulfonate **MMS**), using single molecule counting and single cells of *E. coli* (122). The dynamics of the DNA repair protein Ada has been cast in new light upon DNA damage by this study.

Using the same DNA damage agent **MMS**, another study has probed one of the major repair pathways- Base Excision Repair (**BER**) in live *E. coli* (123). Using photoactivation, localization and tracking for DNA polymerase I and DNA ligase, we have come to learn from their research, how these molecules may search for DNA gaps or nicks and carry out the transient reactions.

A single molecule imaging live cell investigation in *E. coli* has also probed Nucleotide Excision Repair (**NER**) pathway involved in UV mediated DNA damage and repair (124). Using PA-mCherry tagging for the pathway components UvrA and UvrB through photoactivated localization microscopy (PALM) and single particle tracking, they have characterized how UvrA scans the genome for damage and recruits UvrB at lesions.

The 'master regulator' of the DNA damage SOS response in *E. coli*, has also been now put under single molecule fluorescence imaging, unraveling newer details of its localization before and after DNA damage (125). Using RecA-GFP, the article comments on the RecA aggregates (foci, bundles) forming inside cells.

As opposed to individual players and pathways of DNA repair in bacteria, another recent study has elucidated on 'bacterial DNA repair centres' in *B. subtilis* (126). Reporting via single particle tracking for RecN, RecO and RecJ, the authors have described how these repair centres 'arise' and how double strand breaks may be detected and processed.

For the reader who is enthused to know more about how single molecule fluorescence microscopy in combination with live cell imaging is impacting DNA replication and repair, exhaustive reviews have covered wide spanning research (63,110,127,128).

2.11 Coda

Understanding biology has been the overarching goal, albeit however modest, of this thesis and therefore all techniques and methods have been used to primarily serve towards that goal. With Live Cell Imaging, we have been able to peek into processes which are dynamic in

real time, while with Single Molecule Fluorescence Microscopy (SMFM) we have tried to gauge those very processes quantitatively. There are limitations to our approach as described above, but our endeavors described in the forthcoming chapters, has been rewarding and fulfilling to me.

References

1. McGeown, J.G. (2010) Seeing is believing! Imaging Ca²⁺-signalling events in living cells. *Exp Physiol*, **95**, 1049-1060.
2. Vangindertael, J., Camacho, R., Sempels, W., Mizuno, H., Dedeker, P. and Janssen, K.P.F. (2018) An introduction to optical super-resolution microscopy for the adventurous biologist. *Methods Appl Fluoresc*, **6**, 022003.
3. Ford, B.J. (1981) Leeuwenhoek's specimens discovered after 307 years. *Nature*, **292**, 407.
4. Sample, V., Newman, R.H. and Zhang, J. (2009) The structure and function of fluorescent proteins. *Chem Soc Rev*, **38**, 2852-2864.
5. Lichtman, J.W. and Conchello, J.A. (2005) Fluorescence microscopy. *Nat Methods*, **2**, 910-919.
6. Remington, S.J. (2011) Green fluorescent protein: a perspective. *Protein Sci*, **20**, 1509-1519.
7. Chalfie, M., Tu, Y., Euskirchen, G., Ward, W.W. and Prasher, D.C. (1994) Green fluorescent protein as a marker for gene expression. *Science (New York, N.Y.)*, **263**, 802-805.
8. Tsien, R.Y. (1998) The green fluorescent protein. *Annu Rev Biochem*, **67**, 509-544.
9. Shimomura, O., Johnson, F.H. and Saiga, Y. (1962) Extraction, purification and properties of aequorin, a bioluminescent protein from the luminous hydromedusan, *Aequorea*. *J Cell Comp Physiol*, **59**, 223-239.
10. Prasher, D.C., Eckenrode, V.K., Ward, W.W., Prendergast, F.G. and Cormier, M.J. (1992) Primary structure of the *Aequorea victoria* green-fluorescent protein. *Gene*, **111**, 229-233.
11. Inouye, S. and Tsuji, F.I. (1994) *Aequorea* green fluorescent protein. Expression of the gene and fluorescence characteristics of the recombinant protein. *FEBS Lett*, **341**, 277-280.
12. Heim, R., Prasher, D.C. and Tsien, R.Y. (1994) Wavelength mutations and posttranslational autooxidation of green fluorescent protein. *Proc Natl Acad Sci U S A*, **91**, 12501-12504.
13. Ormo, M., Cubitt, A.B., Kallio, K., Gross, L.A., Tsien, R.Y. and Remington, S.J. (1996) Crystal structure of the *Aequorea victoria* green fluorescent protein. *Science (New York, N.Y.)*, **273**, 1392-1395.
14. Wachter, R.M., King, B.A., Heim, R., Kallio, K., Tsien, R.Y., Boxer, S.G. and Remington, S.J. (1997) Crystal structure and photodynamic behavior of the blue emission variant Y66H/Y145F of green fluorescent protein. *Biochemistry*, **36**, 9759-9765.
15. Cubitt, A.B., Heim, R., Adams, S.R., Boyd, A.E., Gross, L.A. and Tsien, R.Y. (1995) Understanding, improving and using green fluorescent proteins. *Trends Biochem Sci*, **20**, 448-455.
16. Matz, M.V., Fradkov, A.F., Labas, Y.A., Savitsky, A.P., Zaraisky, A.G., Markelov, M.L. and Lukyanov, S.A. (1999) Fluorescent proteins from nonbioluminescent Anthozoa species. *Nat Biotechnol*, **17**, 969-973.
17. Alieva, N.O., Konzen, K.A., Field, S.F., Meleshkevitch, E.A., Hunt, M.E., Beltran-Ramirez, V., Miller, D.J., Wiedenmann, J., Salih, A. and Matz, M.V. (2008) Diversity and evolution of coral fluorescent proteins. *PLoS One*, **3**, e2680.

18. Baird, G.S., Zacharias, D.A. and Tsien, R.Y. (2000) Biochemistry, mutagenesis, and oligomerization of DsRed, a red fluorescent protein from coral. *Proc Natl Acad Sci U S A*, **97**, 11984-11989.
19. Campbell, R.E., Tour, O., Palmer, A.E., Steinbach, P.A., Baird, G.S., Zacharias, D.A. and Tsien, R.Y. (2002) A monomeric red fluorescent protein. *Proc Natl Acad Sci U S A*, **99**, 7877-7882.
20. Shaner, N.C., Campbell, R.E., Steinbach, P.A., Giepmans, B.N., Palmer, A.E. and Tsien, R.Y. (2004) Improved monomeric red, orange and yellow fluorescent proteins derived from *Discosoma* sp. red fluorescent protein. *Nat Biotechnol*, **22**, 1567-1572.
21. Shu, X., Shaner, N.C., Yarbrough, C.A., Tsien, R.Y. and Remington, S.J. (2006) Novel chromophores and buried charges control color in mFruits. *Biochemistry*, **45**, 9639-9647.
22. Kogure, T., Karasawa, S., Araki, T., Saito, K., Kinjo, M. and Miyawaki, A. (2006) A fluorescent variant of a protein from the stony coral *Montipora* facilitates dual-color single-laser fluorescence cross-correlation spectroscopy. *Nat Biotechnol*, **24**, 577-581.
23. Ai, H.W., Henderson, J.N., Remington, S.J. and Campbell, R.E. (2006) Directed evolution of a monomeric, bright and photostable version of *Clavularia* cyan fluorescent protein: structural characterization and applications in fluorescence imaging. *Biochem J*, **400**, 531-540.
24. Nienhaus, G.U., Nienhaus, K., Holzle, A., Ivanchenko, S., Renzi, F., Oswald, F., Wolff, M., Schmitt, F., Rucker, C., Vallone, B. *et al.* (2006) Photoconvertible fluorescent protein EosFP: biophysical properties and cell biology applications. *Photochem Photobiol*, **82**, 351-358.
25. Shaner, N.C., Steinbach, P.A. and Tsien, R.Y. (2005) A guide to choosing fluorescent proteins. *Nat Methods*, **2**, 905-909.
26. Rodriguez, E.A., Campbell, R.E., Lin, J.Y., Lin, M.Z., Miyawaki, A., Palmer, A.E., Shu, X., Zhang, J. and Tsien, R.Y. (2017) The Growing and Glowing Toolbox of Fluorescent and Photoactive Proteins. *Trends Biochem Sci*, **42**, 111-129.
27. Specht, E.A., Braselmann, E. and Palmer, A.E. (2017) A Critical and Comparative Review of Fluorescent Tools for Live-Cell Imaging. *Annu Rev Physiol*, **79**, 93-117.
28. Cranfill, P.J., Sell, B.R., Baird, M.A., Allen, J.R., Lavagnino, Z., de Gruiter, H.M., Kremers, G.J., Davidson, M.W., Ustione, A. and Piston, D.W. (2016) Quantitative assessment of fluorescent proteins. *Nat Methods*, **13**, 557-562.
29. Snapp, E.L. (2009) Fluorescent proteins: a cell biologist's user guide. *Trends Cell Biol*, **19**, 649-655.
30. Chudakov, D.M., Matz, M.V., Lukyanov, S. and Lukyanov, K.A. (2010) Fluorescent proteins and their applications in imaging living cells and tissues. *Physiol Rev*, **90**, 1103-1163.
31. Stramer, B.M. and Dunn, G.A. (2015) Cells on film - the past and future of cinemicroscopy. *J Cell Sci*, **128**, 9-13.
32. Landecker, H. (2009) Seeing things: from microcinematography to live cell imaging. *Nat Methods*, **6**, 707-709.
33. Schmid, S.L., Sorkin, A. and Zerial, M. (2014) Endocytosis: Past, present, and future. *Cold Spring Harb Perspect Biol*, **6**, a022509.
34. Dunn, G. and Jones, G. (1998) Michael Abercrombie: the pioneer ethologist of cells. *Trends Cell Biol*, **8**, 124-126.
35. Carrel, A. and Ebeling, A.H. (1926) The Fundamental Properties of the Fibroblast and the Macrophage : li. The Macrophage. *J Exp Med*, **44**, 285-305.

36. Rosenberger, H. (1929) A Standard Microcinematographic Apparatus. *Science (New York, N.Y)*, **69**, 672-674.
37. Zernike, F. (1955) How I discovered phase contrast. *Science (New York, N.Y)*, **121**, 345-349.
38. Frigault, M.M., Lacoste, J., Swift, J.L. and Brown, C.M. (2009) Live-cell microscopy - tips and tools. *J Cell Sci*, **122**, 753-767.
39. Amos, W.B. and White, J.G. (2003) How the confocal laser scanning microscope entered biological research. *Biol Cell*, **95**, 335-342.
40. Dunn, G.A. and Jones, G.E. (2004) Cell motility under the microscope: Vorsprung durch Technik. *Nat Rev Mol Cell Biol*, **5**, 667-672.
41. Denk, W. and Svoboda, K. (1997) Photon upmanship: why multiphoton imaging is more than a gimmick. *Neuron*, **18**, 351-357.
42. Thorn, K. (2016) A quick guide to light microscopy in cell biology. *Mol Biol Cell*, **27**, 219-222.
43. Weber, M. and Huisken, J. (2011) Light sheet microscopy for real-time developmental biology. *Curr Opin Genet Dev*, **21**, 566-572.
44. Sahl, S.J., Hell, S.W. and Jakobs, S. (2017) Fluorescence nanoscopy in cell biology. *Nat Rev Mol Cell Biol*, **18**, 685-701.
45. Duwe, S. and Dedecker, P. (2017) Super-resolution imaging goes fast and deep. *Nat Methods*, **14**, 1042-1044.
46. Galbraith, C.G. and Galbraith, J.A. (2011) Super-resolution microscopy at a glance. *J Cell Sci*, **124**, 1607-1611.
47. Sydor, A.M., Czymmek, K.J., Puchner, E.M. and Mennella, V. (2015) Super-Resolution Microscopy: From Single Molecules to Supramolecular Assemblies. *Trends Cell Biol*, **25**, 730-748.
48. Axelrod, D. (2001) Total internal reflection fluorescence microscopy in cell biology. *Traffic*, **2**, 764-774.
49. Douglass, A.D. and Vale, R.D. (2008) Single-molecule imaging of fluorescent proteins. *Methods Cell Biol*, **85**, 113-125.
50. Biteen, J.S. and Moerner, W.E. (2010) Single-molecule and superresolution imaging in live bacteria cells. *Cold Spring Harb Perspect Biol*, **2**, a000448.
51. Ritchie, K., Lill, Y., Sood, C., Lee, H. and Zhang, S. (2013) Single-molecule imaging in live bacteria cells. *Philos Trans R Soc Lond B Biol Sci*, **368**, 20120355.
52. Rotman, B. (1961) Measurement of activity of single molecules of beta-D-galactosidase. *Proc Natl Acad Sci U S A*, **47**, 1981-1991.
53. Shashkova, S. and Leake, M.C. (2017) Single-molecule fluorescence microscopy review: shedding new light on old problems. *Biosci Rep*, **37**.
54. Hirschfeld, T. (1976) Optical microscopic observation of single small molecules. *Appl Opt*, **15**, 2965-2966.
55. Li, G.W. and Xie, X.S. (2011) Central dogma at the single-molecule level in living cells. *Nature*, **475**, 308-315.
56. Brooks Shera, E., Seitzinger, N.K., Davis, L.M., Keller, R.A. and Soper, S.A. (1990) Detection of single fluorescent molecules. *Chemical Physics Letters*.
57. Moerner, W.E. and Kador, L. (1989) Optical detection and spectroscopy of single molecules in a solid. *Phys Rev Lett*, **62**, 2535-2538.
58. Betzig, E. and Chichester, R.J. (1993) Single molecules observed by near-field scanning optical microscopy. *Science (New York, N.Y)*, **262**, 1422-1425.

59. Schmidt, T., Schutz, G.J., Baumgartner, W., Gruber, H.J. and Schindler, H. (1996) Imaging of single molecule diffusion. *Proc Natl Acad Sci U S A*, **93**, 2926-2929.
60. Stephens, D.J. and Allan, V.J. (2003) Light microscopy techniques for live cell imaging. *Science (New York, N.Y.)*, **300**, 82-86.
61. Yu, J. (2016) Single-Molecule Studies in Live Cells. *Annu Rev Phys Chem*, **67**, 565-585.
62. Yudowski, G.A., Puthenveedu, M.A., Henry, A.G. and von Zastrow, M. (2009) Cargo-mediated regulation of a rapid Rab4-dependent recycling pathway. *Mol Biol Cell*, **20**, 2774-2784.
63. Stracy, M., Uphoff, S., Garza de Leon, F. and Kapanidis, A.N. (2014) In vivo single-molecule imaging of bacterial DNA replication, transcription, and repair. *FEBS Lett*, **588**, 3585-3594.
64. Rust, M.J., Bates, M. and Zhuang, X. (2006) Sub-diffraction-limit imaging by stochastic optical reconstruction microscopy (STORM). *Nat Methods*, **3**, 793-795.
65. Betzig, E., Patterson, G.H., Sougrat, R., Lindwasser, O.W., Olenych, S., Bonifacino, J.S., Davidson, M.W., Lippincott-Schwartz, J. and Hess, H.F. (2006) Imaging intracellular fluorescent proteins at nanometer resolution. *Science (New York, N.Y.)*, **313**, 1642-1645.
66. Hess, S.T., Girirajan, T.P. and Mason, M.D. (2006) Ultra-high resolution imaging by fluorescence photoactivation localization microscopy. *Biophys J*, **91**, 4258-4272.
67. Sustarsic, M. and Kapanidis, A.N. (2015) Taking the ruler to the jungle: single-molecule FRET for understanding biomolecular structure and dynamics in live cells. *Curr Opin Struct Biol*, **34**, 52-59.
68. Lee, J., Miyanaga, Y., Ueda, M. and Hohng, S. (2012) Video-rate confocal microscopy for single-molecule imaging in live cells and superresolution fluorescence imaging. *Biophys J*, **103**, 1691-1697.
69. Huisken, J. and Stainier, D.Y. (2009) Selective plane illumination microscopy techniques in developmental biology. *Development*, **136**, 1963-1975.
70. Huisken, J., Swoger, J., Del Bene, F., Wittbrodt, J. and Stelzer, E.H. (2004) Optical sectioning deep inside live embryos by selective plane illumination microscopy. *Science (New York, N.Y.)*, **305**, 1007-1009.
71. Coelho, M., Maghelli, N. and Tolic-Norrelykke, I.M. (2013) Single-molecule imaging in vivo: the dancing building blocks of the cell. *Integr Biol (Camb)*, **5**, 748-758.
72. Stylianidou, S., Brennan, C., Nissen, S.B., Kuwada, N.J. and Wiggins, P.A. (2016) SuperSegger: robust image segmentation, analysis and lineage tracking of bacterial cells. *Molecular microbiology*, **102**, 690-700.
73. Chiu, S.W. and Leake, M.C. (2011) Functioning nanomachines seen in real-time in living bacteria using single-molecule and super-resolution fluorescence imaging. *Int J Mol Sci*, **12**, 2518-2542.
74. Leake, M.C. (2013) The physics of life: one molecule at a time. *Philos Trans R Soc Lond B Biol Sci*, **368**, 20120248.
75. Sott, K., Eriksson, E., Petelenz, E. and Goksor, M. (2008) Optical systems for single cell analyses. *Expert Opin Drug Discov*, **3**, 1323-1344.
76. Xie, X.S., Choi, P.J., Li, G.W., Lee, N.K. and Lia, G. (2008) Single-molecule approach to molecular biology in living bacterial cells. *Annu Rev Biophys*, **37**, 417-444.
77. Sako, Y., Minoghchi, S. and Yanagida, T. (2000) Single-molecule imaging of EGFR signalling on the surface of living cells. *Nat Cell Biol*, **2**, 168-172.

78. Byassee, T.A., Chan, W.C. and Nie, S. (2000) Probing single molecules in single living cells. *Anal Chem*, **72**, 5606-5611.
79. Leake, M.C. (2010) Shining the spotlight on functional molecular complexes: The new science of single-molecule cell biology. *Communicative & integrative biology*, **3**, 415-418.
80. Dobbie, I.M., Robson, A., Delalez, N. and Leake, M.C. (2009) Visualizing single molecular complexes in vivo using advanced fluorescence microscopy. *J Vis Exp*, 1508.
81. Yu, J., Xiao, J., Ren, X., Lao, K. and Xie, X.S. (2006) Probing gene expression in live cells, one protein molecule at a time. *Science (New York, N.Y.)*, **311**, 1600-1603.
82. Elf, J., Li, G.W. and Xie, X.S. (2007) Probing transcription factor dynamics at the single-molecule level in a living cell. *Science (New York, N.Y.)*, **316**, 1191-1194.
83. Leake, M.C., Chandler, J.H., Wadhams, G.H., Bai, F., Berry, R.M. and Armitage, J.P. (2006) Stoichiometry and turnover in single, functioning membrane protein complexes. *Nature*, **443**, 355-358.
84. Reyes-Lamothe, R., Sherratt, D.J. and Leake, M.C. (2010) Stoichiometry and architecture of active DNA replication machinery in *Escherichia coli*. *Science (New York, N.Y.)*, **328**, 498-501.
85. Delalez, N.J., Wadhams, G.H., Rosser, G., Xue, Q., Brown, M.T., Dobbie, I.M., Berry, R.M., Leake, M.C. and Armitage, J.P. (2010) Signal-dependent turnover of the bacterial flagellar switch protein FliM. *Proc Natl Acad Sci U S A*, **107**, 11347-11351.
86. Ulbrich, M.H. and Isacoff, E.Y. (2007) Subunit counting in membrane-bound proteins. *Nat Methods*, **4**, 319-321.
87. Leake, M.C., Greene, N.P., Godun, R.M., Granjon, T., Buchanan, G., Chen, S., Berry, R.M., Palmer, T. and Berks, B.C. (2008) Variable stoichiometry of the TatA component of the twin-arginine protein transport system observed by in vivo single-molecule imaging. *Proc Natl Acad Sci U S A*, **105**, 15376-15381.
88. Lenn, T., Leake, M.C. and Mullineaux, C.W. (2008) Clustering and dynamics of cytochrome bd-I complexes in the *Escherichia coli* plasma membrane in vivo. *Molecular microbiology*, **70**, 1397-1407.
89. Lenn, T., Leake, M.C. and Mullineaux, C.W. (2008) Are *Escherichia coli* OXPHOS complexes concentrated in specialized zones within the plasma membrane? *Biochem Soc Trans*, **36**, 1032-1036.
90. Xia, T., Li, N. and Fang, X. (2013) Single-molecule fluorescence imaging in living cells. *Annu Rev Phys Chem*, **64**, 459-480.
91. Peterman, E.J., Sosa, H. and Moerner, W.E. (2004) Single-molecule fluorescence spectroscopy and microscopy of biomolecular motors. *Annu Rev Phys Chem*, **55**, 79-96.
92. Watson, J.D. and Crick, F.H. (1953) Molecular structure of nucleic acids; a structure for deoxyribose nucleic acid. *Nature*, **171**, 737-738.
93. Lander, E.S. (2011) Initial impact of the sequencing of the human genome. *Nature*, **470**, 187-197.
94. Snyder, M., Du, J. and Gerstein, M. (2010) Personal genome sequencing: current approaches and challenges. *Genes Dev*, **24**, 423-431.
95. Chin, L., Andersen, J.N. and Futreal, P.A. (2011) Cancer genomics: from discovery science to personalized medicine. *Nat Med*, **17**, 297-303.
96. Hamburg, M.A. and Collins, F.S. (2010) The path to personalized medicine. *N Engl J Med*, **363**, 301-304.

97. Lehman, I.R. (2003) Discovery of DNA polymerase. *J Biol Chem*, **278**, 34733-34738.
98. Lehman, I.R., Bessman, M.J., Simms, E.S. and Kornberg, A. (1958) Enzymatic synthesis of deoxyribonucleic acid. I. Preparation of substrates and partial purification of an enzyme from *Escherichia coli*. *J Biol Chem*, **233**, 163-170.
99. Bessman, M.J., Lehman, I.R., Simms, E.S. and Kornberg, A. (1958) Enzymatic synthesis of deoxyribonucleic acid. II. General properties of the reaction. *J Biol Chem*, **233**, 171-177.
100. Okazaki, R., Okazaki, T., Sakabe, K., Sugimoto, K. and Sugino, A. (1968) Mechanism of DNA chain growth. I. Possible discontinuity and unusual secondary structure of newly synthesized chains. *Proc Natl Acad Sci U S A*, **59**, 598-605.
101. Ogawa, T. and Okazaki, T. (1980) Discontinuous DNA replication. *Annu Rev Biochem*, **49**, 421-457.
102. Cox, M.M., Goodman, M.F., Kreuzer, K.N., Sherratt, D.J., Sandler, S.J. and Mariani, K.J. (2000) The importance of repairing stalled replication forks. *Nature*, **404**, 37-41.
103. Kreuzer, K.N. (2005) Interplay between DNA replication and recombination in prokaryotes. *Annu Rev Microbiol*, **59**, 43-67.
104. McGlynn, P. and Lloyd, R.G. (2002) Recombinational repair and restart of damaged replication forks. *Nat Rev Mol Cell Biol*, **3**, 859-870.
105. Benkovic, S.J., Valentine, A.M. and Salinas, F. (2001) Replisome-mediated DNA replication. *Annu Rev Biochem*, **70**, 181-208.
106. Tanner, N.A., Hamdan, S.M., Jergic, S., Loscha, K.V., Schaeffer, P.M., Dixon, N.E. and van Oijen, A.M. (2008) Single-molecule studies of fork dynamics in *Escherichia coli* DNA replication. *Nature structural & molecular biology*, **15**, 170-176.
107. Spies, M. (2013) There and back again: new single-molecule insights in the motion of DNA repair proteins. *Curr Opin Struct Biol*, **23**, 154-160.
108. Deich, J., Judd, E.M., McAdams, H.H. and Moerner, W.E. (2004) Visualization of the movement of single histidine kinase molecules in live *Caulobacter* cells. *Proc Natl Acad Sci U S A*, **101**, 15921-15926.
109. Sezonov, G., Joseleau-Petit, D. and D'Ari, R. (2007) *Escherichia coli* physiology in Luria-Bertani broth. *J Bacteriol*, **189**, 8746-8749.
110. Li, Y., Schroeder, J.W., Simmons, L.A. and Biteen, J.S. (2018) Visualizing bacterial DNA replication and repair with molecular resolution. *Curr Opin Microbiol*, **43**, 38-45.
111. Beattie, T.R., Kapadia, N., Nicolas, E., Uphoff, S., Wollman, A.J., Leake, M.C. and Reyes-Lamothe, R. (2017) Frequent exchange of the DNA polymerase during bacterial chromosome replication. *Elife*, **6**.
112. Mangiameli, S.M., Merrikh, C.N., Wiggins, P.A. and Merrikh, H. (2017) Transcription leads to pervasive replisome instability in bacteria. *Elife*, **6**.
113. Liao, Y., Li, Y., Schroeder, J.W., Simmons, L.A. and Biteen, J.S. (2016) Single-Molecule DNA Polymerase Dynamics at a Bacterial Replisome in Live Cells. *Biophys J*, **111**, 2562-2569.
114. Lewis, J.S., Spenkelink, L.M., Jergic, S., Wood, E.A., Monachino, E., Horan, N.P., Duderstadt, K.E., Cox, M.M., Robinson, A., Dixon, N.E. *et al.* (2017) Single-molecule visualization of fast polymerase turnover in the bacterial replisome. *Elife*, **6**.
115. Moolman, M.C., Krishnan, S.T., Kerssemakers, J.W., van den Berg, A., Tulinski, P., Depken, M., Reyes-Lamothe, R., Sherratt, D.J. and Dekker, N.H. (2014) Slow unloading leads to DNA-bound beta2-sliding clamp accumulation in live *Escherichia coli* cells. *Nat Commun*, **5**, 5820.

116. Syeda, A.H., Wollman, A.J.M., Hargreaves, A.L., Howard, J.A.L., Bruning, J.G., McGlynn, P. and Leake, M.C. (2019) Single-molecule live cell imaging of Rep reveals the dynamic interplay between an accessory replicative helicase and the replisome. *Nucleic Acids Res.*
117. Thrall, E.S., Kath, J.E., Chang, S. and Loparo, J.J. (2017) Single-molecule imaging reveals multiple pathways for the recruitment of translesion polymerases after DNA damage. *Nat Commun*, **8**, 2170.
118. Henrikus, S.S., Wood, E.A., McDonald, J.P., Cox, M.M., Woodgate, R., Goodman, M.F., van Oijen, A.M. and Robinson, A. (2018) DNA polymerase IV primarily operates outside of DNA replication forks in Escherichia coli. *Plos Genet*, **14**, e1007161.
119. Henrikus, S.S., van Oijen, A.M. and Robinson, A. (2018) Specialised DNA polymerases in Escherichia coli: roles within multiple pathways. *Curr Genet*.
120. Mallik, S., Popodi, E.M., Hanson, A.J. and Foster, P.L. (2015) Interactions and Localization of Escherichia coli Error-Prone DNA Polymerase IV after DNA Damage. *J Bacteriol*, **197**, 2792-2809.
121. Liao, Y., Schroeder, J.W., Gao, B., Simmons, L.A. and Biteen, J.S. (2015) Single-molecule motions and interactions in live cells reveal target search dynamics in mismatch repair. *Proc Natl Acad Sci U S A*, **112**, E6898-6906.
122. Uphoff, S., Lord, N.D., Okumus, B., Potvin-Trottier, L., Sherratt, D.J. and Paulsson, J. (2016) Stochastic activation of a DNA damage response causes cell-to-cell mutation rate variation. *Science (New York, N.Y.)*, **351**, 1094-1097.
123. Uphoff, S., Reyes-Lamothe, R., Garza de Leon, F., Sherratt, D.J. and Kapanidis, A.N. (2013) Single-molecule DNA repair in live bacteria. *Proc Natl Acad Sci U S A*, **110**, 8063-8068.
124. Stracy, M., Jaciuk, M., Uphoff, S., Kapanidis, A.N., Nowotny, M., Sherratt, D.J. and Zawadzki, P. (2016) Single-molecule imaging of UvrA and UvrB recruitment to DNA lesions in living Escherichia coli. *Nat Commun*, **7**, 12568.
125. Ghodke, H., Paudel, B.P., Lewis, J.S., Jergic, S., Gopal, K., Romero, Z.J., Wood, E.A., Woodgate, R., Cox, M.M. and van Oijen, A.M. (2019) Spatial and temporal organization of RecA in the Escherichia coli DNA-damage response. *Elife*, **8**.
126. Rosch, T.C., Altenburger, S., Oviedo-Bocanegra, L., Pediaditakis, M., Najjar, N.E., Fritz, G. and Graumann, P.L. (2018) Single molecule tracking reveals spatio-temporal dynamics of bacterial DNA repair centres. *Sci Rep*, **8**, 16450.
127. Uphoff, S. and Sherratt, D.J. (2017) Single-Molecule Analysis of Bacterial DNA Repair and Mutagenesis. *Annu Rev Biophys*, **46**, 411-432.
128. Hughes, C.D., Simons, M., Mackenzie, C.E., Van Houten, B. and Kad, N.M. (2014) Single molecule techniques in DNA repair: a primer. *DNA Repair (Amst)*, **20**, 2-13.

3

What happens to DnaB upon DNA damage?

This chapter delves on the outcome of the replicative helicase DnaB when the cells are inflicted with UV-mediated DNA damage. DnaB has been speculated to dissociate from the replisome ('fall off') or remain associated with it ('stay put'). Using our snapshot microscopy approach and 'single molecule' sensitivity, we gauge what happens to DnaB after UV exposure, based on three parameters: number of foci, stoichiometry and spatial distribution of foci on the cell long axis. While we do not find any remarkable change in stoichiometry before and after UV exposure, we do report changes on number of foci (e.g., 2 foci category) and for DnaB spatial distribution, when compared to the replisome (β clamp). In line with recent data published while the work was in progress, we hypothesize from our results that DnaB neither 'falls off' nor 'stays put' after UV exposure. Rather, DnaB may be uncoupled from the rest of the replisome machinery, unwinding the chromosome ahead while the other replisome components are stalled behind. Our work should encourage future research on what the role of helicase loaders is (e.g., PriA/PriC) if DnaB does not dissociate from the replisome and how the replication restart pathways work.

3.1 Introduction

The *Escherichia coli* replisome is a multi-subunit (>12 subunits) machine that carries out bidirectional synthesis of the 4.6 Mbp circular genome (1,2). Of these multiple components, the replicative helicase DnaB (encoded by the *dnaB* gene chromosomally, 1416 bp) lies structurally at the forefront of the replisome (**Figure 1.1**, reproduced here) when the replisome is traveling in the direction of DNA synthesis (5'-3'), and unwinds the double-stranded DNA for genome replication (3).

Cellular replicative DNA helicases (such as DnaB), 'universally' form 'donut shaped' hexamers and are hypothesized to encircle one of the two complementary strands, translocating and unwinding the duplex DNA ahead, due to motive force (4,5). These helicases derive the chemical energy that powers the translocation from ATP hydrolysis, which occurs at six coupled ATPase (adenosine triphosphatases) sites located at the interfaces between adjacent monomers. Further, based on the structure of their ATPase domains, the replicative helicases fall under two classes- the DnaB class of bacterial helicases which use the RecA-type ATPase fold and the MCM (mini-chromosome maintenance proteins) class of archaea-eukaryotes, which are AAA+ type ATPases (4).

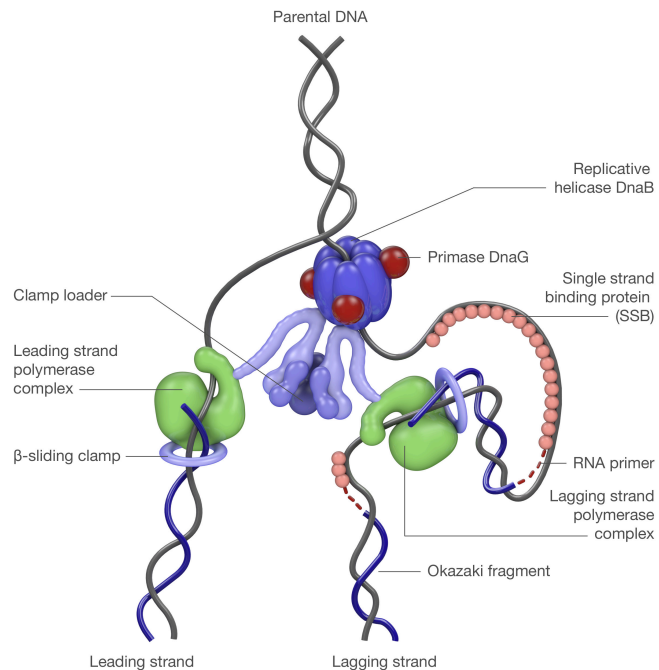


Figure 1.1 The *Escherichia coli* replisome with its multiple components, unwinding the double stranded parental DNA to synthesize new complementary strands.

Apart from universality of replicative helicases as a structural donut, they are also similar in unwinding DNA bidirectionally after assembly. Because of this bidirectional replication, the two helicase motors unwind DNA in opposite direction relative to each other (4). Interestingly, the hexamer structure is stabilized by Mg^{2+} ions, which if chelated or removed leads to the dissociation of hexamer into trimers and monomers (5).

General DnaB characteristics reported in literature

Loading of the replicative helicase DnaB

For replisome assembly in *E.coli*, the helicase DnaB is loaded at the chromosomal site, origin of replication (*oriC*). This loading is done by another protein DnaA belonging to the AAA+ family of ATPases, which recognizes specific sequences within *oriC* (DnaA box, I-site, t-site

and C-site). The ATP bound form of DnaA undertakes unwinding at oriC at AT nucleotides rich regions (5).

For the important step of helicase loading at this melted DNA, DnaB associates with a partner and helicase loader DnaC (DnaC also belongs to AAA+ family of ATPases) and forms a complex with ratio (DnaB₆-DnaC₆). One copy each of this complex is thought to be loaded and tethered on the 'top strand' and 'bottom strand' of oriC elements by DnaA, but in opposite orientations (4) (5). For the ensuing encirclement of single stranded DNA (**ssDNA**) by DnaB hexamer, DnaC is thought to 'crack' open one of the interfaces amongst the DnaB protomers in an ATP facilitated manner (4,5).

Upon loading of one DnaB hexamer on each strand, Single-strand Binding Protein (SSB) prevents further DnaB loading and also protects the melted DNA (6). DnaB, in addition, recruits the DnaG primase for RNA primer synthesis, followed by the subunits of DNA polymerase III (**Pol III**) holoenzyme (6).

Activation of the loaded helicase DnaB

While the precise order of events after DnaB-DnaC loading has been long debated, the ATP bound form of DnaC has been observed to inhibit DnaB activation. To understand how DnaB gets activated, studies now point to ATP hydrolysis by DnaC upon loading of DnaB and eventual 'ejection' of DnaC due to a 'conformational change' of DnaB, which happens upon synthesis of an RNA primer by DnaG primase (4,7). Both these steps are hypothesized to be crucial for DnaB activation and productive DNA unwinding (4,7). Recently, cryo-EM studies also have provided further clarity on how DnaC may aid loading of DnaB (8).

Once DnaB is loaded and activated as a helicase, it is coupled to DNA synthesis (the enzymatic activity of **Pol III**, through its α catalytic subunit) via another replisome subunit called τ (encoded by the gene *dnaX*). The τ subunit is part of the pentameric clamp loader complex ($\tau_3\delta\delta'$), which not only loads the dimeric β sliding clamp for DNA synthesis processivity, but also acts a scaffold for the replisome architecture (9). (**Figure 1.1** shows the positions of the replisome components and their connections, when the replisome travels in the 5'-3' direction).

Kinetics of replicative helicase DnaB unwinding DNA

Research by various groups has also contributed to our knowledge about how fast DnaB helicase may travel while unwinding DNA. While *in vivo* *E.coli* K12, the replisome (and therefore DnaB) has been reported to be progress ~1000 bp/s under certain standardized conditions (10), *in vitro* studies have highlighted how much this processivity of DnaB is dependent on another replisome subunit τ , of the clamp loader complex. In the absence of the τ subunit, DnaB (but in presence of- the ϕ X-type primosomal proteins, SSB, the Pol III core (α , ϵ , and θ subunits), the γ complex (composed of the γ , δ , δ' , χ , and ψ subunits), and the β clamp) unwinds DNA at a rate of ~35 nt/s, while this rate increases 10 fold when the τ -DnaB contact is present, highlighting the role of τ in DnaB unwinding (10). Another *in vitro* study later found different DnaB kinetics (~291 bp/s) (11), and in the presence of translesion polymerases (DNA polymerases II and IV), DnaB rate of movement was reported to be further

affected (1-10 bp/s), using rolling circle replication reactions in the presence and absence of various replisome components to derive this conclusion (12,13).

Bound time of replicative helicase DnaB on DNA

Recent data using super resolution imaging shows that DnaB and other replisome components have quite different 'bound times' on DNA (14). While a core Pol III component such as ϵ subunit (encoded by the chromosomal gene *dnaQ*) remained DNA bound for only 10.4 ± 0.8 s, the β -clamp and DnaB helicase have reported bound times of 47 ± 2.9 s and 913 ± 508 s, respectively (14).

Of the various replisome components assessed for 'stability', DnaB was found to have the highest reported bound time. Much in contrast to Pol III holoenzyme subunits, the authors found out that DnaB does not 'exchange frequently', rather it is a 'stable component' of the replisome (14). This key insight on DnaB stability has significant bearing on our research question as we shall see here.

The replicative helicase DnaB and DNA damage

As introduced in the **sections 1.4. and 1.5., of Chapter 1**, cells suffer frequent DNA damage from internal and external sources. These sources may be natural and recurring, even if external, like ultraviolet radiation (UV) from sunlight. Our functional understanding of DnaB in particular and the replisome in general, remains incomplete and elusive, if we also do not understand how replisome components behave in DNA replication when coping with unavoidable DNA damage from natural sources.

What is pertinent to consider is the apparent conceptual dichotomy that DnaB is at the forefront of a replication machinery poised to meet damaged DNA substrates headlong and also is the most stable component of the replisome (as known so far).

The research question

This thesis chapter asks the research question: what happens to DnaB upon UV mediated DNA damage, as defined by a biological outcome of whether DnaB falls off from the replisome ('dissociates') or stays put at the replisome (or a combination of both outcomes, due to molecular and/or cell-cell heterogeneity, see **Chapter 2, section 2.6**, in the immediate aftermath of UV exposure and DNA damage onset.

This research question of what happens to DnaB upon DNA damage also naturally arises as we try to understand deeper the existing literature on DnaB- replication fork stalling and compare findings from others. The very fact that there exist Replication Restart Proteins **RRPs** (PriA, PriB, PriC and DnaT) and 'replication restart pathways' in *E.coli*, which 'serve to reload' the replicative helicase, emphasizes that DnaB 'falling off' or dissociating from the replisome is a distinct possibility (6). A recent comprehensive review of such restart pathways by Windgassen *et al.*, may interest the reader to appreciate why the helicase dissociation at the replisome is a possible outcome (6).

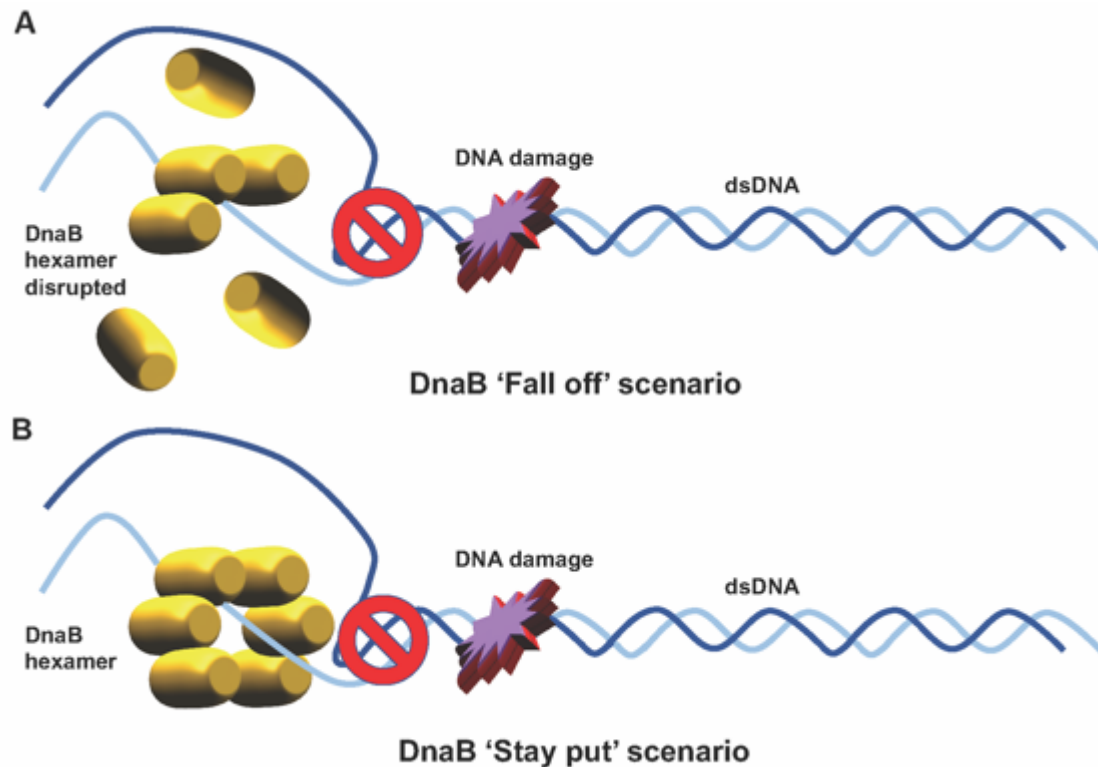


Figure 3.1. A cartoon depicting two hypothesized outcomes when DnaB meets DNA damage as an impediment. A. One hypothesis is that the motor of DnaB hexamers may get disrupted and ‘fall off’ the DNA, upon coming to the DNA damage impediment, leading to replication fork stalling which requires DnaB reloading. **B.** The second hypothesis is that the motor of DnaB hexamers may ‘stay put’ without moving forward, upon coming to the DNA damage impediment, leading to replication fork stalling which does not require DnaB reloading.

On the other hand, research also shows that for efficient replication restart to occur, DnaB (and DnaG) should remain ‘critically associated’ with the stalled replication fork upon UV mediated DNA damage, much in contrast to other replisome subunits (15). In such scenarios, DnaB helicase acts as ‘licensing factor’ for replication restart (15).

In the **Discussion (section 3.5)**, we compare these competing hypotheses in greater detail, especially in light of our data and with the additional perspective of new findings which have emerged while our investigation was in progress.

Before we describe experiments and results in this chapter, in the next section we introduce the concepts of foci and the number of replisomes, and how they are related. In helping navigate the reader on why measuring foci and stoichiometry matter to understand DnaB functions later, we feel that the underlying premise (i.e., the concepts of foci and number of replisomes) should be explained first. We explain to the reader why the number of replisomes is defined by the number of DnaB hexamers and how there may be one as well as two replisomes in the same focus.

3.2 Number of replisomes and number of foci: related but different concepts

The objective of this section is to help understand foci and stoichiometry plots which follow in the results section (**section 3.4.2**).

It is rewarding to review here why replisome components appear as foci during microscopy, because this understanding leads us to appreciate why foci analyses and spatial distribution are relevant to test our hypothesis later. Understanding of this section will also help the reader appreciate why for a structurally hexameric protein (DnaB), we report two fitted peaks of 6 and 12 molecules per focus when studying stoichiometry.

Replisome components, such as DnaB and β clamp, appear as punctate structures (called foci) in microscopy images. These foci are a result of the replisome being DNA bound *in situ*. Further, these foci may be the result of a 'factory' like assembly of replisome proteins *in situ* (16,17) or a translocating multi-molecular machine on a 'track' (18,19). (In the factory model, the replisome is stationary while the DNA loops in and out of it for replication, while in the track model, the replisome traverses the chromosome like an engine on a namesake rail track).

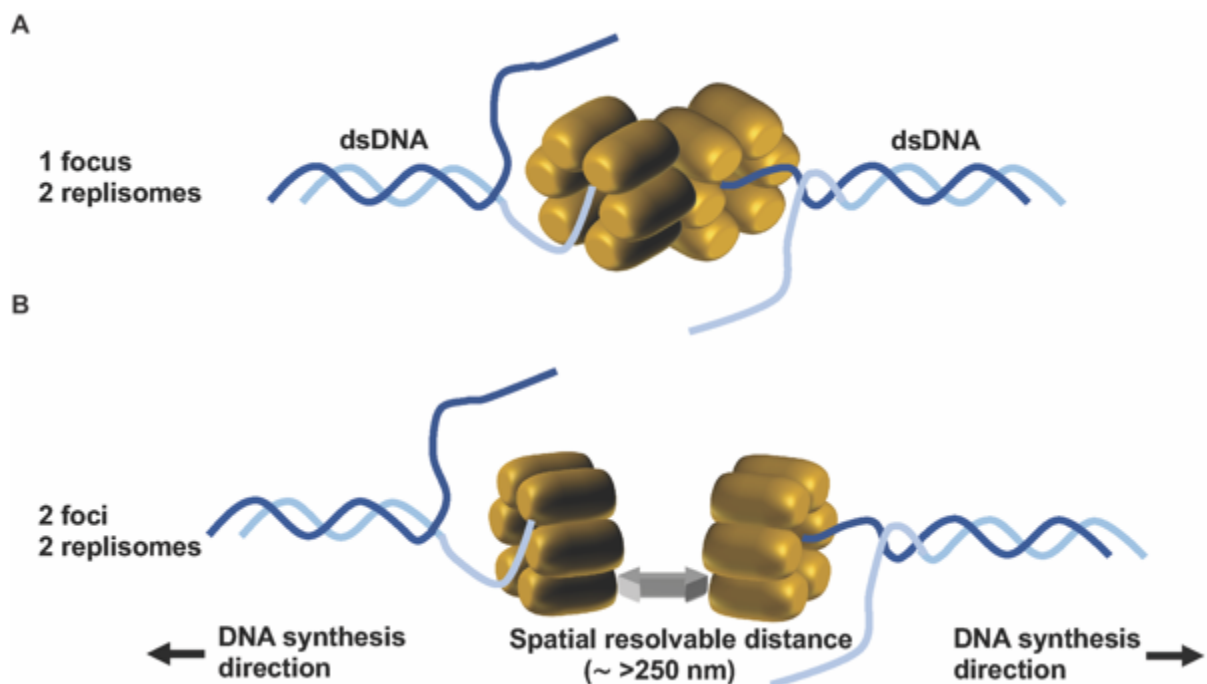


Figure 3.2 A cartoon illustrating the concepts of one focus and two foci, with two replisomes in each situation. Both situations may happen in a cell at different times of its lifetime. **A.** When there are 2 replisomes (defined by the presence of 2 motors of DnaB hexamers) in one light diffraction limited focus, the DnaB stoichiometry is expected to be **12 subunits**. Such a situation may arise at the replication initiation and replication termination. **B.** When there is 1 replisome (also defined by the presence of 1 motor of DnaB hexamer) in a spatial resolved focus observable as separate and distinct from an adjacent focus, the DnaB stoichiometry is expected to be **6 subunits**. Such a situation may be frequently observed when individual replisomes are traversing for bidirectional replication.

Observing these foci that contain replisomes also provides insight on genome replication and cell cycle. During the initiation of genome replication, two replisomes are in close vicinity and poised for bidirectional synthesis of the circular chromosome. Also, at the termination of replication, the two replisomes are in close vicinity, but poised to converge and merge at the Tus-Ter termination at/near the chromosomal *dif* site. Due to the diffraction limit of wide-field fluorescence microscopy (~250 nm, see **section 2.5, Chapter 2** for explanation), the confined proximity of two replisomes in space (proximity defined here on the x-y axes), such circumstances resembling replication initiation and termination may mean that two replisomes (number of replisomes in a focus defined on the basis of DnaB hexamer motors) may be microscopically visible as just a punctate structure or 'one focus' (referred as **one focus-two replisomes** situation, see **figure 3.2A**), an apparent DnaB stoichiometry of **12 subunits** is detected when images are analyzed. However, as the replication proceeds bidirectionally and the spatial distance (x-y axes) between the replisomes increases, the two replisomes may be microscopically visible as two separate and distinct foci (referred as **two foci-two replisomes** situation, see **figure 3.2B**), leading to a DnaB stoichiometry of **6 subunits** when images are analyzed.

The snapshot imaging (please see **section 3.6 Materials and methods** for details) used in this study has been performed on unsynchronized cells (i.e., a population of cells in different stages of replication and cell cycle), which implies the presence of DnaB foci in both situations of 'one focus' and 'two foci'. Furthermore, as shown in **figure 3.3**, when a cell has more than two diffraction limited foci, there may also be the presence of three or four replisomes inside (**figure 3.3D, E**), which may be an occurrence due to the same reasons illustrated by **figure 3.2**. The various possible combinations of number of foci visible and the inherent replisome numbers are also shown in **figure 3.3**. Further combinations of these individual scenarios (**figure 3.3A-E**) for foci-replisome situations can be envisaged, when there are three or four foci in a cell. Because the imaging is on unsynchronized cells, there are also cells found without any foci or replisomes. The reason may be the fact

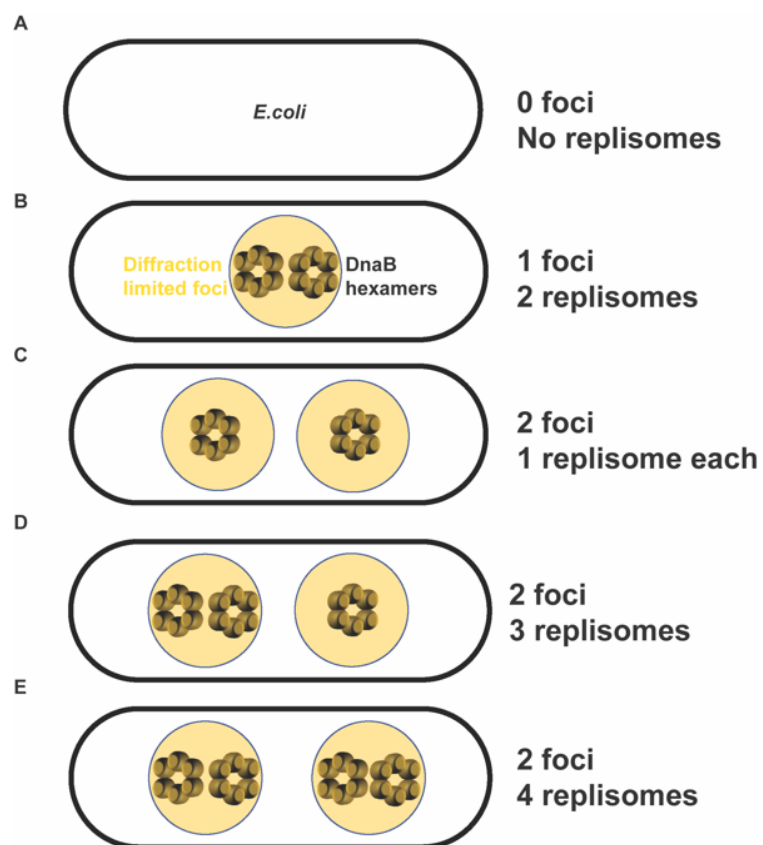


Figure 3.3. A schematic showing the putative foci-replisome scenarios. The number of replisomes is defined by the number of DnaB motors of hexameric stoichiometry. A combination of these possibilities may further give rise to 3 foci and 4 foci scenarios.

that during cell lifetime just after cell birth and before cell division- when there is no genome replication, there are also no foci or replisomes.

As an aside, a recent study measured the ‘stability’ of replisome complexes (*Bacillus subtilis* and *Escherichia coli*) and found that this stability also depended on transcription. By inhibiting initiation of transcription using the antibiotic rifampicin, the authors observed that the stoichiometry distribution of DnaB shifted to a unimodal peak of 12 molecules in ‘replication factories’ (foci), as compared to bimodal peaks of 6 and 12 molecules for the untreated cells (20).

To summarize for this section, we have provided an explanation on why we see punctate structures called ‘foci’ under a microscope and how such foci may harbor one or two replisomes inside them. With this understanding the reader can appreciate why we also we fit two peaks for stoichiometry analyses (DnaB molecules per focus) later. To reiterate here, we define the number of replisomes by the number of DnaB hexamers, because DnaB is the most stable of replisome components reported. To highlight here also for emphasis, we refer to ‘replisome’ as the replication machinery, but to distinguish for our research purposes purely as a concept, we refer to ‘DnaB’ and imply the replicative helicase alone, although the latter is definitely part of the replisome when synthesizing DNA.

With this conceptual understanding behind us, in the next section we describe why and how we have chosen to look at certain parameters or indices and thereby broken down our main research question into sub-questions. Each of these parameters progress our understanding of DnaB outcomes upon UV-mediated DNA damage in a piecemeal manner, which is then considered holistically in **section 3.5 Discussion**.

3.3 How to assess DnaB behavior? The parameters

In order to characterize the DnaB ‘behavior’, we have used three parameters or indices - number of foci, stoichiometry, and spatial distribution of DnaB along the cellular long axis, with respect to the bacterial replisome. The rationale for choosing these three indices has been guided by not just our ability analyze microscopy data, which is crucial, but also whether we could gain biological insights about DnaB and formulate a hypothesis.

These three indices are explained below in the context of understanding DnaB outcomes after UV-mediated DNA damage (**To be noted here again for emphasis:** We refer to ‘replisome’ as the replication molecular machinery, but when we refer to ‘DnaB’ here we imply DnaB helicase only, although the DnaB helicase is definitely also part of the replisome. We distinguish it purely for a conceptual purpose because DnaB is our gene of interest):

- **Number of foci:**

As introduced and explained in **section 3.2**, replisome proteins like DnaB form punctate structures called foci during genome replication, no matter which model of DNA synthesis (factory or track) is considered. Therefore, the number of foci and their distribution reveal details about replisome components.

The number of DnaB foci may be affected by UV exposure if the numbers of replisomes within a diffraction limited focus (foci) has been perturbed. (Furthermore, these numbers of replisomes may vary inside the focus, see **figures 3.2** and **3.3**, for concept illustration).

This ‘perturbation’ of replisomes to which we refer, may lead to number of foci increasing or decreasing, as two DnaB hexamers may move apart from or come closer together. Such situations may happen due to DnaB ‘uncoupling’ from the rest of the replisome components to facilitate DNA repair, according to a new study (21). Interestingly, a distinct outcome hypothesized also in the same report is the assembly of replisome proteins in ‘extra’-replisome loci to facilitate DNA repair, which again may lead to number of foci varying depending on the replisome component under consideration (21). Please see **section 3.5** for further discussion on this uncoupling model in the context of our data.

Using a replisome marker (besides DnaB) for comparison therefore, would inform us if there is any evidence for this uncoupling model, if two replisome components show different number of foci after UV-mediated DNA damage, which otherwise are part of the same molecular machinery. Therefore, this analysis reports on both DnaB and the replisome marker.

- **Stoichiometry:**

The number of DnaB hexamers in a focus (foci) dictates the stoichiometry we observe. Thus, this analysis reports for DnaB only. A reduction in DnaB stoichiometry may point towards whether DnaB ‘fell off’ the replisome as the subunits of the DnaB hexamer may disassemble, while an unchanged stoichiometry may favor the ‘stayed put’ scenario, after DNA damage infliction, see **figure 3.1**. Probing stoichiometry is another way to gauge DnaB, but it may not be the only way that DnaB is impacted due to DNA damage.

- **Spatial distribution:**

As stated above in the ‘Number of foci’ subsection, if the DnaB and replisome foci have moved apart or come closer in the aftermath of UV exposure, then an analyses of the foci spatial distribution would provide evidence for it. As such, this analysis reports on both DnaB and the replisome marker. The localized foci are plotted along on the cellular long axis. The spatial distribution analyses will therefore report on both, DnaB and its position with respect to the replisome.

Our experiments of DnaB behavior are aimed to be understood in the context of the replisome. Because the replisome is a multi-subunit complex, the choices of gene markers as a replisome proxy are also many in principle. However, as mentioned in **section 3.1. Introduction**, the β clamp has the second highest DNA bound time (47 ± 2.9 s) after that of DnaB for the various replisome components tested recently (14). For this primary reason, we have selected it as a replisome marker. Moreover, our understanding that β clamp is a processive marker which follows the Pol III core enzyme, rather than a stationary one like Single strand DNA binding protein SSB which coats DNA at a replication locus for a given time period, also makes it suitable for our study. Additionally, we find in literature the mention of β clamp acting as a

protein-protein interaction hub for replication and has been studied by other researchers as a reliable replisome marker as well (17,20,22-25).

While the β clamp has its merits for usage as a replisome proxy, it should be noted that this component has high copy number at the replisome (~45 molecules when DNA bound (26)), likely reflecting the preceding synthesis of Okazaki fragments just behind the replication fork. However, this high copy number also helps us detect fluorescent signals better.

The same rationale has been extended to the construction of a second strain designated LB3 (*dnaB-mcherry*, *Ypet-dnaN*) as a fluorophore control. In the case of our third strain LB10 (*dnaB-mcherry*, *dnaQ-Ypet*), we have decided to tag the Pol III machinery itself as a second replisome marker, the core exonuclease component involved in DNA proofreading (ϵ subunit). Please see **section 3.6 Materials and methods** for details.

To summarize: with the contextual understanding of foci, replisomes and the parameters involved in this study, we turn towards the results section next. First in **section 3.4.1**, we delve on the strain engineering and validation to address our research. In **section 3.4.2**, we characterize our DnaB observations in undamaged cells, to show the baseline properties. As explained on the rationale behind experimentation in **section 3.3**, the baseline properties are number of foci, stoichiometry and spatial distribution. For emphasis we reiterate here, the reason these parameters lead towards answering our research question (in **section 3.4.3**, upon UV-mediated DNA damage): foci analyses show whether the DnaB foci distribution as categories (0, 1, 2, 3 foci) have been perturbed, stoichiometry analyses show whether there has been reduction in DnaB molecules in a focus and finally, if they (DnaB foci) are perturbed, whether the localization of DnaB foci has changed. While the stoichiometry analyses are only for DnaB, the foci analyses and spatial distribution analyses report on DnaB data with respect to the replisome. Assessing DnaB foci and their spatial distribution with respect to the replisome is insightful because if DnaB hexamers do not ‘fall off’ or dissociate at the replisome, then we can attempt to see what happened to the intact DnaB with respect to the replisome.

3.4 Results

3.4.1 Strain engineering and validation

To address our research question, we have created the three chromosomal fusion strains LB1, LB3 and LB10. Please see **section 3.6 (Materials and methods)** for details on strain engineering.

In the strain **LB1**, DnaB is fluorescently tagged at the C terminus by Ypet (*dnaB-Ypet*) and the replisome is marked by β clamp, fluorescently tagged by mCherry at the N-terminus (*mCherry-dnaN*).

The second strain **LB3**, has the same *E.coli* genes tagged but with fluorophores swapped (*dnaB-mcherry*, *Ypet-dnaN*).

We also constructed a third strain **LB10** in which DnaB has been tagged at the C terminus by mCherry, but the replisome is represented by labelling the DNA Polymerase III core subunit

(ϵ), involved in proofreading during DNA synthesis, which is tagged by Ypet at the C terminus (*dnaB-mCherry*, *dnaQ-Ypet*). **Figure 3.4** provides an overview for the three strains. **Table S3.1** shows a summary of strains used in this study.

The motivation for tagging *dnaB* and *dnaQ* at C terminus for chromosomal fusion proteins has been guided by literature, including previous studies on single molecule fluorescence imaging (1) (18,27).

In the case of *dnaN* fusion proteins, we have used in-house strains BN1109 and BN1682 as templates for further genetic engineering, reported previously in one of the published works of Prof. Nynke Dekker (26).

The choice of linkers is by and large empirical and guided by trial and error. For the strain LB1 we designed a linker 27 amino acids (aa) long, while for strains LB3 and LB10 we designed linkers of 20 aa long.

In the case of strain LB1, the linker downstream to DnaB, *dnaB-Ypet* was derived unaltered from a strain kindly gifted by Prof. David Sherratt, Oxford University, UK. For strains LB3 and LB10, the linker was based on a design from plasmids kindly gifted by Prof. Patricia Foster, Indiana University, USA. However, the linker in LB3 was found to be curtailed (12 aa) after genetic engineering, instead of 20 aa, as designed to be. Nevertheless, we decided to use LB3 for our experimentation, because the curtailed linker was not exceptionally short (we have used linkers as short as 11 aa linkers for functional tagging, ref. (26)), besides the shorter linker provided another measurement control to gauge DnaB activity. However, if DnaB functionality is dependent on long linkers, then this short linker (LB3) may cause problems.

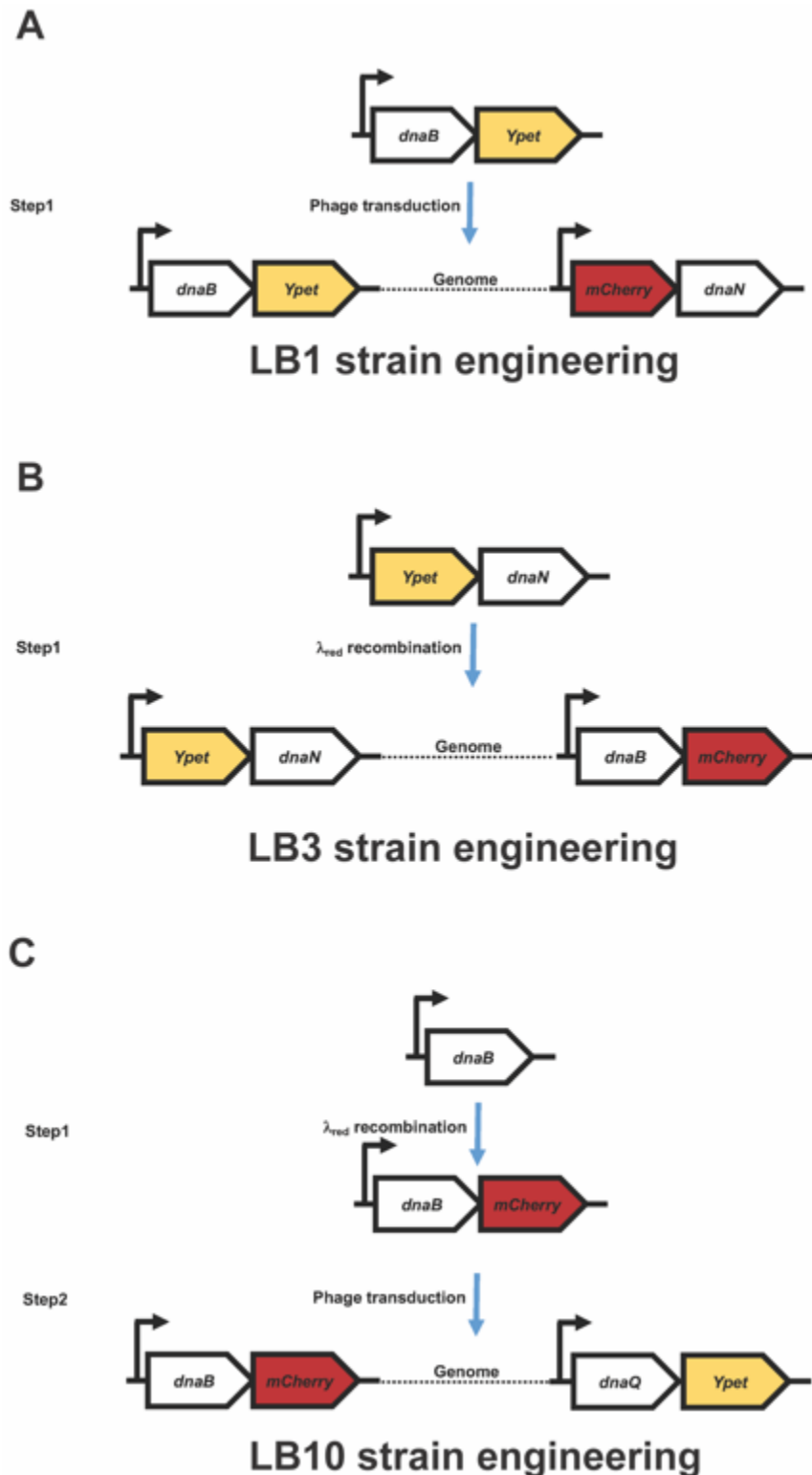


Figure 3.4. An overview of the cloning steps for the genetic engineering of three dual coloured strains created in this study: **LB1**, **LB3** and **LB10**.

All strains have been validated by PCR followed by DNA sequencing. **Figure S1. A, B, C** show the amplification of *dnaB* locus, *dnaN* locus and *dnaQ* locus (colony PCR) respectively, for strains- wild type, LB1, LB3 and LB10. To gauge the health of these strains, we have performed growth curves in regular LB medium (**figure S1. D**). All the strains grew without any apparent defect in this standard assay, with doubling times of 35 min (WT), 34.3 min (LB1), 33 min (LB3) and 33.7 min (LB10). We have also performed serial dilution assay for the four strains under different conditions: undamaged, UV exposures for 1 s (1.218 J/m^2) and 2 s (10.88 J/m^2) (**figure S1. E**). Please see **section 3.6 Materials and methods** on how UV radiation is inflicted on cells, under the heading **UV radiation on cells** and **figure S3.2** for UV dose calibration. The strains grew without any defect in the undamaged condition, in agreement with the results of LB growth curves, which show that the essential and housekeeping functions of the tagged replisome proteins are intact. Interestingly however, when exposed to UV for 1 s, the strain LB1 had apparent perturbation (unlike LB3 and LB10) and the exposure to UV for 2 s, for all strains was quite lethal after overnight incubation. The lethality should be carefully considered as an overnight result, and not necessarily an instantaneous effect of UV dose. Considering that replisome proteins are not known to have exclusive roles in DNA damage repair and tolerance pathways, we are surprised to find this perturbation after UV exposure in strain LB1.

Using these UV exposure times, we also determined the effect of these doses on cell growth using phase contrast microscopy in M9 glycerol- agarose pad. Images were acquired at 10 min intervals without UV exposure (undamaged) and following UV exposure (1 s (1.218 J/m^2) and 2 s (10.88 J/m^2)). Representative phase contrast images (WT and LB1) are shown in **figure S3.3**. Representative growth curves are shown for the same strains (**figure S3.4**), there was no colony formation or growth (based on cell length change) on pad after UV-2 s exposure.

For the undamaged control, the strains WT and LB1 were found to have doubling times of $1.40 \pm 0.05 \text{ h}$ and $1.92 \pm 0.03 \text{ h}$, respectively, in the undamaged condition. While the M9-glycerol is a nutrient deficient medium compared to LB medium, which explains the slower growth of strains, interestingly we also found that the strain LB1 lags behind the WT strain in this type of experiment. After UV-1 s exposure, the growth of LB1 cells was found to be irregular for an exponential fit.

Because the strains grow without any apparent defect in the undamaged condition for rich media experiments (regular growth curves in LB broth and serial dilution assays), we revisited literature to find an explanation into this anomaly of media dependent observations. We are guided by previous studies to say that genetically engineered strains (perhaps particularly for replisome tagged proteins) show behaviour dependent on growth medium or experiment at times (18,20). Moreover, since growth in a rich medium like LB rather requires constitutive and robust protein expression for rapid growth and cell division, we think that our strains show fitness based on the LB medium experiments, but the results may need to be considered carefully for particular assays which may involve minimal media.

To further note about strains and minimal media, we have refrained from reporting experiments from strain LB3 and LB10 eventually after having them validated here, because the stoichiometries for two fusion proteins (*dnaB-mcherry*, *dnaQ-Ypet*) reported in literature could not be ascertained (data not shown). This could be a consequence of a short linker in

the strain LB3 (*dnaB-mcherry*) or the need for further fine-tuning of technical aspects (acquisition, analyses settings) for the strain LB10 (*dnaQ-Ypet*). For the strain LB1, we have been able to perform a comparative check with literature on DnaB stoichiometry and we describe this and other parameters in the next section for undamaged cells.

(**Figure S3.5** shows representative fluorescent cell images for strain LB1 from this study, **figure S3.7** shows autofluorescence intensity comparison of LB1 with respect to WT cells).

3.4.2 DnaB behavior in undamaged cells

For understanding DnaB behavior upon UV-mediated DNA damage, it is useful to see first how DnaB behaves in undamaged cells. These properties of DnaB in the undamaged cells set the baseline condition for observations when UV exposure is applied, mentioned in the next **section 3.4.3**. Furthermore, we also compare the DnaB observations here with that of the replisome (β -clamp), to see how DnaB behaves with respect to the replisome under natural conditions.

As explained in the **section 3.3**, the different DnaB parameters for our research question are: number of foci, stoichiometry and spatial distribution. In the following **sub-section 3.4.2.1**, we begin by describing the characteristics of DnaB foci in undamaged cells and also compare it with β -clamp foci (replisome) later in **section 3.4.2.4**.

3.4.2.1 DnaB foci characteristics in undamaged cells

As mentioned previously in the **section 3.2.**, replication proteins assemble in molecular machines (the replisomes) to carry out DNA synthesis for genome replication. Microscopically, this agglomeration appears to form punctate structures referred here as 'focus' (foci).

From our snapshot microscopy, we have analyzed how these DnaB foci are distributed (cells categorized as having no foci and 1, 2, 3 and 4 foci). About a quarter of cells have no DnaB foci detected (29%), which also could be due to our experimentation on unsynchronized cells while 44% cells show 1 focus (the highest population for any foci category). Approximately one-fourth of cells also show 2 foci

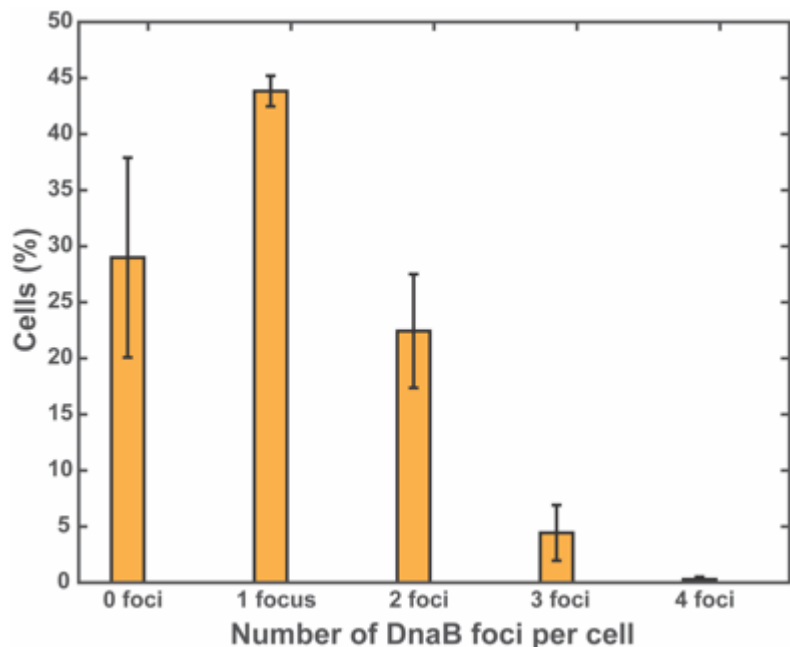


Figure 3.5. Histograms showing percentages of cells with 0, 1, 2, 3, or 4 DnaB-YPet foci in undamaged cells. The bars represent the mean of each foci category and error bars represent the standard deviation. Data from 2171 cells and 2 experimental days.

(22%), while a minority (> 5%) of cell population have 3 and 4 foci. Please see **figure 3.5** to see DnaB foci distribution.

With the visualization of DnaB foci in the undamaged cells here, we report next on the constituents of those foci, i.e., replisomes (single and double).

3.4.2.2 DnaB stoichiometry in undamaged cells

As stated previously in **section 3.2**, the number of replisomes in focus (foci) is defined here as the number of DnaB hexamers, because DnaB is the most stable component of a replisome known so far.

So, to detect the number of replisomes in a focus, one has to detect the number of DnaB hexamers. This principle brings us to stoichiometry analysis of DnaB foci in undamaged cells. Knowing this baseline understanding allows us to subsequently

report on DnaB outcomes when UV exposure is applied onto cells.

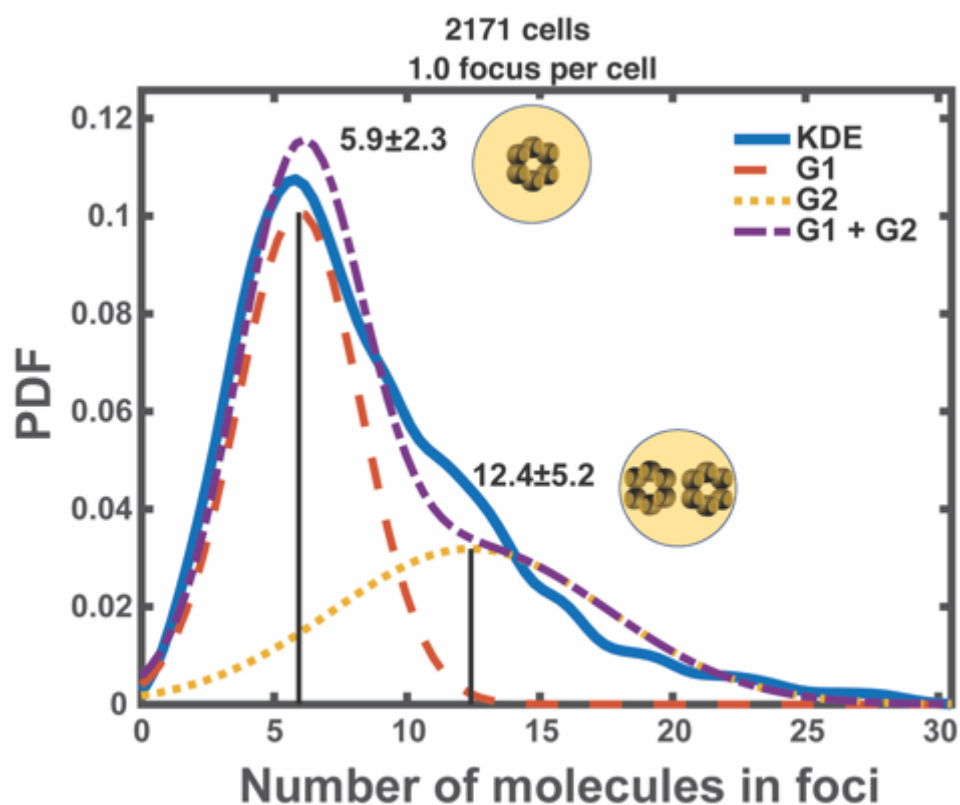


Figure 3.6. Distribution of DnaB-Ypet in foci of undamaged cells. Probability density function (PDF) of the fluorescence intensity (a.u.) of DnaB-YPet foci is divided by the fluorescence intensity of a single YPet molecule (539 a.u.) The blue line represents the kernel density over raw data, while red, dotted yellow and dashed purple lines show represent Gaussian fits G1, G2 and (G1+G2) respectively. Values represent mean Gaussian \pm standard deviation, G1 and G2. During initiation and termination of replication, the two replisomes may be too close (< 250 nm) to be spatially resolved, due to which the foci may appear to have 12 molecules.

We have used snapshot images to determine the DnaB stoichiometry in the undamaged cells. At the outset, our expectation has been that there should be 6 molecules of DnaB in a focus, and in some cases (perhaps during cellular situations of initiation and termination of replication, when replisomes are adjacent or merging respectively) there should be 12 molecules of DnaB in a focus as well. This is because the number of replisomes in a focus detected is also dependent on the spatial resolving limit of the microscope. The spatial resolving limit ($\sim >250$ nm) determines whether we are able to see one or two replisomes in

a diffraction limited focus (This concept is explained in detail, **section 3.2**, and illustrated in **figures 3.2** and **3.3**). For stoichiometry analysis, we have determined first the fluorophore intensity of one Ypet molecule (539 a.u.) *in vivo* by DnaB foci photobleaching (see details on how foci photobleaching yields to single fluorophore intensity calculation in **section 3.6 Materials and methods**, under the heading **Calibration of single Ypet fluorescent molecules**).

In **figure 3.6**, the DnaB-Ypet stoichiometry is shown for undamaged cells. Applying the single fluorophore intensity to DnaB-Ypet from snapshot imaging, we see a bimodal distribution of DnaB in foci. The blue line shows a kernel density over the raw data, the red and yellow lines show two separate Gaussian fits and finally, the purple line shows a sum of these two Gaussian fits. To summarize, there are two peaks of 5.9 ± 2.3 and 12.4 ± 5.2 (means of Gaussians G1 and G2, respectively).

The DnaB stoichiometry with a peak value of 5.9 ± 2.3 molecules (G1, red dashed), has the highest occurrence probability (PDF ~ 0.1) in undamaged cells, while a minority of foci show the prevalence of 12.4 ± 5.2 molecules (G2, yellow dotted) with probability (PDF ~ 0.04). Because our dataset involves unsynchronized cells which are in various stages of the cell cycle, one expects to see such bimodal distribution (as explained in **section 3.2** and **figure 3.2**). Furthermore, the Gaussian G2 has a broader distribution than Gaussian G1 (x-axis), suggesting that there may be more individual DnaB subunits in such diffraction limited foci, apart from presence of just two hexamers (mean peak G2). As an example why there may be more than 12 subunits at certain times, the two replisomes may be close (i.e., distance below diffraction limit) when replication is initiated and DnaB subunits are poised to be loaded as a hexamer from a pool of many DnaB subunits (DnaB has 300 'mean copies delocalized' in the cytoplasm (1)).

Additionally, our results on DnaB stoichiometry of 6 and 12 molecules agree with recent literature (1,20). Further, a recent structural study has confirmed the DnaB hexameric structure (28) using single particle cryo-electron microscopy (cryo-EM), while cellular scenarios for DnaB stoichiometry of 12 molecules in foci may arise (e.g., during replication initiation and termination, when replisome are adjacent), as explained in **section 3.2**.

3.4.2.3 DnaB foci and stoichiometry (combined) in undamaged cells

In sections **3.4.2.1** and **3.4.2.2** above, we have reported on our ability to detect DnaB foci and DnaB stoichiometry. As we shall see in **section 3.4.3**, that these two parameters help us understand DnaB outcomes after UV exposure.

As an additional information, the reader may be interested to know more about how many replisomes reside within a focus. To characterize whether a focus contains single or double replisomes (1 or 2 DnaB-hexamers, respectively), a boundary value separating the two possible outcomes has been set to 10 DnaB molecules. While one might expect such a boundary to lie exactly between 6 and 12, i.e., at 9 DnaB molecules per focus, based on our analyzed stoichiometry of DnaB under undamaged conditions (**figure 3.6**), a boundary set at 10 molecules has been estimated to be a more representative one between the two Gaussians G1 and G2 fitted to our data.

Figure 3.7.A shows that for 2171 cells and 2208 DnaB foci detected, 68% and 32% of DnaB foci contain single and double replisomes, respectively. 39% of the cells have '1 focus' containing a single replisome and 27% of the cells have '1 focus' containing double replisomes, respectively, **figure 3.7.B**. 12% of the cells have '2 foci' that both contain a single replisome and 2% of the cells have '2 foci' that both contain two double replisomes, **figure 3.7.B**. We note that it has been determined that about 12% of cells have a combination of foci containing one and two replisomes (analyses credit: Lisa A. Buller). Taking this into account, it is estimated that ~10% of the cells that actually contain two foci are counted as cells containing either one single-replisome focus or one double-replisome focus. In order to compensate for this analysis artefact, a corrected estimate is shown (**figure 3.7.C**), from which we may conclude that in a '1 focus' scenario, ~30% of cells possess just one replisome (and <20% of cells have double replisome).

Notably, while our study does not address replication with respect to the topic of bacterial transcription, this result of 30% cells with '1 focus' possessing one replisome may be interesting to compare with a recent study (20). The authors reported on *B. subtilis* foci undergoing replication, 41% of which have a 'replication factory' (i.e., a focus) of just 6 DnaC molecules (i.e., a single replisome) and the remaining 59% have double replisomes therein. Upon transcription inhibition (by rifampicin) however, the number of these replication factories with 2 replisomes rose to almost 100% (i.e., a unimodal peak of 12 DnaC molecules), thereby highlighting how transcription affected replication. In case of *E.coli*, 59% and 41% of foci contain single- and double-replisomes, respectively. Similarly, the number of *E.coli* replication factories rose to almost 100% after transcription inhibition. This study has highlighted the partitioning of single and double replisomes in a replication factory and how these replisomes therein are affected by transcription. (In this study, cells were imaged at 30°C). With a caveat that while our result is in terms of cells (30%) showing one replisome in a focus, their observations (which is in terms of foci) in *B.subtilis* (41%) may be similar, rather in *E.coli* (59%).

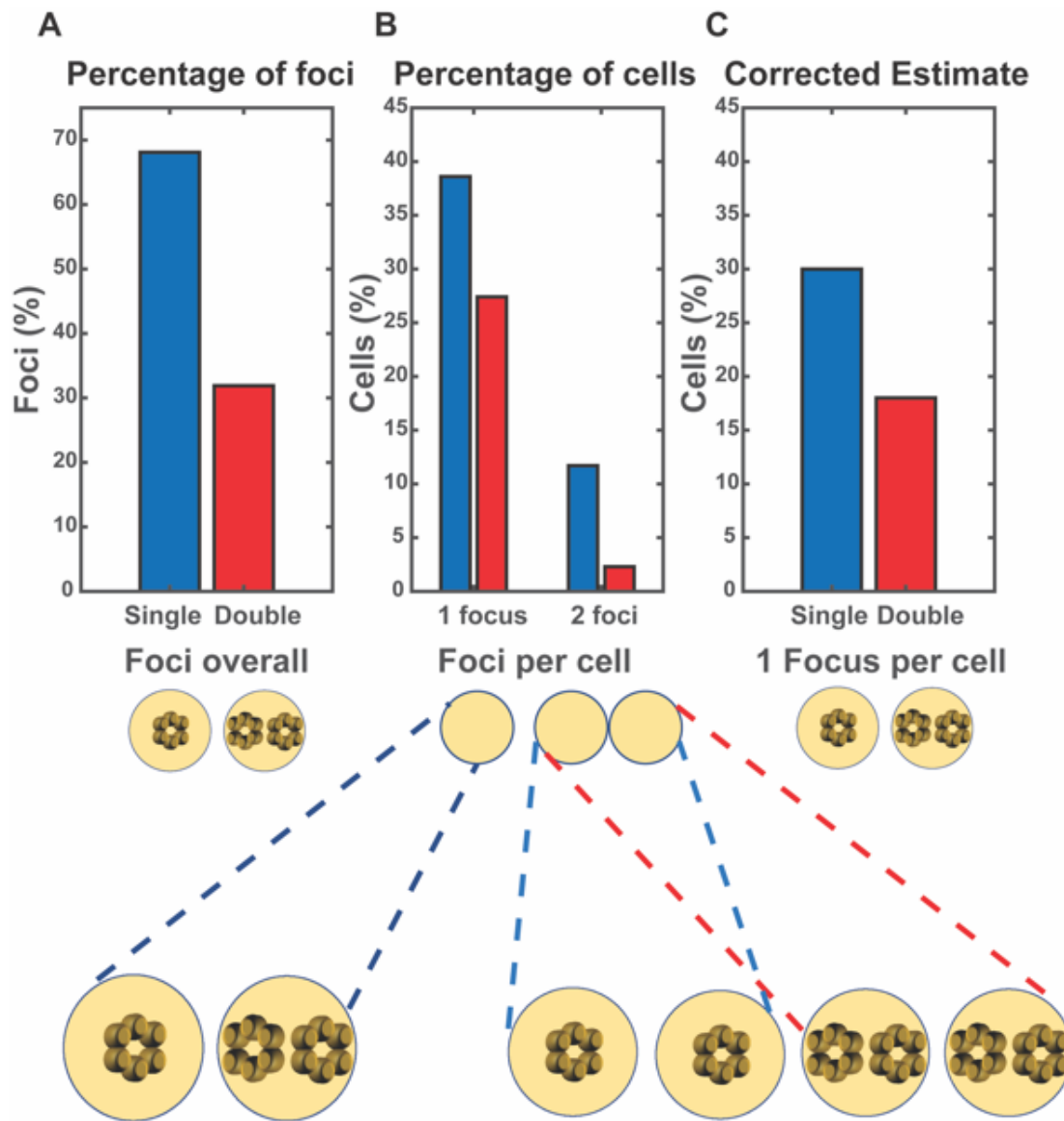


Figure 3.7. Distinguishing between foci containing single replisome and double replisomes based on DnaB stoichiometry. **A.** Percentages of all foci detected in undamaged cells showing single and double replisomes. **B.** Percentages of cells with one and two foci, which may contain single and double replisomes, shown in dashed lines. **C.** Corrected percentages of cells with one focus per cell that contain either a single or a double replisomes. Data from 2171 cells and 2208 DnaB-Ypet foci. (Cell percentages do not add up to 100% because cells of 0, 3 and 4 foci not considered).

3.4.2.4 DnaB overall characteristics (foci & spatial distribution) with respect to the replisome

In **section 3.4.2.1**, we have shown the reader only DnaB foci characteristics, in undamaged cells. In this section, we present a consolidated histogram (**figure 3.8**), wherein DnaB foci and β clamp (replisome) foci characteristics are shown together for a comparison.

For this, we use the same dataset as reported in **section 3.4.2.1**. At the outset, our expectation for this comparison was that both DnaB foci and β -clamp foci should show similar distributions of the number of foci, as they are known to jointly operate at the replisome.

Interestingly when compared to DnaB foci, we find that fewer cells show no foci for β -clamp (8% versus 29% DnaB). However, in line with our expectation the numbers of DnaB (44%) and β -clamp (48%) are similar for '1 focus' distribution; almost half of the cell population. In the '2 foci' category, β -clamp (~33%) shows a close but slightly higher number than DnaB (22%); close to one-fourth of cells, while we refrain from commenting on the 3 and 4 foci situation, because only a few cells show this phenomenon. These cells with 3 and 4 foci may be a result of initiation of replication prior to cell division.

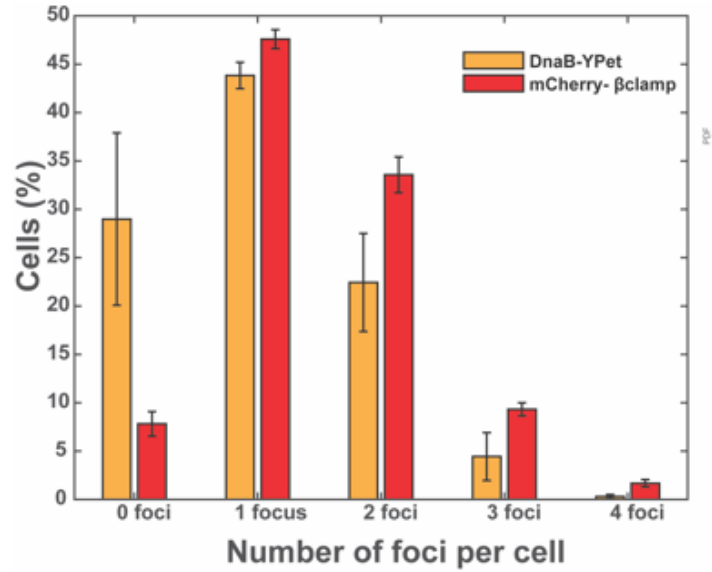


Figure 3.8. Histograms showing percentages of cells with 0, 1, 2, 3, or 4 DnaB-YPet and β -clamp foci in undamaged cells. The height represents the mean of each foci category and error bars represent the standard deviation. Data from 2171 cells and 2 experimental days.

Figure 3.9 shows the overall (i.e., all foci: 1, 2, 3 and 4) spatial distribution for DnaB and β -clamp described above. The locations of the foci have been plotted on the long axis of the cell to show the respective localizations of DnaB and β -clamp. Qualitatively, the profiles of the two proteins closely resemble one other, with a discernible peak at the mid-cell position for undamaged cells and quantitatively, as measured by the **variance** (σ^2) in the dataset, DnaB (0.059) and β -clamp (0.053) are similar as well. Here, the variance is defined as the square of standard deviation for the spatial distribution data; this variance represents the spread of the foci on either side of the mid-cell position 0 (arbitrary units **a.u.**, x- axis). As both the proteins are replisome subunits, similarity in the spatial profiles for DnaB and β -clamp, and thus in their variance, is expected *a priori*.

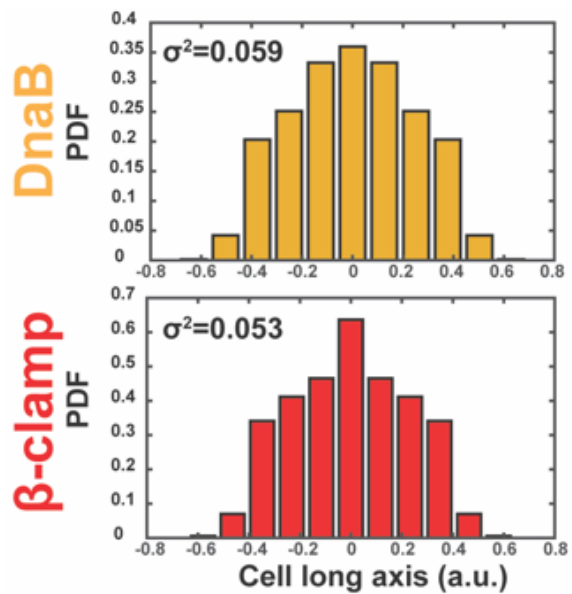


Figure 3.9. Overall spatial distribution for DnaB-YPet and β -clamp in undamaged cells (all foci: 1, 2, 3 and 4). Top yellow figure shows DnaB and bottom red figure shows β -clamp, spatial distribution of foci respectively. Variance (σ^2) is the square of standard deviation of the data (foci), dispersed on the cell long axis (arbitrary units, a.u.) with values close to 0 implying probability for mid-cell position. Analysis from 2171 undamaged cells and 2 experimental days

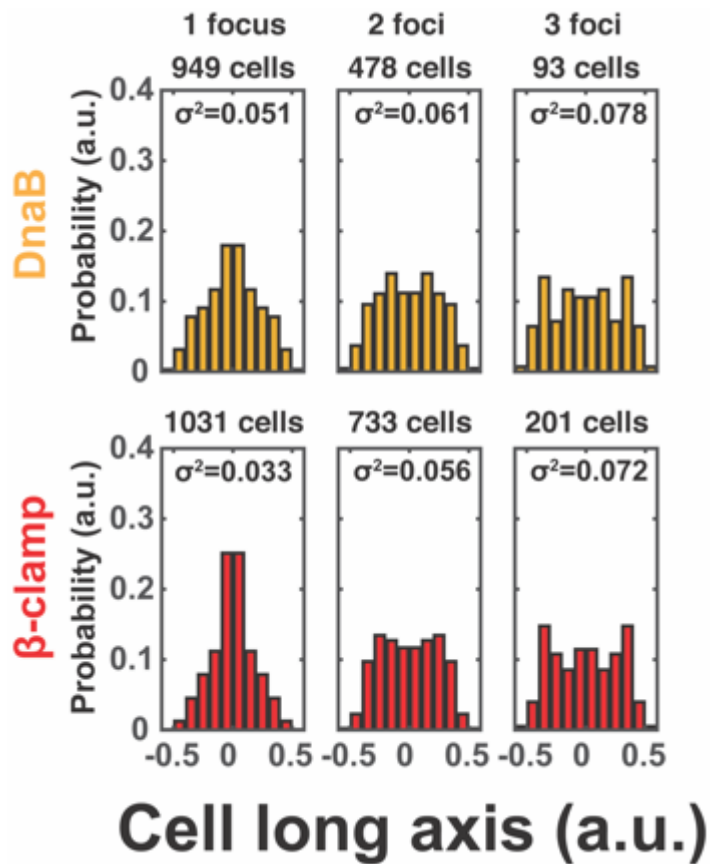
While both the profiles appear similar to a normal distribution, for β -clamp the spatial distribution consists of at least two populations. The first population located at the mid-cell position (leading to the Gaussian shape appearance) and a secondary

population, localized off-center on either side of mid-cell, causing two peaks adjacent to the cell poles in the spatial distribution plot. In the following section, we describe the spatial distribution profile of these proteins when the cell populations are subdivided into individual foci categories, in contrast to overall foci spatial distribution shown here. In the next section, we also explain why we do so.

3.4.2.5 Spatial distribution of DnaB foci (categorized: 1, 2 and 3) with respect to the replisome

In the preceding section, we have shown the reader the number of foci for DnaB and β -clamp (replisome) and also their respective overall spatial distribution (i.e., all foci combined). In this section, we present the same spatial distribution data, but now subdivided into cells containing 1, 2 and 3 foci (we refrain from commenting on cells with 4 foci category, as we have found upon categorizing foci here that fewer cells show such a phenomenon).

in the preceding section, the overall spatial distribution has been shown as part of characterization of the baseline properties, but to probe our research question (i.e., the outcome/behaviour of DnaB upon UV mediated DNA damage), analysing spatial distribution of foci when it is categorized (as 1, 2 and 3) has higher relevance. This is because if the DnaB foci have been perturbed (e.g., if the replisome components are uncoupled, **see section 3.5** for details and hypothesis 3 therein), then studying foci, not as all combined, but as categories shows us whether the spatial localization of different types of foci (1, 2 and 3) have changed with respect to the replisome after UV exposure and especially if and when some foci, if not all, have been affected.



In **figure 3.10**, we show the spatial distribution on the cell long axis for DnaB in yellow (1, 2 and 3 foci). For comparison, we present the spatial distribution data for β -clamp in red (1, 2 and 3 foci) below DnaB plots. As evidenced by variance σ^2 scores (absolute mid-cell position has score 0), in the '1 focus' category both proteins show a strong mid-cell preference, while

Figure 3.10. Spatial distribution for DnaB-YPet and β -clamp in undamaged cells categorized as 1, 2 and 3 foci. The DnaB (top yellow) and β -clamp (bottom red) spatial distribution of foci, respectively. Variance (σ^2) is the square of standard deviation of the data (foci), dispersed on the cell long axis (arbitrary units, a.u.) with values close to 0 implying probability for mid-cell position. Analysis from 2171 undamaged cells and 2 experimental days.

in the '2 foci' category there is a broadened profile for both proteins. These results are in accordance with a recent study wherein the positions of β -clamp foci (and other replisome components) were tracked in *E.coli* (16). β -clamp foci, being proxy for replisomes, were found to have mid-cell localization probability, until replication re-initiation when these foci were then found at quarter cell positions. As a corollary, we add here that DnaB being rather the most stable component of the replisome, should be expected to occupy the same positions as β -clamp *a priori*.

As expected, in the '2 foci' case two small peaks are observed off-center (at approximately the quarter cell positions); these likely represent replisomes that have spatially separated from each other. In the '3 foci' category, a broadened profile is still visible, with the two small peaks even closer to the cell poles, but now also a novel peak at the cell center, suggesting re-initiation of replication in a fraction of the (unsynchronized) cell population. Overall, there is much similarity between the spatial distribution profiles for both DnaB and β -clamp for any foci category, of which the '1 focus' category seemingly has the greatest similarity, as reflected by the variance scores. (We have refrained from presenting on 4 foci scenarios, as few cells show this phenomenon).

In summary here, with the description of the DnaB parameters (foci, stoichiometry and spatial distribution) in undamaged cells as a reference, we move towards addressing our research question in the next section. We measure these parameters again but now after UV exposure onto the cells.

3.4.3 DnaB behavior after UV exposure

In the previous **section 3.4.2**, we have characterized the behavior of DnaB and β -clamp under undamaged conditions, which serves as a baseline for experiments here. We apply the same parameters again: foci, stoichiometry and spatial distribution, but measure them after UV exposure. We describe each of these parameters below and finally we assess them in **section 3.5 Discussion** for what our data implies towards hypotheses.

However, before studying the experimental data, we first highlight the characterization of our UV infliction protocol (see **section 3.6 Materials and methods**, under the heading **UV radiation on cells**). **Figure S3.2** shows how we used a power meter to calculate UV-1 s and UV- 2 s exposures generated by a UV crosslinker machine. Illuminating the machine for 1 s and 2 s produced incident energy doses of 1.21 J/m² and 10.88 J/m², respectively on the bacterial cells. Subsequent time lapse phase contrast images are shown in **figure S3.3** for wild type and LB1 (*dnaB-Ypet*, *mCherry-dnaN*) cells at timepoints 0, 6 and 12 hours (undamaged condition, UV-1 s and UV- 2s exposures). Red and purple boxes highlight filamentous and colony forming cells (as examples) respectively, after UV exposure, demonstrating the deleterious effects of UV exposure. Furthermore, we have ascertained the deleterious effects of UV-1 s and 2 s, on cells by performing growth curves for *E.coli* growing in the M9-agarose pad, shown in **figure S3.4**. The strains WT and LB1 were calculated to have doubling times of 1.40 ± 0.05 h and 1.92 ± 0.03 h, respectively, in the undamaged condition.

3.4.3.1 DnaB foci behavior after UV exposure with respect to the replisome

First, we present here the results of mean number of foci per cell for both DnaB and the β -clamp. As shown in **figure 3.11A, B**, the mean number of foci (DnaB and β -clamp) per cell for undamaged condition and for timepoints 5, 10 and 20 minutes after UV-exposure (1 s: 1.21 J/m² energy dose) and (2 s: 10.88 J/m² energy dose) is tracked.

After UV-1 s exposure, the mean number of DnaB foci per cell shows no remarkable change across time. However, the mean number of β -clamp foci per cell seems to decrease over time. This pattern is also similar for both proteins for same timepoints after UV-2 s exposure. Our results here are similar to a recent study, which also reported a ‘small’ decrease from ~ 1.57 to ~ 1.39 for average number of DnaB foci per cell after 5 min of varying UV exposure (0, 10, 25, 50 J/m²), see **section 3.5 Discussion** for further comparison (21)).

While, analysis of the mean number of foci (and change thereof) provides a useful overview and indicates whether there has been any

effect of UV exposure on the number of foci, however, such analysis of mean number of foci may also mask or average out the effects of UV exposure, especially if there are changes only to a particular foci distribution but not to others. Thus, we next visualize how the numbers of cells containing foci numbers are distributed (i.e., as categories: 0, 1, 2, 3 and 4 foci) for both DnaB and β -clamp, under the same conditions of UV-1 s and UV-2 s and imaging at timepoints 5, 10 and 20 min after UV exposure (**figure 3.12**)

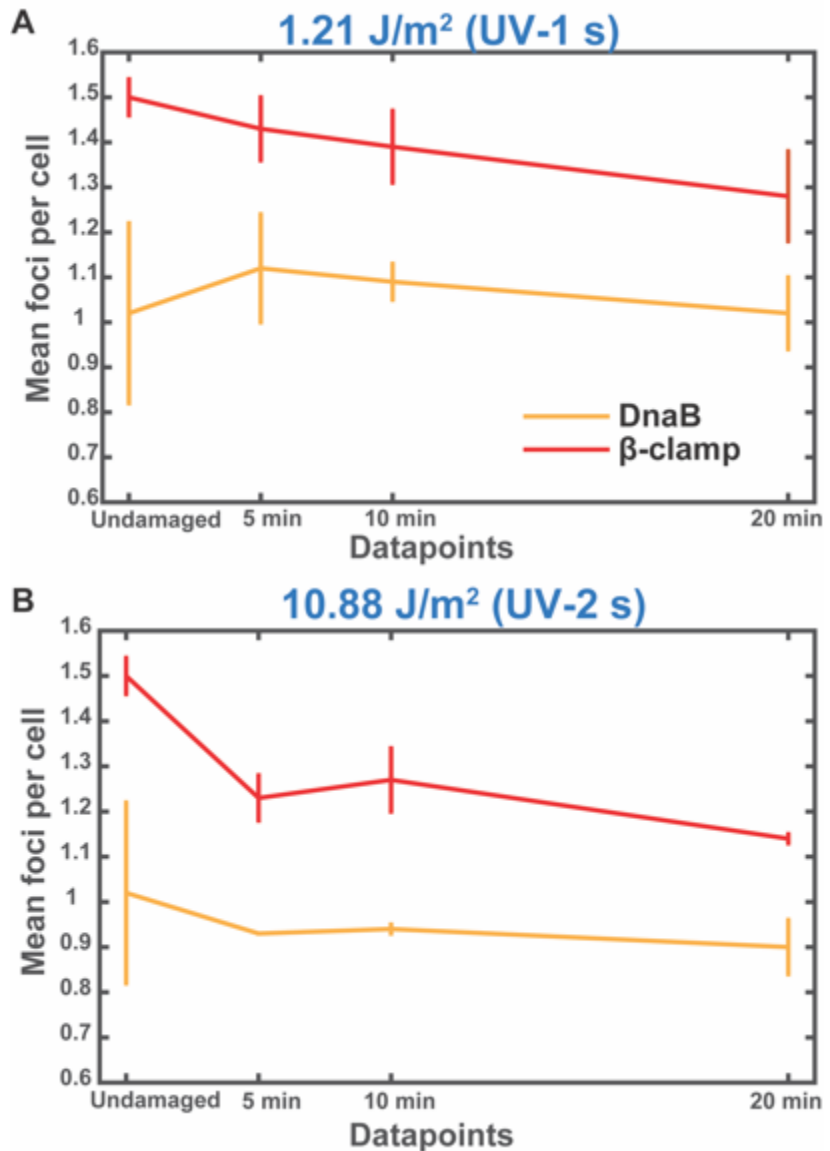


Figure 3.11. DnaB-YPet and β -clamp foci after UV exposure. **A.** The mean foci per cell, for undamaged condition (2171 cells) and cells at timepoints 5, 10 and 20 min after UV-1 s exposure (1473, 1295 and 1522 cells respectively). **B.** The mean foci per cell, for undamaged condition and cells at timepoints 5, 10 and 20 min after UV-2 s exposure (758, 775 and 682 cells respectively). Errors bars represent standard deviation. Datasets from at least 2 experimental days for all datapoints.

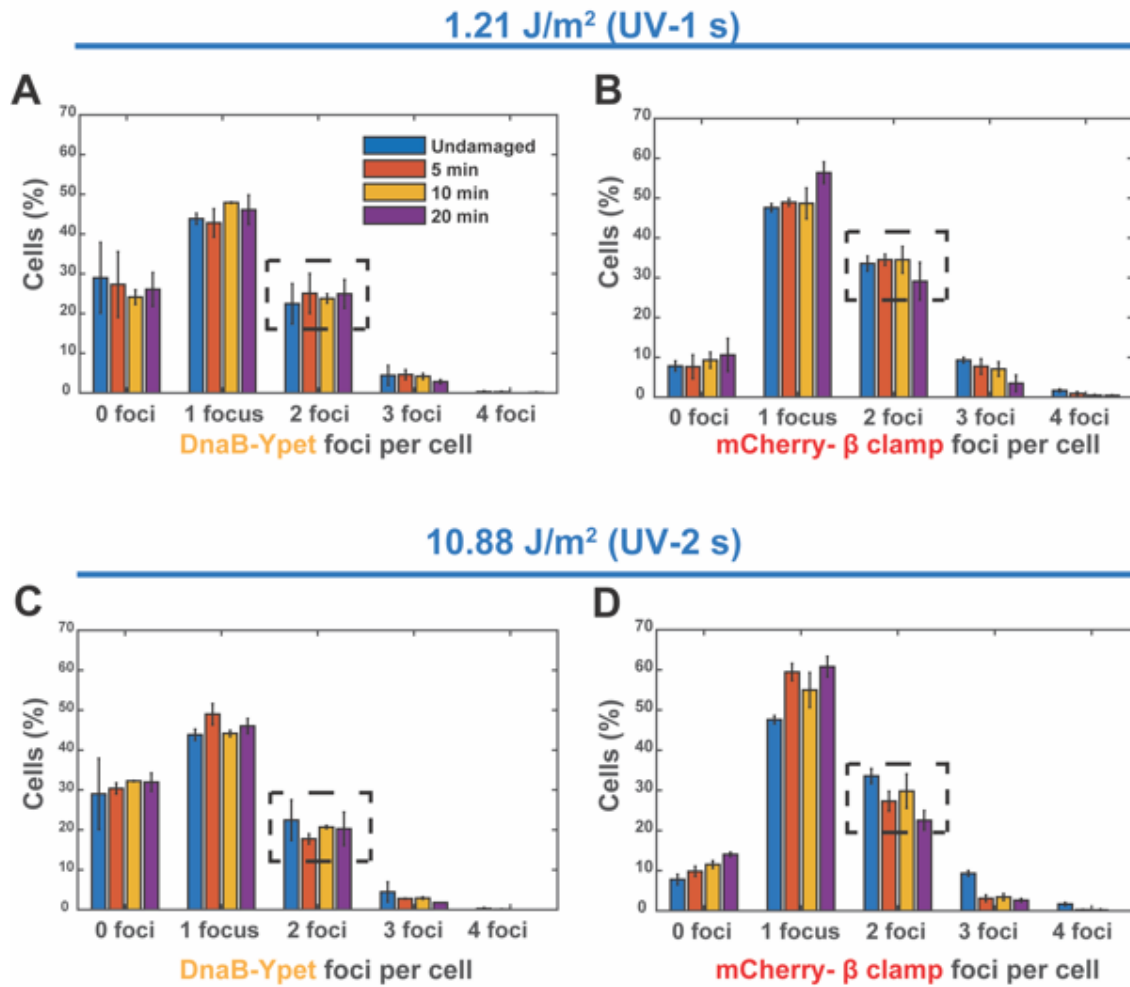


Figure 3.12. DnaB-YPet and β-clamp foci after UV exposure. **A, B** describe how categorized foci (0, 1, 2, 3 and 4 foci) are distributed after UV-1 s exposure (analysis from 2171, 1473, 1295 and 1522 cells for undamaged, 5, 10 and 20 min timepoints after UV exposure respectively) for DnaB (top left) and β-clamp (top right). **C, D** represent the same data characteristics but after UV- 2 s exposure (analysis from 2171, 758, 775 and 682 cells for undamaged, 5, 10 and 20 min timepoints after UV exposure, respectively), DnaB (bottom left) and β-clamp (bottom right). Errors bars represent standard deviation. Datasets from at least 2 experimental days for all datapoints. Note: Black dashed boxes shown to highlight '2 foci' histograms for DnaB (almost steady) and β-clamp (decreasing trend) with time (undamaged versus t=20 min) after UV exposure (1 s and 2 s).

Furthermore, in **figure 3.12 C, D** showing the effects of UV-2 s exposure on DnaB and β-clamp respectively, DnaB perturbation is minimal across foci categories and time points. Interestingly, the data for the β-clamp still holds an upward pattern for the '0 foci' and '1 focus' categories, while '2 foci' and '3 foci' histograms show a decreasing pattern, as seen after UV-1 s exposure.

Furthermore, in **figure 3.12 C, D** showing the effects of UV-2 s exposure on DnaB and β-clamp respectively, DnaB perturbation is minimal across foci categories and time points. Interestingly, the data for the β-clamp still holds an upward pattern for the '0 foci' and '1 focus'

categories, while '2 foci' and '3 foci' histograms show a decreasing pattern, as seen after UV-1 s exposure.

As shown in black boxes (dashed lines) for '2 foci' histograms of **figure 3.12**, when we compare the undamaged condition histograms with that of timepoint t=20 min (UV- 1 s and 2 s), DnaB is almost steady, but β -clamp shows a decline.

In summary here, our observations on the effects of 2 s UV-exposure on cells here show a decrease of β -clamp foci per cell over time at 20 min timepoint for the '2 foci' category, which is progressive with higher UV exposure. This decrease in β -clamp '2 foci' category at 20 min timepoint for both UV- 1 s and UV- 2 s may be important to notice and we find it relevant for discussion in **section 3.5**. (We have refrained from commenting 3 foci and 4 foci categories, as few cells show this phenomenon).

3.4.3.2 DnaB stoichiometry after UV exposure

As described in **section 3.3** about the three parameters (number of foci, stoichiometry and spatial distribution) to probe our research question, the stoichiometry parameter is unique. As opposed to number of foci and spatial distribution analyses, which are also compared to the replisome marker to test hypotheses (see **section 3.5 Discussion**), the stoichiometry analysis is relatively straightforward. This is simply because a reduction in DnaB stoichiometry after UV exposure, without any further comparison to the replisome marker, may provide evidence of DnaB 'fall off' or dissociation hypothesis. Therefore, in this section, we seek evidence of DnaB outcomes (fall off/ stay put, see **section 3.1 Introduction**), by just studying the numbers.

As reported in **section 3.4.2.2**, we see two peaks for DnaB molecules in foci (corresponding to 6 and 12 DnaB molecules, respectively). We have explained previously in **section 3.2** why this may happen when we see a focus under the microscope. In **figure 3.13** we present the DnaB stoichiometry analyses after UV exposure (**Figure 3.13 A** (undamaged cells) is reproduced here for comparison).

In **figure 3.13 B, C, D**, the stoichiometry results of UV-1 s (1.21 J/m^2) exposure are presented, for imaging done at timepoints 5, 10 and 20 min after UV exposure, respectively. Using the same analysis protocol as seen for graphs in **section 3.4.2.2**, we find that the DnaB stoichiometry has not been perturbed after UV-1 s exposure. In each case of 5, 10 and 20 min, the two peaks of DnaB report a stoichiometry of about 6 and 12 molecules and importantly, stays constant with time passage after UV exposure. In **figure 3.13 E, F, G**, the stoichiometry results of UV-2 s (10.88 J/m^2) exposure are presented, for imaging done at timepoints 5, 10 and 20 min after UV exposure, respectively. In each case of 5, 10 and 20 min, DnaB stoichiometry is again close to 6 and 12 molecules and stays constant, irrespective of time passage after UV exposure. Because the stoichiometry of DnaB is unchanged after UV-1 s and UV- 2 s exposures, with respect to the undamaged cells, we do not find any direct evidence of DnaB 'fall off' or dissociation, so far from our analyses here.

Furthermore, while there is no change of stoichiometry after UV exposure and time passage, we also looked at our data here to see the width (i.e., x- axis values) of the Gaussians G1 (red) and G2 (yellow). This is because if there is a change in the width of the Gaussians, it

may be an evidence that partial dissociation or disintegration of DnaB may have occurred. Partial disintegration is a scenario envisioned wherein some DnaB monomers may remain bound to the DNA despite the absence of an encircling hexamer.

In this regard, the **figure 3.13 B, C and D** for DnaB stoichiometry at different timepoints after UV-1 s exposure show no change for Gaussian G1, with x-axis values extending from 0 to ~15, similar to the undamaged cells. Moreover, the values for Gaussian G2 also show no remarkable change with x-axis values extending from 0 to ~25. Additionally, **figure 3.13 E, F and G** for DnaB stoichiometry at different timepoints after UV-2 s exposure (likewise UV-1 s) show no change for Gaussian G1, with x-axis values extending from 0 to ~15, similar to the undamaged cells. The values for Gaussian G2 also show no remarkable change.

In summary here, the stoichiometry analyses inform us that we do not see a DnaB 'fall off' scenario. Moreover, by carefully observing the width of the Gaussians G1 and G2 we also do not gather evidence for a partial DnaB dissociation, compared to undamaged cells.

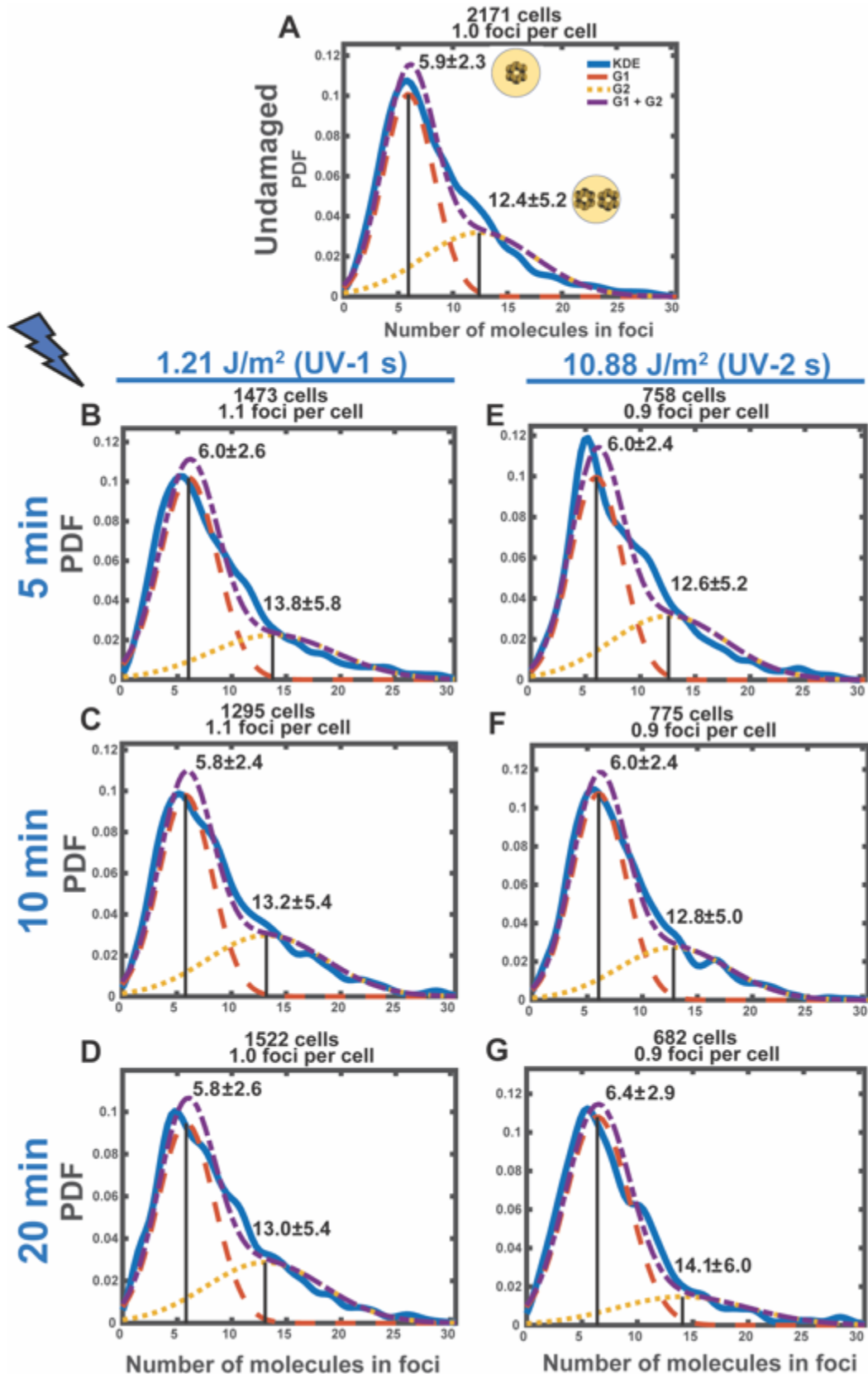


Figure 3.13. DnaB-YPet stoichiometry after UV exposure. **A.** DnaB Stoichiometry in undamaged cells. **B, C** and **D** profiles represent DnaB-YPet stoichiometry at 5, 10 and 20 min (UV- 1s) respectively. **E, F** and **G** profiles represent DnaB-YPet stoichiometry at 5, 10 and 20 min (UV- 2s) respectively. The blue line represents the kernel density over raw data, while the red, dotted yellow and dashed purple lines show represent Gaussian fits G1, G2 and their sum (G1+G2) respectively. Values represent mean Gaussian \pm standard deviation, G1 and G2.

3.4.3.3 Spatial distribution of DnaB foci after UV exposure, with respect to the replisome

As seen from our foci analyses (**figure 3.12**, 0, 1, 2, 3 and 4 foci) of DnaB and β -clamp upon UV exposure in **section 3.4.3.1**, we have noted that number of foci (DnaB) remains almost constant before and after UV exposure. However, specifically for the '2 foci' category at $t=20$ min, both for UV-1 s and UV-2 s exposures, β -clamp progressively shows a decreasing trend, which is more profound after UV-2 s.

If this implies that DnaB and β -clamp foci have moved apart or de-localized after UV exposure, then spatial distribution analysis of foci should provide evidence for it. We first report on the overall (i.e., all foci combined: 1, 2, 3 and 4) spatial distribution of DnaB and β -clamp upon UV exposure (**figure 3.14**) and then delve on spatial distribution of categorized foci (i.e., cells with 1, 2 and 3 foci separately) for both proteins, also upon UV exposure (**figure 3.15**).

In **figure 3.14 B, C and D**, the overall spatial distributions of DnaB and β -clamp foci over time after 1 second of UV-exposure are shown. We first describe on the spatial distribution of DnaB, which seems to show slight changes 5 minutes after the exposure, variance (σ^2) = 0.069, compared to the undamaged condition. The mid-cell peak as seen in the undamaged situation has flattened and seems like a plateau, indicating a broader spatial distribution over the length of the cell, after UV-damage. This broadening effect persists qualitatively after 10 min ($\sigma^2 = 0.066$) and 20 min ($\sigma^2 = 0.067$), though after 20 minutes there is a rise in the number of DnaB foci at the mid-cell position again, as the variance score also shows (variance score closer to 0 implies mid-cell position). In stark contrast to DnaB foci, the position of β -clamp foci stays mostly located in the mid-cell position, at all timepoints (5, 10 and 20 min) after UV-1 s exposure ($\sigma^2 = 0.049$, 0.046 and 0.047, respectively). While the β -clamp qualitatively showed a broad distribution in the undamaged situation ($\sigma^2 = 0.053$), after UV-exposure it displays a stronger mid-cell position, which indicates perhaps that DnaB and β -clamp respond differently to UV-mediated DNA damage. For both two proteins, we see in **figure 3.14 D-F** that the spatial profiles do not differ much after UV-2s exposure relative to UV-1s.

Having looked at the overall spatial distribution here, next we comment on the spatial distribution of categorized foci (i.e., cells with 1, 2 and 3 foci separately). We do so because the effect of UV exposure on foci dynamics may be masked or averaged out, if only a particular foci category has been perturbed rather than all of them. Moreover, this has significance for the **hypothesis 3**: a model of DnaB 'uncoupling' from the replisome (see **section 3.5 Discussion**), which is easier to study if foci are separately categorized (as 1, 2 and 3) and their spatial distribution profile compared to that of the replisome marker in each case.

In **figure 3.15 B, C and D**, which show the spatial distribution of DnaB and at time points of 5, 10 and 20 min respectively after UV 1 s exposure, DnaB '1 focus' seems to have a broad distribution but with a preference for mid-cell localization at all time points. In the case of DnaB '2 foci' category, there seems to be 2 off-centre peaks (1/4 and 3/4 long axis cell positions) across timepoints. After UV-1 s exposure, β -clamp '1 focus' holds a strong mid-cell preference while β -clamp '2 foci' holds off-centre positions but in closer proximity to mid-cell than DnaB does. Overall, we find that profiles of DnaB and β -clamp do not exactly overlap each other. After UV-1 s exposure, this is also reflected in the variance scores for the two proteins (shown for each plot therein). The DnaB (σ^2) score for '1 focus' is ~ 0.059 , while that of β -clamp '1

focus' score is ~ 0.034 across timepoints. Similarly, the DnaB (σ^2) score for '2 foci' and '3 foci' exist at ~ 0.072 and ~ 0.078 respectively, while that of β -clamp (σ^2) scores for '2 foci' and '3 foci' scores come to ~ 0.051 and ~ 0.067 , across timepoints.

Next, in figure **3.15 E- G**, which shows the spatial distribution of DnaB after UV-2 s and at time points of 5, 10 and 20 min respectively, we find the DnaB profile ('1 focus' and '2 foci') shapes almost similar as in UV-1 s, except that they are more pronounced here (i.e., if there are peaks after UV- 1 s, those peaks are higher (y-axis) after UV- 2 s) . Interestingly and at the same time, β -clamp '1 focus' holds the same mid-cell position across timepoints. Further, the β -clamp '2 foci' off-centre peaks seen in UV-1 s treatment, get more pronounced here. Overall, it is striking to see that β -clamp favour a mid-cell or off-centre position constantly, while DnaB profile seems to evolve with timepoints. Moreover, the variance scores also underscore this qualitative description of UV- 2 s exposure on cells. The DnaB (σ^2) score for '1 focus' is ~ 0.056 , while that of β -clamp '1 focus' score is ~ 0.027 across timepoints. Similarly, the DnaB (σ^2) score for '2 foci' and '3 foci' exist at ~ 0.068 and ~ 0.078 respectively, while that of β -clamp (σ^2) scores for '2 foci' and '3 foci' scores come to ~ 0.044 and ~ 0.061 , across timepoints.

In summary, our data on spatial distribution qualitatively and quantitatively tracks DnaB and replisome foci, before and after UV exposure. While **figure 3.14** on overall spatial distribution presents an overview, **figure 3.15** on spatial distribution of categorized foci shows how the spatial distribution of the DnaB 1 'focus' evolves or changes with timepoints after UV, while β -clamp '1 focus' is always steady with a sharp mid-cell peak. This has consequences for hypothesis 3 mentioned in **section 3.5**, because the replisome may have a preferred mid-cell localization, while DnaB seemingly does not.

Furthermore, our observations of '2 foci' and '3 foci' extend support to the idea that these two proteins, which nevertheless work together at the replisome, respond differently to UV exposure. After UV-2 s, DnaB has a flattened profile for both foci categories, while the β -clamp always displays an off-centre or quarter cell position for the 2 foci category (this observation being most pronounced at $t=20$ min).

In the next section, we put together our observations on foci, stoichiometry and spatial distribution and see what is the probable 'fate' of DnaB after UV exposure.

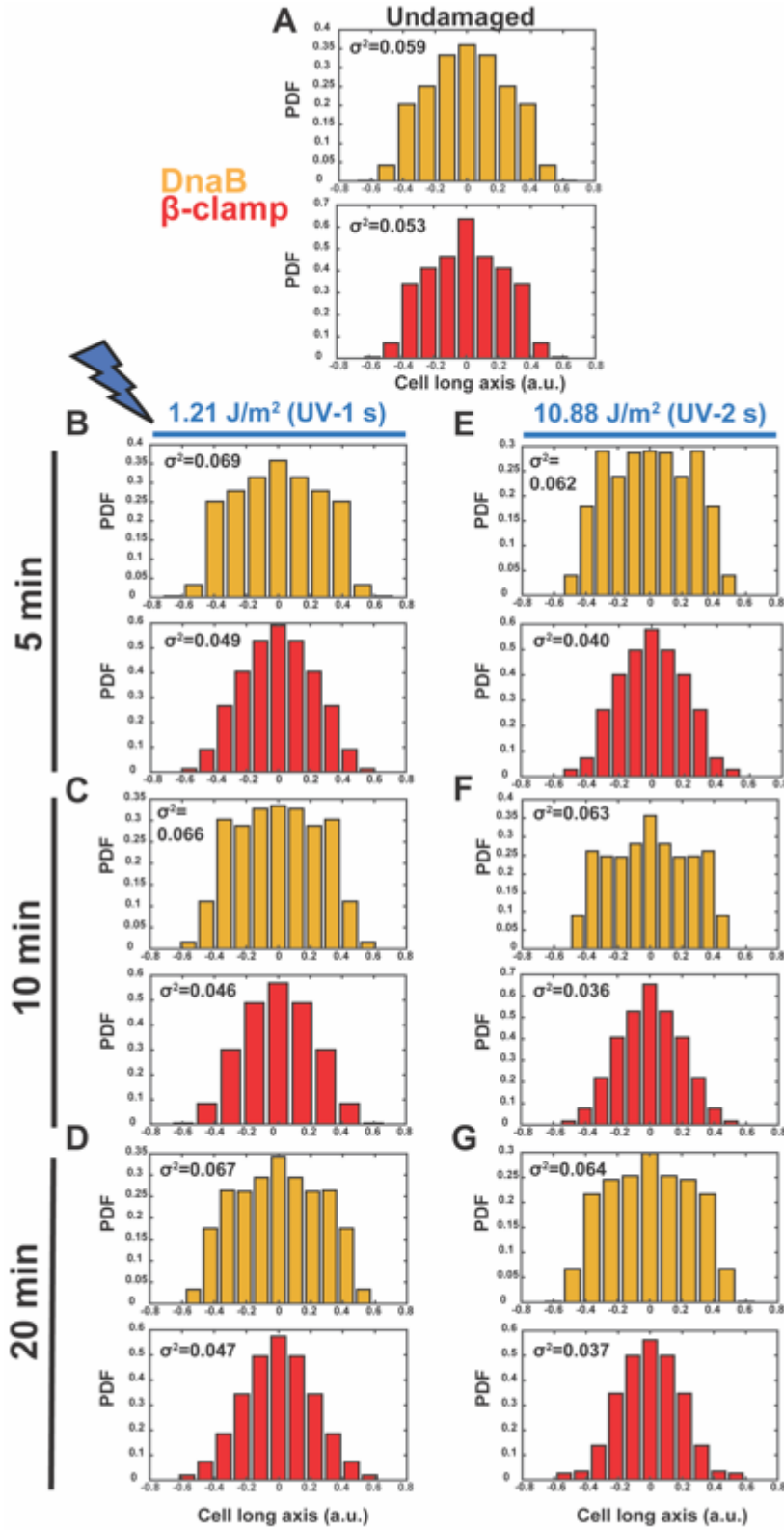


Figure 3.14. Spatial distribution for DnaB-YPet and β -clamp (all foci). **A.** Spatial distribution in undamaged cells for all foci. **B, C** and **D** show spatial distribution after UV-1 s at timepoints 5, 10 and 20 min respectively for all foci. **E, F** and **G** show spatial distribution for all foci after UV-2 s for the same time points. The variance (σ^2) is the square of standard deviation of the data (foci), dispersed on the cell long axis (arbitrary units, a.u.) with values close to 0 implying probability for mid-cell position.

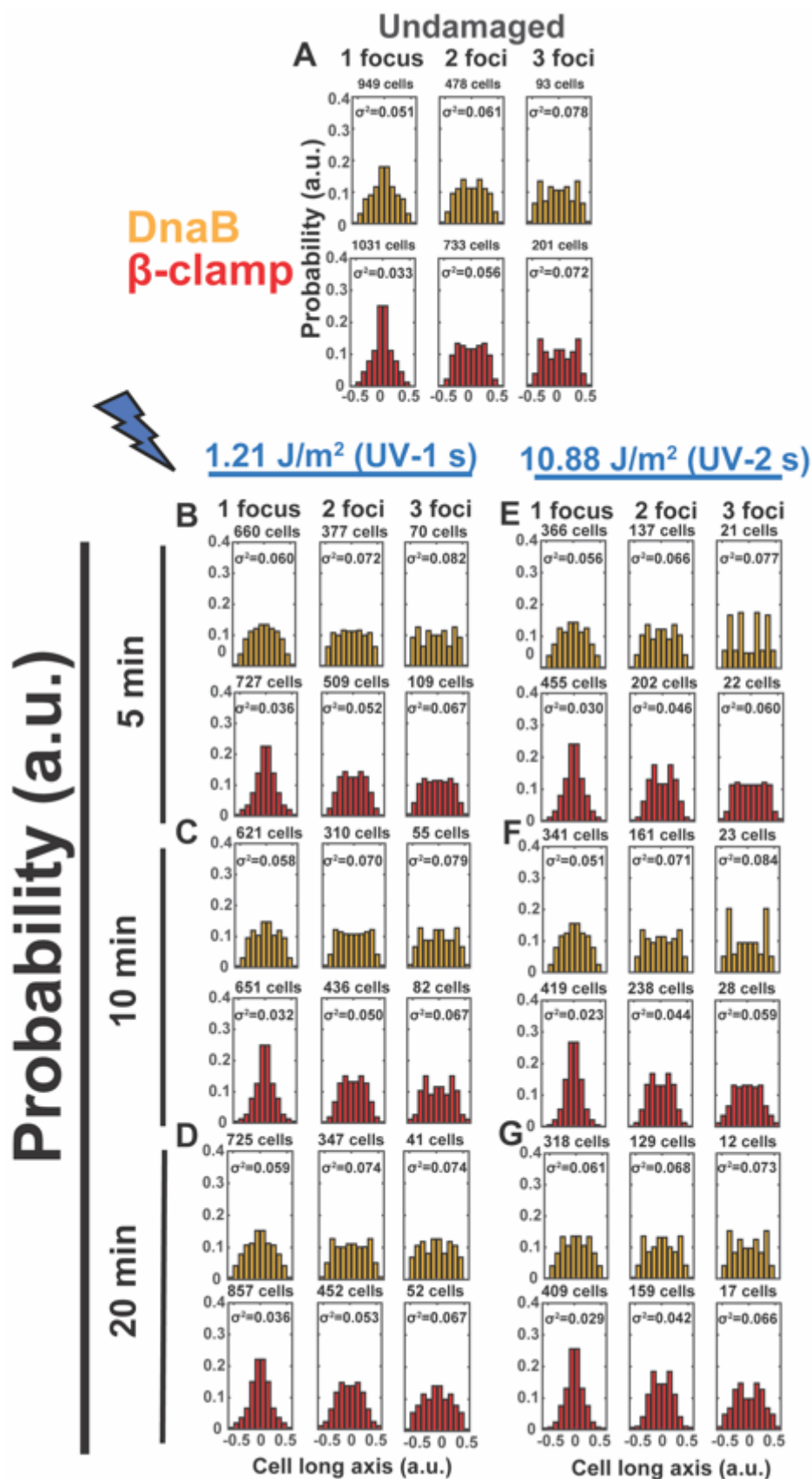


Figure 3.15. Spatial distribution on cell long axis for DnaB-YPet and β -clamp (1, 2 and 3 foci). **A.** Spatial distribution of foci in undamaged cells. **B, C** and **D** show spatial distribution for foci categories after UV-1 s at timepoints 5, 10 and 20 min respectively. **E, F** and **G** show spatial distribution for foci categories after UV-2 s for the same time points. The variance (σ^2) is the square of standard deviation of the data (foci), dispersed on the cell long axis (arbitrary units, a.u.) with values close to 0 implying probability for mid-cell position.

3.5 Discussion

We began this research project with the aim of understanding DnaB helicase behaviour *in vivo*, upon UV mediated damage and since the outset, our assumptions have been shaped by existing literature. The existing literature provides an excellent understanding on DnaB and the replisome in general. However, when we juxtaposed and compared studies from different laboratories, we aimed to find a consensus and thereby arrived at our research question. Our research question on the fate of DnaB, thus began as an attempt to synthesize new knowledge from already existing evidences.

But then, even after being cognizant of differences which *in vitro* versus *in vivo* approaches may exert, we could not arrive at a clear conclusion after comparing literature. The different viewpoints are detailed below, which were introduced briefly in the **section 3.1**:

Hypothesis 1: Our knowledge over the years that helicase loaders exist (apart from DnaC which is involved at replication initiation), and that multiple proteins (such as PriA, PriC, PriC and DnaT) are involved in multiple pathways, to act together and rescue stalled replication forks reveals the importance of restart mechanisms. There are at least 3 restart pathways *in vivo* hypothesized with these factors, all of which serve to reload DnaB helicase on genomic sites far removed from the origin of replication, as a key step in replication after fork stalling (6). In other words, replicative helicase reloading is conceivable only if the helicase no longer 'loaded' on DNA and has 'fallen off' the intact replisome traversing on DNA. This may be thought of as the orthodox view from the evolutionary standpoint, due to the fact that helicase re-loaders also exist.

Hypothesis 2: A seminal study published in 2013 challenged this view, when they found evidence that DnaB helicase and DnaG primase may avoid such conceivable fall off, rather remain associated with the stalled replication fork to act as a 'licensing' factor for impending replication restart (15). While the study has an impressive array of experiments for such hypothesis, this viewpoint begets the question- when do helicase re-loaders, which exist, work if DnaB never falls off the replisome and reloading is not required? In other words, do both 'fall off' and 'stay put' DnaB scenarios occur in principle and arbitrarily, without being mutually exclusive?

Hypothesis 3: While our research was in progress, an interesting study emerged in 2019 which suggested an alternative hypothesis- DnaB may rather 'uncouple' from other replisome components at a stalled replication fork (21). 'Uncoupling' as the term implies, DnaB no longer works in coordination with PolIIIHE- the former unzipping DNA ahead while the latter is stalled behind. In this model, DnaB neither stays put *in situ* nor falls off the replisome for reassembly. Importantly in this hypothesis, the role of the restart pathways and helicase re-loaders remain also unclear, if and when they operate to reload DnaB.

Thus, in this context and acknowledging different viewpoints of DnaB outcomes after UV exposure, we analyse our research findings here to find a consensus. We state first the stoichiometry results because they were the only analyses which did not show any perturbation after UV exposure.

From our stoichiometry results (**figure 3.13**) we are not able to comment directly on the DnaB fate. The unchanged stoichiometry (undamaged and UV damage) we see, could be the result of at least three reasons, now in light of recent literature- that the helicase DnaB stays put at the replisome after UV exposure (in agreement with **Hypothesis 2**) or keeps unwinding DNA after UV exposure with intact hexamers as a necessity (in agreement with **Hypothesis 3**). The third possibility may be our technical inadequacy to detect such a stoichiometry change on wide-field fluorescence microscopy. Surely, we did not find here any evidence for DnaB fall off (**Hypothesis 1**), as stoichiometry reduction would have pointed.

However, foci distribution analyses (**figure 3.12**) of DnaB with respect to the replisome (β -clamp) has shed light on some interesting observations. While the '**0 foci**' category distribution is almost unchanged for both proteins (the distributions for UV-1 s and UV- 2 s relative to undamaged), which is also expected because UV light would not be a causative factor for replication or for formation of replisome foci to our knowledge, there is a marginal increase for **β -clamp-0 foci** increase from 8% (undamaged) to 14% (UV-2 s, 20 min).

The greatest number of cells (~ 50%) show '**1 focus**' for both proteins and under any condition in our study. **DnaB** seems to show almost no change in this category after UV exposure, while **β -clamp** seems to have an upward trend after UV exposure (47%, undamaged to 60%, UV-2 s at 20 min).

Further, about a quarter of cells, show '**2 foci**' in undamaged conditions for both proteins, but interestingly these numbers change with UV exposure and timepoints. For helicase **DnaB**, the numbers of '2 foci' category remain almost constant -from 26% through 24% to 23% after 1 s UV (5, 10 and 20 min respectively). However, right after UV-2 s exposure, these numbers drop for DnaB to 18% (5 min) and then gradually rise to 21% (10 min). In the case of **β -clamp** and '2 foci' distribution, β -clamp is responsive to UV for both exposure times 1 s and 2 s. There is a discernible decreasing trend from 35% through 34% to 30% in the case of 1 s exposure (5, 10 and 20 min respectively), the percentage distribution stays almost constant (but lower than undamaged condition: 34%). Also compared to this undamaged condition, the β -clamp '2 foci' numbers are lower after UV-2 s exposure- 27%, 31% and 23% for 5, 10 and 20 min respectively, suggesting that our observation is perhaps not arbitrary or artefactual for β -clamp decrease here.

To compare our foci distributions with that of reported literature, we find that another laboratory (β -clamp, undamaged cells) also finds about half the analysed cell population (58%) having 1 foci distribution (16). They also report a cumulative distribution for a quarter of cells (26%) for 2 foci (15% of these '2 foci' are proximal, and 11% of these '2 foci' are spatially distant), in close agreement with us on the cumulative number. However, they find lower number of cells with 0 foci (10%), unlike our observations. To be noted, the study was also performed with imaging at 25°C.

The study which forms the basis of **Hypothesis 3** (ref. (21), figure 1 therein), reported the overall marginal decrease of DnaB 'foci per cell' (~1.57 to 1.39) with increasing amount of UV dosage (0, 10, 25 and 50 J/m²) (21). The authors report of a DnaB foci 'frequency' of about ~10 (0 foci), ~30 (1 focus) and ~50 (2 foci), which only changes marginally (<10 units, in each foci category): increase (after UV 25 J/m², 5 min after exposure) for the 0 foci and 1 focus categories and decrease for the 2 foci category. We find these changes not huge and similar to our numbers which show marginal difference in any category.

Interestingly, their investigation reveals a rise in β -clamp foci (1.9 to 2.5 average foci per cell) after 5 min of 25 J/m², in agreement with our β -clamp-1 focus numbers which rise (47%- 60%, all timepoints), although 2 foci numbers decrease (34%- 23%, all timepoints).

From the foci distribution analyses to conclude, we find that there is a gradual increase in **ratio (DnaB/ β -clamp)** for the 2 foci category, positively correlated with UV exposure and time passage. These ratios are 0.64, 0.76 and 0.82 (undamaged, UV-1 s 20 min and UV-2 s 20 min respectively). While the numbers of DnaB double foci category remain almost steady, the decrease of β -clamp double foci category has contributed to these ratios. Based on this observation, while we are unable to comment about **Hypothesis 1** and **2**, although we understand that **Hypothesis 3** may provide an explanation on the premise that replisome components and their respective foci are uncoupled. We think they (DnaB and replisome) are uncoupled because the foci numbers of these replisome components are affected after UV exposure independently of each other (compared to undamaged). If they are uncoupled and there has been spatial distance developed consequently, this should be evident in the spatial distribution analyses, which we turn next to.

To our understanding the spatial distribution should provide us with robust evidence for the uncoupling model, because the foci from the two replisome components should have same localization patterns in **undamaged** cells undergoing replication. This holds true if one looks at the undamaged cell profiles of **DnaB** and **β -clamp** in **figure 3.15 A**, for foci categories shown. The variance scores (σ^2) are also similar; the '1 focus' (0.051, 0.033), '2 foci' (0.061, 0.056) and '3 foci' (0.078, 0.072) profiles show a mid-cell peak, a broad or flattened profile with peaks off-centre and a broad or flattened profile with peaks closer to the cell poles, respectively, for both proteins (DnaB, β -clamp).

When compared to the undamaged situation, the profile of DnaB (**1 focus**) is found evolving in **both cases of UV-1 s and UV-2 s** across time points. The σ^2 scores are (UV-1 s 0.060, 0.058, 0.059; UV-2 s 0.056, 0.051, 0.061) In contrast, the profile of **β -clamp (1 focus)** is always with sharp mid-cell peak with σ^2 scores closer to 0 or mid-cell position (UV-1 s 0.036, 0.032, 0.036; UV-2 s 0.030, 0.023, 0.029), across all timepoints.

Furthermore, when compared to the undamaged situation, the profile of **DnaB (2 foci)** is found evolving in **both cases of UV-1 s and UV-2 s** across time points, with appearance of peaks towards the poles (UV-1 s: 10 min (σ^2 =0.070) and 20 min (σ^2 =0.074) timepoints, UV-2 s: all timepoints (σ^2 =0.066, 0.071, 0.068)). In contrast, the profile of **β -clamp (2 focus)** is always with two small peaks (smaller with respect to peak height (y-axis) of 1 focus profile) off centered with $\frac{1}{4}$ and $\frac{3}{4}$ cell long axis positions, across timepoints 5, 10 and 20 min. The corresponding σ^2 scores are: 0.052, 0.050 and 0.053 (UV-1 s) and 0.046, 0.044 and 0.042 (UV- 2s). Notably, the σ^2 scores for β -clamp here are closer to 0 or mid-cell than for DnaB. Moreover, to note with interest and significance, this twin peak profile is sharper and narrower qualitatively on the x-axis (UV 2 s- all timepoints, compared to undamaged and UV 1 s- all timepoints).

In conclusion, the spatial distribution analysis qualitatively and quantitatively shows that the two components of replisome, as plotted by their foci localization on the long cell axis, have profile shapes not similar to each other at the greatest dose applied and with time passage (UV-2 s, 20 min). This, we think provides evidence to the recently postulated **hypothesis 3** of replisome uncoupling. In support of their model (21), we hypothesize the reason that DnaB (**figure 3.15 G**) has a broadened profile after UV exposure is because it is still unwinding DNA and working through the chromosome. While the β -clamp or replisome, being subject to replisome stalling according to the hypothesis 3 model, may be localized at the mid-cell

position or near mid-cell (1 focus and 2 foci respectively, **figure 3.15 G**), notably this mid-cell localization which has also been reported by another study(16).

As a summary, while our observations provide further support for an alternative hypothesis of no fall off/ no stay put on DnaB fate (i.e., neither DnaB dissociation nor DnaB stalled, rather uncoupling) after UV mediated DNA damage, we remain curious as to what roles the reloading proteins and pathways may play biologically, especially with respect to DnaB. Future experiments with individual deletion of genes and in combination thereof, which work in reloading pathways will shed further light into DnaB functionality.

3.6 Materials and methods

Strain Engineering

All strains mentioned in this chapter are derivatives of *Escherichia coli* AB1157. A combination of two main methods- λ_{red} recombination and P1 phage transduction, has been mainly used to engineer strains.

For constructing the strain **LB1 (*dnaB-Ypet*, *mCherry-dnaN*)**, we have used a strain harboring YPet fluorescence tag at the C terminus of DnaB (a kind gift from Prof. David Sherratt, Oxford University). The genetic fragment *dnaB-Ypet* from this gifted strain was transferred to *E.coli* AB1157 wild type by P1 phage transduction, to create SDR7 (*dnaB-Ypet* with *kanR*) and SDR14 (*dnaB-Ypet* without *kanR*). By bringing the genetic fragment (*mCherry-dnaN* with *kanR*) in SDR14 by P1 phage transduction, the strain SDR35 was created. Because this strain harbored the *kanR* gene upstream of *mCherry-dnaN* (5'-3'), which may affect the expression of *dnaN*, the *kanR* gene was deleted by FLP recombination to create the final strain LB1.

For creating the strain **LB3 (*dnaB-mcherry*, *Ypet-dnaN*)**, we have used the strain BN1109 (26) as a host with the gene fragment (*Ypet-dnaN* with *kanR*). The gene *kanR* was deleted by FLP recombination (thereafter called strain LB2) and fluorescently tagged the gene locus *dnaB* with *mCherry* in LB2, for a C terminus fusion protein (*dnaB-mCherry* with *kanR*), using λ_{red} recombination.

The strain **LB10 (*dnaB-mCherry*, *dnaQ-Ypet*)** was created by first fluorescently tagging *dnaB* with *mCherry* in the wild type, for a C terminus fusion protein (*dnaB-mCherry* with *kanR*), using λ_{red} recombination (thereafter called strain LB4). Next, the fragment *kanR* was deleted by FLP recombination (thereafter called strain LB5), so that the fragment (*dnaQ-Ypet* with *kanR*) could be transferred into LB5 via P1 phage transduction from an in-house strain BN1514 and thereafter called LB10.

Please refer to the **Table S3.1.** for a summary on strain engineering. **Tables S3.2., S3.3 and S3.4.** further provide a summary of plasmids, linkers and DNA primers respectively used for this work.

Biochemicals, reagents, and media

All materials reported were purchased from Sigma- Aldrich, unless specified otherwise. Luria Bertani (LB) medium was used in bulk experiments, and M9-glycerol medium supplemented with the amino acids threonine, leucine, proline, histidine and arginine was used in imaging experiments, unless specified otherwise.

Growth curves

Strains were grown in LB broth for 16 h at 37 °C while shaking at 200 rpm. The next day, the culture was diluted in fresh LB medium (1:500) and the Optical Density at 600 nm wavelength (OD_{600}) was measured on a spectrophotometer (Ultrospec10, Amersham) at 30 min time intervals until a value of ~1.00 was recorded. Growth curves were obtained for three biological replicates measured on different days.

UV radiation on cells

For producing UV mediated DNA damage on cells, we have used a 254 nm UV crosslinker (Herolabs, GmbH) at 20°C, for a preset time: 1 s and 2 s. UV radiation was inflicted after 10 min of warm-up before every experiment. **Figure S3.2** shows UV dose calibration using a power meter (19196-C, Newport) after placing an agarose pad (1 cm*1 cm*0.2 cm) on the sensor area, also after 10 min warm-up.

Serial dilution assay to assess labeled strain functionality- undamaged versus UV damaged

Strains were grown in LB broth for 16 h at 37 °C while shaking at 200 rpm. LB agar plates were prepared by mixing LB-agar (1.5% w/v) and cast. For each strain, cells were plated from dilutions ranging from 10^{-1} to 10^{-8} and incubated for 16 h. In the case of UV damage, the plates with cells were irradiated inside the UV 254 nm crosslinker, prior to overnight incubation. The following day, the plates were photographed in a Gel Documentation System (Bio-Rad). Serial dilution experiments were obtained from at least two biological replicates done on different days.

Washing of microscope slides and coverslips

All washing steps were performed ultrasonically in Coplin jars, in the following order: 0.2% Hellmanex wash for 20 min, Milli-Q water wash twice for 5 min each, 100% ethanol wash for 20 min and finally, two repeats of a Milli-Q water wash for 5 min each. The slides and coverslips were then air-dried using a nitrogen pressure gun.

Preparation of cells for microscopy

The strains for imaging were grown in a primary culture overnight (M9-glycerol) at 37 °C while shaking at 200 rpm. The next day, these cells were diluted (1:10) in fresh M9-glycerol and grown under the same conditions for ~1.5 to 2 h, so that the OD_{600nm} ranged from ~0.15 to 0.20. These cells were centrifuged in a volume of 500 μ l to obtain a pellet. This pellet was then re-dissolved in fresh 50 μ l M9 glycerol. A volume of 2 μ l was loaded onto the agarose pad for imaging.

Preparation and loading of agarose pads for microscopy

To prepare agarose pads, 1.5% agarose (Ultrafine agarose, Invitrogen) in M9-glycerol was heated, cast and cut into pads (1 cm*1 cm*0.2 cm). Next, a cell suspension was placed on the top of the agarose pad and air dried. Thereafter, this pad was placed on a clean round cover-slip (# 1, Menzel Glaser), in such a way that the cell suspension side of the pad now faced the cover-slip. The casting of the pad and the loading of cells, were performed at room temperature.

Microscopy hardware

The time-lapse microscopy experiments were performed on a commercial Nikon Ti-E inverted microscope equipped with a 1.49 NA Apo TIRF 100X Oil immersion objective, a standard Nikon halogen lamp, a Nikon DS-Fi2 Charged Couple Device camera used for phase contrast imaging, and an iXon Ultra EMCCD camera (Andor) used for fluorescence detection. The microscope was surrounded by a temperature cage (Okolab) regulated via a temperature controller (Okolab Touch). Excitation light of wavelengths of 515 nm and 561 nm (provided by diode laser and a diode-pumped solid state laser, respectively; both lasers from Cobolt) was delivered at the objective via a laser combiner LightHUB (Omicron). Inside the microscope, custom filter sets were used, specifically z514, ET540/30m, zt514rdc (Chroma) for EYFP/YPet and z561, ET605/52m, zt561rdc (Chroma) for mCherry.

Imaging acquisition settings

All images were acquired using a personal computer (Dell PC, Windows OS) equipped with NIS-Elements software (Nikon). At timepoints after UV irradiation, three sequential images or snapshots (0.5 frames per second) were acquired for each field of view. These snapshots include one image from the phase contrast channel and two images from the yellow and red fluorescence channels, respectively. The fluorescence images in the yellow and the red channel were acquired by emitting 515 nm and 561 nm excitation light respectively. **Table 3.1** shows a summary of the acquisition settings.

Gene-fluorescent protein	Laser (nm)	Laser power (%/mW)	Exposure time (ms)	EMgain
<i>dnaB-YPet</i>	515	50% / 0.87	75	300
<i>mCherry-dnaN</i>	561	10% / 1.87	100	300
<i>dnaB-mCherry</i>	561	50% / 10.75	75	300
<i>YPet-dnaN</i>	515	50% / 0.87	75	300
<i>dnaQ-YPet</i>	515	50% / 0.87	75	300

Table 3.1. A summary of image acquisition settings.

Image analyses

The image analyses presented in this study have been done in three parts, which are explained below:

- Pre-processing of images
- Supersegger: a MATLAB based automated image processing and analyses package (credit: Paul Wiggins, University of Washington, USA)
- Post processing of images

Pre-processing of images:

In the first step, a custom-built MATLAB based script 'HelicaseLCI' (credit: Filip M. Asscher, TU Delft) was run on the raw images for a rough alignment of phase contrast and fluorescence images which were captured by two different cameras, followed by a correction of these images for laser beam-shape profiles and conversion of images with raw file format '.nd2' to '.tif' format.

Supersegger:

The second step has been the usage of Supersegger, a free MATLAB based image processing and analyses tool (29). Suited for bacterial live cell imaging involving fluorescence signals, Supersegger offers quantitative analyses and involves 'machine learning algorithms' to correct and optimize cell boundaries. Further, this software links cells from frame to frame 'reliably', which is essential for tracking processes due to live cell imaging and enables to 'segment' cells (i.e., recognition of cell and non-cell areas in a field of view) in a colony formation as well. The package also has a range of capabilities including the ability to recognize cell division events (mother, daughter and neighboring cells), offers statistics on cellular fluorescence and importantly for our studies, the location and intensity of foci.

The software loads images at each timepoint, aligns images, recognizes cell regions from the background, 'tracks' each region of the cell from frame to frame and links them, and finally computes 'fluorescence and structural characteristics' for each cell and frame after frame. Supersegger output is in three file formats: Frame files, Clist matrices and Cell files.

Supersegger broadly follows the following order in image analyses:

- Image alignment
- Cell segmentation
- Frame to frame linking of cells
- Cytometry
- Data output

For further details of this analysis package, an interested reader may like to consult the reference (29).

Post-processing of images:

After the images have been analyzed, the Supersegger graphical user interface (GUI further offers post-processing data visualization tools for 'single cells and population level analysis'. These tools include kymographs, histograms, movies, frame mosaics and consensus images to name a few.

Additionally, for our analyses we have used our above-mentioned script 'HelicaseLCI' to extract the following information from Supersegger analyzed files:

- Number of cells detected.
- Number of foci detected per cell.
- Intensity of foci over cell population
- Spatial distribution of foci within cells

From the above information, we have computed graphs for foci, stoichiometry and spatial distribution of replisome components and studied them for comparison of undamaged cells with cells undergoing UV-mediated DNA damage.

Calibration of single Ypet fluorescent molecules

E.coli strain LB1 (*dnaB-Ypet*, *mCherry-dnaN*) was grown in M9-glycerol, primary culture overnight and secondary culture on the following day. Cells were harvested when the secondary culture attained an OD₆₀₀ of ~0.15- 0.20 and 2 µl of this culture loaded on 1.5% agarose- M9 glycerol pads for imaging (as described under the heading **Preparation of cells for time-lapse microscopy, section 3.6.**).

With an exposure time of 75 ms, 50% power of 515 nm laser and fast acquisition at 10 frames per second (fps) (see **Table 3.1.** for a detailed summary for image acquisition settings), videos were captured of Ypet foci until the fluorescence was bleached.

We applied two approaches/tools sequentially (credit: Filip M. Asscher, TU Delft) for determining single fluorophore intensity:

- Trackmate
- Supersegger and Autostepfinder

In the first attempt we used the ImageJ based single particle tracking plugin Trackmate (30), to track DnaB foci over time as they bleach. The focus intensity at the very beginning of the video I_0 and also at the end of the video I_{single} (i.e., just before TrackMate stopped recognizing all but one fluorophore in the focus) are noted. By dividing the values I_0 / I_{single} , we calculated the number of molecules in the focus.

In our case, Trackmate could not detect single fluorophores as desired, but just two fluorophores at the minimum. Therefore, we tried a second approach by step fitting the bleaching traces.

To do this, the videos were first analyzed by the software Supersegger (29) to consider the spot intensity of Ypet foci over time (please see **section Image analyses**). We generated intensity traces from spot intensity analyses. Subsequently, a step fitting algorithm

Autostepfinder (credit: Luuk Loeff and Jacob Kerssemakers, TU Delft) was applied to the intensity traces to determine the number of bleaching steps.

Next, we obtained the fluorescence intensity value of a single Ypet molecule as determined from a singular bleaching step. We have calculated this value by step fitting the last bleaching step, beyond which there is a flat baseline (or bleaching), see **figure S3.6.A**.

Figure S3.6.B shows histograms plotted for intensity drop by bleaching during three experiments and then applied for a Gaussian fit. The mean value of a single Ypet fluorophore has been found to be 539 a.u. by doing so (**figure S3.6.C**). Further, by dividing the total intensity of a Ypet focus by this value of one fluorophore, yielded the number of tagged molecules present in a focus.

In our study, we detected the number of DnaB molecules in a focus to be ~6 and 12 (see **figure 3.6** stoichiometry plots of undamaged cells), by this second approach, as previously reported in literature.

To be noted, in order to obtain this graph one SuperSegger value has been needed to be manually set, in addition to the calibrated intensity of a single fluorophore, namely the minimal score of a focus (minScore). Depending on imaging settings and the range of the fluorescence intensity in the data, the minScore may vary. For the analysis of DnaB-Ypet foci, the minScore has been set so that the mean of the main peak in fluorescence intensity (**figure 3.6**) divided by the intensity of a single Ypet fluorophore, yields a value of 6 DnaB molecules (analyses credit: Lisa A. Buller, see **table 3.2** for fluorophore intensity and minscore parameters).

Gene-fluorescent protein	Laser (nm)	Laser power (%/mW)	Mean intensity single fluorophore (a.u.)	minScore used (a.u.)
<i>dnaB-Ypet</i>	515	50% / 0.87	539	400-480
<i>mCherry-dnaN</i>	561	10% / 1.87	191	173

Table 3.2. A summary of fluorophore calibration settings.

3.7. Supplementary information

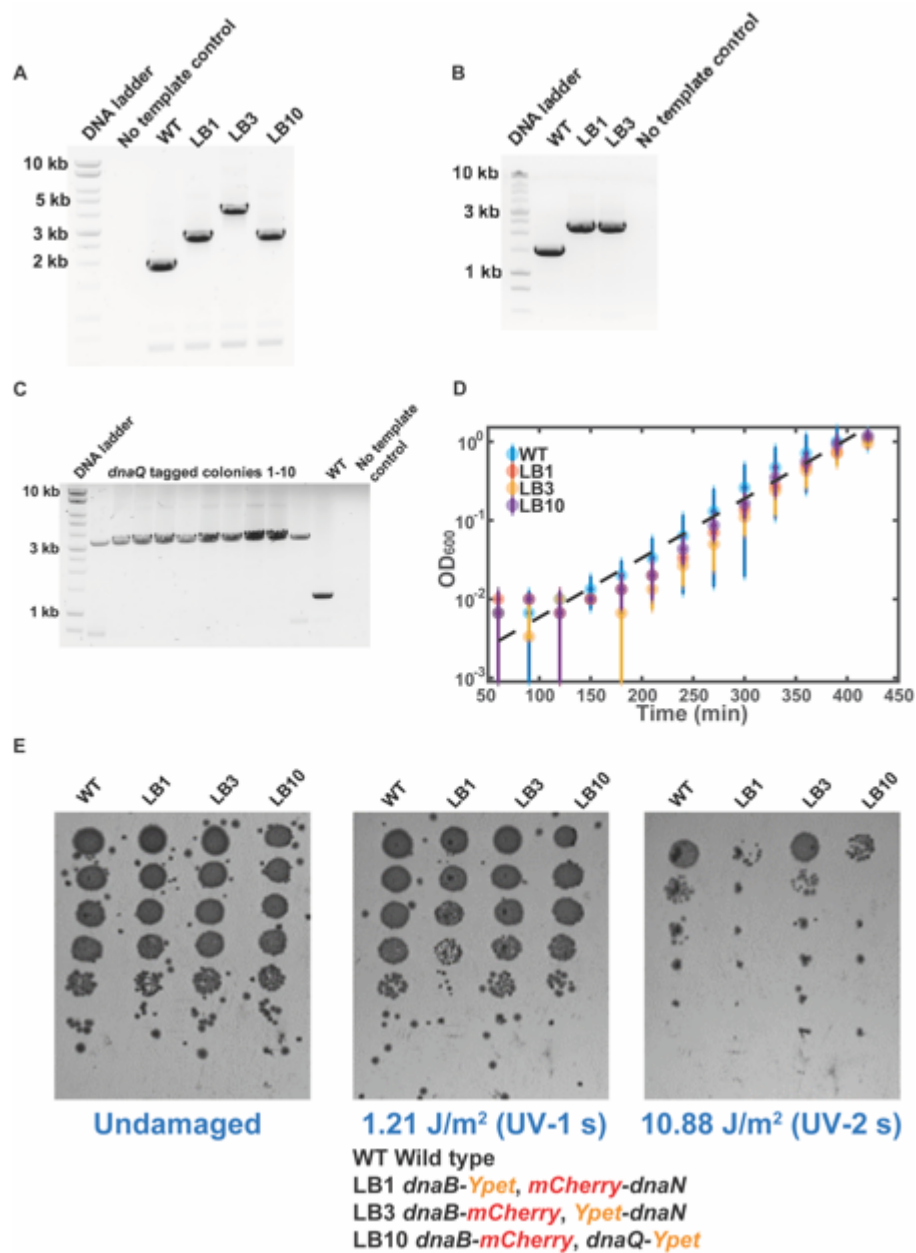
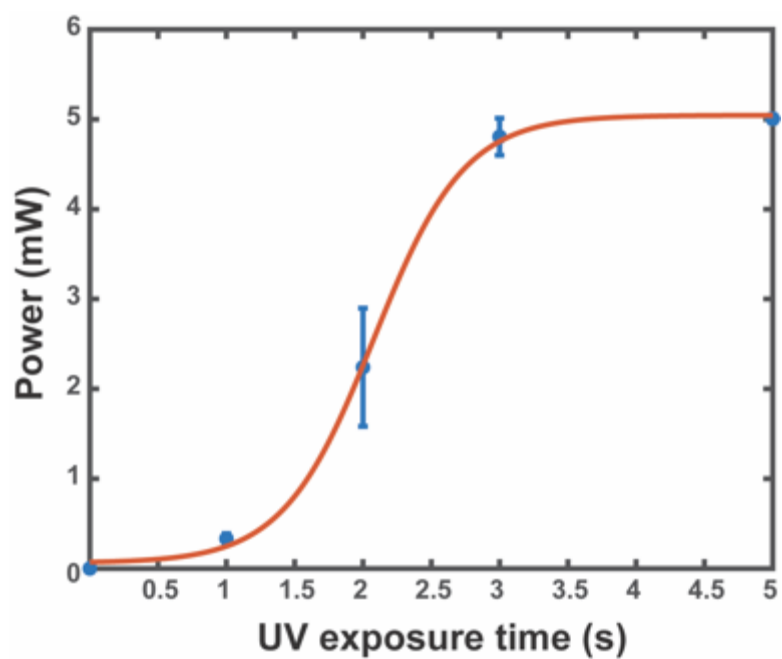
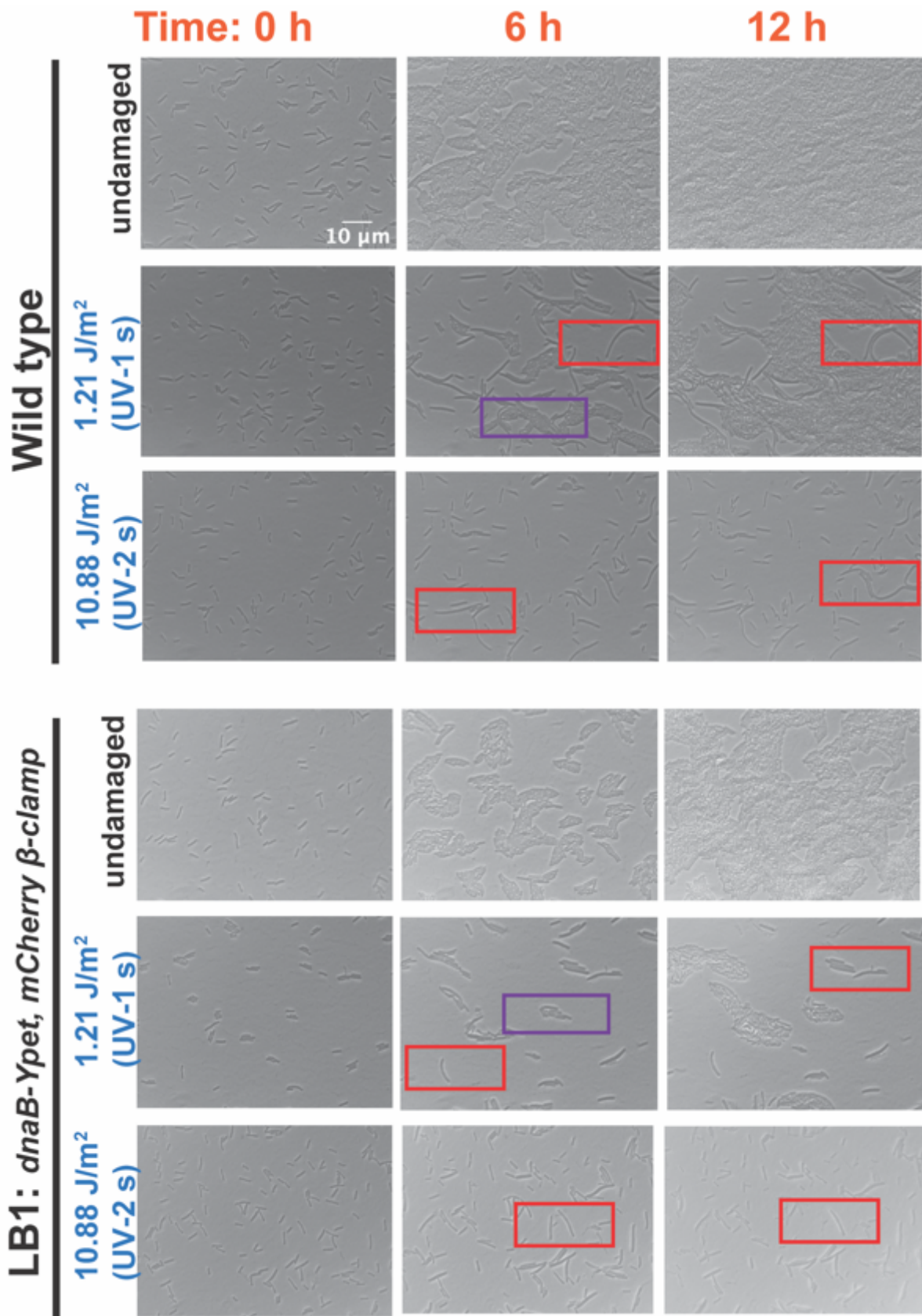


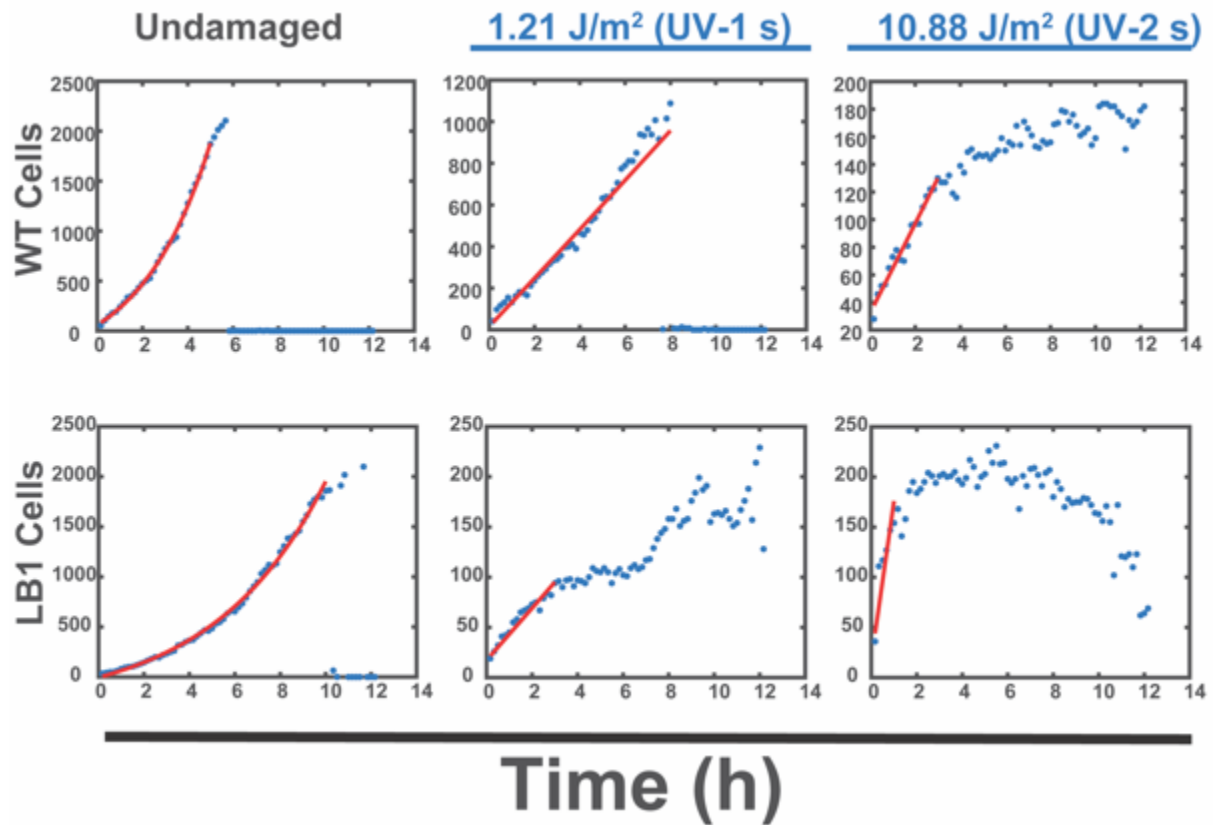
Figure S3.1. Validation experiments for the engineered strains. **A.** PCR amplification for the *dnaB* gene locus. LB3 has a higher band due to presence of *KanR* gene. **B.** PCR amplification for the *dnaN* gene locus. **C.** Colony PCR results for the *dnaQ* gene locus. **D.** Growth curves in Luria Bertani medium with exponential fit (dashed lines). The coloured dots represent the OD₆₀₀ datapoints and error bars represent the standard deviation. The doubling time was calculated to be 35 min (WT), 34.3 min (LB1), 33 min (LB3) and 33.7 min (LB10). **E.** Serial dilution assays performed on LB-agar plates without and with UV exposures.



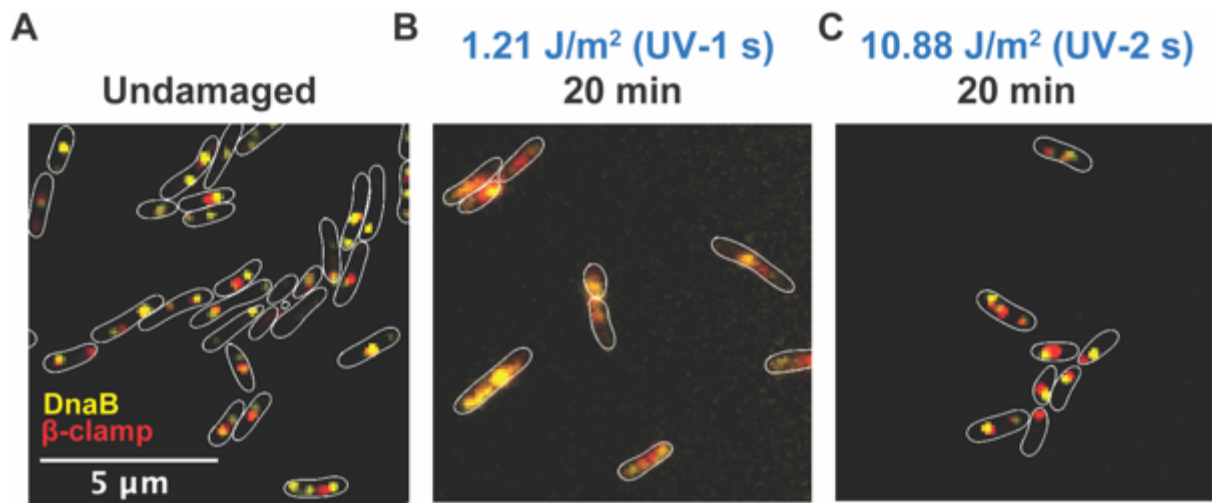
S3.2. Crosslinker calibration. A sigmoidal fit has been applied for power measurements (mW) for the UV exposure times (1, 2, 3 and 5 s). Errors bars represent the standard deviation. Please see section 3.6 **UV radiation on cells** for measurement details. Datapoints were collected in triplicate, at the least. UV-1 s and UV- 2 s exposures used in the study produced 1.21 J/m² and 10.88 J/m² incident energy on bacterial cells.



S3.3. Representative cell phase contrast images: undamaged and after UV exposure. Images of Wild type and LB1 cells acquired at 0, 6 and 12 h after UV-1 s and UV- 2s exposure. Red and purple frames indicate filamentous and colony forming cells respectively, after UV exposure.

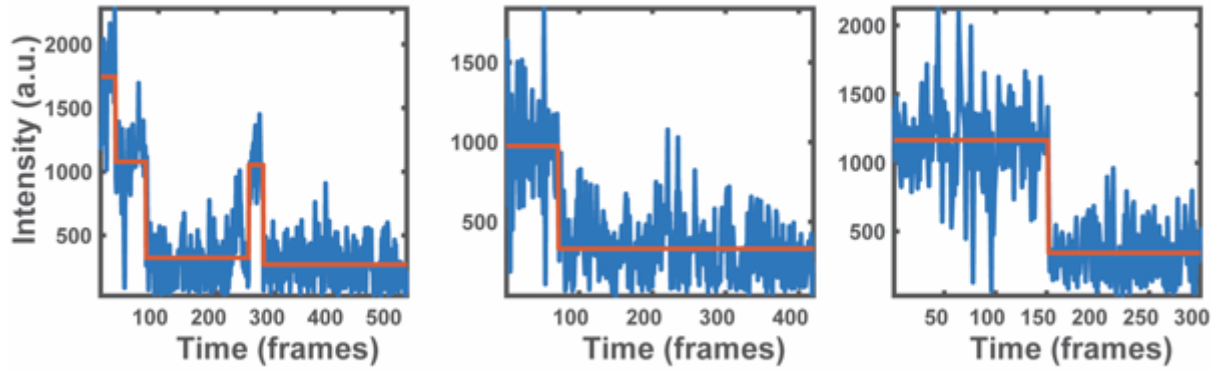


S3.4 Representative in-pad growth curves: undamaged and after UV exposure. Phase contrast images of Wild type and LB1 cells acquired every 10 min for 12 h. Blue dots indicate datapoints, while red lines indicate attempted exponential fit. The strains WT and LB1 were calculated to have doubling times of 1.40 ± 0.05 h and 1.92 ± 0.03 h, respectively, in the undamaged condition.

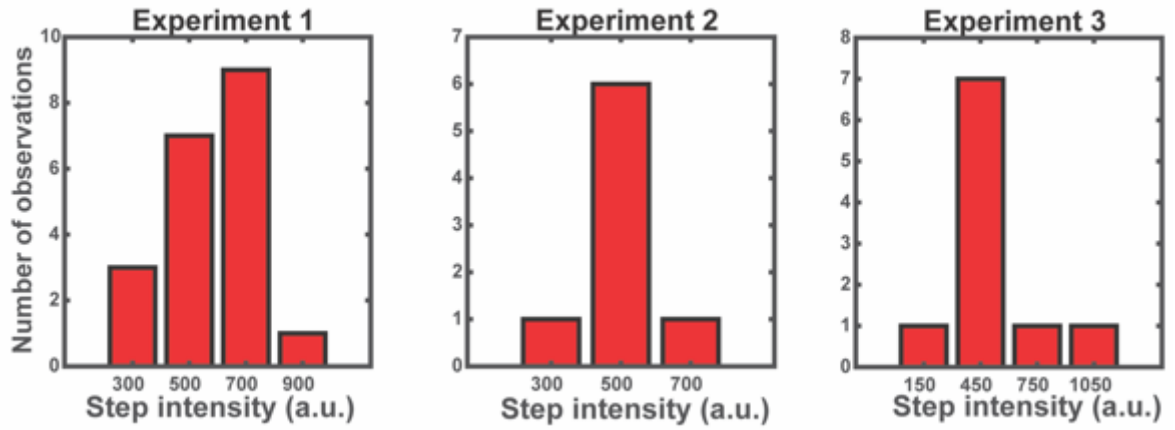


S3.5. Representative cell fluorescence images: undamaged and after UV exposure. Cell boundaries in white and foci shown by Supersegger curveFilter function. **A.** DnaB and β-clamp foci in undamaged cells. **B.** DnaB and β-clamp foci imaged at 20 min after UV-1 s expoure. **C.** DnaB and β-clamp foci imaged at 20 min after UV-2 s expoure. Strain LB1.

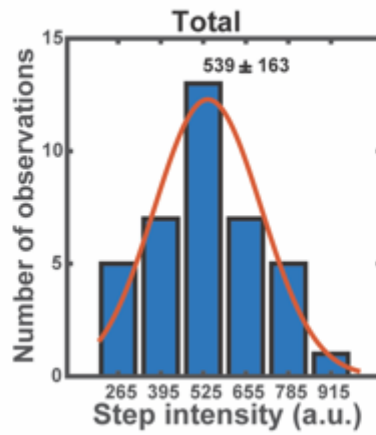
A



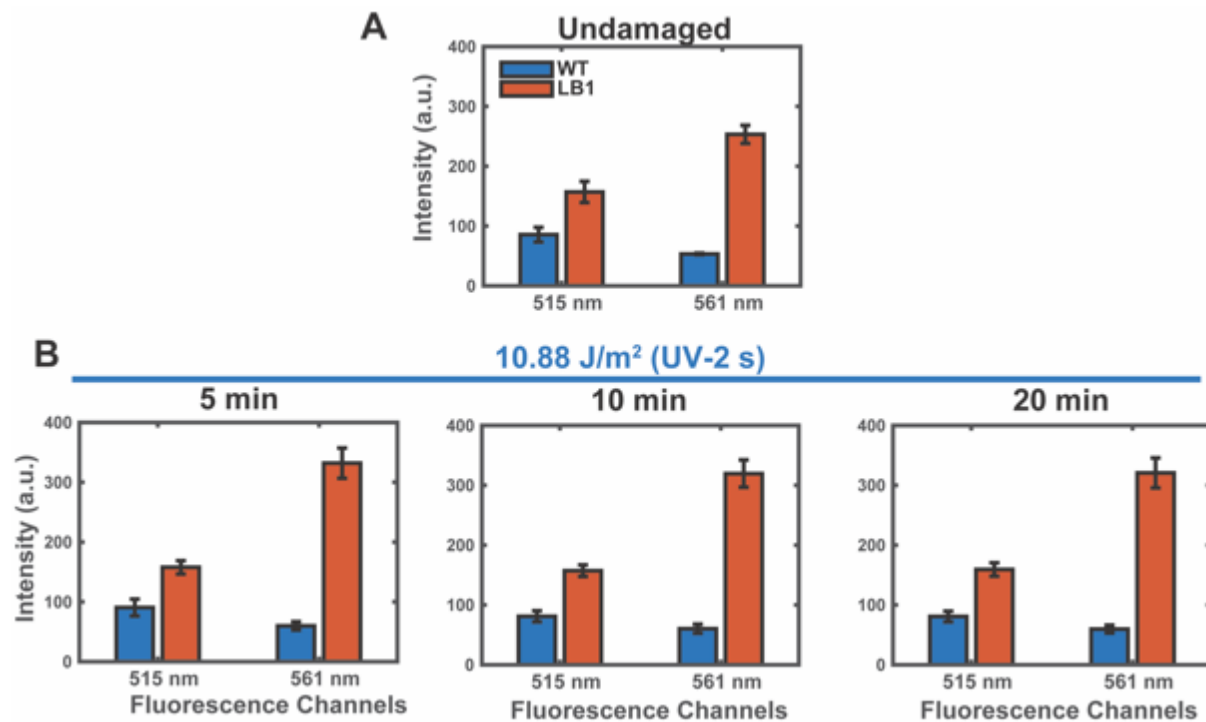
B



C



S3.6. Fluorophore Calibration *in vivo* for single molecule intensity. **A.** Three examples are shown of final bleaching steps used to calculate fluorophore intensity. **B.** Histograms plotted for fluorescent intensity drop by photobleaching during three experiments. **C.** Gaussian fit is applied for the data from three experiments to obtain the fluorescent intensity of one YPet molecule, 539 a.u.



S3.7. Autofluorescence intensity. Whole cell fluorescence comparison for wild type and LB1 cells using 515 nm laser (YPet) and 561 nm laser (mCherry). Data shown for undamaged conditions and after 5, 10 and 20 min of UV-2 s exposure (10.88 J/m²). LB1 shows higher fluorescence levels compared to WT cells.

Strains	Relevant genotype	Construction
BN1110	<i>E.coli</i> AB1157 with pKD46 plasmid	<i>E.coli</i> K12 derivative
BW25142	<i>E.coli</i> host for plasmids with R6K γ origin of replication	Coli Genetic Stock Center (CGSC# 7840), Yale University
BN1682	<i>mCherry-dnaN</i> with <i>kan^R</i>	Previous study*
BN1109	<i>Ypet-dnaN</i> with <i>kan^R</i>	Previous study*
BN1116	<i>E.coli</i> BW25142 host for plasmid with <i>mCherry</i> and <i>kan^R</i>	Previous study*
SDR5	Plasmid with R6K γ origin (Patricia Foster 20 amino acid linker- <i>mcherry</i>)	Gibson assembly with BN1116
SDR7	<i>dnaB-Ypet</i> with <i>kan^R</i>	Phage transduction in BN1110
SDR14	<i>dnaB-Ypet</i>	<i>Flp-frt</i> recombination (<i>kan^R</i> flipped out from SDR7)
SDR35	<i>dnaB-Ypet</i> , <i>mCherry-dnaN</i> with <i>kan^R</i>	Phage transduction (BN1682→SDR14)
LB1	<i>dnaB-Ypet</i> , <i>mCherry-dnaN</i>	<i>Flp-frt</i> recombination (<i>kan^R</i> flipped out from SDR35)
LB2	<i>Ypet-dnaN</i>	<i>Flp-frt</i> recombination (<i>kan^R</i> flipped out from BN1109)
LB3	<i>Ypet-dnaN</i> , <i>dnaB-mCherry</i> with <i>kan^R</i>	λ -red recombination: SDR5→LB2
LB4	<i>dnaB-mCherry</i> with <i>kan^R</i>	λ -red recombination: SDR5→BN1110
LB5	<i>dnaB-mCherry</i>	<i>Flp-frt</i> recombination (<i>kan^R</i> flipped out from LB4)
LB10	<i>dnaB-mCherry</i> , <i>dnaQ-Ypet</i> with <i>kan^R</i>	Phage transduction (BN1514→LB5)

Table S3.1. A summary of bacterial strains used in this study.

*Previous study here refers to ref. (26)

Plasmids	Relevant genotype	Construction
pKD46	Plasmid with genes for λ -red recombination under arabinose promoter	Previous study*
pCP20	Plasmid with yeast <i>Flp</i> recombinase gene for <i>Flp-frt</i> recombination	Previous study*
BN1116	Plasmid from same strain, used as PCR template, for cloning SDR5 plasmid (R6KY origin of replication)	Previous study*
SDR5	<i>mCherry</i> with <i>kan^R</i> (Template for λ -red recombination)	Gibson assembly on BN1116 plasmid backbone

Table S3.2. A summary of plasmids used in this study.

Linkers	Sequence (5'-3')
<i>dnaB-Ypet</i>	(t)CAGCAGAAGCTGCAGCCAAAGAGGCCGCGAGCGAAAGAAGCAGCGGCGAAAGAGGCCA GCAGCTAAAGCGGCCGCGAGAATTC
<i>dnaB-mcherry</i>	GGATCCGCTGGCTCCGCTGCTGGTTCTGGCGCTGGCTCCGCTGCTGGTTCTGGCGAATTC
<i>dnaQ-Ypet</i>	CGGCTGGCTCCGCTGCTGGTTCTGGCGAATTC
<i>mCherry-dnaN</i>	*Previous study
<i>Ypet-dnaN</i>	*Previous study

Table S3.3. A summary of linkers used for gene tagging in this study. Please note that for the *dnaB-Ypet* tagging, (t) nucleotide is contributed by the genome.

*Previous study here refers to ref. (26)

Primers	Sequence (5'-3')
2925	taatccgctgggtagcgatggcggc
2926	cttcttcgagacgggctacgcaaa
2927	accgggggtaaacaccggttatgacg
2928	ttattatcgtcgtcgactgcggc
SDR7	gacaatagcggccatcaactccata
SDR8	tcgaaccgcgaccccctgcgtgaca
LB13	gtcaatggtcgcgcttcgacaactatgcggggccgcagtacgacgacgaaGG ATCCGCTGGCTC
LB14	gtgttccttgataagtgtttgctttaattacctaattcataaaataattaCATATGAA TATCCTCCTTAG
LB15	gtcaatggtcgcgcttcgacaactatgcggggccgcagtacgacgacgaaGG ATCCGCTGGCTCCGCTGCTGGTTCTGGCGCT
ND33	attacgaattcgagcggatccgctggctccgctgctggttctggcgctggctccg ctgctggttctggcgaattcgtgagcaagggcgaggagg
ND34	cagcctacaccggggttactgtacag
ND35	gagctgtacaagtaaccggggtgtagg
ND36	ggagccagcggatccgctcgaattcgtaatcatggtca
1045	cgttggcacctaccagaaag
1628	gcaggaaaaactggtcaccatc

Table S3.4. A summary of DNA primers used in this study.

References:

1. Reyes-Lamothe, R., Sherratt, D.J. and Leake, M.C. (2010) Stoichiometry and architecture of active DNA replication machinery in *Escherichia coli*. *Science (New York, N.Y.)*, **328**, 498-501.
2. Kurth, I. and O'Donnell, M. (2013) New insights into replisome fluidity during chromosome replication. *Trends Biochem Sci*, **38**, 195-203.
3. LeBowitz, J.H. and McMacken, R. (1986) The *Escherichia coli* dnaB replication protein is a DNA helicase. *J Biol Chem*, **261**, 4738-4748.
4. Bleichert, F., Botchan, M.R. and Berger, J.M. (2017) Mechanisms for initiating cellular DNA replication. *Science (New York, N.Y.)*, **355**.
5. Bell, S.P. and Kaguni, J.M. (2013) Helicase loading at chromosomal origins of replication. *Cold Spring Harb Perspect Biol*, **5**.
6. Windgassen, T.A., Wessel, S.R., Bhattacharyya, B. and Keck, J.L. (2018) Mechanisms of bacterial DNA replication restart. *Nucleic Acids Res*, **46**, 504-519.
7. Makowska-Grzyska, M. and Kaguni, J.M. (2010) Primase directs the release of DnaC from DnaB. *Mol Cell*, **37**, 90-101.
8. (!!! INVALID CITATION !!! (Arias-Palomo et al., 2019)).
9. Beattie, T.R. and Reyes-Lamothe, R. (2015) A Replisome's journey through the bacterial chromosome. *Front Microbiol*, **6**, 562.
10. Kim, S., Dallmann, H.G., McHenry, C.S. and Marians, K.J. (1996) Coupling of a replicative polymerase and helicase: a tau-DnaB interaction mediates rapid replication fork movement. *Cell*, **84**, 643-650.
11. Galletto, R., Jezewska, M.J. and Bujalowski, W. (2004) Unzipping mechanism of the double-stranded DNA unwinding by a hexameric helicase: the effect of the 3' arm and the stability of the dsDNA on the unwinding activity of the *Escherichia coli* DnaB helicase. *Journal of Molecular Biology*, **343**, 101-114.
12. Indiani, C., Langston, L.D., Yurieva, O., Goodman, M.F. and O'Donnell, M. (2009) Translesion DNA polymerases remodel the replisome and alter the speed of the replicative helicase. *Proc Natl Acad Sci U S A*, **106**, 6031-6038.
13. Ribeck, N., Kaplan, D.L., Bruck, I. and Saleh, O.A. (2010) DnaB helicase activity is modulated by DNA geometry and force. *Biophys J*, **99**, 2170-2179.
14. Beattie, T.R., Kapadia, N., Nicolas, E., Uphoff, S., Wollman, A.J., Leake, M.C. and Reyes-Lamothe, R. (2017) Frequent exchange of the DNA polymerase during bacterial chromosome replication. *Elife*, **6**.
15. Jeiranian, H.A., Schalow, B.J., Courcelle, C.T. and Courcelle, J. (2013) Fate of the replisome following arrest by UV-induced DNA damage in *Escherichia coli*. *Proc Natl Acad Sci U S A*, **110**, 11421-11426.
16. Mangiameli, S.M., Veit, B.T., Merrikh, H. and Wiggins, P.A. (2017) The Replisomes Remain Spatially Proximal throughout the Cell Cycle in Bacteria. *Plos Genet*, **13**, e1006582.
17. Mangiameli, S.M., Cass, J.A., Merrikh, H. and Wiggins, P.A. (2018) The bacterial replisome has factory-like localization. *Curr Genet*, **64**, 1029-1036.
18. Reyes-Lamothe, R., Possoz, C., Danilova, O. and Sherratt, D.J. (2008) Independent positioning and action of *Escherichia coli* replisomes in live cells. *Cell*, **133**, 90-102.
19. Bates, D. and Kleckner, N. (2005) Chromosome and replisome dynamics in *E. coli*: loss of sister cohesion triggers global chromosome movement and mediates chromosome segregation. *Cell*, **121**, 899-911.

20. Mangiameli, S.M., Merrikh, C.N., Wiggins, P.A. and Merrikh, H. (2017) Transcription leads to pervasive replisome instability in bacteria. *Elife*, **6**.
21. Soubry, N., Wang, A. and Reyes-Lamothe, R. (2019) Replisome activity slowdown after exposure to ultraviolet light in *Escherichia coli*. *Proc Natl Acad Sci U S A*, **116**, 11747-11753.
22. Amarh, V., White, M.A. and Leach, D.R.F. (2018) Dynamics of RecA-mediated repair of replication-dependent DNA breaks. *J Cell Biol*, **217**, 2299-2307.
23. Lovett, S.T. (2018) Between sisters: Watching replication-associated recombinational DNA repair. *J Cell Biol*, **217**, 2225-2227.
24. Wang, X., Lesterlin, C., Reyes-Lamothe, R., Ball, G. and Sherratt, D.J. (2011) Replication and segregation of an *Escherichia coli* chromosome with two replication origins. *Proc Natl Acad Sci U S A*, **108**, E243-250.
25. Wegrzyn, K.E., Gross, M., Uciechowska, U. and Konieczny, I. (2016) Replisome Assembly at Bacterial Chromosomes and Iteron Plasmids. *Front Mol Biosci*, **3**, 39.
26. Moolman, M.C., Krishnan, S.T., Kerssemakers, J.W., van den Berg, A., Tulinski, P., Depken, M., Reyes-Lamothe, R., Sherratt, D.J. and Dekker, N.H. (2014) Slow unloading leads to DNA-bound beta2-sliding clamp accumulation in live *Escherichia coli* cells. *Nat Commun*, **5**, 5820.
27. Syeda, A.H., Wollman, A.J.M., Hargreaves, A.L., Howard, J.A.L., Bruning, J.G., McGlynn, P. and Leake, M.C. (2019) Single-molecule live cell imaging of Rep reveals the dynamic interplay between an accessory replicative helicase and the replisome. *Nucleic Acids Res*.
28. Arias-Palomo, E., Puri, N., O'Shea Murray, V.L., Yan, Q. and Berger, J.M. (2019) Physical Basis for the Loading of a Bacterial Replicative Helicase onto DNA. *Mol Cell*, **74**, 173-184 e174.
29. Stylianidou, S., Brennan, C., Nissen, S.B., Kuwada, N.J. and Wiggins, P.A. (2016) SuperSegger: robust image segmentation, analysis and lineage tracking of bacterial cells. *Molecular microbiology*, **102**, 690-700.
30. Tinevez, J.Y., Perry, N., Schindelin, J., Hoopes, G.M., Reynolds, G.D., Laplantine, E., Bednarek, S.Y., Shorte, S.L. and Eliceiri, K.W. (2017) TrackMate: An open and extensible platform for single-particle tracking. *Methods*, **115**, 80-90.

4

Drug dosage and timing influence the spatial distribution of DNA Polymerase IV

In Escherichia coli, upon DNA damage translesion polymerases are upregulated during the SOS response. DNA polymerase IV (Pol IV), one such polymerase, plays a key role in cellular survival. Using live cell imaging, we report here on Pol IV dynamics in vivo in real time, tracing its response to two different DNA damage drugs, methyl methanesulfonate (MMS) and nitrofurazone (NFZ), from the onset of DNA damage to beyond the peak of its upregulation during SOS response. Overall, the findings are quite similar for MMS and NFZ. We find that the magnitude of the Pol IV response to DNA damage depends strongly on the dosage of DNA damage drug and evolves over time. The spatial positioning of DNA-bound Pol IV in the cell is found to evolve from being uniform at low (cumulated) drug dosage, to favoring the cell poles at higher (cumulated) drug dosage. While its colocalization with the replisome is found to exceed that of random chance, many Pol IV molecules are recruited to the DNA in a damage-dependent manner via replication-independent means. At the highest (cumulated) drug dosages tested, the mid-cell localization of the replisome tends to broaden, enhancing the apparent colocalization with Pol IV. With this probing of Pol IV at the single-molecule level over a range of DNA damage drug dosages and time, we provide further insights into the response of translesion polymerases to different kinds of DNA damage.

A manuscript based on this chapter is under peer review.

4.1 Introduction

Cell growth and division are essential to life, and a key underlying process is the replication of the genome. A full understanding of DNA replication includes understanding its progression in the context of DNA damage and repair (1). DNA damage may be caused by extrinsic factors, e.g. UV radiation and chemicals in the environment, or by intrinsic factors such as spontaneous DNA breakage or by-products of cellular metabolism (2-4).

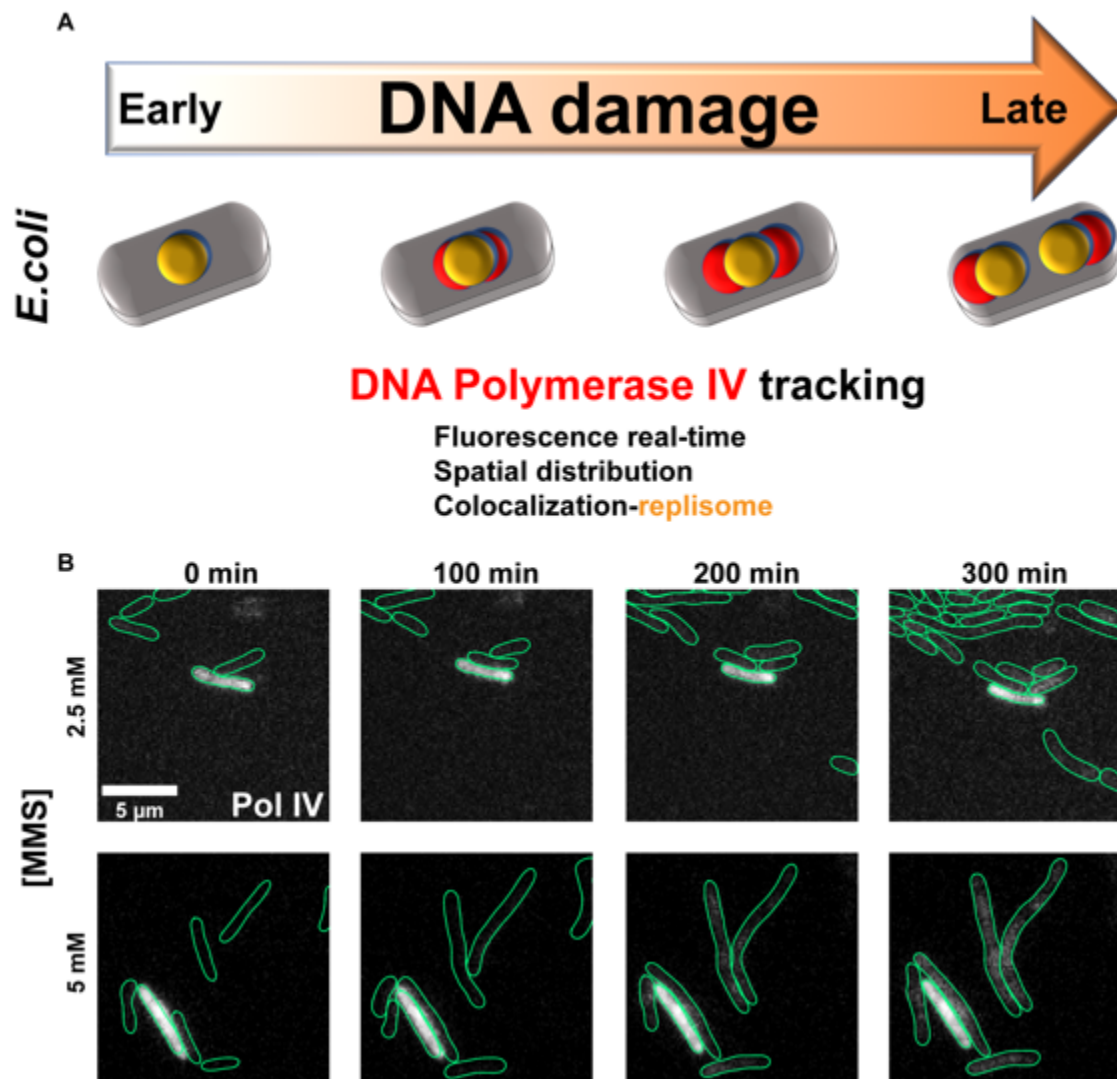


Figure 4.1 The cellular response to different doses of DNA damage drugs. **A.** Schematic of the successive stages of the SOS response. Live cell imaging of Pol IV response is performed in this context. **B.** Images of *E. coli* cells subject of 2.5 mM (top series) or 5 mM (bottom series) of the DNA damage drug MMS over time. Green lines indicate the cell boundaries assessed via phase contrast microscopy (**Materials and Methods**) and white signal reflects Pol IV-mCherry fluorescence. Quantitative image analysis (**Materials and Methods**) is used to probe the whole-cell fluorescence and to track the behaviour of fluorescent foci.

In the bacterium *Escherichia coli*, the response to DNA damage (known as the 'SOS' response) triggers the transcription of a cascade of genes involved in repair processes. Genes

that are transcribed early on are thought to be involved in 'error-free' pathways; these include repair proteins such as RecA and RecN. When these repair mechanisms do not suffice, e.g. in the case of persistent DNA damage, the SOS response invokes more 'error-prone' pathways in which specialized DNA polymerases bypass DNA lesions (and, in consequence, contribute to mutagenesis) (6,7). In *E. coli*, the presence of three such translesion synthesis (TLS) polymerases, Pol II, Pol IV, and Pol V (in addition to the replicative polymerases Pol I and Pol III) suggests an important role for translesion synthesis and repair (8,9). Thus, upon substantial DNA damage, a cell will progress from an undamaged, healthy state, to a state of early DNA damage and onset in which the first responders of 'error-free' pathways should prevail, to a state in which mutations and damage effects are established and late responders of 'error prone pathways' can act for damage 'tolerance'. In a final late cell state, a cell will either divide, provided that it can tolerate or has repaired DNA damage, or may even lapse into cell death due to high toxicity and mutation (**Figure 4.1A**).

The bacterial TLS DNA polymerase IV (Pol IV), encoded by *dinB* gene and discovered nearly two decades ago (11), has a substantial presence both in undamaged cells and in stationary phase culture relative to other TLS polymerases (12-14). Early measurements using Western blots indicated the presence of 250 Pol IV molecules in the undamaged cell, and upregulation to 2500 in the presence of the SOS response (12,15). More recently, single-molecule measurements have measured lower copy numbers for Pol IV, namely 20 in the absence of damage and 250 upon treatment of cells with the antibiotic ciprofloxacin (13). Pol IV can bypass N² adducts on guanines as well as alkyl adducts (16,17), resulting in low fidelity, 'error-prone' DNA synthesis as described above. Pol IV may also possess UV lesion bypass ability, although *dinB* knockout cells are not hypersensitive to UV damage for survival (18). Whether Pol IV exhibits a uniform response towards different types of DNA damage remains an open question. Furthermore, roles for Pol IV have also been suggested in other contexts, such as nucleotide excision repair - one of the first responders to DNA damage - and recombination, both processes that are considered 'error-free' (19,20). This raises the question whether Pol IV dynamically switches between different pathways over time.

In order to bypass bulky adducts during 'error-prone' DNA synthesis, a likely scenario may involve displacement of the active Pol III (the canonical DNA synthesis polymerase) by Pol IV, but how and when this occurs is not well understood. One model known as the 'toolbelt' model (21,22) proposes that under damage conditions Pol IV is always present in the vicinity of Pol III through its established binding site to the dimeric sliding β -clamp (23,24), ready to take over upon replication fork stalling. Evidence in support of this model was provided by a recent *in vitro* single-molecule force spectroscopy study that identified the polymerases by their differences in DNA synthesis rates (25). However, it has also been proposed that the exchange between Pol III and Pol IV occurs at a rate determined by their respective cellular concentrations (26,27). This might seem plausible in the presence of damage, where the ratio of Pol IV to Pol III can vary between 5-15 over time (13,28); however, even in the absence of damage the ratio of Pol IV to Pol III is of order one (13,28), which suggests that further regulation of the access of Pol IV to the replisome should be necessary. Lastly, the exchange between Pol III and Pol IV could occur following the recruitment of Pol IV at specific sites of DNA damage, as certain DNA damage adducts or substrates have higher affinity for Pol IV action (17).

Several recent studies have started to shed light on the behavior of Pol IV using the high-resolution visualization capacity of single-molecule fluorescence microscopy. For example, a recent *in vitro* colocalization study (27) has provided evidence refuting the toolbelt model by showing that Pol IV alternates with Pol III in binding to the sliding clamp. Exchange between the two polymerases was not provoked by the introduction of N²-dG furfuryl DNA damage lesion. Instead, it was concluded that the probability of exchange is governed by mass action alone. Given the reported higher copy number of Pol IV over Pol III, especially in the context of DNA damage, this would predict frequent colocalization of Pol IV with the replisome. *In vivo*, one recent single-molecule study reported a degree of colocalization between Pol IV and the replisome of 10-20% (compared to 5% expected by random chance) upon treatment with ciprofloxacin or methyl methanesulfonate (MMS), and concluded that the spatial distribution of Pol IV was independent of the type of DNA damage incurred (13). A second recent *in vivo* single-molecule study found that in the presence of MMS, the average distance between Pol IV and a replisome marker (SSB) decreased by 42% (relative to untreated cells), resulting in a degree of colocalization that exceeded that of random chance by a factor of ~6. Furthermore, the same study found that in the presence of nitrofurazone (NFZ), the average distance decreased by 13% (relative to untreated cells), resulting in a degree of colocalization that did not exceed that of random chance (29), thereby concluding that the degree of colocalization between Pol IV and the replisome depended on the DNA damage drug probed. Nonetheless, both *in vivo* investigations find conditions in which the colocalization between Pol IV and the replisome exceeds that expected by random chance. Thus, the authors suggest that mass action alone does not govern the spatial distribution of Pol IV in cells and propose either the existence of Pol IV populations with distinct diffusive properties (29), or post-replicative translesion synthesis by Pol IV (13). In the latter context, Pol IV activity would take place after replication, requiring no exchange with the replisome.

Both these *in vivo* studies reached their conclusions by sampling the localization of Pol IV over a limited range of DNA damage drug dosages. However, the response of a bacterial cell could certainly vary depending on drug dosage and potentially evolve (or change) over long timescales. Therefore, we have here examined the behavior of Pol IV using wide-field fluorescence-based live cell imaging for different dosages of DNA damage and tracked the response from an undamaged state, through a gradual onset of DNA damage and beyond the peak of SOS response. We have investigated how the overall upregulation of Pol IV, its binding to DNA, and its spatial distribution along the long axis of the *E. coli* cell depend on drug dosage, duration of drug exposure, and type of DNA damage drug employed. Throughout, we have compared these response characteristics of Pol IV with those of the replisome, using the β -clamp as a replisome marker (30,31). The choice of the β -clamp marker has been an important one because, besides it having a higher DNA bound time than most components other than DnaB (32), that allows reliable reporting of the replisome position, the marker is also a hub for Pol IV interactions (25). This allows us to conclude, for the DNA damage drugs tested, that at low cumulative levels of DNA damage Pol IV is uniformly distributed throughout the cell; in this regime, it can transiently colocalize with the replisome. Conversely, at high cumulative levels of DNA damage, the Pol IV distribution shifts towards the cell poles, as does, to a lesser extent, that of the replisome. Under these conditions, Pol IV may colocalize with the replisome but in a manner that is unlikely to reflect its primary role in the DNA damage response. These findings contribute, at the single-molecule level, to an overall understanding of the response of bacterial cells to DNA damage.

4.2 Results

4.2.1 Strain creation with fluorescently labelled DNA Polymerase IV and β -clamp

To track DNA Polymerase IV (Pol IV) relative to the replisome in live cell imaging experiments in response to DNA damage drugs, we have genetically engineered two chromosomal fusion strains in *Escherichia coli* (**Materials and Methods**; **Figure S4.1A**; **Table S4.1**). In a first strain (SDR33), we have labeled Pol IV in the *dinB* locus at its C-terminus with mCherry and, as a marker of the replisome, each monomer of the homo-dimeric sliding β -clamp in the *dnaN* locus at its N-terminus with YPet (31). In a second strain (SDR32), Pol IV is labeled with EYFP and each monomer of the homo-dimeric β -clamp is labeled with mCherry. The choice for the Pol IV labels (and their linkers) is motivated by published characterization of effective tagging approaches for this polymerase (33). The use of the β -clamp as a replisome marker is motivated by its being a bright and integral part of a processive replisome (30,31). All strains were validated by PCR (**Figure S4.1B**) followed by DNA sequencing. For all strains, characterization of growth curves in flasks with LB medium revealed a typical doubling time of ~38 min (**Figure S4.1C**). On agarose pads containing supplemented M9-glycerol medium (see **Materials and Methods** for supplemented amino acids), the typical doubling time of labeled strains was reduced to 76 ± 18 min (**Figure S4.1D**), in agreement with previous studies (31). Labeled strains showed mean cell lengths of ~3 μ m when first placed on agarose pads, with slight reductions over the course of time-lapse experiments lasting several hours (**Figure S4.1E**). Averaged over the course of such experiments, cells divided at lengths of 3.5–4 μ m (**Figure S4.1F**). The functionality of Pol IV chromosomal fusion strains in the presence of DNA damage agents MMS and NFZ, which are known to produce different kinds of adducts or lesions (CH_3 (16) and N^2 -dG (17), respectively), was examined in serial dilution assays and compared to that of a wild-type strain (**Figures S4.2A,B**). Images of individual *E. coli* cells on agarose-M9 glycerol pads show the response of fluorescent Pol IV for two dosages of the DNA damage drug MMS (**Figure 4.1B**). Qualitatively, despite the cell-to-cell heterogeneity common to single-cell observations (34–37), one can observe that a higher dosage of DNA damage drugs elicits an upregulation of fluorescently labeled Pol IV.

4.2.2 Observing *in vivo* Pol IV response to DNA damage drugs

To determine the most suitable range of drug dosage conditions for in-depth probing, we first monitor the total fluorescence emitted by Pol IV-mCherry within individual cells every 2 min in time-lapse experiments lasting for 12 h (**Figure 4.2A**, and identical **Figure S4.5A**). One of two DNA damage agents, MMS or NFZ, was added to the agarose pad 20 min prior to the start of the time-lapse experiments. The drug dosages ranged from 0 mM to 10 mM (MMS) and 0 μ M to 100 μ M (NFZ). Focusing first on MMS, we observe that the cellular response as assayed by total Pol IV-mCherry fluorescence increases for increasing concentrations of MMS (**Fig 4.2A**, and identical **Figure S4.5A**), saturating at the highest concentration shown here (10 mM). In these experiments, we have normalized the results by the total cell area, which is necessary because we observe that an increasing dosage of MMS increases the probability of observing a population of longer, ‘filamentous’ cells (top panels of **Figures S4.4A,B**), in agreement with published observations (13,38). The presence of such cells is thought to

derive from delayed cell division until the effects of damage have been eliminated to tolerable levels (39). The impact of higher dosages of MMS up to those employed in previous experiments (e.g. 100 mM, see Ref. (29)) was examined in similar fashion; however, under these conditions, phase contrast imaging revealed the frequent appearance of black spots in the cell interior (**Figure S4.3**), which we interpreted as deleterious consequences of high cytotoxicity (see **Discussion**). Thus, we did not analyze the results from such experiments. Starting at MMS concentrations of 2.5 mM and upwards, the total Pol IV fluorescence is observed to peak after 300 min (5 h); at later timepoints, the total Pol IV fluorescence decreases, possibly as a result of the DNA damage-mediated SOS response. Control experiments monitoring total cellular fluorescence in wild type cells (including no fluorescent label) under identical laser excitation showed a much-reduced response (e.g. < 100 a.u. for 10 mM MMS, **Figure S4.5B**). A comparable set of experiments in which Pol IV was labeled with EYFP showed overall similar trends despite slightly increased cellular autofluorescence at the corresponding excitation wavelength (~200 a.u. for 10 mM MMS, **Figures S4.5C,D**).

To specifically assess the response of Pol IV molecules that are DNA-bound, we next used selection criteria to identify foci of enhanced fluorescence (representative images for both DNA damage drugs and fluorescent strains shown in **Figure S4.6**) that would reflect the presence of immobilized, and presumably DNA-bound, Pol IV molecules (40) (**Materials and Methods**). The intensity of the fluorescence contained within such Pol IV foci as a function of MMS dosage over the same time period (again normalized per area) is shown in **Figure 4.2B** (and identical **Figure S4.8A**). At low dosages of MMS, we observe that Pol IV rarely binds to DNA, in agreement with previous observations (13): the number of DNA-bound Pol IV molecules per square micron (obtained via conversion of the calibrated fluorescence intensity, **Figure S4.7**) is nearly zero. At higher dosages of MMS, the number of DNA-bound Pol IV molecules per square micron increases, reaching a maximum of 5 after 5 h at 10 mM MMS, and declining again for longer observation times, similar to the whole-cell fluorescence (**Figure 4.2A**). Control experiments monitoring the fluorescence intensity within identified foci (again normalized by total cell area) in wild type cells (including no fluorescent label) under identical laser excitation also showed a much-reduced response (no observable Pol IV foci even at 10 mM MMS, **Figure S4.8B**). A comparable set of experiments in which Pol IV was labeled with EYFP showed overall similar trends (**Figures S4.8C,D**).

The experiments at different dosages of NFZ show, broadly speaking, similar results: the whole-cell Pol IV-mCherry fluorescence (**Figure 4.2C**, and identical **Figure S4.5E**) initially increases with time for all tested NFZ concentrations, with the strongest response observed at a dosage of 5 μ M. Except at the highest NFZ dosage tested (100 μ M), the whole-cell Pol IV-mCherry fluorescence is observed to peak around 300 min (5 h) and to decrease at later timepoints. As in the case of MMS, the whole-cell fluorescence was normalized by the total cell area, because increasing the dosage of NFZ also enhanced (though to a lesser extent than with MMS) the probability of observing a population of longer, 'filamentous' cells (bottom

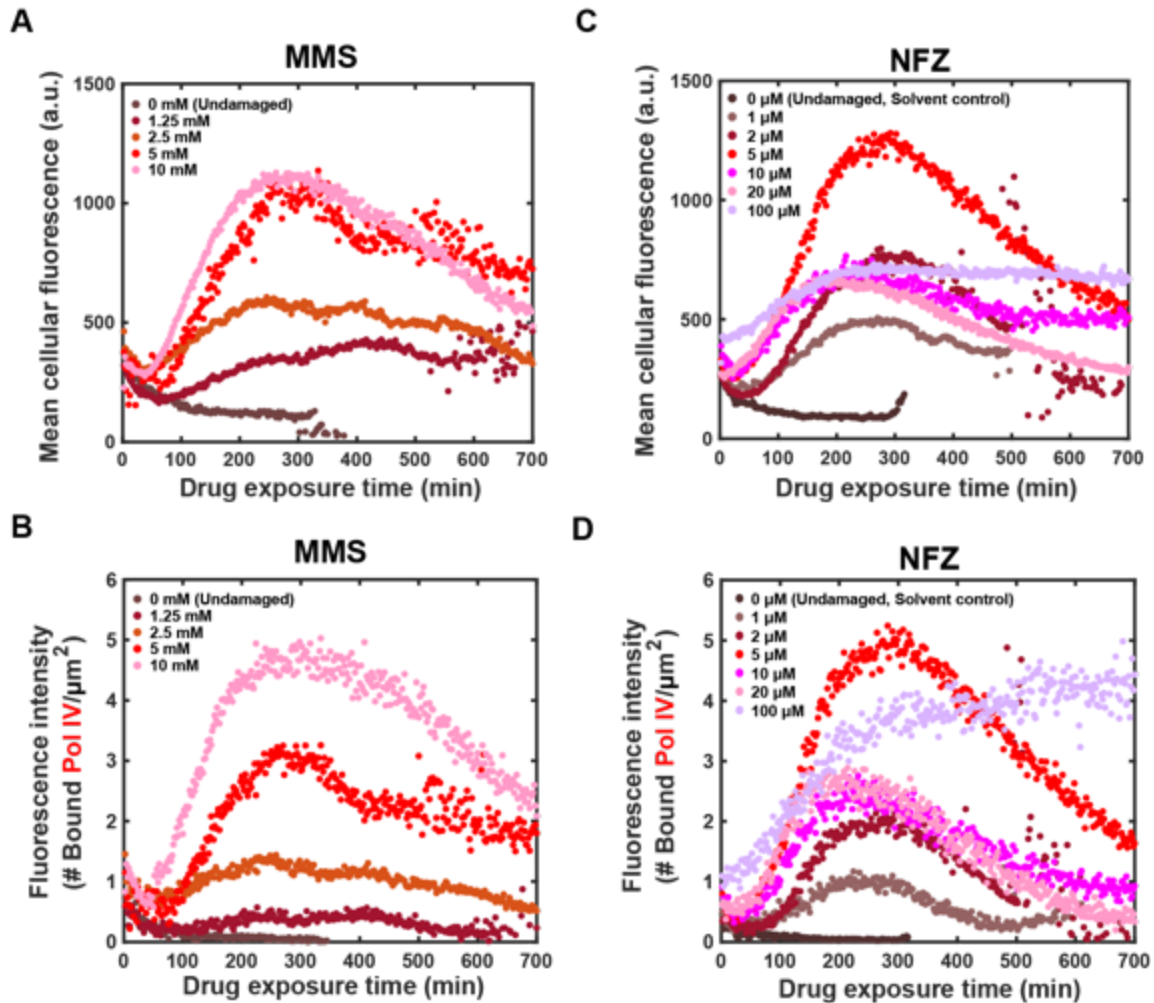


Fig 4.2 DNA damage drugs MMS and NFZ elicit a Pol IV response over the course of several hours, with an overall intensity that depends on drug concentration. A. Response over time to different dosages (0 mM, 1.25 mM, 2.5 mM, 5 mM, and 10 mM) of MMS, as assayed by total fluorescence of Pol IV-mCherry in the cell, normalized per cell area. **B.** Response over time to the same dosages of MMS as in (A), as assayed by the fluorescence in Pol IV-mCherry foci, normalized per area. **C.** Response over time to different dosages (0 μM, 1 μM, 2 μM, 5 μM, 10 μM, 20 μM, and 100 μM) of NFZ, as assayed by total Pol IV-mCherry fluorescence in the cell, normalized per cell area. **D.** Response over time to the same dosages of NFZ as in (B.), as assayed by the fluorescence in Pol IV-mCherry foci, normalized per area.

panels of **Figures S4.4A,B**), in agreement with published observations (39). Control experiments monitoring total cellular fluorescence in wild type cells (including no fluorescent label) under identical laser excitation showed a much-reduced response (e.g. ~200 a.u. at 20 μM NFZ, **Figure S4.5F**), except at 100 μM NFZ. Similarly, the increase of the whole-cell fluorescence in the yellow even at low dosages of NFZ (**Figure S4.5H**) comprised the detection of a Pol IV-specific response for Pol IV labeled with EYFP (**Figure S4.5G**). The response of Pol IV foci (again normalized per area) to NFZ dosage over the same time period is shown in **Figure 4.2D** (and identical **Figure S4.8E**). At low dosages of NFZ, we observe that Pol IV again rarely binds to DNA (in agreement with previous observations (13)), with less than one DNA-bound Pol IV molecule found per square micron. At higher dosages of NFZ up to 20 μM, the number of DNA-bound Pol IV molecules per square micron increases, reaching

a maximum of 5 after 5 h at 20 μ M NFZ, and declining again for longer observation times, similar to the whole-cell fluorescence (**Figure 4.2C**). Control experiments monitoring the fluorescence intensity within identified foci (again normalized by total cell area) in wild type cells (including no fluorescent label) under identical laser excitation showed a much-reduced response (no observable Pol IV foci at 5 h, **Figure S4.8F**), except at 100 μ M NFZ. A comparable set of experiments in which Pol IV was labeled with EYFP detected overall similar trends in the foci (**Figures S4.8G,H**), it being less sensitive to NFZ fluorescence than the whole-cell analysis under similar conditions (**Figures S4.5G,H**).

4.2.3 The spatial distribution of Pol IV depends on dosage of DNA damage drugs and elapsed time.

To gain further insight into the response of Pol IV to DNA damage drugs, we analyzed the spatial distribution of Pol IV foci along the long axes of the cells as a function of MMS or NFZ dosage and time. We first examined the spatial distribution of Pol IV foci at the peak of the Pol IV temporal response (5 h, see **Figure 4.2**) for different MMS dosages (**Figure 4.3A**, red histograms; the full set of histograms including all times is shown in **Figure S4.9A**). To report on the replisome under the same conditions, we co-plot the spatial distribution of foci observed in the yellow channel, which reflects DNA-bound β -clamps in the vicinity of the replication fork (30,31) (**Figure 4.3A**, yellow histograms). As expected, the density of Pol IV foci is very low in the absence of MMS; the replisome, in contrast, is readily observable and exhibits a spatial position that peaks at mid-cell, in agreement with published findings (30,31,41). As the MMS dosage is increased, we observe an increase in the density of Pol IV foci. These Pol IV foci are distributed relatively uniformly along the long axis of the cell, until the highest MMS dosage (10 mM) is reached and Pol IV foci are most prominent at the cell poles. The foci representing the replisome, in contrast, maintain their highest probability at mid-cell irrespective of MMS dosage. We have also examined the evolution of the spatial distribution of foci over time up to the peak of Pol IV temporal response at modest MMS dosages below 5 mM (**Figure 4.3B**; Pol IV foci, red histograms; β -clamp foci, yellow histograms). We consider the response of cells at such dosages to be most representative of a response in which cells go through the process of recovery from DNA damage, because cells remain capable of cell division within the time course of the experiment (**Figure S4.11A**). We observe only a mild increase in the density of Pol IV foci over time, together with a slight shift of the spatial distribution of Pol IV foci from peaked at mid-cell to more uniformly distributed along the long axis of the cell. The spatial distribution of the replisome, while most pronouncedly peaked at mid-cell at time zero, nonetheless maintains a peak at mid-cell even after 5 h. These results (for which strain controls are included in **Figures S4.9B** and **S4.10A,B**) illustrate that the spatial distribution of Pol IV foci varies with the cumulated MMS dosage, slightly favoring the mid-cell position in the absence of MMS to favoring the poles upon prolonged exposure to higher concentrations of MMS.

We have similarly examined the spatial distribution of Pol IV foci at the peak of the Pol IV temporal response (5 h, see **Figure 4.2**) for different NFZ dosages (**Figure 4.3D**, red histograms; the full set of histograms including all times is shown in **Figure S4.9C**). As above, we co-plot the spatial distribution of β -clamp foci (**Figure 4.3D**, yellow histograms). Again, we observe that the density of Pol IV foci in the absence of NFZ is essentially zero, as expected, whilst the replisome signal is clear and its spatial localization peaks at mid-cell. As the NFZ

dosage is increased, we observe an increase in the density of Pol IV foci. At the maximal response (in terms of the density of Pol IV foci) at [NFZ] = 5 μ M, it is already apparent that the distribution of Pol IV foci shows high density at the cell poles. Interestingly, at this NFZ dosage the spatial distribution of foci representing the replisome has also broadened relative to its clearly peaked mid-cell position in the absence of NFZ. At higher NFZ dosages (10 μ M and beyond), the density of Pol IV foci is observed to decrease while the peaks in the spatial position at the cell poles are maintained. At these higher dosages, the spatial positioning of the replisome appears still further disrupted (i.e., the broadened replisome profile further prevails). We have also examined the spatial distribution of Pol IV and β -clamp foci over time at more modest NFZ concentrations (where cell division remains observable over the course of the experiment, **Figure S4.11B**), as shown in **Figure 4.3E** ([NFZ] = 2 μ M; Pol IV foci, red histograms; β -clamp foci, yellow histograms). Under these conditions, we observe an increase in the density of Pol IV foci over time, with these foci being relatively uniformly distributed along the long axis of the cell; the spatial distribution of the replisome, while most strongly peaked at mid-cell at time zero, continues to peak at mid-cell even after 5 h. These results (for which strain controls are included in **Figures S4.9D** and **S4.10D,E**) illustrate that the spatial distribution of Pol IV foci varies with the cumulated NFZ dosage, being uniformly distributed throughout the cell at low cumulated dosage and favoring the poles at high cumulated dosage.

These results can be summarized in more concise form by defining a polarization P that describes whether the majority of the foci are to be found in the central two quartiles of the cell or in the poles. We define $P = \frac{N_{poles}}{N_{total}}$, where N_{poles} is the number of molecules found in foci located in the poles and N_{total} is the number of molecules found in foci in the cell. Thus, when foci are concentrated in the central two quartiles of the cell, P is close to zero; in contrast, as the foci become more concentrated in the poles, P approaches one. Three-dimensional plots showing the evolution of Pol IV and β -clamp polarization as a function of MMS dosage and time are shown in **Figure 4.3C** (top and bottom panels, respectively). The corresponding set of three-dimensional plots showing the evolution of polarization as a function of NFZ dosage and time are shown **Figure 4.3F**. Overall, one can observe that increases in cumulated drug dosage yield the same trend in the evolution of Pol IV and β -clamp polarization, namely large increases in the Pol IV polarization and smaller increases in the β -clamp polarization, irrespective of whether the DNA damage drug is MMS or NFZ. The trends are more pronounced, however, in the presence of NFZ. Strain controls for these experiments can be found in **Figure S4.10C,F**.

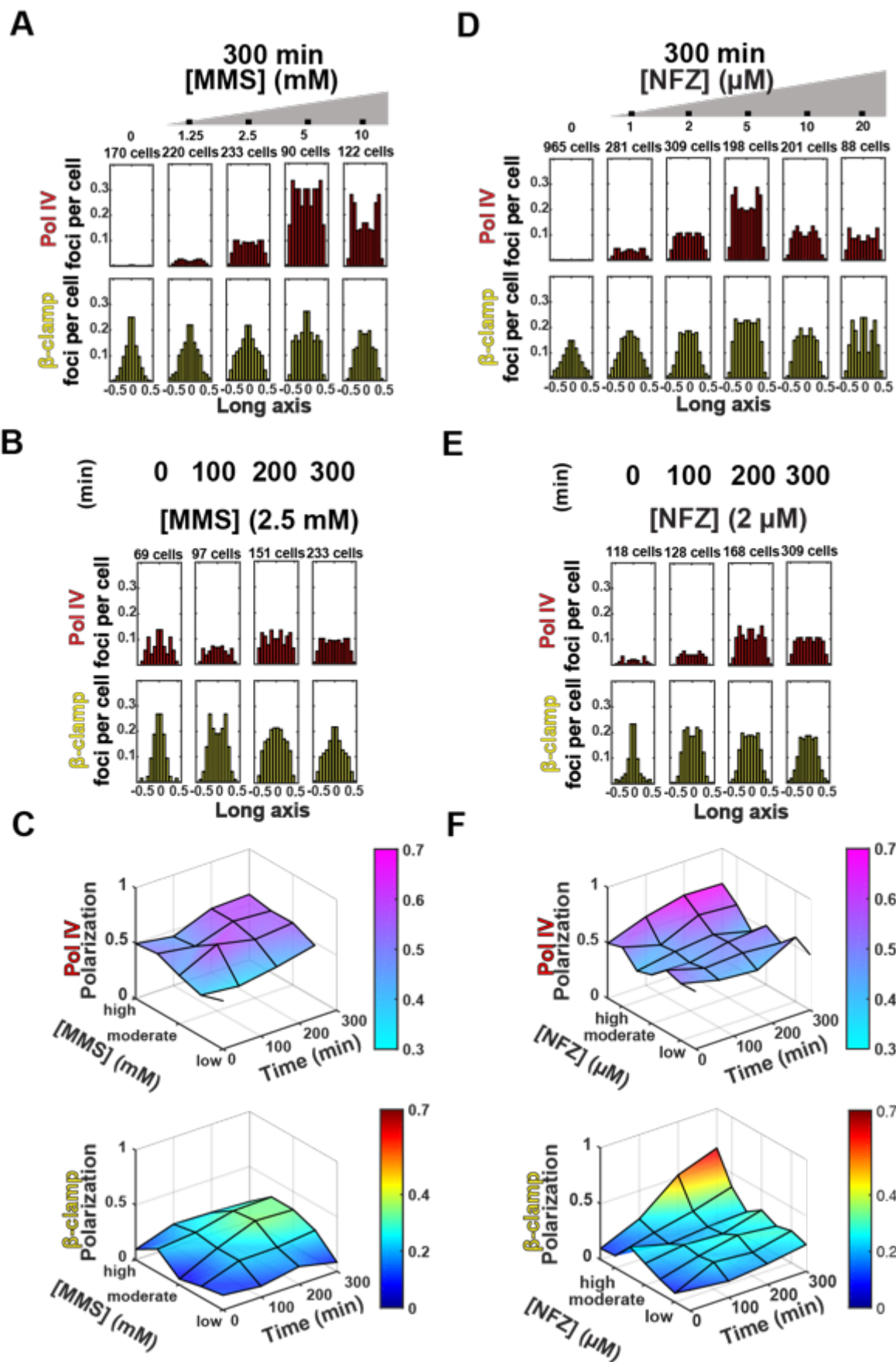


Figure 4.3 The influence of DNA damage drugs MMS and NFZ on the spatial distributions of Pol IV and the replisome. **A.** Spatial distributions of Pol IV-mCherry and the YPET- β clamp sampled 5 h following different dosages (0 mM, 1.25 mM, 2.5 mM, 5 mM, and 10 mM) of MMS. **B.** Spatial distributions of Pol IV-mCherry and the YPET- β clamp over time at an MMS dosage of 2.5 mM. **C.** Spatial distributions of Pol IV-mCherry and the YPET- β clamp sampled 5 h following different dosages (0 μ M, 1 μ M, 2 μ M, 5 μ M, 10 μ M, 20 μ M, and 100 μ M) of NFZ. **D.** Spatial distributions of Pol IV-mCherry and the YPET- β clamp over time at an NFZ dosage of 2 μ M. **E.** Degree of spatial polarization (see main text) of Pol IV-mCherry (left) and YPET- β clamp (right) as a function of MMS dosage and time. **F.** Degree of spatial polarization (see main text) of Pol IV-mCherry (left) and YPET- β clamp (right) as a function of NFZ dosage and time.

4.2.4 Examination at the single-cell level of colocalization between Pol IV and the replisome in the presence of DNA damage drugs

In the preceding measurements, we have examined the spatial distributions of Pol IV and the replisome and described our findings as a function of cumulated dosage of the DNA damage drugs MMS and NFZ. The results reflect the behavior of Pol IV and replisome averaged over many cells (varying between 50 and 900, depending on drug effects/dosage and time). While this approach reveals the main trends, it comes with two drawbacks: first, the averaging over many cells may wash out interesting signatures of Pol IV or replisome dynamics that occur at the single-cell level; second, and related, the cellular population over which is averaged is diverse, and, particularly at the higher cumulated drug dosages, may include cells in which DNA replication has stalled and cell division no longer occurs. Indeed, in our experiments cell division times are observed to increase even at low to moderate concentrations of MMS and NFZ (**Figures S4.11B,C** respectively), and reliable cell division (and an estimate of the timescale between cell birth and division) is only observed at MMS dosages up to (and including) 2.5 mM, and at NFZ dosages up to (and including) 2 μ M. Whether in such situations even behavior that does clearly emerge from cell averages reflects any TLS-specific interactions between Pol IV and the replisome is not *a priori* clear; certainly, the disruption of the spatial distribution of the replisome away from a pronounced peak at mid-cell at high cumulated dosages of NFZ (**Figure 4.3F**) could argue against this. For this reason, we have set out to examine the colocalization between Pol IV and replisome at the single-cell level at concentrations of MMS (2.5 mM) and NFZ (2 μ M) where upregulation of Pol IV is clearly discernible, but where replication and subsequent cell division remain intact.

In these experiments (**Figure 4.4**), we examine the spatial location of Pol IV and β -clamp foci over the course of the cell division cycle and use this information to compute the degree of colocalization between Pol IV and β -clamp. Here, the degree of colocalization is defined as the fraction of Pol IV foci that include a β -clamp focus (**Materials and Methods** and Ref. (13)). As can be seen by examining the dynamics over the course of the cell division cycle, the degree of colocalization can vary substantially within a single cell. Furthermore, by comparing traces resulting from different individual cells, it is clear that different cells do not share identical trends over the course of the cell cycle: the temporal unfolding of colocalization varies substantially from cell to cell. Overall, the degree of colocalization is observed to fluctuate

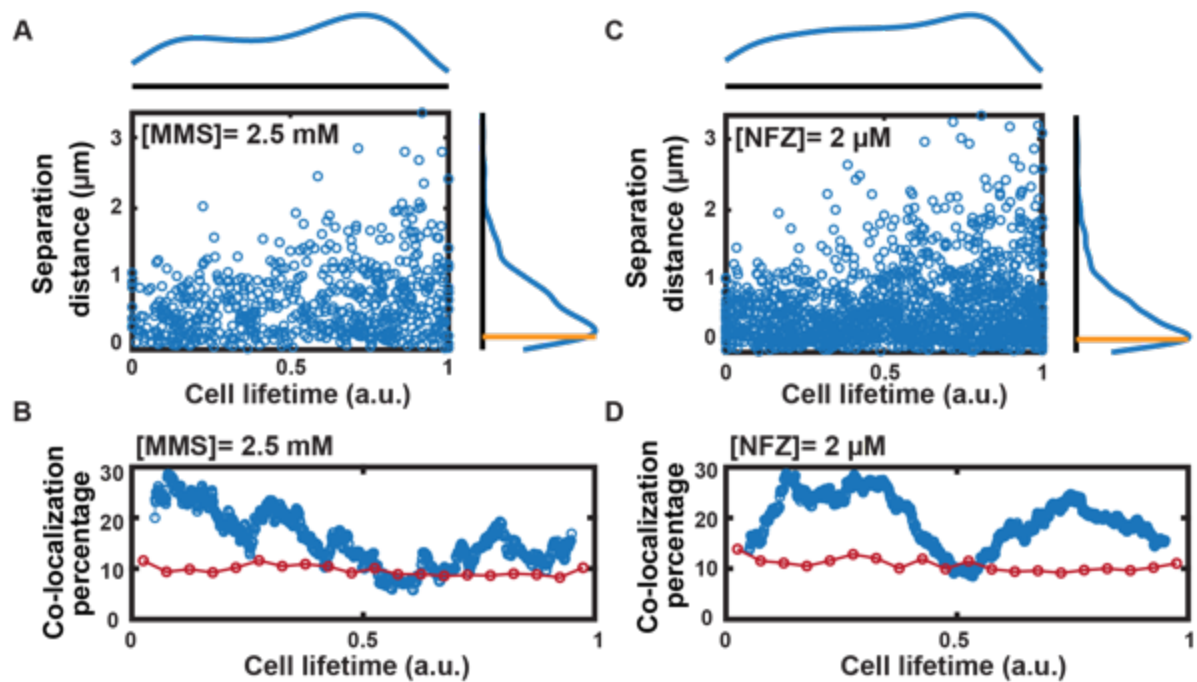


Fig 4.4 Assessment of Pol IV and replisome colocalization within the lifespan of a single cell. Colocalization data is assessed as a function of the normalized cell lifetime, defined from cell birth ($t=0$) to cell division ($t=1$) for drug dosages at which DNA damage effects are clearly present, but cell division cycles are not halted. **A.** Scatter plot of the separation distance between a Pol IV-mCherry focus and the nearest replisome focus (monitored via the YPET- β clamp) versus the normalized cell lifetime in the presence of 2.5 mM MMS. The probability distribution of finding foci at a certain cell lifetime is provided above the scatter plot, and the probability distribution of finding foci at a certain separation distance is indicated to the right of the scatter plot. The colocalization threshold for separation distance of 200 nm is indicated by the yellow line. $N = 26$ cells. **B.** The percentage of Pol IV foci colocalized with a replisome as a function of normalized cell lifetime in the presence of 2.5 mM MMS (blue line), calculated from the same dataset as panel (A.). The percentage of colocalization that would be expected from random foci localization (red line) is calculated considering the cell area, the number of replisomes present and the area occupied by each replisome as a disk with a radius of 200 nm. and. **C.** As in panel (A.), but now in the presence of 2 μ M NFZ. $N = 46$ cells. **D.** As in panel (B.), but now in the presence of 2 μ M NFZ and calculated using the same dataset as in panel (C.). The cell lifetime is indicated in arbitrary units (a.u.), where 0 and 1 represent cell birth and division, respectively.

between 10-30%, both within a single cell cycle or when averaging over different cells (**Figures 4.4B,D**). The degree of colocalization that occurs by chance can vary over the course of a cell cycle, as the number of active replisomes may fluctuate (42) and the cell volume increases as the cell grows. Taking the number of replisomes and the cell area into account, we calculated the expected percentage of colocalization from random foci localization and find it to be ~10% (**Materials and Methods**; red lines in **Figures 4.4B,D**; red lines in **Figures S4.12B,D**). It is only at a little over half of the cell lifetime, which coincides with the typical time at which replication terminates, that the colocalization percentages reduce to the random expectancy level. This point in the cell cycle is characterized by the absence of clear replisome foci positioning, after the principal replication has finished and before replication of daughter chromosomes is re-initiated. At all other times, while replication is carried out, we observe a colocalization percentage that is considerably elevated above the random expectancy value.

Thus, we deduce that under these low dosages of DNA damage drugs, colocalization between Pol IV and replisome occurs, while at the same time a population of Pol IV foci remains that does not colocalize with the replisome. This suggests that multiple pathways of Pol IV mediated DNA repair may coexist, both at the replisome and independent of it, as previously reported (29). However, while we observe clear fluctuations in the size of the replisome-colocalized population of Pol IV foci over the course of the cell cycle, in contrast to the findings of Ref. (29), we do not find a dependency of the colocalization percentage on the type of DNA damage at play.

4.3 Discussion

In this work, we have performed long time-lapse imaging with single-molecule sensitivity to probe the response over time of the bacterial TLS polymerase Pol IV to different dosages of the DNA damage drugs MMS and NFZ, selected for their differences in molecular reactivity. Our findings expand on those of the recent literature by systematically sampling the effect of cumulated dose of DNA damage drugs. Our observations indicate that Pol IV is upregulated over the course of several hours following the addition of these DNA damage drugs, and that this upregulation results in more stationary Pol IV clustered in foci. While our Pol IV fusion proteins are not as fully functional as the wild type proteins (**figure S4.2**, serial dilution assays), our strains still retain activity. This partial functionality may be related to the choice of linkers that connect the gene of interest and fluorophore DNA (33). At low cumulated dose of DNA damage, these foci, which likely report on DNA-bound Pol IV, are predominantly uniformly distributed throughout the cell; however, as the cumulated DNA damage dose increases, they are more likely to be found towards the cell poles (**Figures 4.3A,C,E**). Thus, we conclude that Pol IV does not have a unique localization feature, but rather that its response is dosage dependent. Under conditions where the DNA damage load did not preclude cell division, Pol IV colocalizes more frequently with the replisome than would be expected by chance (**Figures 4.4B,D and S4.12B,D**), but most Pol IV molecules do not colocalize with the replisome.

We now compare our more detailed findings with those of several recent investigations of Pol IV and cellular response to the presence of DNA damage drugs (13,27,29). We selected the two drugs (MMS, NFZ) because we found that most Pol IV studies have been characterized using drugs eliciting N²-dG adducts or alkylation residues (7,17,23,33). Additionally, while our research was in progress, two publications emerged using the same drugs, allowing for direct comparison (13,29). We find agreement in certain aspects of the response, for example in the upregulation of Pol IV over the course of the first few hours following addition of DNA damage drugs (13) and in its spatial positioning in the cell in response of high (cumulated) dosages of NFZ (29). But we find differences in others, for example in the dependence of Pol IV colocalization with replisome on type of DNA damage drug (29). Where relevant, we comment on how differing experimental conditions, including dosages, may have resulted in different types of response observed. Subsequently, we describe which aspects require further elucidation in the context of proposed models for Pol IV response to DNA damage.

The effect of DNA damage drugs on the upregulation of Pol IV and its subsequent DNA binding

In the absence of DNA damage drugs, Pol IV is present at low copy number in *E. coli* (**Figure 4.4.1B**) (13). From the whole-cell fluorescence, we estimate ~20 Pol IV molecules per cell (data not shown). This agrees with the low Pol IV copy number (and, on average, 0.5 ± 0.5 Pol IV foci per cell) described for Pol IV-YPet in Ref. (13) in EZ glucose medium (43,44), a richer medium than the M9 medium employed in our studies. When cells constitutively expressed the SOS response (via an engineered frame shift in the *lexA* gene) (13,29), wide-field fluorescence imaging similarly did not reveal observable Pol IV foci (13). However, under similar conditions the authors of Ref. (29) were able to use PALM imaging (45) observe “sharp” Pol IV-PAmCherry foci with a 250 ms integration time. We attribute this difference to the reduced background (and improved signal-to-noise) and more precise tracking of individual molecules obtainable using PALM. Nonetheless, there appears to be agreement amongst *in vivo* studies (ours and Refs. (13,29)) that the number of immobile, presumably DNA-bound Pol IV is low in the absence of DNA damage.

In the presence of DNA damage drugs MMS and NFZ, we find that a substantial presence of Pol IV builds up in a concentration-dependent manner (**Figure 4.1B**, **Figure 4.2**). We observe a 5.5-fold relative increase in the whole-cell fluorescence (**Figures 4.2A,C**) and a similar increase in the fluorescence intensity of Pol IV foci (**Figures 4.2B,D**). At the moderate drug concentrations of 2.5 mM MMS and 2 μ M NFZ, we counted approximately 1–4 Pol IV molecules per focus (data not shown). Both a similar build-up of Pol IV and a corresponding number of Pol IV per foci were observed in cells treated with the fluoroquinolone antibiotic ciprofloxacin (13), an antibiotic that through its direct inhibition of DNA gyrase ultimately results in the formation of DNA double-strand breaks and induction of the SOS response (46). Both these *in vivo* experiments support the hypothesis that DNA damage is essential for the recruitment of Pol IV to DNA. The decrease in Pol IV response observed in our experiments on timescales exceeding 5 h, may reflect the recovery of cells from incurred DNA damage (47). These data are consistent with error-free DNA repair occurring in the early stages of the SOS response and translesion synthesis being catalyzed by Pol IV in the middle stage of the SOS response. Whether the reduction in Pol IV presence in the late stage of the SOS response, as observed in our experiments, is functionally linked to further repair activities carried out by e.g. Pol V, as suggested in Ref. (13), remains to be determined.

The effects of different concentrations of DNA damage drugs on overall cellular behavior.

Several lines of evidence lead us to conclude that the increased cumulated dosages of DNA damage drugs do indeed increase the actual extent of DNA damage. Even at low dosages of MMS and NFZ, the mean cell division time is observed to increase (**Figures S4.11**). Once these dosages have reached 5 mM (MMS) or 10 μ M (NFZ), little cell division is observed within the 12 h duration of our experiments. Furthermore, with an increase in the cumulated dose of DNA damage drugs, the fraction of cells that shows filamentation, reflecting continued growth in the absence of cell division (39,48), is increased (**Figure S4.4**), particularly strongly so in the case of MMS (**Figure S4.4A**). At the highest MMS dosages tested (50 and 100 mM), the extent of filamentation is reduced, but black spots are observed within the cells (**Figure S4.3**), suggesting aggregation of cellular contents as a result of the cumulated damage. These

conditions, which were accompanied by a cessation of cell growth, and a reduction in cell length as in Ref. (29), were not included in further analysis. The highest NFZ dosage tested (100 μ M) was also not analyzed, simply because at this high dosage the fluorescence of NFZ itself prevented accurate tracking of Pol IV-mCherry.

If we compare the dosages of MMS and NFZ employed in our experiments to those utilized in Refs. (13,29), some notable differences emerge. In Ref. (13), the MMS dosage employed was fixed at 0.3 ng/ml, or 3 nM, six orders of magnitude lower than in our experiments. While it initially appears surprising that Pol IV foci were observed under these conditions, it must be noted that the experimental conditions included exposing cells to a continuous flow of solution containing MMS, whereas in our experiments the addition of MMS to an agarose pad was performed only once, ~20 min prior to imaging on the microscope (**Materials and Methods**). In contrast, in Ref. (29), the dosages of DNA damage drugs employed were typically higher: 100 mM for MMS and 40 or 100 μ M for NFZ. These higher dosages may simply result from a shorter (20 min) incubation time (in the case of MMS); or from the incubation of cells with drug in broth, rather than on the agarose pad during imaging (in the case of NFZ). Alternatively, the fact that these experiments were performed on cells that constitutively expressed Pol IV permitted the cells to tolerate higher concentrations of DNA damage drugs. At these high dosages of DNA damage drugs, average cell length was observed to decrease (29), as it did in our experiments (**Figure S4.4**).

The effects of different concentrations of DNA damage drugs on Pol IV spatial location, and on its colocalization with the replisome.

We now compare the patterns of Pol IV spatial localization in our wide-field fluorescence imaging experiments to those described in Ref. (29), obtained using super-resolution microscopy. In the absence of DNA damage drugs, we did not analyze the spatial distribution of Pol IV foci, as too few of them were observed (see above); the authors of Ref. (29), however, detected a static Pol IV population that was uniformly distributed along the long axis the cell. Under the same conditions, the replisome distribution (monitored via SSB-mYPet) peaked at $\frac{1}{4}$ and $\frac{3}{4}$ positions. This differs from our observation that the replisome displays a preference for mid-cell positions, as elsewhere described in the literature (49); possibly, differences in strains or growth conditions contribute to this. Accordingly, only weak colocalization between Pol IV and the replisome was found in the absence of DNA damage drugs.

At low dosages of both MMS and NFZ, we observe that Pol IV foci are distributed uniformly throughout the cell, while the replisome maintains its preference for mid-cell (**Figures 4.3A,B,D,E**). This results in an intermediate value (~0.5) of the polarization for Pol IV (top panels in **Figures 4.3C,F**) and a slightly lower value of the polarization for the replisome (bottom panels in **Figures 4.3C,F**). As either the concentrations of MMS or NFZ (**Figures 4.3A,D**) or the overall time elapsed increase (**Figures 4.3B,E**), the distribution of Pol IV foci includes more density towards the cell poles; also the spatial distribution of the replisome broadens. Accordingly, the polarization for both increases to higher values (**Figures 4.3C,F**). For the case of MMS, it is challenging to compare our findings to those of Ref. (29), as the experiments were not performed at similar concentrations. For the case of NFZ, these findings confirm and extend the observation of dosage-dependent movement of Pol IV towards the poles found in Ref. (29).

Assuming that (dis)similarity in the polarization between Pol IV and replisome implies (a lack of) proximity between the two, it follows that the spatial overlap between Pol IV and replisome increases with the cumulated drug dosage for both MMS and NFZ. However, care should be taken in the interpretation of this statement. First, because at the highest cumulated drug concentrations the spatial distribution of both the Pol IV and the replisome increase in density towards the poles, such overlap may merely result from changes in overall cellular processing under conditions of damage, e.g. the confinement of damaged DNA and misfolded proteins at the poles (50-52), as opposed to resulting from a functional interaction. Thus, while extrapolating the data in **Figures 4.3C,F** to 100 mM MMS might lead one to expect a high degree of spatial overlap between Pol IV and replisome, in agreement with Ref. (29), such overlap might not reflect any functional interaction between Pol IV and the replisome. Second, the data displayed in **Figures 4.3** reflect the population-wide situation for many cells, and do not report directly on whether in any particular cell, Pol IV and replisome have spatial overlap.

To address these points, we have quantified the degree of colocalization between Pol IV and replisome in individual cells, and only at low to moderate dosages of MMS and NFZ (**Figure 4.4, Figure S4.12**). Here, we find that there is a degree of colocalization that exceeds that of random chance, irrespective of the number of Pol IV foci, for both MMS and NFZ. For the case of higher concentrations of MMS (100 mM) and NFZ (40 or 100 μ M), similar analysis was performed in Ref. (29). There, the presence of MMS decreased of the average distance between Pol and the replisome by 42% (relative to untreated cells), resulting in a degree of colocalization that exceeded that of random chance by \sim 6-fold and was influenced by interaction with the β -clamp; in contrast, despite observations of dosage-dependent movement of Pol IV to the poles as in our experiments, the presence of NFZ increased the average distance between Pol and the replisome by 13% (relative to untreated cells), resulting in a degree of colocalization that did not exceed that of random chance. Possibly, the use of SSB as a replisome marker in Ref. (29) contributes to this discrepancy between our findings, as SSB binding may reports not only on DNA replication but more broadly on DNA damage; alternatively, it may derive from differences in strains or growth conditions that warrant further investigation (53).

Models and general pathways.

Based on our findings and those of others, we now consider the overall response of Pol IV to the DNA damage drugs MMS and NFZ. Clearly, our data indicate that any description of this response must take into account the cumulated drug dosage. By and large, we find that the response of Pol IV to these drugs is relatively similar, with the upregulation of Pol IV occurring on similar timescales and its spatial distribution along the long axis of the cell being in both cases evolving from uniformly distributed at low cumulated drug dosages to slightly preferring the poles at higher cumulated drug dosages. Our finding that the spatial distribution of Pol IV is independent of the type of DNA damage drug employed contrasts with the findings of Ref. (29), obtained at higher dosages of MMS and NFZ. We also find the degree of colocalization between Pol IV and replisome to be similar for both types of DNA damage drugs, in both cases being substantially above that expected by random chance. Similar, for both DNA damage drugs tested, a large fraction of the static Pol IV is not found in the vicinity of a replisome. These Pol IV may be recruited to sites of DNA damage through mechanisms that remain to be determined (13); interestingly, as we have compared the colocalization between Pol IV and the β -clamp as marker of the replisome, we can also conclude that interactions with the β -

clamp alone, irrespective of replication (31), do not suffice to recruit all Pol IV to the DNA (29). In agreement with other reports, this suggests that while “mass action” may govern exchange with Pol III at the replisome, it does not dictate the behavior of all Pol IV present in live cells (13,29).

Conclusions

We have examined the response of cells to DNA damage drugs MMS and NFZ by examining the behavior of the TLS polymerase Pol IV, and its relationship to the replisome. Overall, we find the response to be similar for the two drugs. While a substantial fraction of Pol IV appears to colocalize with the replisome, an even larger fraction does not, suggesting replication-independent (or post-replicative) roles for Pol IV. In future experiments, it will be interesting to probe the response of Pol IV to a wider array of DNA damage. It will also be pertinent to extend such investigations to the other types of translesion polymerases present in bacterial cells (54-56) in order to probe their affinities for different DNA damage substrates (57), and to explore possible redundancy amongst them. Similar investigations will inform future studies of antibiotic resistance (58-60).

4.4 Materials and methods

Genetic engineering of *E. coli* strains

All strains reported here are *Escherichia coli* K12 AB1157 derivatives. The fluorescently tagged strains for *dinB* and *dnaN* genes (SDR32 and SDR33) were both created by a two-step process, first by λ_{red} recombination (for the *dinB* gene) and then by phage transduction (for the *dnaN* gene) (S1A Fig). As a result of FLP-mediated recombination via plasmid pCP20, the final strains do not include the kanamycin antibiotic resistance gene. As a negative control, we also used λ_{red} recombination to create a $\Delta\text{dinB}::\text{FRT-Kanamycin-FRT}$ strain (designated SDR19) in which the *dinB* chromosomal locus is deleted and replaced by a short fragment (FRT-Kanamycin-FRT) that is a relic of λ_{red} recombination. To avoid disrupting any regulatory sites in the neighboring genes, 50 bp at both the beginning and end of the *dinB* coding sequence were kept intact. Further details on strains, plasmids and primers are provided in **Tables S4.1-S4.3**. The PCR amplification gel images shown in **Figure S4.1B** are for *dinB* (left) and *dnaN* (right) loci, using primer pairs 2601-2602 and 1045-1628, respectively. (In **Table S4.2**, plasmids pCP20 and pKD46 are originally derived from studies described in Refs. (61,62), respectively).

Biochemicals, reagents, and media employed

All materials reported were purchased from Sigma- Aldrich, unless specified otherwise. Luria Bertani (LB) medium was used in bulk experiments, and M9-glycerol medium supplemented with the amino acids threonine, leucine, proline, histidine and arginine was used in imaging experiments, unless specified otherwise.

Growth curves

Strains were grown in LB broth for 16 h at 37 °C while shaking at 200 rpm. The next day, the culture was diluted in fresh LB medium (1:5000) and the Optical Density at 600 nm wavelength (OD₆₀₀) was measured on a spectrophotometer (Ultrospec10, Amersham) at 45 min time intervals until a value of ~1.00 was recorded. For each strain of interest, growth curves were obtained for two biological replicates, on different days. None of the strains tested exhibited aberrant phenotypes in the growth curves (**Figure S4.1C**).

Serial dilution assay to assess labeled strain functionality in presence of DNA damage

Strains were grown in LB broth for 16 h at 37 °C while shaking at 200 rpm. LB agar plates were prepared by mixing LB-agar (1.5% w/v) with either of DNA damage drugs MMS or NFZ, and then cast. For each strain, cells were plated from dilutions ranging from 10⁻¹ to 10⁻⁸ and incubated for 16 h. The following day, the plates were photographed in a Gel Documentation System (Bio-Rad). In the case of NFZ, N,N-Dimethyl formamide was used as a solvent. Also for each strain, serial dilution experiments were obtained for two biological replicates, on different days. These data show that the newly generated strains in which *dinB* and *dnaN* were tagged retain a high degree of functionality relative to the Δ *dinB*::FRT-*kanamycin*-FRT strain (**Figure S4.2**).

Washing of microscope slides and coverslips

All washing steps were performed ultrasonically in Coplin jars, in the following order: 0.2% Hellmanex wash for 20 min, Milli-Q water wash twice for 5 min each, 100% ethanol wash for 20 min and finally, two repeats of a Milli-Q water wash for 5 min each. The slides and coverslips were then air-dried using a nitrogen pressure gun.

Preparation of cells for time-lapse microscopy

The strains for imaging were grown in a primary culture overnight (M9-glycerol) at 37 °C while shaking at 200 rpm. The next day, these cells were diluted (1:10) in fresh M9-glycerol and grown under the same conditions for ~1.5 to 2 h, so that the OD_{600nm} ranged from ~0.15 to 0.20. These cells were centrifuged in a volume of 500 µl to obtain a pellet. This pellet was then re-dissolved in fresh 50 µl M9 glycerol. A volume of 2 µl was loaded onto the agarose pad for imaging.

Preparation and loading of agarose pads for time-lapse microscopy

To prepare agarose pads, 1.5% agarose (Ultrafine agarose, Invitrogen) in M9-glycerol was heated, cast and cut into pads (1 cm*1 cm*0.2 cm). Next, a cell suspension was placed on the top of the agarose pad and air dried. Thereafter, this pad was placed on a clean round cover-slip (# 1, Menzel Glaser), in such a way that the cell suspension side of the pad now faced the cover-slip and DNA damage drugs (diluted in M9 glycerol to reach the desired concentration) could be placed on the other (now top) surface of the pad. All final drug concentrations were calculated to accommodate the pad volume of 200 µl, and for consistency, every experiment

had 2 μ l (final drug volume) on the surface of the pad (irrespective of dilution). The casting of the pad, and the loading of cells and drug onto it, were performed at room temperature.

Microscopy hardware

The time-lapse microscopy experiments were performed on a commercial Nikon Ti-E inverted microscope equipped with a 1.49 NA Apo TIRF 100X Oil immersion objective, a standard Nikon halogen lamp, a Nikon DS-Fi2 Charged Couple Device camera used for phase contrast imaging, and an iXon Ultra EMCCD camera (Andor) used for fluorescence detection. The microscope was surrounded by a temperature cage (Okolab) regulated via a temperature controller (Okolab Touch). Excitation light of wavelengths of 515 nm and 561 nm (provided by diode laser and a diode-pumped solid state laser, respectively; both lasers from Cobolt) was delivered at the objective via a laser combiner LightHUB (Omicron). Inside the microscope, custom filter sets were used, specifically z514, ET540/30m, zt514rdc (Chroma) for EYFP/YPet and z561, ET605/52m, zt561rdc (Chroma) for mCherry.

Protein purification for fluorophore calibration in single-molecule experiments

The coding sequences for EYFP and mCherry were cloned into vector pRSETB (Thermo Fisher Scientific) by performing Gibson assembly (Promega). Proteins were expressed in *E. coli* BL21 DE3 (Biolabs) and purified by nickel pulldown followed by gel-filtration on a Superdex 200 increase column (GE Healthcare). Further details on the primers employed are provided in **Tables S4.1-4.3**.

Calibration of the fluorophore intensity in single-molecule experiments

A schematic of the flow cell used to calibrate the fluorophore intensities *in vitro* is shown in **Figure S4.7A**. Briefly, equidistant holes of diameter ~ 0.2 cm were drilled into a 24*60 mm coverslip (#1, Menzel Glaser) using a laser cutter (Lion Lasers). A pre-cut parafilm spacer was placed between two such cover-slips to form a channel spanning the two holes of the coverslip. The resulting flow cell was then heat-sealed at 80 $^{\circ}$ C for 3-4 min. Once the flow cell had cooled to room temperature, a (1:1) 100 μ l mix of antibody dissolved in M9-glycerol (1:100 JL8 Clontech for EYFP, 1:100 Living Colors 632543 Clontech for mCherry) and fluorescent protein diluted in M9-glycerol ($\sim 1:25$ for 3.3 mg/ml EYFP, $\sim 1:10$ for 1.7 mg/ml mCherry) was prepared. A small fraction of this mix (5 μ l) was then loaded into each channel. In a negative control experiment, only the solution of M9-glycerol with antibody was loaded into the channel. For each fluorophore, the calibration experiment was performed at least twice, on different days (**Figures S4.7B-D**).

Imaging settings

All images were acquired using a personal computer (Dell PC, Windows OS) equipped with NIS-Elements software (Nikon). Long time-lapse videos (~ 12 h) acquired a set of three images at two-minute intervals. The three images include one image from the phase contrast channel and two images from the yellow and red fluorescence channels, respectively. The fluorescence images in the yellow channel were acquired by providing 515 nm excitation light (0.3 mW at the objective) for an exposure time of 100 ms (for both Pol IV and β -clamp). The

fluorescence images of Pol IV in the red channel were acquired by providing 561 nm excitation light (1.9 mW at the objective) for an exposure time of 100 ms; for imaging the β -clamp in the red channel, the power was reduced (to 1.0 mW at the objective).

Image analysis

The original image files are saved as in an *nd2* format and exported as *tif* files. Fluorescence images are flattened through division by illumination profiles, which were determined by imaging fluorescence slides (Chroma Technology Corp) and subsequently applying a low-pass Gaussian filter. These illumination profiles were measured for each laser individually.

Image registration is applied in two parts. The first part introduces microscope-specific rigid transformation parameters, and the second part corrects for day-to-day variations in the translational component of this rigid transformation. First, the built-in functionality in the NIS Elements Advanced Research software for determining camera pixel size and rotation with respect to the *xy*-stage are used to correct for differences in rotation and magnification between the phase-contrast and fluorescence cameras. Furthermore, any translational mismatch between the cameras is restored, and appropriate cropping is subsequently applied to eliminate non-overlapping image areas. Second, in each experiment the three first frames of the time-lapse imaging (corresponding to the images deriving from phase-contrast, excitation at 515 nm, and excitation at 561 nm) are cross-correlated with each other to deduce translational shift with subpixel precision.

Cell segmentation, linking, and fluorescence statistics calculations such as spot finding and fitting, is performed using SuperSegger (63). To assess the spatial distributions of fluorescent foci, individual frames (at 0, 100, 200, and 300 min) were selected from the time-lapse imaging dataset. Any potential errors in cell segmentation were manually corrected using the built-in functionality in SuperSegger. Cell gating based on morphological and phase-contrast intensity parameters was applied to eliminate certain cells (e.g. overlapping cells) in which segmentation errors could not be corrected. These user inputs for segmentation correction and gating were performed by two scientists independently. Measurements as a function of cell lifetime (**Fig 4.4**) were constructed using a cell gating that selects for cells that were reliably segmented and linked from birth until division.

Foci gating is performed by considering the raw intensity of each focus (i.e. the pixel value of the fluorescence image at the centroid of the Gaussian fit) and subtracting from it the mean pixel value of the fluorescence channel inside the cell. For this 'corrected raw focus intensity', a threshold is set. The value of this threshold was empirically determined by measuring the natural variations in autofluorescence (i.e. from the unlabeled strain) that got recognized as foci by SuperSegger. Since these foci are very dim compared to the ones observed in the labeled strains, we are able to find a threshold value for corrected raw focus intensity that separates false positives (originating from autofluorescence), from true positives (originating from fluorescent protein).

Colocalization analysis

To assess the degree of co-localization between Pol IV foci and replisomes, we have calculated the distances between all pairs of Pol IV foci and replisomes. These distances are

determined by taking the foci locations returned by SuperSegger and calculating the Euclidean distance between them. Subsequently, we considered for each Pol IV focus the closest replisome only, leaving us with an array of numbers that we call the separation distances. We classify a pair of Pol IV and replisome foci co-localized if their separation distance is smaller than 200 nm. The percentage of co-localization represents the percentage of Pol IV – replisome foci pairs that meet this criterion.

We have calculated the co-localization percentage that would result from random Pol IV binding as follows. We identify the replisome foci in a cell and calculate the area they occupy by considering a 200 nm radius (the co-localization threshold) around them. The area occupied by replisomes is divided by the total cell area to determine the probability of co-localization upon random binding. As a result of this method, this probability is not a single number, but varies over the cell cycle because it is modulated by the cell length and the number of replisomes present. However, as a rule of thumb a 10% probability of co-localization from random binding can be generally applied.

Acknowledgments

We thank Patricia Foster for supplying strains, Belen Solano Hermosilla for help with designing and making figures, and Anjana Badrinarayanan, Jacob Kerssemakers, Joseph Loparo, Houra Merrikh, Andrew Robinson, and Elizabeth Thrall for insightful discussions.

4.5 Supplementary information

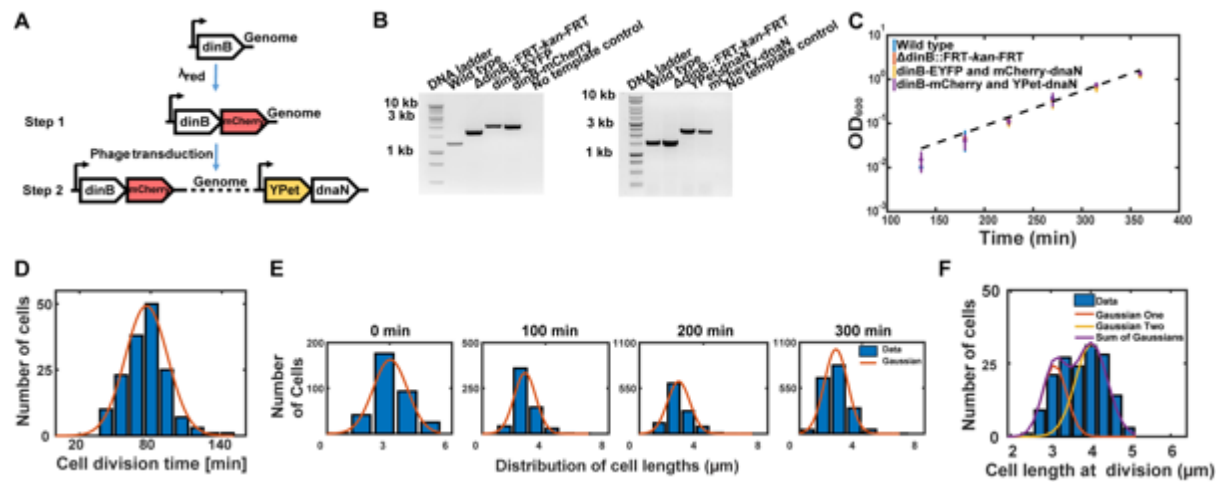


Figure S4.1 Strain creation and characterization. **A.** Cloning schematic for a single strain. **B.** PCR results for *dinB* and *dnaN* loci. Lanes 2-6 show the results for different strains: wild type, SDR19 (\square *dinB*), SDR32 (*dinB*-EYFP, *mCherry*-*dnaN*), SDR33 (*dinB*-*mCherry*, *YPet*-*dnaN*) and No template control. **C.** Growth curves in LB medium for the four strains in (B.), with fitted doubling times of 38 min (wild type), 39 min (SDR19), 38 min (SDR32), and 37 min (SDR33). **D-F.** Characterization of cells in M9 medium on agarose pad in the absence of DNA damage drugs. **D.** Cell division (doubling) times. **E.** Distributions of cell lengths over time. **F.** Cell lengths at division.

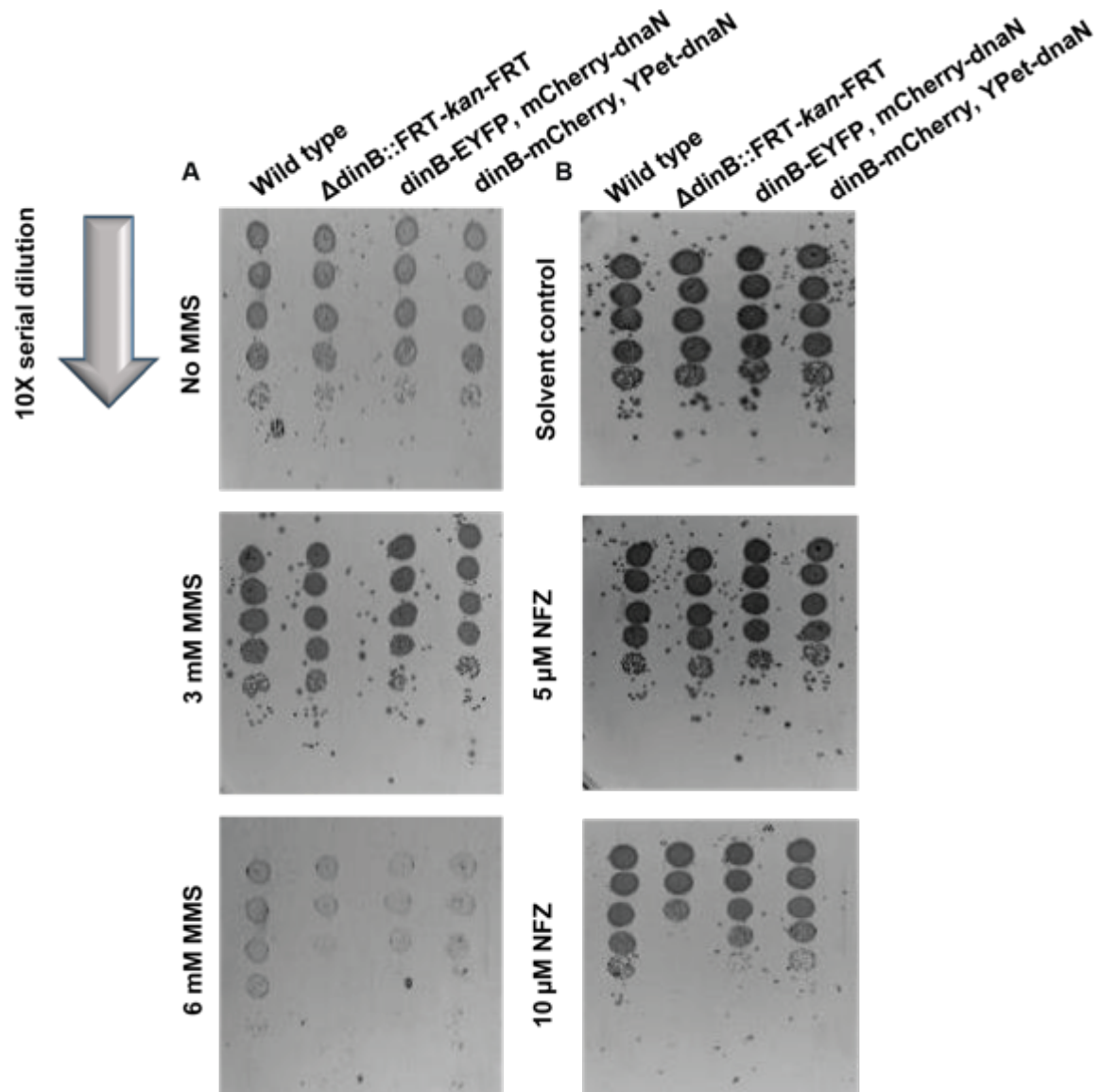


Figure S4.2 Functionality of the tagged Pol IV strains assayed by the bulk cellular response to DNA damage drugs. A. Serial dilution assays for the created strains in response to different MMS dosages (0 mM (solvent control), 3 mM, and 6 mM). **B.** Serial dilution assays for the created strains in response to different NFZ dosages (0 μ M (solvent control), 5 μ M, and 10 μ M).

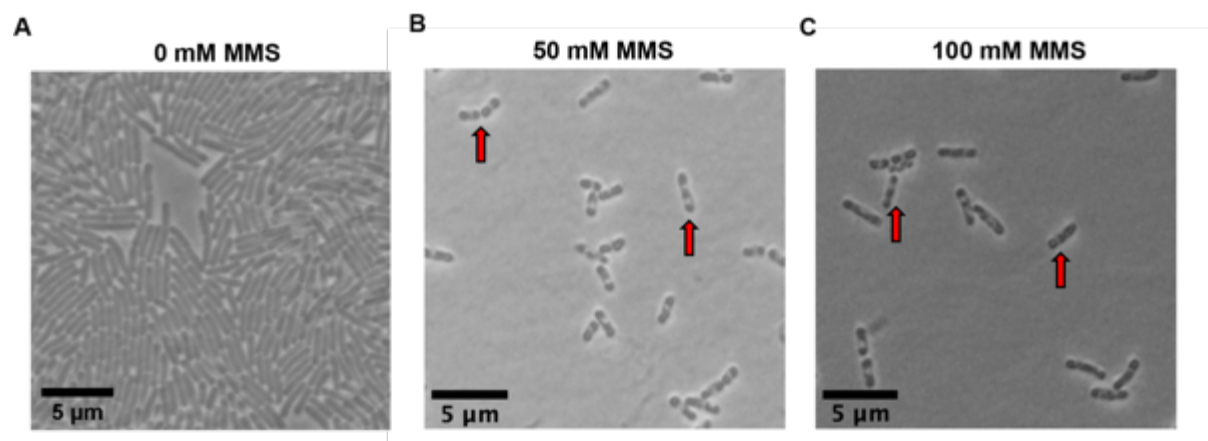


Figure S4.3 Appearance of black spots at the highest dosages of DNA damage drug MMS. Fields of view of cells incubated with M9 medium on agarose pad for the cases: **A.** no MMS added, **B.** an MMS dosage of 50 mM, and **C.** an MMS dosage of 100 mM. All images were collected at the same timepoint, corresponding to 10 h after the addition (or not) of MMS to the agarose pad. In panels (B.) and (C.), identifiable black spots are observed in the cells. These appear from 75 min onwards.

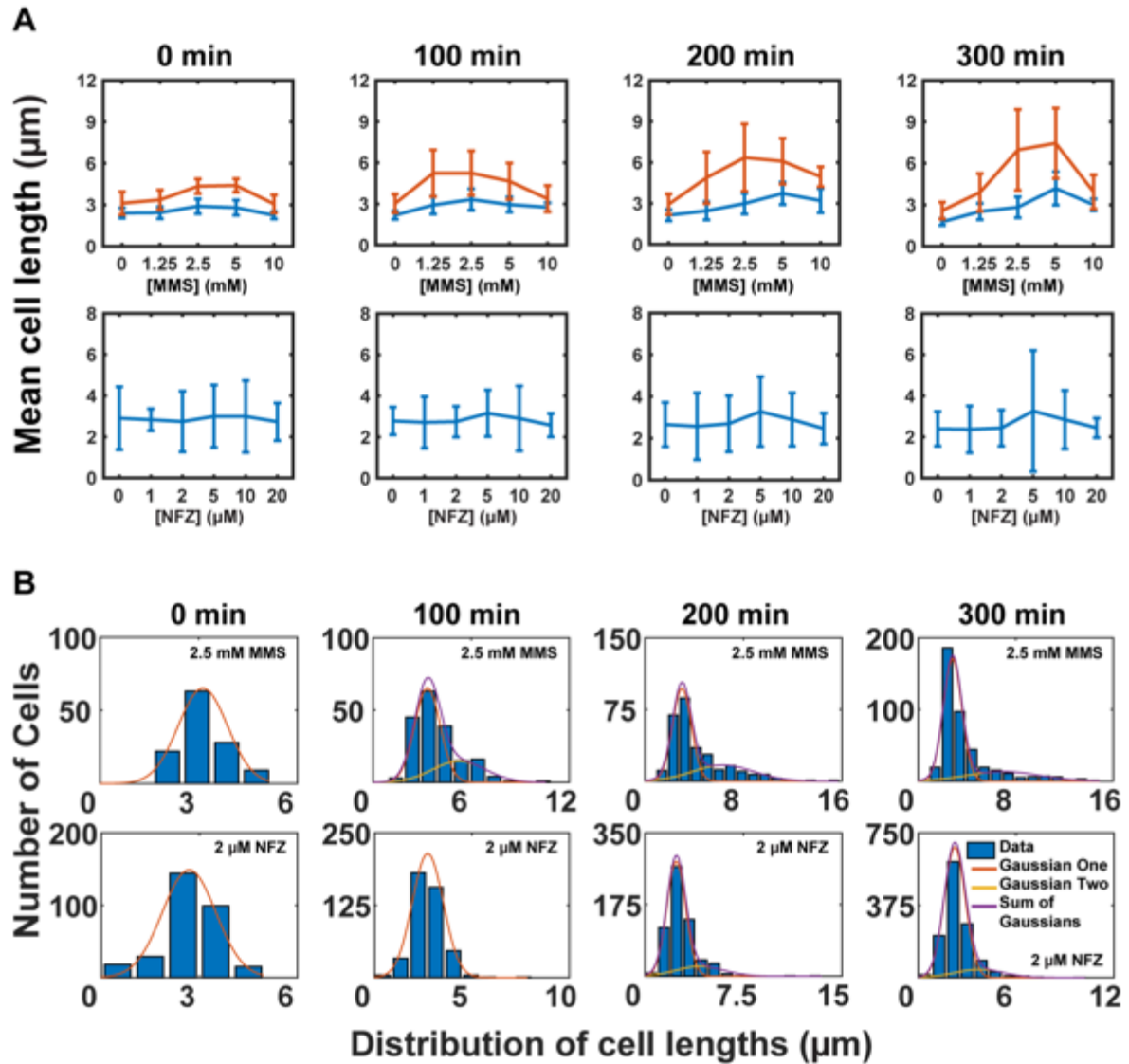
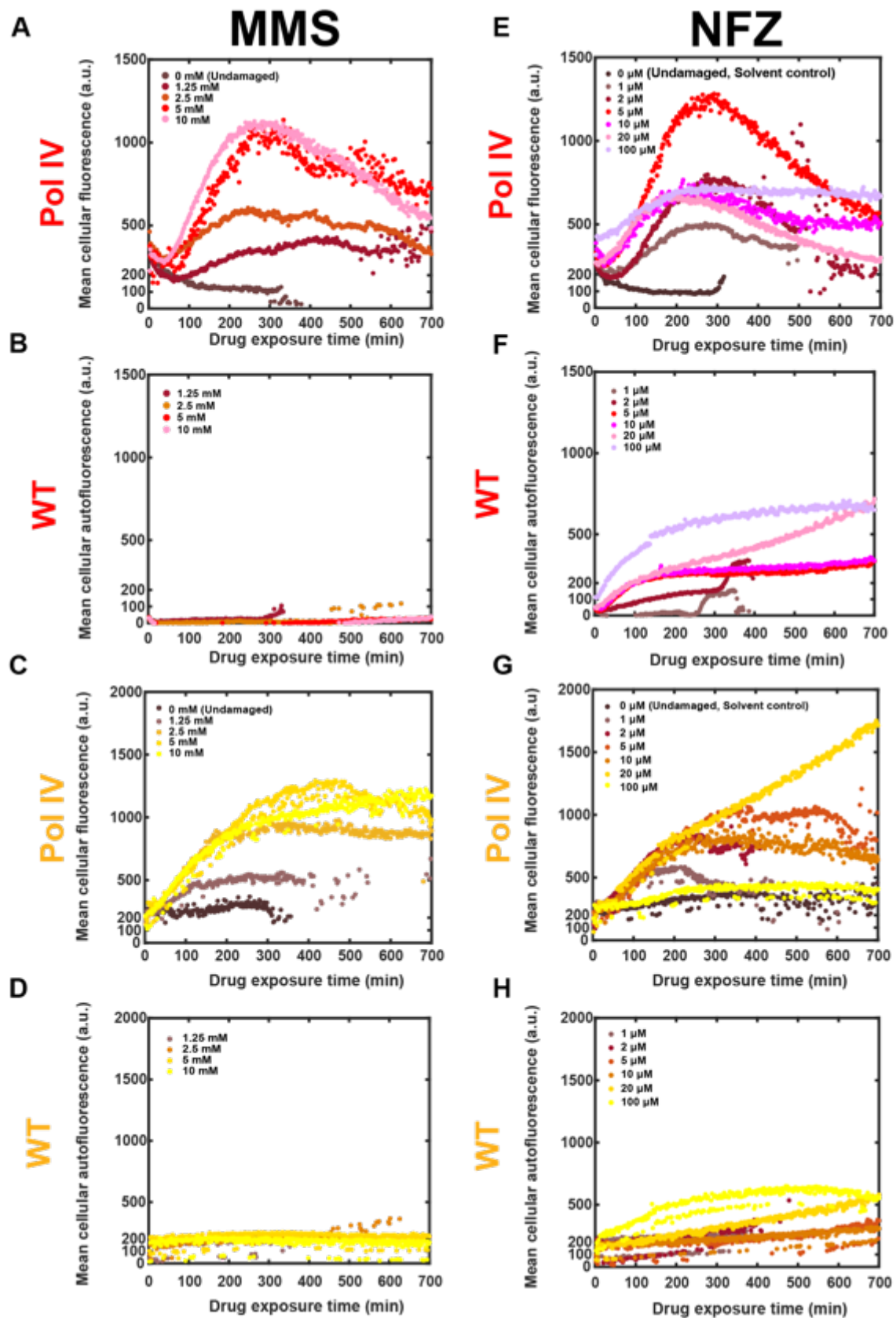
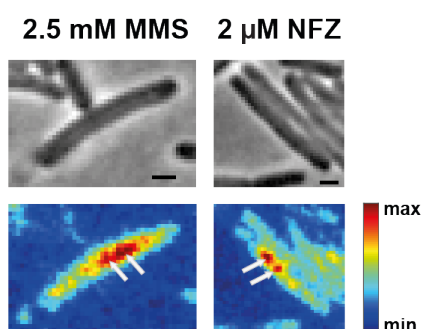
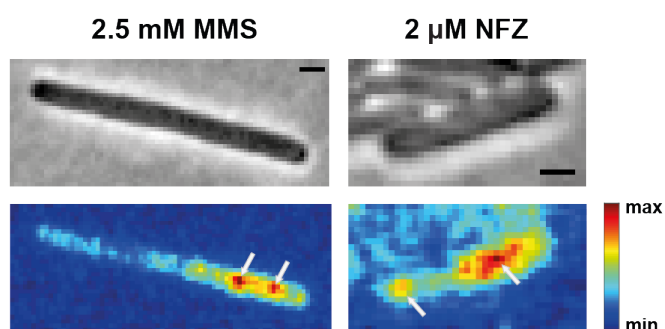


Figure S4.4 Measurement of mean cell length in response to DNA damage drugs MMS and NFZ. A. Top: Response over time to different dosages (0 mM, 1.25 mM, 2.5 mM, 5 mM, and 10 mM) of MMS, as assayed by mean cell length for strains SDR33 and SDR32 (combined). Here, the population distribution, shown in panel (B.) for 2.5 mM MMS, was fitted to a double Gaussian function. The red and blue datapoints represent the two fitted means, and the error bars correspond to the respective standard deviations. Bottom: Response over time to different dosages (0 μM , 1 μM , 2 μM , 5 μM , 10 μM , and 20 μM) of NFZ, as assayed by mean cell length for strains SDR33 and SDR32 (combined). Here, the population distribution, shown in panel (B.) for 2 μM NFZ, was fitted to a single Gaussian function. The datapoints represent the fitted means, and the error bars correspond to the standard deviations. **B.** Distributions of cell lengths over time at 2.5 mM MMS (top) and 2 μM NFZ (bottom). Data in both panels obtained for cells incubated with M9 medium on agarose pad.



S4.5 Fig. Controls for the whole-cell fluorescence response to DNA damage drugs MMS and NFZ. **A.** Response over time to different dosages (0 mM, 1.25 mM, 2.5 mM, 5 mM, and 10 mM) of MMS, as assayed by total fluorescence in strain SDR33 with Pol IV-mCherry labeling. **B.** As in (A.), but reporting the total cellular autofluorescence upon excitation at 561 nm in a WT strain. **C.** Response over time to different dosages (0 mM, 1.25 mM, 2.5 mM, 5 mM, and 10 mM) of MMS, as assayed by total fluorescence in strain SDR32 with Pol IV-EYFP labeling. **D.** As in (C.), but reporting the total cellular autofluorescence upon excitation at 515 nm in a WT strain. **E.** Response over time to different dosages (0 μ M, 1 μ M, 2 μ M, 5 μ M, 10 μ M, 20 μ M, and 100 μ M) of NFZ, as assayed by total fluorescence in strain SDR33 with Pol IV-mCherry labeling. **F.** As in (E.), but reporting the total cellular autofluorescence upon excitation at 561 nm in a WT strain. **G.** Response over time to different dosages (0 μ M, 1 μ M, 2 μ M, 5 μ M, 10 μ M, 20 μ M, and 100 μ M) of NFZ, as assayed by total fluorescence in strain SDR32 with Pol IV-EYFP labeling. **H.** As in (G.), but reporting the total cellular autofluorescence upon excitation at 515 nm in a WT strain. Data in all panels obtained for cells incubated with M9 medium on agarose pad.

A**B**

S4.6 Fig. Pol IV forms foci after treatment with DNA damage drugs. A. Images of cells in phase-contrast mode (top, grayscale) and in the Pol IV fluorescence channel (bottom, normalized false colour scale) for strain SDR33 after 300 min of exposure to an MMS dosage of 2.5 mM (left) and to an NFZ dosage of 2 μ M (right). White arrows point at the identified Pol IV foci (**Materials and Methods**). **B.** Similar to (A.), but for strain SDR32. Scale bar represents 1 μ m.

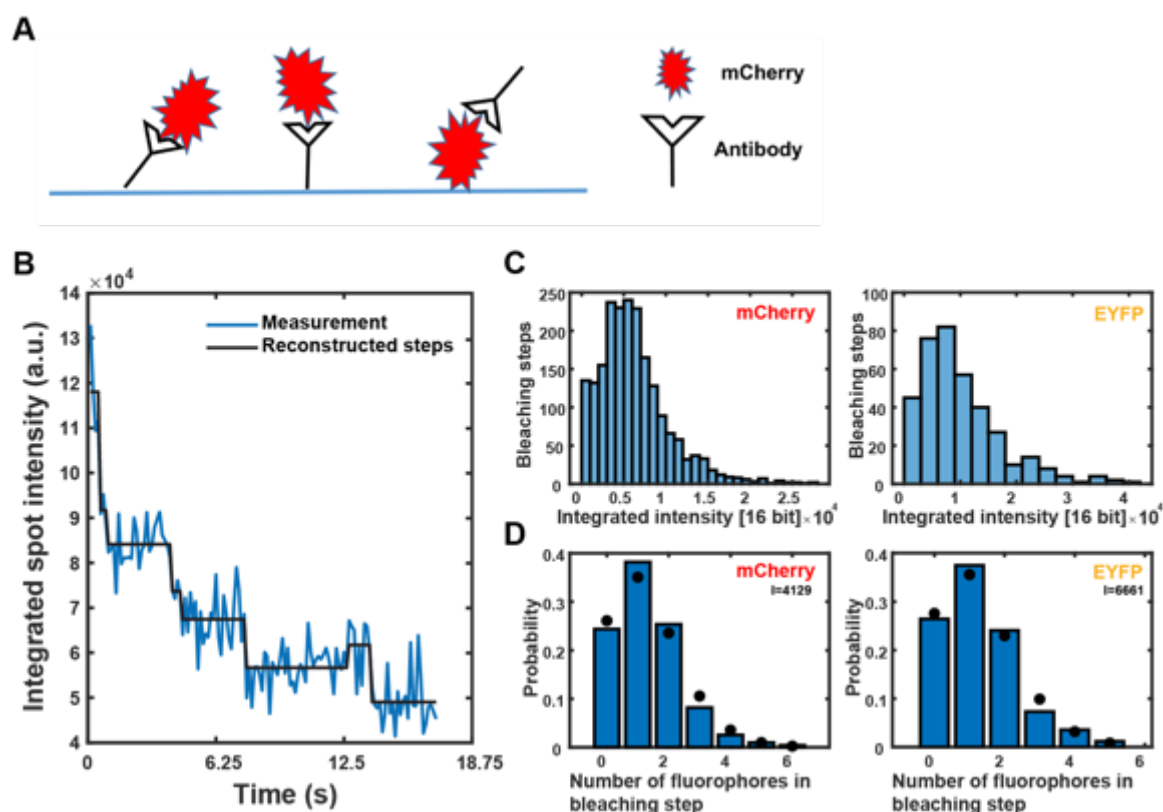


Figure S4.7 Calibration of fluorescent dye intensity. **A.** Schematic of dye attachment to antibodies adhered to the surface of a flow cell surface in M9-Glycerol. The proteins are attached to a glass surface as described in the **Materials and Methods**. **B.** The intensities of single fluorophores are calibrated by assessing photobleaching events of purified proteins, as shown. Spots are detected by finding local minima in smoothed versions of the time-lapse images and two-dimensional Gaussian functions are fit to these spots. From the fit parameters the integrated intensity is calculated and the sub-pixel precision spot locations are retrieved. Spots are linked between frames based on these centroid locations by a microscopy tracking algorithm (5), and steps are fitted using an improved algorithm based on Ref. (10). **C.** Histograms of the sizes of several hundreds bleaching steps retrieved from the fits described in (B.). Left panel: mCherry; right panel: EYFP. **D.** Bleaching step sizes from panel (C.) fit to a Poisson distribution. Here, an initial guess for the intensity of a single fluorophore is used to bin the bleaching steps by the number of fluorophores that bleached in the same image frame (blue bars). This single-fluorophore intensity is then allowed to vary to optimize the Poisson fit (black dots) by considering the squared error. This optimization results in an integrated intensity of 4129 counts for a single mCherry fluorophore (left), and in an integrated intensity of 6661 for a single EYFP fluorophore (right).

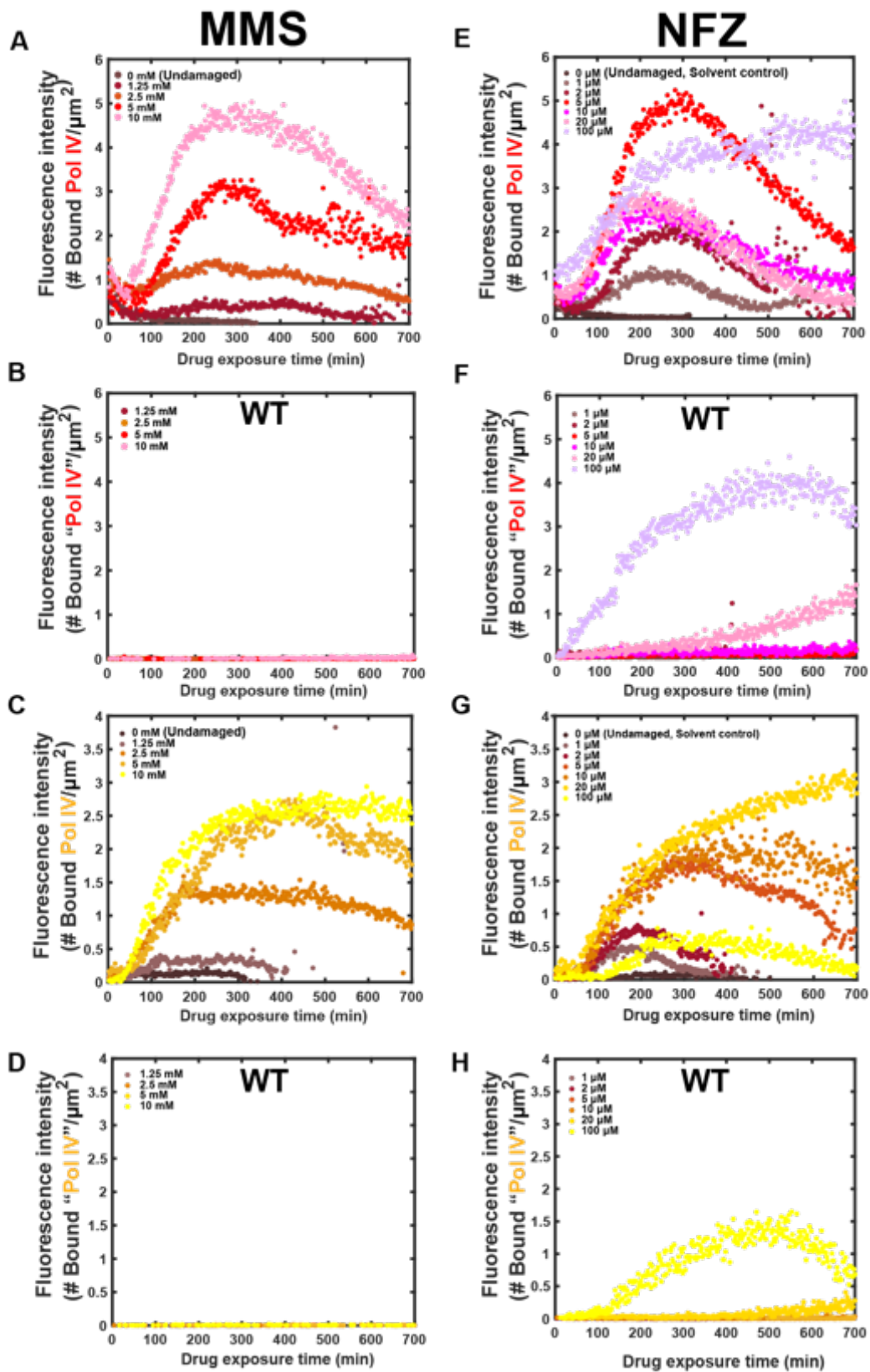


Figure S4.8 Controls for the response of fluorescent Pol IV foci to DNA damage drugs MMS and NFZ. **A.** Response over time to different dosages (0 mM, 1.25 mM, 2.5 mM, 5 mM, and 10 mM) of MMS, as assayed by the fluorescence in foci in strain SDR33 with Pol IV-mCherry labeling. **B.** As in (A.), but reporting the total cellular autofluorescence upon excitation at 561 nm in a WT strain. **C.** Response over time to different dosages (0 mM, 1.25 mM, 2.5 mM, 5 mM, and 10 mM) of MMS, as assayed by total fluorescence in strain SDR32 with Pol IV-EYFP labeling. **D.** As in (C.), but reporting the total cellular autofluorescence upon excitation at 515 nm in a WT strain. **E.** Response over time to different dosages (0 μ M, 1 μ M, 2 μ M, 5 μ M, 10 μ M, 20 μ M, and 100 μ M) of NFZ, as assayed by total fluorescence in strain SDR33 with Pol IV-mCherry labeling. **F.** As in (E.), but reporting the total cellular autofluorescence upon excitation at 561 nm in a WT strain. **G.** Response over time to different dosages (0 μ M, 1 μ M, 2 μ M, 5 μ M, 10 μ M, 20 μ M, and 100 μ M) of NFZ, as assayed by total fluorescence in strain SDR32 with Pol IV-EYFP labeling. **H.** As in (G.), but reporting the total cellular autofluorescence upon excitation at 515 nm in a WT strain. Data in all panels obtained for cells incubated with M9 medium on agarose pad.

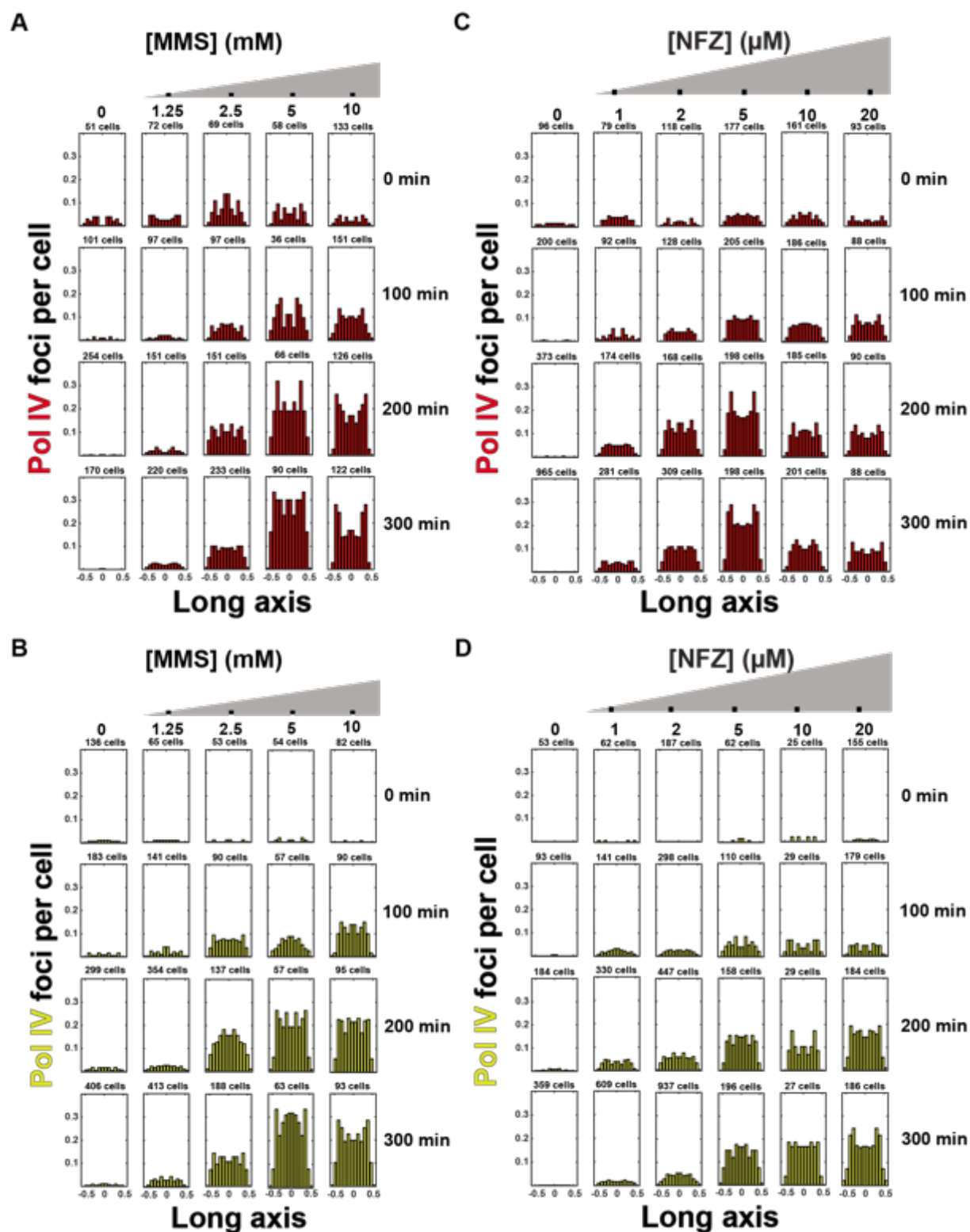


Figure S4.9 Full set of histograms showing the influence of DNA damage drugs MMS and NFZ on the spatial distribution of Pol IV foci for the two strains. **A.** Spatial distributions of Pol IV-mCherry foci in strain SDR33 for different dosages of MMS over time. **B.** Spatial distributions of Pol IV-EYFP foci in strain SDR32 for different dosages of MMS over time. **C.** Spatial distributions of Pol IV-mCherry foci in strain SDR33 for different dosages of NFZ over time. **D.** Spatial distributions of Pol IV-EYFP foci in strain SDR32 for different dosages of NFZ over time. Data in all panels obtained for cells incubated with M9 medium on agarose pad.

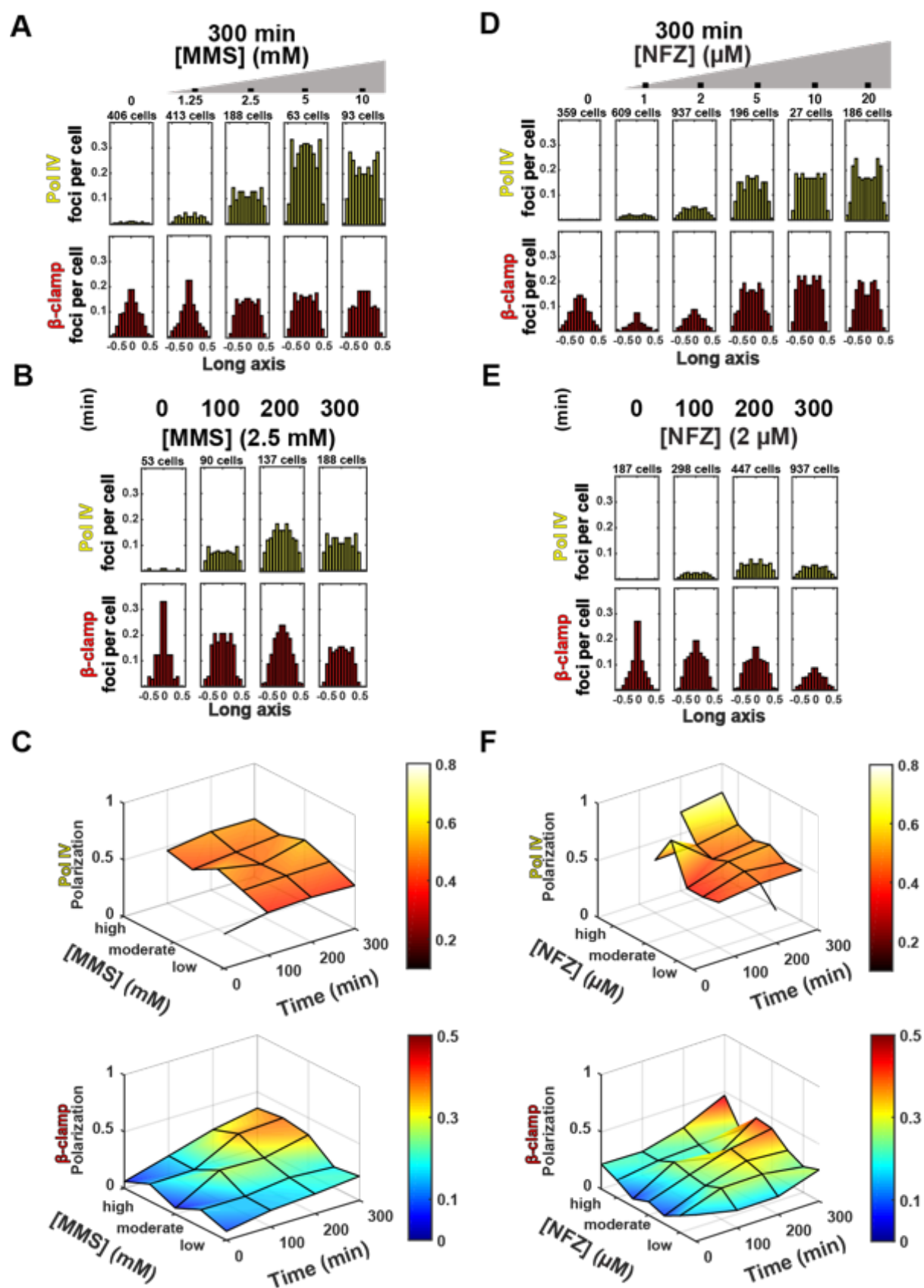


Figure S4.10 Strain control for the influence of DNA damage drugs MMS and NFZ on the spatial distributions of Pol IV and the replisome. Here, strain SDR32 is used, whereas the data in figure 3 in the main text derives from strain SDR33 (**Materials and Methods**). **A.** Spatial distributions of Pol IV-EYFP foci and mCherry- β clamp foci, sampled at 5 h following different dosages (0 mM, 1.25 mM, 2.5 mM, 5 mM, and 10 mM) of MMS. **B.** Spatial distribution of Pol IV-EYFP foci and mCherry- β clamp foci over time at an MMS dosage of 2.5 mM. **C.** Spatial distributions of Pol IV-EYFP foci and mCherry- β clamp foci, sampled at 5 h following different dosages (0 μ M, 1 μ M, 2 μ M, 5 μ M, 10 μ M, and 20 μ M) of NFZ. **D.** Spatial distribution of Pol IV-EYFP foci and mCherry- β clamp foci over time at an NFZ dosage of 2 μ M. **E.** Degree of spatial polarization (see main text) of Pol IV-EYFP foci (left) and mCherry- β clamp foci (right) as a function of MMS dosage and time. **F.** Degree of spatial polarization (see main text) of Pol IV-EYFP foci (left) and mCherry- β clamp foci (right) as a function of NFZ dosage and time. Data in all panels obtained for cells incubated with M9 medium on agarose pad.

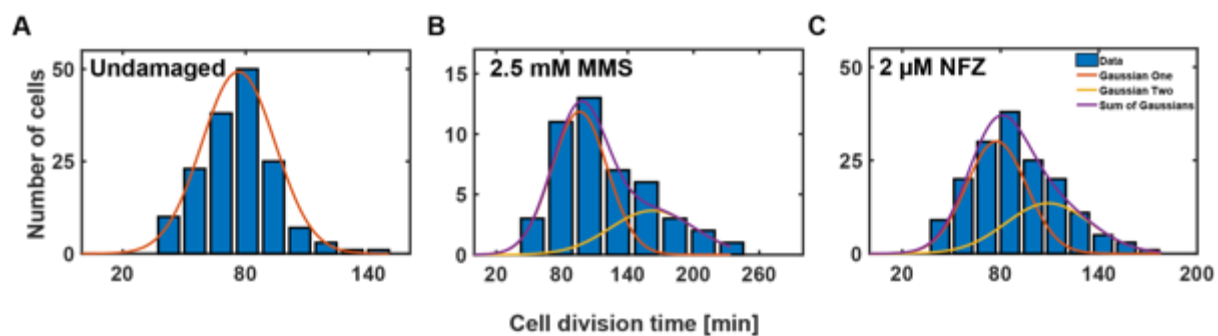


Figure S4.11 Division times in the presence of low dosages of DNA damage drugs MMS and NFZ for cells subjected to individual analysis. **A.** Division times in the absence of DNA damage drugs. **B.** Division times in the presence of 2.5 mM MMS. **C.** Division times in the presence of 2 μ M NFZ. Data in all panels obtained for cells incubated with M9 medium on agarose pad.

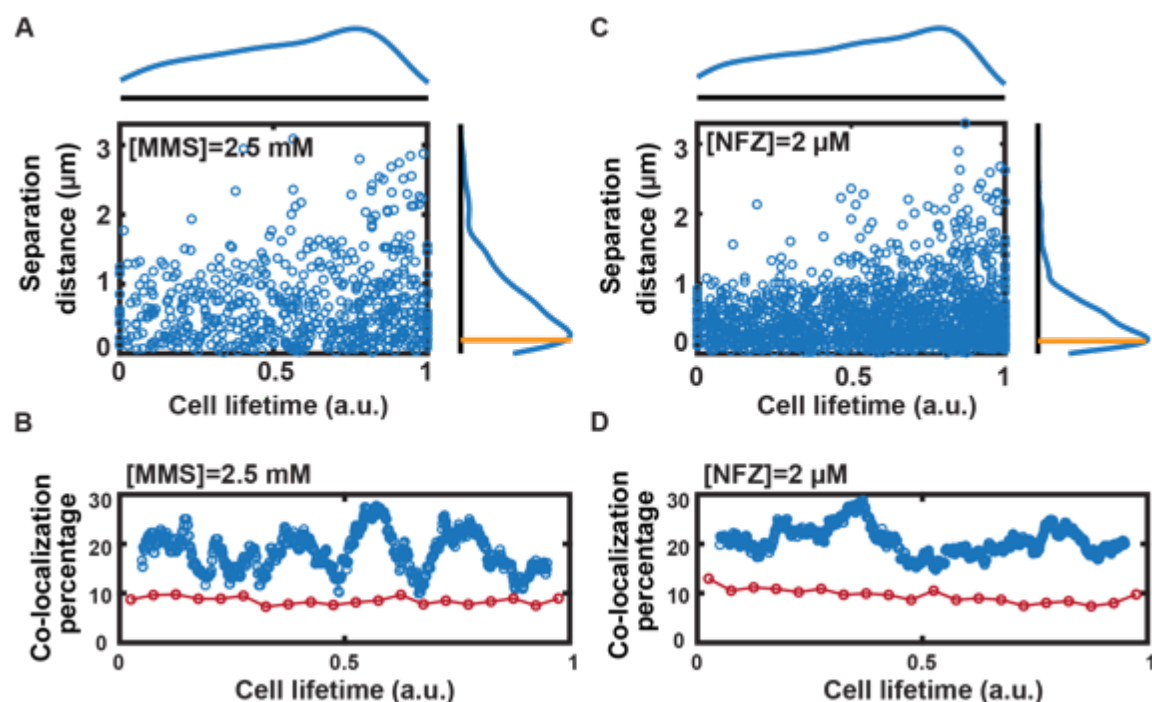


Figure S4.12 Strain control for the colocalization between Pol IV and replisome within the lifespan of a single cell. Colocalization data is assessed as a function of the normalized cell lifetime, defined from cell birth ($t=0$) to cell division ($t=1$) for drug dosages at which DNA damage effects are clearly present, but cell division cycles are not halted. Here, strain SDR32 is used, whereas the data in **Figure 4** in the main text derives from strain SDR33 (**Materials and Methods**). **A.** Scatter plot of the separation distance between a Pol IV-EYFP focus and the nearest replisome focus (monitored via the mCherry- β clamp) versus the normalized cell lifetime in the presence of 2.5 mM MMS. The probability distribution of finding foci at a certain cell lifetime is provided above the scatter plot, and the probability distribution of finding foci at a certain separation distance is indicated to the right of the scatter plot). The colocalization threshold for separation distance of 200 nm is indicated by the yellow line. $N = 19$ cells. **B.** The percentage of Pol IV foci colocalized with a replisome as a function of normalized cell lifetime in the presence of 2.5 mM MMS (blue line), calculated from the same dataset as panel (A.). The percentage of colocalization that would be expected from random foci localization (red line) is calculated considering the cell area, the number of replisomes present and the area occupied by each replisome as a disk with a radius of 200 nm. and. **C.** As in panel (A.), but now in the presence of 2 μM NFZ. $N = 110$ cells. **D.** As in panel (B.), but now in the presence of 2 μM NFZ and calculated using the same dataset as in panel (C.). Data in all panels obtained for cells incubated with M9 medium on agarose pad. The cell lifetime is shown in arbitrary units (a.u.), where 0 and 1 represent cell birth and division, respectively.

Strains	Relevant genotype	Construction
BN1110	<i>E.coli</i> AB1157 with pKD46 plasmid	<i>E.coli</i> K12 derivative
BW25142	<i>E.coli</i> host for plasmids with R6K γ origin of replication	Coli Genetic Stock Center (CGSC# 7840), Yale University
BN1682	<i>mCherry-dnaN</i> with Kan ^R	Previous study*
BN1109	<i>YPet-dnaN</i> with Kan ^R	Previous study*
BN1114	<i>E.coli</i> BW25142 host for plasmid with <i>mYPet</i> and Kan ^R	Previous study*
BN1116	<i>E.coli</i> BW25142 host for plasmid with <i>mCherry</i> and Kan ^R	Previous study*
SDR1	<i>dinB-EYFP</i> with Kan ^R	λ -red recombination: SDR4 \rightarrow BN1110
SDR2	<i>dinB-mCherry</i> with Kan ^R	λ -red recombination: SDR5 \rightarrow BN1110
SDR11	<i>dinB-EYFP</i>	<i>Flp-frt</i> recombination (Kan ^R flipped out from SDR1)
SDR12	<i>dinB-mCherry</i>	<i>Flp-frt</i> recombination (Kan ^R flipped out from SDR2)
SDR19	Δ <i>dinB</i> (<i>dinB</i> ::FRT-Kan ^R -FRT)	λ -red recombination: Kan ^R from BN1114 \rightarrow BN1110
SDR29	<i>dinB-EYFP</i> and <i>mCherry-dnaN</i> with Kan ^R	Phage transduction (BN1682 \rightarrow SDR1)
SDR30	<i>dinB-mCherry</i> and <i>YPet-dnaN</i> with Kan ^R	Phage transduction (BN1109 \rightarrow SDR12)
SDR32	<i>dinB-EYFP</i> and <i>mCherry-dnaN</i>	<i>Flp-frt</i> recombination (Kan ^R flipped out from SDR29)
SDR33	<i>dinB-mCherry</i> and <i>YPet-dnaN</i>	<i>Flp-frt</i> recombination (Kan ^R flipped out from SDR30)

Table S.4.1 Summary of bacterial strains employed. Previous study* refers to ref. 31

Plasmids	Relevant genotype	Construction
BN1114	Plasmid from same strain, used as PCR template, for cloning SDR4 plasmid (R6K γ origin of replication)	Previous study*
BN1116	Plasmid from same strain, used as PCR template, for cloning SDR5 plasmid (R6K γ origin of replication)	Previous study*
SDR4	<i>EYFP</i> with <i>kanR</i> (Template for λ -red recombination)	Gibson assembly on BN1114 plasmid backbone
SDR5	<i>mCherry</i> with <i>kanR</i> (Template for λ -red recombination)	Gibson assembly on BN1116 plasmid backbone
pKD46	Plasmid with genes for λ -red recombination under arabinose promoter	Previous study*
pCP20	Plasmid with yeast <i>Flp</i> recombinase gene for <i>Flp-frt</i> recombination	Previous study*

Table S4.2 Summary of plasmids employed. Previous study* refers to ref. 31

Primers	Sequence (5'-3')
ND17	AGCCAGCGGATCCGCTCGAATTCGTAATCATGGTCA
ND18	CTGTACAAGTAACCCGGGTGTAGGCTGG
ND19	ACGAATTCGAGCGGATCCGCTGGCTCCG
ND20	GCCTACACCCGGGTACTTGTACAGCTCGTCCATGCCG
ND27	ATGTGACGTTGCTTGACCCGCAAATGGAAAGACAACCTGGTGCTG GGATTAGGATCCGCTGGCTCCGCTGCTGGTTCTGGCGCTGGCTC CGCTGCTGGTTCTGGCGAATTC
ND28	CAGTGATACCCTCATAATAATGCACACCAGAATATACATAATAGT ATACACATATGAATATCCTCCTTAG
ND33	ATTACGAATTCGAGCGGATCCGCTGGCTCCGCTGCTGGTTCTGG CGCTGGCTCCGCTGCTGGTTCTGGCGAATTCGTGAGCAAGGGCG AGGAGG
ND34	CAGCCTACACCCGGGTACTTGTACAG
ND35	GAGCTGTACAAGTAACCCGGGTGTAGG
ND36	GGAGCCAGCGGATCCGCTCGAATTCGTAATCATGGT CA
SDR1	ATGCGTAAATCATTCATGTGGATATGGACTGCTTTTTTCGCCGCA GTGGACTGGAGCTGCTTCGAAGTTCCTATACTTTCTAGAGAA
SDR2	TCATAATCCCAGCACCAGTTGTCTTTCCATTTGCGGGTCAAGCAA CGTCACTCCTTAGTTTCTATTCCGAAGTTCCTATTCTCT
1045	CGTTGGCACCTACCAGAAAG
1628	GCAGGAAAAACTGGTCACCATC
2601	GCTTTCGCAGCGAACGCG
2602	GCGAGAATTCGATGCATACAG

Table S4.3 Summary of DNA primers employed. Previous study* refers to ref. 31

References

1. Friedberg, E.C. (2003) DNA damage and repair. *Nature*, **421**, 436-440.
2. Baharoglu, Z. and Mazel, D. (2014) SOS, the formidable strategy of bacteria against aggressions. *FEMS Microbiol Rev*, **38**, 1126-1145.
3. Pennington, J.M. and Rosenberg, S.M. (2007) Spontaneous DNA breakage in single living *Escherichia coli* cells. *Nature genetics*, **39**, 797-802.
4. Zgur-Bertok, D. (2013) DNA damage repair and bacterial pathogens. *PLoS Pathog*, **9**, e1003711.
5. Crocker, J.C. and Grier, D.G. (1996) Methods of digital video microscopy for colloidal studies. *J Colloid Interf Sci*, **179**, 298-310.
6. Goodman, M.F. and Woodgate, R. (2013) Translesion DNA polymerases. *Cold Spring Harb Perspect Biol*, **5**, a010363.
7. Henrikus, S.S., van Oijen, A.M. and Robinson, A. (2018) Specialised DNA polymerases in *Escherichia coli*: roles within multiple pathways. *Curr Genet*.
8. Fuchs, R.P. and Fujii, S. (2013) Translesion DNA synthesis and mutagenesis in prokaryotes. *Cold Spring Harb Perspect Biol*, **5**, a012682.
9. Curti, E., McDonald, J.P., Mead, S. and Woodgate, R. (2009) DNA polymerase switching: effects on spontaneous mutagenesis in *Escherichia coli*. *Molecular microbiology*, **71**, 315-331.
10. Kerssemakers, J.W., Munteanu, E.L., Laan, L., Noetzel, T.L., Janson, M.E. and Dogterom, M. (2006) Assembly dynamics of microtubules at molecular resolution. *Nature*, **442**, 709-712.
11. Wagner, J., Gruz, P., Kim, S.R., Yamada, M., Matsui, K., Fuchs, R.P. and Nohmi, T. (1999) The *dinB* gene encodes a novel *E. coli* DNA polymerase, DNA pol IV, involved in mutagenesis. *Mol Cell*, **4**, 281-286.
12. Kim, S.R., Matsui, K., Yamada, M., Gruz, P. and Nohmi, T. (2001) Roles of chromosomal and episomal *dinB* genes encoding DNA pol IV in targeted and untargeted mutagenesis in *Escherichia coli*. *Mol Genet Genomics*, **266**, 207-215.
13. Henrikus, S.S., Wood, E.A., McDonald, J.P., Cox, M.M., Woodgate, R., Goodman, M.F., van Oijen, A.M. and Robinson, A. (2018) DNA polymerase IV primarily operates outside of DNA replication forks in *Escherichia coli*. *Plos Genet*, **14**, e1007161.
14. Pomerantz, R.T., Goodman, M.F. and O'Donnell, M.E. (2013) DNA polymerases are error-prone at RecA-mediated recombination intermediates. *Cell Cycle*, **12**, 2558-2563.
15. Janion, C. (2008) Inducible SOS response system of DNA repair and mutagenesis in *Escherichia coli*. *Int J Biol Sci*, **4**, 338-344.
16. Scotland, M.K., Heltzel, J.M., Kath, J.E., Choi, J.S., Berdis, A.J., Loparo, J.J. and Sutton, M.D. (2015) A Genetic Selection for *dinB* Mutants Reveals an Interaction between DNA Polymerase IV and the Replicative Polymerase That Is Required for Translesion Synthesis. *Plos Genet*, **11**, e1005507.
17. Jarosz, D.F., Godoy, V.G., Delaney, J.C., Essigmann, J.M. and Walker, G.C. (2006) A single amino acid governs enhanced activity of DinB DNA polymerases on damaged templates. *Nature*, **439**, 225-228.
18. Courcelle, C.T., Belle, J.J. and Courcelle, J. (2005) Nucleotide excision repair or polymerase V-mediated lesion bypass can act to restore UV-arrested replication forks in *Escherichia coli*. *J Bacteriol*, **187**, 6953-6961.

19. Pomerantz, R.T., Kurth, I., Goodman, M.F. and O'Donnell, M.E. (2013) Preferential D-loop extension by a translesion DNA polymerase underlies error-prone recombination. *Nature structural & molecular biology*, **20**, 748-755.
20. Williams, A.B., Hetrick, K.M. and Foster, P.L. (2010) Interplay of DNA repair, homologous recombination, and DNA polymerases in resistance to the DNA damaging agent 4-nitroquinoline-1-oxide in *Escherichia coli*. *DNA Repair (Amst)*, **9**, 1090-1097.
21. Indiani, C., McInerney, P., Georgescu, R., Goodman, M.F. and O'Donnell, M. (2005) A sliding-clamp toolbelt binds high- and low-fidelity DNA polymerases simultaneously. *Mol Cell*, **19**, 805-815.
22. Furukohri, A., Goodman, M.F. and Maki, H. (2008) A dynamic polymerase exchange with *Escherichia coli* DNA polymerase IV replacing DNA polymerase III on the sliding clamp. *J Biol Chem*, **283**, 11260-11269.
23. Scotland, M.K., Heltzel, J.M.H., Kath, J.E., Choi, J.S., Berdis, A.J., Loparo, J.J. and Sutton, M.D. (2015) A Genetic Selection for *dinB* Mutants Reveals an Interaction between DNA Polymerase IV and the Replicative Polymerase That Is Required for Translesion Synthesis. *Plos Genet*, **11**.
24. Heltzel, J.M., Maul, R.W., Wolff, D.W. and Sutton, M.D. (2012) *Escherichia coli* DNA polymerase IV (Pol IV), but not Pol II, dynamically switches with a stalled Pol III* replicase. *J. Bacteriol.*, **194**, 3589-3600.
25. Kath, J.E., Jergic, S., Heltzel, J.M., Jacob, D.T., Dixon, N.E., Sutton, M.D., Walker, G.C. and Loparo, J.J. (2014) Polymerase exchange on single DNA molecules reveals processivity clamp control of translesion synthesis. *Proc Natl Acad Sci U S A*, **111**, 7647-7652.
26. Sutton, M.D. (2010) Coordinating DNA polymerase traffic during high and low fidelity synthesis. *Biochim Biophys Acta*, **1804**, 1167-1179.
27. Zhao, G., Gleave, E.S. and Lamers, M.H. (2017) Single-molecule studies contrast ordered DNA replication with stochastic translesion synthesis. *Elife*, **6**.
28. Fijalkowska, I.J., Schaaper, R.M. and Jonczyk, P. (2012) DNA replication fidelity in *Escherichia coli*: a multi-DNA polymerase affair. *FEMS Microbiol Rev*, **36**, 1105-1121.
29. Thrall, E.S., Kath, J.E., Chang, S. and Loparo, J.J. (2017) Single-molecule imaging reveals multiple pathways for the recruitment of translesion polymerases after DNA damage. *Nat Commun*, **8**, 2170.
30. Mangiameli, S.M., Veit, B.T., Merrih, H. and Wiggins, P.A. (2017) The Replisomes Remain Spatially Proximal throughout the Cell Cycle in Bacteria. *Plos Genet*, **13**, e1006582.
31. Moolman, M.C., Krishnan, S.T., Kerssemakers, J.W., van den Berg, A., Tulinski, P., Depken, M., Reyes-Lamothe, R., Sherratt, D.J. and Dekker, N.H. (2014) Slow unloading leads to DNA-bound beta2-sliding clamp accumulation in live *Escherichia coli* cells. *Nat Commun*, **5**, 5820.
32. Beattie, T.R., Kapadia, N., Nicolas, E., Uphoff, S., Wollman, A.J., Leake, M.C. and Reyes-Lamothe, R. (2017) Frequent exchange of the DNA polymerase during bacterial chromosome replication. *Elife*, **6**.
33. Mallik, S., Popodi, E.M., Hanson, A.J. and Foster, P.L. (2015) Interactions and Localization of *Escherichia coli* Error-Prone DNA Polymerase IV after DNA Damage. *J Bacteriol*, **197**, 2792-2809.
34. Cai, L., Friedman, N. and Xie, X.S. (2006) Stochastic protein expression in individual cells at the single molecule level. *Nature*, **440**, 358-362.
35. Vera, M., Biswas, J., Senecal, A., Singer, R.H. and Park, H.Y. (2016) Single-Cell and Single-Molecule Analysis of Gene Expression Regulation. *Annu Rev Genet*, **50**, 267-291.

36. Osella, M., Tans, S.J. and Cosentino Lagomarsino, M. (2017) Step by Step, Cell by Cell: Quantification of the Bacterial Cell Cycle. *Trends Microbiol*, **25**, 250-256.
37. Norman, T.M., Lord, N.D., Paulsson, J. and Losick, R. (2015) Stochastic Switching of Cell Fate in Microbes. *Annu Rev Microbiol*, **69**, 381-403.
38. Sikora, A., Mielecki, D., Chojnacka, A., Nieminuszczy, J., Wrzesinski, M. and Grzesiuk, E. (2010) Lethal and mutagenic properties of MMS-generated DNA lesions in Escherichia coli cells deficient in BER and AlkB-directed DNA repair. *Mutagenesis*, **25**, 139-147.
39. Wehrens, M., Ershov, D., Rozendaal, R., Walker, N., Schultz, D., Kishony, R., Levin, P.A. and Tans, S.J. (2018) Size Laws and Division Ring Dynamics in Filamentous Escherichia coli cells. *Curr Biol*, **28**, 972-979 e975.
40. Xie, X.S., Choi, P.J., Li, G.W., Lee, N.K. and Lia, G. (2008) Single-molecule approach to molecular biology in living bacterial cells. *Annu Rev Biophys*, **37**, 417-444.
41. Mangiameli, S.M., Cass, J.A., Merrikh, H. and Wiggins, P.A. (2018) The bacterial replisome has factory-like localization. *Curr Genet*, **64**, 1029-1036.
42. Mangiameli, S.M., Merrikh, C.N., Wiggins, P.A. and Merrikh, H. (2017) Transcription leads to pervasive replisome instability in bacteria. *Elife*, **6**.
43. Kouzine, F., Liu, J., Sanford, S., Chung, H.J. and Levens, D. (2004) The dynamic response of upstream DNA to transcription-generated torsional stress. *Nature structural & molecular biology*, **11**, 1092-1100.
44. Neidhardt, F.C., Bloch, P.L. and Smith, D.F. (1974) Culture medium for enterobacteria. *J Bacteriol*, **119**, 736-747.
45. Betzig, E., Patterson, G.H., Sougrat, R., Lindwasser, O.W., Olenych, S., Bonifacino, J.S., Davidson, M.W., Lippincott-Schwartz, J. and Hess, H.F. (2006) Imaging intracellular fluorescent proteins at nanometer resolution. *Science (New York, N.Y.)*, **313**, 1642-1645.
46. Torres-Barcelo, C., Kojadinovic, M., Moxon, R. and MacLean, R.C. (2015) The SOS response increases bacterial fitness, but not evolvability, under a sublethal dose of antibiotic. *Proc Biol Sci*, **282**, 20150885.
47. Badrinarayanan, A. (2018).
48. Kreuzer, K.N. (2013) DNA damage responses in prokaryotes: regulating gene expression, modulating growth patterns, and manipulating replication forks. *Cold Spring Harb Perspect Biol*, **5**, a012674.
49. Kuwada, N.J., Traxler, B. and Wiggins, P.A. (2015) Genome-scale quantitative characterization of bacterial protein localization dynamics throughout the cell cycle. *Molecular microbiology*, **95**, 64-79.
50. Coquel, A.S., Jacob, J.P., Primet, M., Demarez, A., Dimiccoli, M., Julou, T., Moisan, L., Lindner, A.B. and Berry, H. (2013) Localization of protein aggregation in Escherichia coli is governed by diffusion and nucleoid macromolecular crowding effect. *PLoS Comput Biol*, **9**, e1003038.
51. Lindner, A.B., Madden, R., Demarez, A., Stewart, E.J. and Taddei, F. (2008) Asymmetric segregation of protein aggregates is associated with cellular aging and rejuvenation. *Proc Natl Acad Sci U S A*, **105**, 3076-3081.
52. Ghodke, H., Paudel, B.P., Lewis, J.S., Jergic, S., Gopal, K., Romero, Z.J., Wood, E.A., Woodgate, R., Cox, M.M. and van Oijen, A.M. (2019) Spatial and temporal organization of RecA in the Escherichia coli DNA-damage response. *Elife*, **8**.
53. Loparo, J.J. and Thrall, E.S. (2019). personal communication ed.
54. Vaisman, A. and Woodgate, R. (2017) Translesion DNA polymerases in eukaryotes: what makes them tick? *Crit Rev Biochem Mol Biol*, **52**, 274-303.

55. Stallons, L.J. and McGregor, W.G. (2010) Translesion synthesis polymerases in the prevention and promotion of carcinogenesis. *J Nucleic Acids*, **2010**.
56. Jansen, J.G., Temviriyankul, P., Wit, N., Delbos, F., Reynaud, C.A., Jacobs, H. and de Wind, N. (2014) Redundancy of mammalian Y family DNA polymerases in cellular responses to genomic DNA lesions induced by ultraviolet light. *Nucleic Acids Res*, **42**, 11071-11082.
57. Jarosz, D.F., Cohen, S.E., Delaney, J.C., Essigmann, J.M. and Walker, G.C. (2009) A DinB variant reveals diverse physiological consequences of incomplete TLS extension by a Y-family DNA polymerase. *Proc Natl Acad Sci U S A*, **106**, 21137-21142.
58. Cirz, R.T., Chin, J.K., Andes, D.R., de Crecy-Lagard, V., Craig, W.A. and Romesberg, F.E. (2005) Inhibition of mutation and combating the evolution of antibiotic resistance. *PLoS Biol*, **3**, e176.
59. Frisch, R.L., Su, Y., Thornton, P.C., Gibson, J.L., Rosenberg, S.M. and Hastings, P.J. (2010) Separate DNA Pol II- and Pol IV-dependent pathways of stress-induced mutation during double-strand-break repair in *Escherichia coli* are controlled by RpoS. *J Bacteriol*, **192**, 4694-4700.
60. Fitzgerald, D.M., Hastings, P.J. and Rosenberg, S.M. (2017) Stress-Induced Mutagenesis: Implications in Cancer and Drug Resistance. *Annu Rev Cancer Biol*, **1**, 119-140.
61. Cherepanov, P.P. and Wackernagel, W. (1995) Gene disruption in *Escherichia coli*: TcR and KmR cassettes with the option of Flp-catalyzed excision of the antibiotic-resistance determinant. *Gene*, **158**, 9-14.
62. Datsenko, K.A. and Wanner, B.L. (2000) One-step inactivation of chromosomal genes in *Escherichia coli* K-12 using PCR products. *Proc Natl Acad Sci U S A*, **97**, 6640-6645.
63. Stylianidou, S., Brennan, C., Nissen, S.B., Kuwada, N.J. and Wiggins, P.A. (2016) SuperSegger: robust image segmentation, analysis and lineage tracking of bacterial cells. *Molecular microbiology*, **102**, 690-700.

Summary

The basis of this thesis has been the curiosity, however modest, to understand how DNA replication happens *in vivo*, particularly during the onset of DNA damage and beyond. DNA damage is a recurring phenomenon, which a (bacterial) cell faces in its lifetime from the environment or even its inherent metabolism. While we understand much about replication in general from decades of research, our understanding is not comprehensive without understanding how replication is affected, when the cell is under DNA damage and/ or under repair.

In terms of genome replication, the effects of DNA damage may be at the level of:

- a. Replisome components
- b. Accessory components of the replisome

In this thesis and with a limited time span of a PhD research, I (along with my colleagues) have reported on one component each of the two categories stated above in the bacterial model *Escherichia coli*. In the former case, we have investigated the replicative helicase DnaB and in the latter case, the translesion DNA polymerase IV (Pol IV).

Chapter 1 introduces the concept of DNA replication and components of the DNA synthesis machinery- the replisome. Besides the integral components of the replisome, there are accessory components involved in DNA replication or acting in special circumstances thereof (e.g., DNA damage). Thereafter, I invoke the idea of replication fork stalling and describe the different causes of it, one of which is DNA damage. Subsequently, the types of DNA damage are discussed: exogenous and endogenous factors. Finally, I underscore the motivation behind this thesis, the questions of biological significance and a thesis outline for the reader.

Chapter 2 provides a summary and review of live cell imaging and single molecule fluorescence microscopy (SMFM) techniques. Beginning with a conceptual introduction of 'molecular flashlight' and a brief history of technical development to acknowledge the seminal contribution of various researchers across the years, I describe the different modalities which may be used combining live cell imaging and single molecule fluorescence microscopy. Thereafter, I describe the merits of studying live cells by single molecule imaging and how such studies have produced an upheaval in the field of bacterial cell biology. Subsequently, I consider the technical and biological considerations driving the choice of such imaging (live cell imaging-single molecule fluorescence microscopy) techniques. The chapter concludes by bringing up how the usage of these two techniques is suitable for our research, by reviewing how these single molecule imaging had led to recent progress of DNA replication and repair mechanisms particularly.

Chapter 3 delves on the outcome of the replicative helicase DnaB when the cells are inflicted with UV-mediated DNA damage. DnaB has been speculated to dissociate from the replisome ('fall off') or remain associated with it ('stay put'). Using our snapshot microscopy approach and 'single molecule' sensitivity, we gauge what happens to DnaB after UV exposure, based on three parameters: number of foci, stoichiometry and spatial distribution of foci on the cell long axis. While we do not find any remarkable change in stoichiometry before and after UV exposure, we do report changes on number of foci (e.g., 2 foci category) and for DnaB spatial

distribution, when compared to the replisome (β clamp). In line with recent data published while the work was in progress, we hypothesize from our results that DnaB neither ‘falls off’ nor ‘stays put’ after UV exposure. Rather, DnaB may be uncoupled from the rest of the replisome machinery, unwinding the chromosome ahead while the other replisome components are stalled behind. Our work should encourage future research on what the role of helicase loaders is (e.g., PriA/PriC) if DnaB does not dissociate from the replisome and how the replication restart pathways work.

Chapter 4 is a study about DNA damage translesion polymerases which are upregulated during the SOS response in *Escherichia coli*. DNA polymerase IV (Pol IV), one such polymerase, plays a key role in cellular survival. Using live cell imaging, we report here on Pol IV dynamics *in vivo* in real time, tracing its response to two different DNA damage drugs, methyl methanesulfonate (MMS) and nitrofurazone (NFZ), from the onset of DNA damage to beyond the peak of its upregulation during SOS response. Overall, the findings are quite similar for MMS and NFZ. We find that the magnitude of the Pol IV response to DNA damage depends strongly on the dosage of DNA damage drug and evolves over time. The spatial positioning of DNA-bound Pol IV in the cell is found to evolve from being uniform at low (cumulated) drug dosage, to favoring the cell poles at higher (cumulated) drug dosage. While its colocalization with the replisome is found to exceed that of random chance, many Pol IV molecules are recruited to the DNA in a damage-dependent matter via replication-independent means. At the highest (cumulated) drug dosages tested, the mid-cell localization of the replisome tends to broaden, enhancing the apparent colocalization with Pol IV. With this probing of Pol IV at the single-molecule level over a range of DNA damage drug dosages and time, we found further insights into the response of translesion polymerases to different kinds of DNA damage.

The research described here has been an interdisciplinary endeavor, ranging from bacterial cell biology to instrumentation and analyses, and chemistry of DNA damage drugs. This work could not have been possible without the various technical advances from other groups, not just limited to microscopy. Undoubtedly, genome replication being a complex process, even in *Escherichia coli*, we have much to learn on how DNA damage affects replication and the ensuing repair is carried out. Moreover, with multiple pathways at play involving numerous factors (e.g., different helicases or DNA polymerases), we understand barely how these factors coordinate in the cell cycle. Significantly, such DNA damage studies also have translational implication for society beyond curiosity and bench science. In summary, this work will have served its purpose for me, if it serves others to ask relevant and more introspective questions for future research.

Samenvatting

De basis van dit proefschrift is de nieuwsgierigheid, hoe bescheiden ook, om te begrijpen hoe DNA-replicatie *in vivo* plaatsvindt, vooral tijdens het ontstaan van DNA-schade en daarna. DNA-schade is een terugkerend fenomeen, waarmee een (bacteriële) cel in zijn leven wordt geconfronteerd, geïnduceerd door de omgeving of zelfs door het eigen metabolisme. Hoewel we uit tientallen jaren van onderzoek veel over replicatie weten, is ons begrip niet volledig zonder de kennis van hoe replicatie wordt beïnvloed wanneer de cel beschadigd is en/of wordt gerepareerd.

Bij genoomreplicatie kunnen de effecten van DNA-schade liggen op het niveau van:

- a. Replisoom componenten
- b. Accessoire (of extra) componenten van het replisoom

In dit proefschrift en binnen de beperkte tijdsduur van een doctoraatsonderzoek, heb ik (samen met mijn collega's) gerapporteerd over één component van elk van de twee hierboven genoemde categorieën in de bacterie *Escherichia coli*. In het eerste geval hebben we de replicatieve helicase DnaB onderzocht en in het tweede geval de Translesie DNA polymerase IV (Pol IV).

Hoofdstuk 1 introduceert het concept van DNA-replicatie en componenten van het DNA-synthesecomplex- het replisoom. Naast de integrale (of basis) componenten van het replisoom zijn er accessoire componenten die betrokken zijn bij DNA replicatie of die optreden in speciale omstandigheden daarvan (bijvoorbeeld bij DNA-schade). Daarna licht ik het verschijnsel van stagnatie van de replicatievork toe en beschrijf de verschillende oorzaken ervan, waaronder DNA-schade. Vervolgens worden de soorten DNA-schade besproken: exogene en endogene factoren. Tot slot benadruk ik de motivatie achter dit proefschrift, de vragen van biologische betekenis en een proefschriftoverzicht voor de lezer.

Hoofdstuk 2 geeft een samenvatting en overzicht van technieken voor beeldvorming en single-molecule fluorescentie microscopie (SMFM) in levende cellen. Beginnend met een conceptuele introductie van de 'moleculaire zaklamp' en een korte geschiedenis van technische ontwikkelingen om de verkennende bijdrage van verschillende onderzoekers door de jaren heen te erkennen, beschrijf ik de verschillende modaliteiten die kunnen worden gebruikt in combinatie met beeldvorming van levende cellen en fluorescentie-microscopie van een enkel molecuul. Daarna beschrijf ik de verdiensten van het bestuderen van levende cellen door middel van beeldvorming van individuele moleculen en hoe dergelijke studies een omwenteling hebben veroorzaakt op het gebied van bacteriële celbiologie. Vervolgens overweeg ik de technische en biologische afwegingen die van belang zijn bij de keuze voor dergelijke beeldvormingstechnieken (live-celbeeldvorming -fluorescentie-microscopie van een enkel molecuul). Het hoofdstuk concludeert met de vraag hoe het gebruik van deze twee technieken toepasselijk is voor ons onderzoek door te bekijken hoe deze enkele-molecuul beeldvorming met name heeft geleid tot recente vooruitgang van DNA replicatie- en herstelmechanismen.

Hoofdstuk 3 gaat dieper in op de reactie van de replicatieve helicase DnaB wanneer de cellen worden blootgesteld aan UV-geïnduceerde DNA-schade. Er is gespeculeerd dat DnaB zich

distantieert van het replisoom ('afvallen') of ermee geassocieerd blijft ('blijven zitten'). Met behulp van onze fotografische microscopie methode die een gevoeligheid op het niveau van een enkel molecuul heeft, meten we wat er met DnaB gebeurt na blootstelling aan UV. Dit doen we op basis van drie parameters: het aantal lokalisaties, de hoeveelheid van het eiwit en de ruimtelijke verdeling van deze lokalisaties over de as van de cel. Hoewel we geen opmerkelijke verandering in stoichiometrie voor en na UV-blootstelling vinden, rapporteren we wel veranderingen in het aantal lokalisaties (bijv. in de categorie met 2 lokalisatie) en ook een verandering in de ruimtelijke verdeling van DnaB ten opzichte van replisoom (β -clamp). In lijn met resultaten die recentelijk zijn gepubliceerd, terwijl dit werk aan de gang was, veronderstellen we op basis van onze experimenten dat DnaB niet 'valt' of 'blijft zitten' na blootstelling aan UV. In plaats daarvan kan DnaB worden losgekoppeld van de rest van de replisoom machine, waardoor het chromosoom voorop wordt afgewikkeld terwijl de andere replisoom componenten achter blijven. Ons werk zou toekomstig onderzoek moeten aanmoedigen over wat de rol van helicase-laders is (bijvoorbeeld PriA/ PriC) als DnaB niet afvallen van het replisoom en hoe de mechanismen voor herstart van de replicatie werken.

Hoofdstuk 4 is een studie over DNA-schade translesie polymerasen, waarvan de concentratie verhoogd is tijdens de SOS respons in *Escherichia coli*. DNA-polymerase IV (Pol IV), zo'n polymerase, speelt een sleutelrol bij cellulaire overleving. Met behulp van live-celbeeldvorming rapporteren we hier over Pol IV-dynamica *in vivo*, en de reactie van Pol IV op twee verschillende DNA-beschadigende middelen: methyl methanesulfonate (MMS) en nitrofurazone (NFZ). Dit doen we vanaf het begin van DNA-schade tot voorbij de piek van de verhoogde concentratie tijdens SOS respons. Over het algemeen zijn de bevindingen vergelijkbaar voor MMS en NFZ. We vinden dat de omvang van de Pol IV-respons op DNA-schade sterk afhangt van de toegediende dosering van DNA-schadeveroorzakende middelen en dat de respons ook evolueert met de tijd. De ruimtelijke positionering van DNA-gebonden Pol IV in de cel blijkt te evolueren van uniform (bij een lage dosis), tot een voorkeur van lokalisatie in de uiteinden van de cel bij een hogere (geaccumuleerde) dosis. Hoewel de co-lokalisatie van Pol-IV en het replisoom die van willekeurige kans overtreft, worden veel Pol IV-moleculen via replicatie-onafhankelijke middelen gerekruteerd naar het DNA op een schade-afhankelijke manier. Bij de hoogste (geaccumuleerde) dosis die wordt getest, heeft de lokalisatie van het replisoom in het midden van de cel de neiging om te verbreden, waardoor de schijnbare co-lokalisatie met Pol IV wordt versterkt. Met deze observatie van Pol IV op het niveau van een enkel molecuul over een reeks doseringen en incubatietijd van DNA-beschadiging, vonden we meer inzicht in de reactie van translesie polymerasen op verschillende soorten DNA-schade.

Het hier beschreven onderzoek is een interdisciplinaire inspanning geweest, variërend van bacteriële celbiologie tot instrumentatie en analyse, en chemie van geneesmiddelen voor DNA-schade. Dit werk was niet mogelijk geweest zonder de verschillende technische vorderingen van andere groepen, niet alleen beperkt tot microscopie. Omdat genoomreplicatie ongetwijfeld een complex proces is, zelfs in *Escherichia coli*, moeten we veel leren over hoe DNA-schade de replicatie beïnvloedt en over hoe het daaropvolgende herstel wordt uitgevoerd. Daarnaast, met meerdere mechanismen die spelen (bijv. verschillende helicases of DNA polymerasen), begrijpen we nauwelijks hoe deze factoren in de celcyclus gecoördineerd worden. Het is opmerkelijk dat dergelijke DNA-schadeonderzoeken ook implicaties hebben voor de samenleving, naast nieuwsgierigheid en laboratoriumwetenschap.

Samengevat zal dit werk in mijn ogen een succes zijn als het anderen dient om relevante en meer introspectieve vragen te stellen voor toekomstig onderzoek.

Acknowledgements

The PhD journey of one person is, not just the result of bench science, but also the sum of all interactions and conversations which happen during that period. Such interactions may inspire the candidate towards aiming higher and also lead towards course correction when one is astray. Many times, inspiration may come when attending a Friday seminar while getting exposed to new ideas or talking to a colleague who has decided to take a bold step in his/her career. Moreover, such inspiration may last way beyond just the few years as a PhD student. Perhaps one carries such inspiration throughout life, as can be seen by reading biographies of scientists in particular and leaders in general. A pursuit may be considered truly worthwhile if it has a lasting beneficial impact on one's life, and beyond just the short-term recognition or instant fruits of labour.

First and foremost, I thank my promoter and supervisor Prof. Nynke H. Dekker for accepting me as a PhD student. I have learned much from her on many aspects of science, on how a scientific grant proposal is written, how a scientific question is formulated and how a publication is written. She has striven for perfection in details, for which she sets an example before me. I am forever grateful for all the support from her, especially when my father passed away in March 2018. During a time of personal grief, she offered more than words of commiseration which meant a world to me. Thank you Nynke!

My special word of gratitude for the thesis committee members, who found time amidst their busy schedule to read my thesis and agreed to be on the committee. I have the highest regard for this generosity: Prof. Marileen Dogterom, Prof. Sander Tans, Prof. Tom Shimizu and Dr. Greg Bokinsky.

My scientific journey is deeply indebted to Dr. Belen Solano Hermosilla. Without her guidance on planning and advice, asking critical questions on 'why' rather than only 'how', my work would have moved slower. In fact, she not only helped me, but actively participated in the planning of my students as well. I have enjoyed all the conversations I have had with her on diverse topics, because of her broad curiosity and wide-spanning career experience. In the course of time, I also became acquainted with her three beautiful children and her husband Javier- with whom I have had a great time talking to! I will always remember the great time with guitar, piano and songs at your place.

With my first student for a Master's thesis project, Filip M. Asscher, it was my pleasure to supervise someone who always wanted to do more than asked. My appreciation for his work ethic and love of life soon blossomed into true friendship, one of the contributing factors perhaps why he also decided to join as a technician later, to help me run the 'live cell imaging' sub-group. Joining in February/March 2017, his tenure overlaps with the time when our department shifted from Building 22 to Building 58 in the campus and thereby started our research anew. He was my only colleague at that time in 'live cell imaging' and we laid the basis for our research together, beginning from discussion of literature to buying microscopy software. Today, our friendship has gone beyond office and he has also helped with my career. In fact, through him I became acquainted with Mr. Maarten Asscher, a Dutch litterateur and columnist, when I was seeking professional advice on how to build a career in scientific publishing. (Thank you, Maarten!). We enjoyed many rounds of beer and discussing Dutch

life, which I will cherish to remember always. His analyses support has contributed seminally to my research.

Kirsten van Kooij joined in the helicase project in 2018 for her Bachelor's thesis. She was hard working, well-planned and dependable to do a thorough job. Her results really encouraged me to go deeper in this project. I am sure you will do great in whatever you would go on to do!

Loes Menken also decided to do her Bachelor's thesis project with me in 2019. I was amazed by her motivation to come early in the office and work hard. She was a fast learner and put her best foot forward in understanding biological concepts, coming as she did from a Physics background.

In January 2019, Lisa A. Buller joined me as a Master's student on the helicase project. I was struck by her meticulousness right from the outset. Lisa could be almost the best student I could have asked for. While she had much experimental experience, she was also inclined to undertake image analyses to drive the project and thereby learn new things. She has a sharp mind and thinks of steps to be taken at present for future progress. I was simply amazed and inspired by her ability to focus for long hours and this exemplified her drive. Lisa, your work is also the basis of this thesis undoubtedly.

Theo van Laar, my office mate in the last few months, I have the greatest respect for your kindness and willingness to help others always. Your knowledge in biological aspects is profound and I always learnt something new by talking to you. I wish I could have got to work with you more.

To my lab members: Louis Kuijpers you have a bright future ahead and I wish you the best for it. Richard Janissen, your advice has always been appreciated and your expertise on graphics I have admired. Kaley McCluskey, you have a quality amongst many others, to describe a complex idea in simple terms which I find fascinating! You are well-read and have a variety of topics for conversation. Humberto Sanchez, the most important observation I had to learn from you was the relentless focus to achieve results. You have always replied back with a smile! Good luck to Daniel Ramirez for the road ahead!

Roland Dries, you have been a trusted friend, I could discuss almost anything with you! Your depth and breadth of understanding of human nature and the world, is remarkable. I would always like to be friends with you in the future!

Sacha Khaiboulov and Susanne de Hage, you are perhaps two of the most important people in the department, carrying the department alarms 24*7. Anytime and anything I asked of you, I have got instant help. I really cannot thank you enough, from day one!

Eli van der Sluis, Esengul Yildirim and Jaco van der Torre, thank you for all the conversations.

I can never forget the wonderful lunch conversations with Dr. Martin Depken and Dr. Bertus Beaumont. Discussing about life, meditation and how you deal with or solve your problems cemented my respect for you both.

I am indebted Dr. Chirlmin Joo for taking me as a Teaching Assistant when as a biologist I contributed little to his Physics classes to begin with. It was a learning experience! Moreover, you have always had the time and advice for my career. I really appreciate your habit of replying emails as promptly as you could. Your pizza treats after the completion of our teaching assignments were truly nice!

I also offer my thanks to Prof. Cees Dekker, with whom I had many enjoyable discussions including on bluegrass songs and while writing for Kavli Newsletters.

Jeremie Capoulade you were always there to take my questions on the microscope. Your expert advice was always useful. You also helped me on and off with taking care of the microscope.

Margreet Doctor, I admire your passion to dive deep into optical systems. I learned many things from you. You were one of the few people who always visited my students' presentations.

Aditya Ananth, you were one guy with whom I could talk in Hindi while in Delft and made me remember that there is another language I can speak. Great jokes we cracked and made fun of everything! For both of us, our outlook towards the life changed while doing our PhD, we came to consider what a good life should be. I hope you continue with cricket in the future.

To my foosball partners, Sam Leachman, Luuk Loeff and Thijs Cui, it was great fun knowing you. Luuk and Thijs, it was an incredible time sharing office corner with you!

Jacob Kerssemakers, you are a man of many talents, yet always kind and humble. You exemplify calm as always.

I am grateful to Stefania Usai for the time and advice to help my career, thank you! My thanks also to Marije Boonstra for taking my requests for certificates on and off.

For all the paperwork and emails handled, the secretaries- previous and current, I am thankful to them. Dijana Boric, who processed my papers on lab joining in 2014, Jolijn Leeuwenburgh who was always helpful, Emmylou van Hartrop who helped me with inviting guests for departmental seminars, Amanda van der Vlist, who I could always ask for information. Thank you also to Nadine Kuijvenhoven and Tracey de Ruijter.

Without great support staff like Jan Wignand and Anke Amweg-Welter, I would have been unable to perform my experiments.

During my initial years at TU Delft, I shared office with Seungkyu Ha and Zhongbo Yu who were some of the friendliest colleagues I have ever had. I learnt much working with Sriram Krishnan about bacterial techniques. Bojk Berghuis and Maarten van Oene were so much fun to be with always!

In the recent years, I shared offices with Artur Kaczmarczyk and Orkide Ordu, who were really nice people. It was a pleasure coming to office every day!

In the past few years in the department, I made many acquaintances which I will fondly remember: Siddharth Deshpande, Jakub Wiktor, Sergii Pud, Daniel Verschuren, Stephanie Heerema, Jorine Eeftens, Anthony Birnie.

Jetty van Ginkel for all the career advice and interesting conversations!

My paths intersected with many people in the department during these days, each of whom may have enriched my career and thoughts in some way. I hope they forgive me if I have not named them individually here.

My housemates made my life wonderful during my stay in Delft: Nick Antonopoulos and Stuart Pearson. Thank you for all the conversations!

Finally, I would like to thank my parents for all the love and support always, without which no endeavor would have been possible. No words suffice to express my gratitude.

Sumitabho Deb Roy, May 2020

Curriculum Vitae

Sumitabho DEB ROY

13-12-1984	Born in Shillong, India
2003-2006	B.Sc. Biotechnology Bharati Vidyapeeth University, India
2006-2009	M.Sc. Biotechnology Berhampur University, India
2011-2014	Senior Project Fellow CSIR- Institute of Genomics & Integrative Biology, India
2014-2020	Ph.D. Department of Bionanoscience, Delft University of Technology, The Netherlands Promoter: prof.dr. Nynke H. Dekker

List of Publications

- **S. Deb Roy***, F.M. Asscher*, T. van Laar, N.H. Dekker. Drug dosage and timing influence the spatial distribution of DNA Polymerase IV. (*denotes equal contribution). Submitted, 2019.
- A.K. Mukherjee, S. Sharma, S. Sengupta, D. Saha, P. Kumar, T. Hussain, V. Srivastava, **S. Deb Roy**, J.W. Shay, S. Chowdhury. Telomere length-dependent transcription and epigenetic modifications in promoters remote from telomere ends. PLoS Genet 14(11): e1007782 (2018).
- M. Netravathi, S. Kapoor, R. Kumari, P. Dakle P, M.K. Dwivedi, **S. Deb Roy**, P. Pandey, J. Saini, A. Ramakrishna, D. Navalli, P. Satishchandra, P.K. Pal, M. Faruq, A. Kumar. Genetic analysis of an Indian family with Coats plus syndrome and dextrocardia: whole exome sequencing identifies homozygous novel CTC1 and a rare HES7 variation. BMC Medical Genetics **16**, 5 (2015).
- V.K. Yadav, A. Kumar, A. Mann, S. Aggarwal, M. Kumar, **S. Deb Roy**, S.K. Pore, R. Banerjee, J. M. Kumar, R.K. Thakur, S. Chowdhury. Engineered reversal of drug resistance in cancer cells-metastases suppressor factors as change agents. Nucleic Acids Research **42**, 764 (2013).